TU Delft

Delft University of Technology

Biological Production of Spatially Organized Functional Materials

Yu, K.

DOI
10.4233/uuid:57651a9a-5dab-4459-a320-302b6c680b8e

Publication date
2021

Document Version
Final published version

Citation (APA)
Yu, K. (2021). *Biological Production of Spatially Organized Functional Materials*. [Dissertation (TU Delft), Delft University of Technology]. https://doi.org/10.4233/uuid:57651a9a-5dab-4459-a320-302b6c680b8e

Important note
To cite this publication, please use the final published version (if applicable).
Please check the document version above.

Copyright
Other than for strictly personal use, it is not permitted to download, forward or distribute the text or part of it, without the consent of the author(s) and/or copyright holder(s), unless the work is under an open content license such as Creative Commons.

Takedown policy
Please contact us and provide details if you believe this document breaches copyrights.
We will remove access to the work immediately and investigate your claim.

This work is downloaded from Delft University of Technology.
For technical reasons the number of authors shown on this cover page is limited to a maximum of 10.

Biological Production of Spatially Organized Functional Materials

Kui YU

Biological Production of Spatially Organized Functional Materials

Dissertation

for the purpose of obtaining the degree of doctor
at Delft University of Technology
by the authority of the Rector Magnificus, Prof. dr. ir. T.H.J.J. van der Hagen.,
chair of the Board for the Doctorates
to be defended publicly on
Friday 18th June 2021 at 10:00 o'clock

by

Kui YU

Master of Engineering in Material Science and Engineering,
Donghua University, China
born in Henan, China

This dissertation has been approved by the promotors.

Composition of the doctoral committee:

Rector Magnificus	chairperson
Dr. M.-E. Aubin-Tam	Delft University of Technology, promotor
Dr. Y. Lin	Delft University of Technology, copromotor

Independent members:

Prof. dr. A. A. Zadpoor	Delft University of Technology
Prof. dr. G. H. Koenderink	Delft University of Technology
Prof. dr. M. M. G. Kamperman	University of Groningen
Dr. K. Masania	Delft University of Technology
Prof. dr. M. Linder	Aalto University

This work was financially supported by China Scholarship Council (CSC), Whitespace at Lululemon, Air Force Office of Scientific Research, Asian Office of Aerospace Research and Development, AOARD, the Netherlands Organization for Scientific Research (NWO/OCW), and the Advanced Materials NWO-NSFC program.

Keywords: *Bioinspired materials, bacterial cellulose, living materials, 3D bioprinting*
Cover designed by: Kui Yu and Xiangxiang Zhou
Printed by: Gildeprint, Enschede

Copyright © 2021 by K. Yu
ISBN 978-90-8593-479-0
Casimir PhD Series, Delft-Leiden 2021-13
An electronic version of this dissertation is available at
https://repository.tudelft.nl/

Contents

Summary ..... **vii**

Samenvatting ..... **xi**

1 Introduction **1**

1.1 Bioinspired Materials 3

1.2 Processing Methods of Bioinspired Materials 5

1.3 Biological Fabrication Methods 6

1.4 Bacterial Cellulose and Composites 7

1.5 The Importance of Spatial Organization 11

1.6 Challenges and Research Aim 11

1.7 Thesis Outline 11

1.8 References 13

2 Scalable Bacterial Production of Moldable and Recyclable Biomineralized Cellulose with Tunable Mechanical Properties **21**

2.1 Introduction 23

2.2 Results and Discussion 25

2.3 Conclusions 36

2.4 References 37

2.5 Supplementary Information 42

3 Spiral Honeycomb Microstructured Bacterial Cellulose for Increased Strength and Toughness **51**

3.1 Introduction 53

3.2 Results and Discussion 55

3.3 Conclusions 62

3.4 References 62

3.5 Supplementary Information 67

4 Bacterially Grown Cellulose/ Graphene Oxide Composites Infused with γ-Poly (glutamic acid) as Biodegradable Structural Materials with Enhanced Toughness 75

4.1 Introduction.... 77

4.2 Results and Discussion 80

4.3 Conclusions.... 88

4.4 References.... 88

4.5 Supplementary Information 94

5 Three-dimensional Patterning of Engineered Biofilms with a Do-it-yourself Bioprinter 101

5.1 Introduction.... 103

5.2 Protocol.... 104

5.3 Results 108

5.4 Discussion.... 112

5.5 References.... 115

6 Bioprinting of Regenerative Photosynthetic Living Materials 119

6.1 Introduction.... 121

6.2 Results 123

6.3 Conclusion 133

6.4 References.... 135

6.5 Supplementary Information 140

7 Conclusions and Outlook 159

Acknowledgements 165

Curriculum Vitae 169

List of Publications 171

Summary

Catastrophic breakage of a material might bring severe accidents in aerospace engineering, construction, and transportation field. Therefore, engineering material with high toughness values is very important for these special applications.

Many biological materials in nature, such as nacre, silk, and wood, possess high toughness values because of their highly organized micro- and nanostructure. Inspired by these natural materials, many scientists tried to build tough materials by improving their orientation of the micro- and nanostructure. However, most of the current fabrication methods are either energy-consuming or labor-intensive, the mild and scalable production of engineering tough materials remains challenging.

In this thesis, several bioinspired materials or living materials were fabricated with specific spatial organizations, using *ex situ* (Chapter 2), *in situ* (Chapter 3 and 4) and 3D bioprinting (Chapter 5 and 6) techniques. It should be noted that all the materials in this thesis are biologically produced with microorganisms.

As a biologically produced natural material, bacterial cellulose (BC) showed promising applications in the next generation of structural materials because of its excellent tensile strength, finely layered nanofibrous structure, biodegradability, and scalable producibility. However, the toughness values of BC still requires improvement. Besides, to endow BC with certain functions (photosynthetic, electrical, magnetic, biological), additional components need to be inserted into the BC fibrous network, so that functional BC composites with high toughness can be developed.

To construct BC based inorganic/organic composites, inorganic particles need to be inserted, which remains difficult, into the BC layered structure. To solve this problem, in Chapter 2, we used a kitchen blender to mechanically disintegrate the BC solid pellicle into a fibrous suspension. A microorganism-induced calcium carbonate ($CaCO_3$) precipitation method was utilized to make the BC suspension highly biomineralized. The biomineralized BC slurry could reassemble into a layered 3D bulk material simply by air-drying. The biomineralized BC composites are extremely compressible (could resist 100 kN force) and show high toughness values (22 MJ m^{-3}), over five folds higher than pure BC. Due to these attractive mechanical properties, its rapid, scalable mild and green fabrication procedure (12 hours, 28 °C, no hazardous chemicals involved), and its fire-resistance, moldability and recyclable properties, this biomineralized BC composite shows promising applications in the

industry, including production of furniture, cellphone holders, helmets, and protective garments.

Although the *ex situ* method of Chapter 2 successfully inserted $CaCO_3$ into the BC network, the mechanical disintegration method might reduce the tensile strength of BC composite. To avoid the mechanical disintegration, in Chapter 3, we used an *in situ* fermentation method to introduce polyvinyl alcohol (PVA) into the BC network. PVA polymers were added into the liquid fermentation medium, and a BC/PVA composite could be grown by bacteria. By regulating the PVA concentration and post treatment procedure, we could self-assemble the BC/PVA film in a honeycomb microstructure. Compared to controlled BC, the resulted honeycomb BC/PVA film showed a 2X increase in tensile strength (315 MPa for honeycomb BC) and a 5X increase in toughness (17.8 MJ m^{-3} for honeycomb BC).

Although the *in situ* fermentation method shown in Chapter 3 successfully inserted PVA into the BC network, this method only applies to water soluble polymers. The construction of inorganic/BC composites is difficult because most inorganic particles are unstable during days of fermentation. To overcome this disadvantage, in Chapter 4, we used a surface charged inorganic component-graphene oxide (GO), which could remain stable in the liquid fermentation medium. BC/GO composites with excellent toughness values (35 MJ m^{-3}) were successfully grown by bacteria.

The composites in Chapter 2-4 are fabricated by living microorganisms, but they are all "dead" materials since the living cells were killed and removed in the post treatment procedure. However, some functions, like photosynthesis, require cells to stay alive in the final materials. Therefore, living materials are also important in the development of advanced functional materials.

3D bioprinting is an emerging technique and remains a very useful tool in the spatial patterning of living materials. In Chapter 5 and 6, we used this technique to construct functional living materials with shapes that can be controlled spatially at the millimeter scale. In Chapter 5, we printed a calcium-alginate hydrogel containing bacteria and optimized the printing resolution. In Chapter 6, based on the same calcium-alginate hydrogel, we printed microalgae. The bioprinting was done on the top of a dried BC film, in order to improve the mechanical properties of the fragile calcium-alginate hydrogel. Notably, the presence of microalgae endows the material with photosynthetic properties, which makes it promising in diverse applications including photosynthetic skin, artificial leaves, bio-garments, photosynthetic adhesive labels, *etc*.

Overall, by varying the raw materials (BC, $CaCO_3$, PVA, GO, *etc*.) and processing methods (*ex situ*, *in situ*, 3D printing), multiple bioinspired materials or living materials could be produced by different microorganisms, while being organized at the nano-, micro-, and/or macroscales. These microorganism-based processing methods are very promising in the green and scalable production of advanced functional materials.

Samenvatting

Catastrofale breuk van een materiaal kan leiden tot ernstige ongevallen vooral op het gebied van lucht- en ruimtevaarttechniek, constructie, en transport. Daarom zijn materialen met hoge taaiheidswaarden erg belangrijk voor deze speciale toepassingen.

Veel biologische materialen in de natuur, zoals parelmoer, zijde, en hout, hebben hoge taaiheidswaarden vanwege hun sterk georganiseerde micro- en nanostructuur. Geïnspireerd door deze natuurlijke materialen, probeerden veel wetenschappers taaie materialen te bouwen door de oriëntatie van de micro- en nanostructuur van het materiaal te verbeteren. Meeste van de huidige fabricagemethoden zijn echter energieverbruikend of arbeidsintensief, hierdoor blijft de milde en schaalbare productie van technisch taaie materialen blijft een uitdaging.

In dit proefschrift zijn verschillende biogeïnspireerde materialen of levende materialen vervaardigd met specifieke ruimtelijke organisaties, gebruikmakend van *ex situ* (Hoofdstuk 2), *in situ* (Hoofdstuk 3 en 4) en 3D bioprinting (Hoofdstuk 5 en 6) technieken. Alle materialen in dit proefschrift biologisch zijn geproduceerd met micro-organismen.

Als biologisch geproduceerd natuurlijk materiaal vertoond bacteriële cellulose (BC) veelbelovende toepassingen in de volgende generatie structurele materialen vanwege zijn uitstekende treksterkte, fijn gelaagde nanovezelstructuur, biologische afbreekbaarheid en schaalbare produceerbaarheid. De taaiheidswaarden van BC moeten echter nog worden verbeterd. Bovendien, om BC bepaalde functies te geven (fotosynthetisch, elektrisch, magnetisch, biologisch), moeten aanvullende componenten in het BC-vezelnetwerk worden ingebracht, zodat functionele BC-composieten met een hoge taaiheid kunnen worden ontwikkeld.

Om op BC gebaseerde anorganische/ organische composieten te construeren, moeten anorganische deeltjes worden ingebracht, wat moeilijk blijft, in de gelaagde structuur van BC. Om dit probleem op te lossen, hebben we in Hoofdstuk 2 een keukenblender gebruikt om de vaste BC-pellicle mechanisch te desintegreren tot een vezelige suspensie. Een door micro-organismen geïnduceerde calciumcarbonaat ($CaCO_3$) -precipitatiemethode werd gebruikt om de BC-suspensie in hoge mate gemineraliseerd te maken. De biomineralized BC-slurry kan eenvoudig worden samengevoegd tot een gelaagd 3D-bulkmateriaal door het aan de lucht te drogen. De biomineralized BC-composieten zijn extreem samendrukbaar (ze kunnen 100 kN-kracht weerstaan) en vertonen hoge taaiheidswaarden (22 MJ m^{-3}), meer dan vijf keer hoger dan puur BC. Vanwege deze aantrekkelijke mechanische eigenschappen, de snelle,

schaalbare milde en groene fabricageprocedure (12 uur, 28 °C, zonder gevaarlijke chemicaliën) en de brandwerende, vormbare en recycleerbare eigenschappen, vertoont dit biomineralized BC-composiet veelbelovende toepassingen in de industrie, inclusief de productie van meubels, houders voor mobiele telefoons, helmen en beschermende kleding.

Hoewel de *ex situ*-methode van Hoofdstuk 2 met succes $CaCO_3$ in het BC-netwerk heeft ingebracht, kan de mechanische desintegratiemethode de treksterkte van BC-composiet verminderen. Om mechanische desintegratie te voorkomen, hebben we in Hoofdstuk 3 een *in situ* fermentatiemethode gebruikt om polyvinylalcohol (PVA) in het BC-netwerk te introduceren. PVA-polymeren werden toegevoegd aan het vloeibare fermentatiemedium en een BC/ PVA-composiet kon door bacteriën worden gevormd. Door de PVA-concentratie en de nabehandelingsprocedure te reguleren, konden we de BC/ PVA-film zelf assembleren in een honingraatmicrostructuur. Vergeleken met gecontroleerde BC vertoonde de resulterende honingraat BC/ PVA-film een 2x toename in treksterkte (315 MPa voor honingraat BC) en een 5x toename in taaiheid (17.8 MJ m^{-3} voor honingraat BC).

Hoewel de *in situ* fermentatiemethode van Hoofdstuk 3 met succes PVA met in het BC-netwerk heeft ingebracht, is deze methode alleen van toepassing op wateroplosbare polymeren. De constructie van anorganische/ BC-composieten is moeilijk omdat de meeste anorganische deeltjes instabiel zijn tijdens fermentatiedagen. Om dit nadeel te ondervangen, hebben we in Hoofdstuk 4 een aan het oppervlak geladen anorganisch component-grafeenoxide (GO) gebruikt, dat stabiel zou kunnen blijven in het vloeibare fermentatiemedium. BC / GO-composieten met uitstekende taaiheidswaarden (35 MJ m^{-3}) werden met succes gemaakt door bacteriën.

De composieten in Hoofdstuk 2-4 worden vervaardigd door levende micro-organismen, maar dit zijn allemaal "dode" materialen aangezien de levende cellen werden gedood en verwijderd tijdens de nabehandelingsprocedure. Sommige functies, zoals fotosynthese, vereisen echter dat cellen in het uiteindelijke materiaal in leven blijven. Daarom zijn levende materialen ook belangrijk bij de ontwikkeling van geavanceerde functionele materialen.

3D-bioprinting is een opkomende techniek en blijft een zeer nuttig hulpmiddel bij het maken van ruimtelijk patroon met levende materialen. In Hoofdstuk 5 en 6 hebben we deze techniek gebruikt om functionele levende materialen te construeren met vormen die ruimtelijk op millimeterschaal kunnen worden bestuurd. In Hoofdstuk 5 hebben we een calcium-alginaat hydrogel met bacteriën geprint en de printresolutie geoptimaliseerd. In Hoofdstuk 6, gebaseerd op dezelfde calcium-alginaat hydrogel, hebben we microalgen geprint. De bioprinting werd uitgevoerd op een gedroogde BC-film om de mechanische eigenschappen van de kwetsbare calciumalginaat-hydrogel te verbeteren. Met name de

aanwezigheid van microalgen verleent het materiaal fotosynthetische eigenschappen, waardoor het veelbelovend is voor diverse toepassingen, waaronder fotosynthetische huid, kunstmatige bladeren, biokledingstukken, fotosynthetische zelfklevende etiketten, enz.

Door de grondstoffen (BC, $CaCO_3$, PVA, GO, *etc*.) en verwerkingsmethoden (*ex situ*, *in situ*, 3D-printen) te variëren, kunnen in het algemeen meerdere bio-geïnspireerde materialen of levende materialen worden geproduceerd door verschillende micro-organismen, terwijl ze georganiseerd worden op de nano-, micro- en/ of macroschaal. Deze op micro-organismen gebaseerde verwerkingsmethoden zijn veelbelovend voor de groene en schaalbare productie van geavanceerde functionele materialen.

1

Introduction

Abstract: Living systems, such as muscle, bone, nacre, wood or skin, possess excellent mechanical properties with limited number of raw components. The advantageous mechanical properties originate from their hierarchical structure. Inspired by such structure, many methods are currently being developed to fabricate biomimetic materials. However, these human methods are generally either energy-intensive or labour-intensive, and cannot easily achieve the ideal structure as nature did. The use of microorganisms as factory, is attracting increasing attention in material science, as it replicates fast and can be genetically engineered to achieve multiple functions. Using microorganisms for fabricating bioinspired materials is still at its early stage in material science but of critical importance in the green and scalable production of high-performance functional materials.

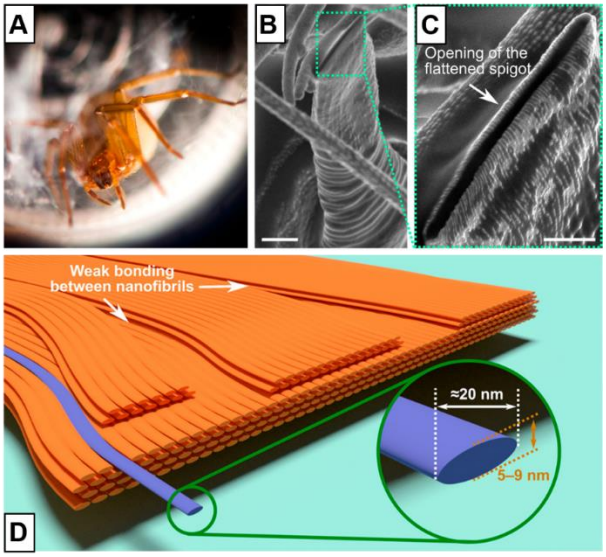

Figure 1.1 Nanofibrous layered structure of spider silk. (A-C) Spider (*Loxosceles laeta*) and the flattened *Loxosceles* spigot from which silk ribbons are extruded. (D) Scheme of the fibrous layered organization of a *Loxosceles* silk. Scale bars of (B) and (C) are 5 μm and 2 μm, separately. This image is reproduced with permission from ref [1] (Copyright 2018 American Chemical Society).

1.1 Bioinspired Materials

In living systems, many biological materials possess remarkable properties due to their highly organized nano- and microstructure.[2, 3] Spider silk (**Figure 1.1**) is one of the toughest (*Loxosceles laeta* spider, toughness value = 150.6 MJ m^{-3}) natural materials due to its multi-layered ribbon-like microstructure.[1] Wood (**Figure 1.2**) possesses excellent mechanical performance due to its hierarchical structure.[4] Nacre (**Figure 1.3**), as the inner layer of the mollusk *Mytilus edulis* shell, has a very high mineral content (over 95 % of calcium carbonate ($CaCO_3$));[5, 6] yet, because of its special "brick and mortar" multi-layer structure (**Figure 1.3**), the toughness value of natural nacre is over 1000 times higher than pure $CaCO_3$.[5]

All such biological materials are composed of a very limited number of raw components, from organic polymers (cellulose, chitin, silk, collagen)[2] to inorganic minerals ($CaCO_3$, hydroxyapatite, magnetite).[7] Nevertheless, excellent mechanical performance can be achieved by simply regulating their nano- and microstructures.[7] Inspired by the structure-property relationship of these natural materials, researchers across the world are trying to

obtain high-performance structural materials by mimicking the structure of these natural materials.[8]

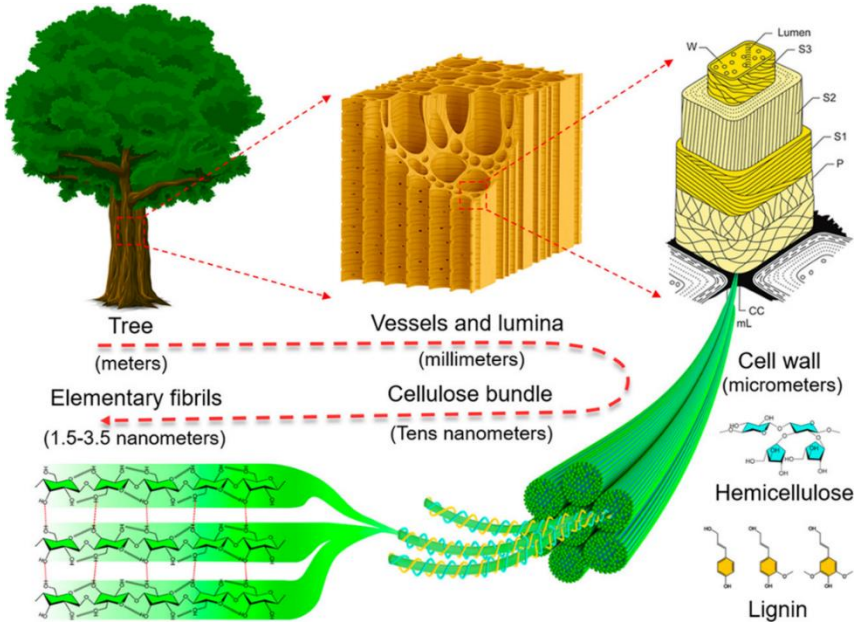

Figure 1.2 The hierarchical structure of wood, from molecular, nano-, micro- to macroscopic scale. This image is adapted with permission from ref [4] (Copyright 2018 American Chemical Society).

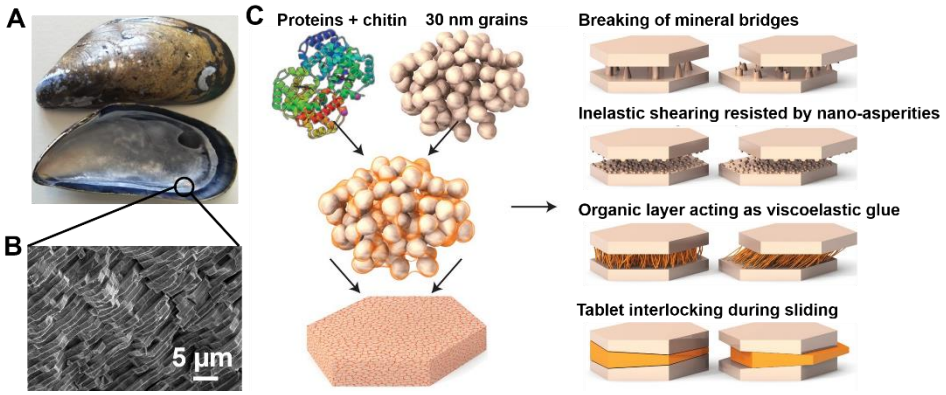

Figure 1.3 Structure and toughening mechanism of natural nacre. (A) Optical image of nacre; (B) SEM image of the cross section of natural nacre; (C) Composition of a single platelet in nacre and the toughening mechanism of natural nacre. Figure 1.3 C is reproduced with permission from ref [5] (Copyright 2015 Springer Nature).

1.2 Processing Methods of Bioinspired Materials

To construct the biomimetic fibrous or layered nano- and microstructure, many fabrication techniques were developed (**Figure 1.4**).[8] Spinning[9] (including electrospinning,[10] wet spinning,[11] and melt spinning[12]) or extrusion methods[8] are generally used for one dimensional (1D) fiber fabrication. Coating[8] (including spin-coating,[13] spray coating,[14] dip-coating[15] and blading[16]), vacuum filtration,[17] layer-by-layer,[18] biomineralization[19] and self-assembly[20] methods can be utilized for two dimensional (2D) films preparation. Three dimensional (3D) printing,[21] freeze-casting,[22] sintering[23] and hot-pressing[24] can be used for the construction of 3D bulk materials.

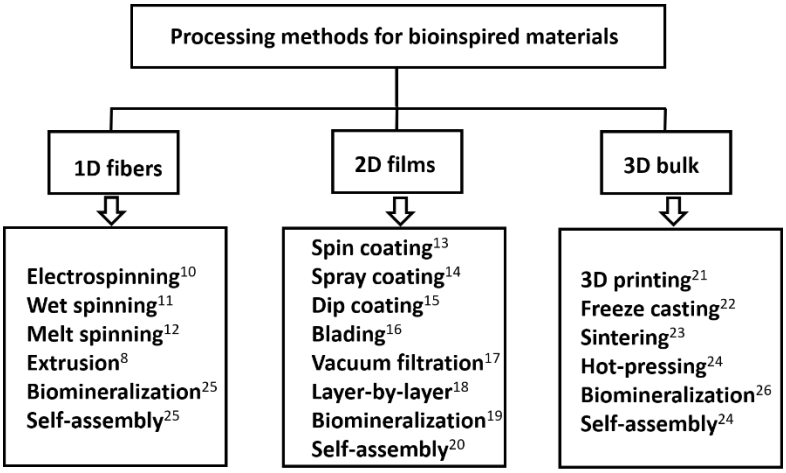

Figure 1.4 Summary of the processing methods for bioinspired materials.

It should be noted that biomineralization and self-assembly methods can also be used as 1D fiber[25] or 3D bulk material[26] fabrication. Sintering is specifically for the metal-based composites fabrication approaches.[23] The current biomimetic materials are generally produced by the combination of two or more of the above-mentioned methods.[19, 24]

However, most of the current fabrication methods are either labour-intensive, energy-intensive, environmental-unfriendly, or with limited scalable abilities.[8, 27] The development of green and mild fabrication methods with scalable productibility becomes increasingly important.

The elaboration of novel biological fabrication methods would open a new window in the mild and scalable production of bioinspired materials and living materials.[28-30]

1.3 Biological Fabrication Methods

Microorganisms,[29, 31] including bacteria, fungi and algae, can replicate fast, grow under mild conditions and secrete many biological enzymes, which could be used as bio-catalysts in chemical reactions[32] and in material science applications.[33] Moreover, as microorganisms require very little space to be stored and can usually stay alive upon freezing, they draw increasingly attention in the fabrication of bioinspired materials and living materials.[28, 33-35]

Compared to the traditional fabrication methods, biological fabrication methods are mild and easily scalable. A common material processing procedure consists of spreading living cells within a polymer matrix.[29, 30] In this case, living cells usually secrete or produce materials with certain functions.

It should be noted that during the biological production stage, it is important to keep the living cells alive. Nutrients, polymer substrates and cross-linking methods are three major factors that need to be considered in the biological production design (**Figure 1.5**).

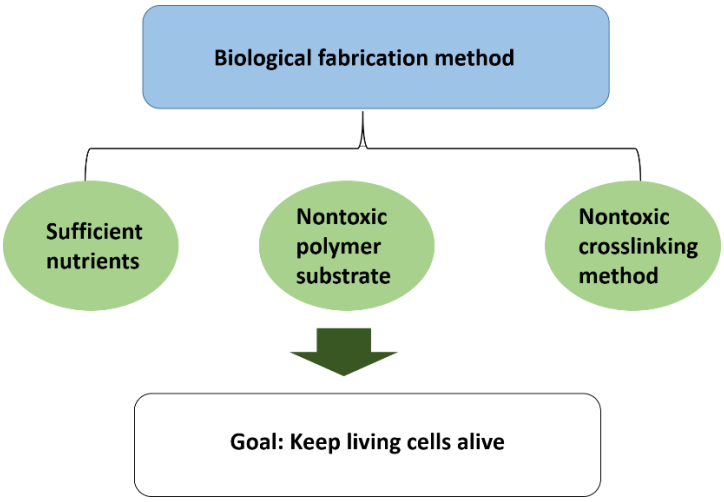

Figure 1.5 Designing principles for the biological production of bioinspired and/or living materials.

Living microorganisms in the final composite could have different functions. One is to produce the components for the material (such as $CaCO_3$,[34] cellulose[30]), which might for example influence the mechanical performance of the final composite.[35] The other is to bring certain functions (*e.g.*, algae could bring photosynthetic function[31]). Recent examples of

biological production of materials include Heveran *et al*[33], who developed an engineered living building material by microorganism-based $CaCO_3$ precipitation. A photosynthetic cyanobacteria was employed to grow $CaCO_3$ crystals into a gelatin hydrogel scaffold, endowing the living material with enhanced fracture toughness. In addition, Xin *et al*[35] exploited living bacteria and 3D-printed materials to grow biomimetic mineralized composites with ordered microstructures. The final composites exhibited outstanding specific strength and fracture toughness.[35] Also, Sushila Maharjan *et al*[31] produced a photosynthetic living material with 3D printing technique, and the microalgae living cells were utilized as an oxygen generator in the final living composite.

1.4 Bacterial Cellulose and Composites

Among all the biologically-produced materials, bacterial cellulose (BC) is one of the most extensively investigated material.[28, 36, 37]

BC is a biopolymer produced by the fermentation of bacteria.[38] During fermentation, cellulose producing bacteria could polymerize glucose into cellulose macromolecules.[39] Due to the inter- and intra- molecular hydrogen bonding, these cellulose macromolecules can be hierarchically packed together to form BC nanofibers (**Figure 1.6**).[37] Pure BC is a hydrogel-like wet pellicle, with a layered nanofibrous microstructure.[39, 40] Compared to plant cellulose, BC is not associated with impurities (*e.g.*, hemicellulose, lignin, pectin).[40] Therefore, BC purification does not involve the chemically hazardous delignification process.[41] As wet BC hydrogel can be produced in large scale at the air-liquid interface during static fermentation, the shape and size of BC is easily tunable.[38, 42] Meanwhile, due to several advantages, including high tensile strength, high water holding capacity, high purity, mild production temperature, *etc.*, BC draws increasingly attention in the fabrication of next generation bioinspired structural materials.[43]

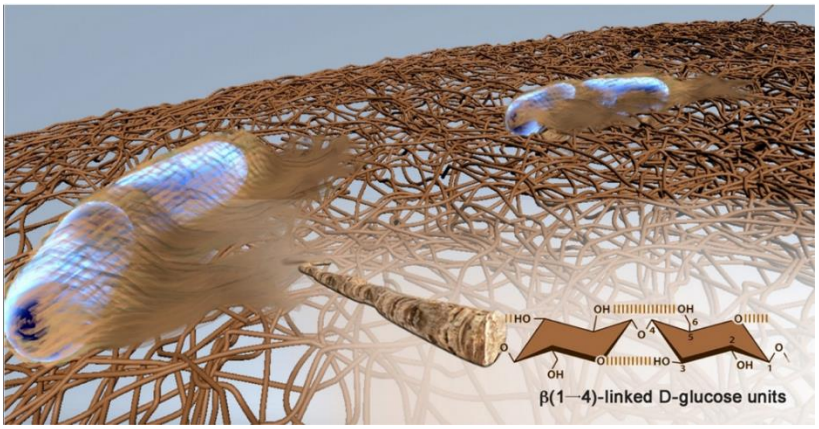

Figure 1.6 Scheme of the 3D fibrous network of BC. This image is adapted with permission from ref [42] (Copyright 2016 Elsevier).

Although BC possesses multiple advantages, it lacks certain functions,[36] including conductivity, biocompatibility, photosynthetic, magnetic properties, *etc*. Therefore, inserting other materials with such functions into the BC network are necessary to prepare BC composites for food, construction, waste water treatment and biomedical applications.[36, 37]

There are three basic methods for incorporating other ingredients into the BC network: *ex situ* blend, *in situ* impregnation and *in situ* fermentation (**Figure 1.7**).[36] The *ex situ* blending method is a widely used method, where a BC wet pellicle is first mechanically disintegrated into a BC nanofiber suspension, followed by mixing the nanofiber suspension with water soluble polymers,[44] nanoparticles,[45, 46] inorganic materials,[47] *etc*. Alternatively, other functional ingredients can also be grown together with the BC nanofiber suspension and reassembled into a functional material, endowing BC with certain functions. Zhu *et al*[48] used a hydrothermal method to grow metal oxide nanodiscs together with BC nanofibers and the reassembled BC membrane was used in visible light photodegradation applications. Huang *et al*[45] mixed halloysite nanotubes with a BC nanofibrous suspension and removed the liquid by vacuum filtration to obtain a membrane as lithium ion battery separators. Wang *et al*[49] grafted polypyrrole onto the surface of BC nanofibers and prepared a BC membrane used for bendable and flexible supercapacitor. Moreover, agarose,[50] chitosan,[51] aramid nanofiber,[52] zein nanoparticles,[46] polyaniline,[53] epoxy resin,[54] MXene,[55] and soy protein insolate,[44] were also introduced to produced BC composites for diverse applications, including lithium ion battery,[52] food packaging,[46] biosensor,[53] supercapacitor,[55] and air filtration.[44]

However, the mechanical disintegration impairs the natural BC pellicle network, and the dried BC films assembled from such BC nanofiber suspension shows lower tensile strength values compared to dried BC films originating from a natural BC pellicle. To avoid destroying the natural BC network, *in situ* impregnation methods are also being developed. In the *in situ* impregnation methods,[56] a pristine BC wet pellicle is immersed into a solution, where other ingredients are added in. The ingredients can diffuse into the BC network.[57] Many components including silver nitrates,[58] aluminium nitrate,[59] poly (vinyl alcohol) (PVA),[60] collagen,[61] graphite,[62] and aniline[63] have been impregnated into the BC network.

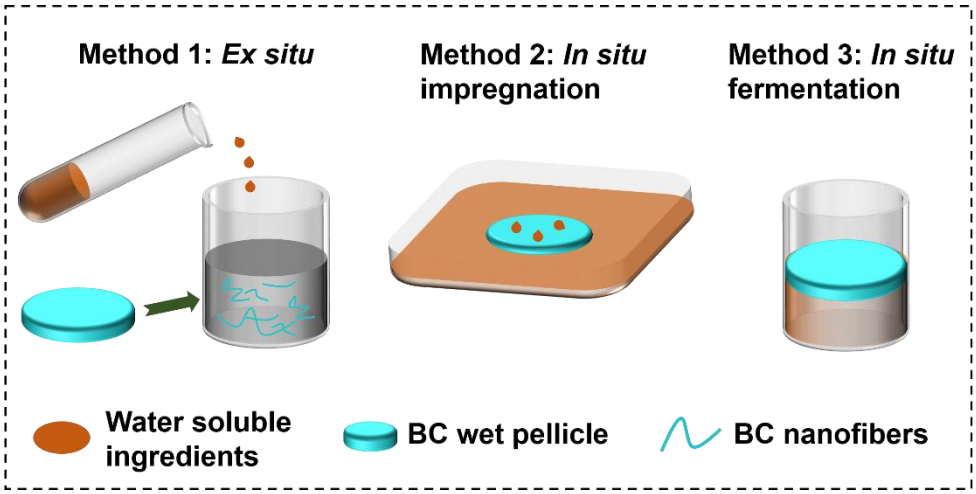

Figure 1.7 Summary of BC composites fabrication methods. In the *ex situ* methods, a BC pellicle is mechanically disintegrated into a BC nanofiber dispersion, followed by the addition of water-soluble ingredients into the BC nanofiber suspension to realize the insertion of water-soluble ingredients into the BC nanofibrous network and form the BC composites. In the *in situ* impregnation methods, BC wet pellicles are immersed into a solution containing other ingredients that can diffuse into the BC network to form the final composites. In the *in situ* fermentation methods, ingredients are added into the BC fermentation flask before the BC solid pellicle is formed, such that the BC pellicle would form in the presence in these other ingredients, resulting in a grown BC pellicle containing the desired ingredients within its network.

However, the diffusion inside BC is limited to low molecular weight molecules[58] or to nanoscale particles.[62] When it comes to macromolecules[60, 64] and microparticles,[65, 66] the diffusion becomes very slow and the ingredients cannot diffuse into the BC network homogeneously. To enhance the impregnation speed, energy-consuming vacuum filtration procedure[67] or other treatment with external forces[64] are needed.

Compared to the previous two methods, *in situ* fermentation method[68] can achieve a homogeneous distribution of viscous polymers into the BC network. In the *in situ* fermentation method, other water soluble components are added into the bacterial culture medium. The BC wet pellicle forms at the air-liquid interface. Together with the medium, the dissolved ingredients can therefore be entrapped into the BC network during the growing procedure of BC. Many polymers including sodium alginate,[69] keratin,[70] pectin,[71] gelatin,[68] carboxyl methyl cellulose,[69] starch,[71] silk[72] and PVA[73] have been introduced into the BC network with an *in situ* fermentation method.

Although the *in situ* fermentation method is an effective way of producing polymer/BC composites, it is difficult to insert inorganic particles into the BC network with this method, as sedimentation of such particles would occur during the several days of *in situ* fermentation. To solve this problem, an aerosol assisted spray method[74] was developed. Several inorganic particles including silver nanowires,[75] graphene oxide[76] and clay[77] have been grown into the BC network successfully with this spray culture method. However, the spray procedure increases the chances of contamination, and the homogeneous spray might be difficult when it comes to large surface area. These two disadvantages need to be optimized in future developments.

In summary, BC is one of the most extensively studied bacterial polymer. Many other materials, including organic polymers[69] and inorganic particles,[77] have been inserted into the BC network, with *ex situ*, *in situ* impregnation and *in situ* fermentation methods (**Figure 1.7**), to form BC composites. Among these methods, *in situ* fermentation method is the most promising one, as the general *in situ* fermentation could realize the homogeneous distribution of viscous polymers into the BC network,[68] while the improved *in situ* fermentation (aerosol assisted spray method)[74] could insert inorganic particles into the BC network. Due to the mild fabrication temperature, tailored material geometry, scalable production ability and excellent material comprehensive properties, BC based composites[36] show promising applications in human daily life, including batteries,[45] food packaging,[46] biosensors,[53] tissue engineering,[70] and sustainable plastics,[77] *etc*.

1.5 The Importance of Spatial Organization

From considering several natural materials (silk,[1] wood,[4] nacre[6] and BC[37]), scientists learned that the spatial organization across scales (from the molecular or nanoscale, to the micro- and macroscopic scales) is crucial for the construction of advanced functional materials with excellent mechanical performance.[7] Several production approaches, including self-assembly,[78] biomineralization,[26] layer-by-layer,[18] 3D printing,[29] draw increasingly attention for the construction of the hierarchical structure. Among these approaches, self-assembly,[78] biomineralization[19] and layer-by-layer[18] can be used for nano- and microscale design, while 3D printing[29] can be utilized for structural design at the macroscopic scale. The combination of these approaches would benefit for the future design of high-performance functional materials with structures controlled at different scales.[21]

1.6 Challenges and Research Aim

High-performance materials are highly demanded in the industry. However, the current fabrication methods are either energy-consuming or labour-intensive, and the mild and scalable production of bioinspired high-performance structural materials remain challenging. As a new starting biomaterial, bacterial cellulose is drawing increasing attention in the fabrication of bioinspired materials, as it can be produced in large scale under mild fabrication temperature (30 °C) by bacteria. However, pure bacterial cellulose lacks toughness, biocompatibility, conductivity and photosensitivity. To broaden the application field of this new material, functional components, including biopolymers, inorganic particles, living microorganisms, *etc*., need to be inserted into the densely packed bacterial cellulose layered microstructure.

The overall aim of this thesis is to construct spatially organized bioinspired functional materials using various microorganisms. "**How to produce a composite material biologically?**", "**How to improve their mechanical properties?**" and "**How to spatially organise the material?**" are three major challenges to be solved in this thesis.

1.7 Thesis Outline

This thesis entitled "Biological Production of Spatially Organized Functional Materials" is organized in seven chapters.

In **Chapter 1**, the background information and the current fabrication techniques of bioinspired materials were described. The research progress of BC-based composites was summarized.

In **Chapter 2**, inorganic $CaCO_3$ particles were inserted into the BC network and BC/$CaCO_3$ structural materials with tuneable mechanical properties were constructed. Due to the densely packed layered structure of BC, it remains difficult to insert $CaCO_3$ particles into the natural BC network. In this chapter, we used a kitchen blender to disintegrate BC wet pellicle into a fibrous suspension, the BC suspension was then biomineralized by a microorganism-induced $CaCO_3$ precipitation method to form a BC/$CaCO_3$ slurry. Due to the BC fiber and $CaCO_3$ crystal entanglements, the biomineralized slurry could reassemble into a layered structure. The resulting BC/$CaCO_3$ composites are very tough and extremely compressible. They could resist a 100 kN compression force and could be dropped from 10-meter-height without breakage. More importantly, this new material is moldable and recyclable, and is produced fully by bacteria in large scale. Due to these advantages, this material is promising as the next generation sustainable structural materials.

In **Chapter 3**, a water-soluble polymer-PVA was inserted into the BC network following an *in situ* fermentation approach. Before the solid BC pellicle was formed, PVA was added into the liquid fermentation medium. As PVA was dissolved in the medium, the newly formed BC pellicle at the air-liquid interface could entrap PVA and medium into its fibrous network during fermentation. The final BC/PVA wet pellicle was post-treated with a "freezing-thawing" (FT) procedure and dried. Interestingly, when the PVA concentration is up to 10 %, the final BC/PVA composite could self-assemble into a spiral honeycomb microstructure. Because of this special microstructure organization, the honeycomb BC/PVA composite shows improved tensile strength ($\times 2$) and toughness ($\times 5$) compared to pure BC.

In **Chapter 4**, graphene oxide (GO) particles were inserted into the BC network with a semi-static *in situ* fermentation method. Unlike water soluble polymers, most inorganic particles cannot remain stable in the liquid medium and aggregate easily during *in situ* fermentation. This aggregation process makes the *in situ* fermentation of BC/inorganic particle composites difficult. Unlike normal inorganic particles (clay, $CaCO_3$, *etc*.), GO particles possess abundant functional groups on its surface. These charges help GO to remain stable in the liquid solution over months. Therefore, GO could be inserted into the BC network with an *in situ* fermentation method. However, only a thin layer (<2 mm) of GO could grow into the bottom side of BC. To insert GO into the whole BC pellicle, we simply shook the incubation flask once a day during fermentation, so that some GO-containing liquid could be present on the top of the freshly formed BC and then be entrapped into the newer

BC layers. The BC/GO composites show competitive toughness values (35 MJ m^{-3}) compared to most BC-based materials.

In **Chapter 5**, a simple 3D printing technique was developed to pattern living microorganisms onto certain substrates. We printed a bioink (sodium alginate and genetically engineered bacteria producing curli) onto a $CaCl_2$ containing agar surface. As sodium alginate and Ca^{2+} can form an "egg-box" chelation, the bioink could be solidified into a Ca^{2+}-alginate hydrogel upon contacting the agar surface. After incubating the 3D prints for several days, the curli-producing bacteria produced curli within the hydrogel, enabling the Ca^{2+}-alginate bacterial hydrogel to resist citrate treatment.

In **Chapter 6**, based on the same Ca^{2+}-alginate and 3D printing technique, we printed microalgae onto a BC substrate, and constructed a self-standing photosynthetic living material. The presence of BC substrate mechanically strengthened the bioprints and helped this material to resist various physical distortions, which is hardly achievable in most 3D printed living materials. Moreover, the microalgae living cells endow this material with photosynthetic properties.

Overall, the genetically engineered possibility and fast replicability of microorganisms make them promising in creating new materials, inducing chemical reactions and bringing new functions to materials. Although the utilization of microorganisms in material science is still at its infant stage, it will become increasingly important in the fabrication of next generation functional materials and living materials.

1.8 References

1. Wang, Q.; Schniepp, H. C. Strength of Recluse Spider's Silk Originates from Nanofibrils. ACS Macro Lett. 2018, *7* (11), 1364-1370.

2. Ling, S.; Chen, W.; Fan, Y.; Zheng, K.; Jin, K.; Yu, H.; Buehler, M. J.; Kaplan, D. L. Biopolymer Nanofibrils: Structure, Modeling, Preparation, and Applications. Prog. Polym. Sci. 2018, *85*, 1-56.

3. Zhang, B.; Han, Q.; Zhang, J.; Han, Z.; Niu, S.; Ren, L. Advanced Bio-inspired Structural Materials: Local Properties Determine Overall Performance. Mater. Today 2020, *41*, 177-199.

4. Chen, C.; Hu, L. Nanocellulose toward Advanced Energy Storage Devices: Structure and Electrochemistry. Acc Chem. Res. 2018, *51* (12), 3154-3165.

5. Wegst, U. G. K.; Bai, H.; Saiz, E.; Tomsia, A. P.; Ritchie, R. O. Bioinspired Structural Materials. Nat. Mater. 2015, *14* (1), 23-36.

6. Barthelat, F. Nacre from Mollusk Shells: A Model for High-Performance Structural Materials. Bioinspir. Biomim. 2010, *5* (3), 035001.

7. Huang, W.; Restrepo, D.; Jung, J. Y.; Su, F. Y.; Liu, Z.; Ritchie, R. O.; McKittrick, J.; Zavattieri, P.; Kisailus, D. Multiscale Toughening Mechanisms in Biological Materials and Bioinspired Designs. Adv. Mater. 2019, *31* (43), 1901561.

8. Zhao, H.; Yang, Z.; Guo, L. Nacre-inspired Composites with Different Macroscopic Dimensions: Strategies for Improved Mechanical Performance and Applications. NPG Asia Mater. 2018, *10* (4), 1-22.

9. Shang, L.; Yu, Y.; Liu, Y.; Chen, Z.; Kong, T.; Zhao, Y. Spinning and Applications of Bioinspired Fiber Systems. ACS Nano 2019, *13* (3), 2749-2772.

10. Xue, J.; Wu, T.; Dai, Y.; Xia, Y. Electrospinning and Electrospun Nanofibers: Methods, Materials, and Applications. Chem. Rev. 2019, *119* (8), 5298-5415.

11. Yao, J.; Chen, S.; Chen, Y.; Wang, B.; Pei, Q.; Wang, H. Macrofibers with High Mechanical Performance Based on Aligned Bacterial Cellulose Nanofibers. ACS Appl. Mater. Interfaces 2017, *9* (24), 20330-20339.

12. Zhong, F.; Thomann, R.; Thomann, Y.; Burk, L.; Mülhaupt, R. Melt-Processable Nacre-Mimetic Hydrocarbon Composites via Polymer 1D Nanostructure Formation. Macromolecules 2019, *52* (23), 9272-9279.

13. Zhang, Y.; Tian, J.; Zhong, J.; Shi, X. Thin Nacre-Biomimetic Coating with Super-Anticorrosion Performance. ACS Nano 2018, *12* (10), 10189-10200.

14. Xie, H.; Lai, X.; Wang, Y.; Li, H.; Zeng, X. A Green Approach to Fabricating Nacre-inspired Nanocoating for Super-efficiently Fire-safe Polymers *via* One-step Self-assembly. J. Hazard. Mater. 2019, *365*, 125-136.

15. Zhang, B.; Wang, Q.; Zhang, Y.; Gao, W.; Hou, Y.; Zhang, G. A Self-assembled, Nacre-mimetic, Nano-laminar Structure as a Superior Charge Dissipation Coating on Insulators for HVDC Gas-insulated Systems. Nanoscale 2019, *11* (39), 18046-18051.

16. Mirkhalaf, M.; Barthelat, F. Nacre-like Materials Using a Simple Doctor Blading Technique: Fabrication, Testing and Modeling. J. Mech. Behav. Biomed. Mater. 2016, *56*, 23-33.

17. Liu, Y.; Yu, S.-H.; Bergström, L. Transparent and Flexible Nacre-Like Hybrid Films of Aminoclays and Carboxylated Cellulose Nanofibrils. Adv. Funct. Mater. 2018, *28* (27), 1703277.

18. Finnemore, A.; Cunha, P.; Shean, T.; Vignolini, S.; Guldin, S.; Oyen, M.; Steiner, U. Biomimetic Layer-by-Layer Assembly of Artificial Nacre. Nat. Commun. 2012, *3*, 966.

19. Spiesz, E. M.; Schmieden, D. T.; Grande, A. M.; Liang, K.; Schwiedrzik, J.; Natalio, F.; Michler, J.; Garcia, S. J.; Aubin-Tam, M. E.; Meyer, A. S. Bacterially Produced, Nacre-Inspired Composite Materials. Small 2019, *15* (22), 1805312.

20. Yao, H. B.; Tan, Z. H.; Fang, H. Y.; Yu, S. H. Artificial Nacre-like Bionanocomposite Films from the Self-assembly of Chitosan-montmorillonite Hybrid Building Blocks. Angew Chem. Int .Ed. 2010, *49* (52), 10127-10131.

21. Yang, Y.; Li, X.; Chu, M.; Sun, H.; Jin, J.; Yu, K.; Wang, Q.; Zhou, Q.; Chen, Y. Electrically Assisted 3D Printing of Nacre-inspired Structures with Self-sensing Capability. Sci. Adv. 2019, *5* (4), eaau9490.

22. Zhao, N.; Yang, M.; Zhao, Q.; Gao, W.; Xie, T.; Bai, H. Superstretchable Nacre-Mimetic Graphene/Poly(vinyl alcohol) Composite Film Based on Interfacial Architectural Engineering. ACS Nano 2017, *11* (5), 4777-4784.

23. Grossman, M.; Bouville, F.; Erni, F.; Masania, K.; Libanori, R.; Studart, A. R. Mineral Nano-Interconnectivity Stiffens and Toughens Nacre-like Composite Materials. Adv. Mater. 2017, *29* (8), 1605039.

24. Gao, H. L.; Chen, S. M.; Mao, L. B.; Song, Z. Q.; Yao, H. B.; Colfen, H.; Luo, X. S.; Zhang, F.; Pan, Z.; Meng, Y. F.; Ni, Y.; Yu, S. H. Mass Production of Bulk Artificial Nacre with Excellent Mechanical Properties. Nat. Commun. 2017, *8* (1), 287.

25. Liu, B.; Cao, Y.; Huang, Z.; Duan, Y.; Che, S. Silica Biomineralization *via* the Self-assembly of Helical Biomolecules. Adv. Mater. 2015, *27* (3), 479-497.

26. Mao, L. B.; Gao, H. L.; Yao, H. B.; Liu, L.; Colfen, H.; Liu, G.; Chen, S. M.; Li, S. K.; Yan, Y. X.; Liu, Y. Y.; Yu, S. H. Synthetic Nacre by Predesigned Matrix-directed Mineralization. Science 2016, *354* (6308), 107-110.

27. Zhao, C.; Zhang, P.; Zhou, J.; Qi, S.; Yamauchi, Y.; Shi, R.; Fang, R.; Ishida, Y.; Wang, S.; Tomsia, A. P.; Liu, M.; Jiang, L. Layered Nanocomposites by Shear-flow-induced Alignment of Nanosheets. Nature 2020, *580* (7802), 210-215.

28. Moradali, M. F.; Rehm, B. H. A. Bacterial Biopolymers: From Pathogenesis to Advanced Materials. Nat. Rev. Microbiol. 2020, *18* (4), 195-210.

29. Schaffner, M.; Ruhs, P. A.; Coulter, F.; Kilcher, S.; Studart, A. R. 3D Printing of Bacteria into Functional Complex Materials. Sci. Adv. 2017, *3* (12), eaao6804.

30. Gilbert, C.; Tang, T. C.; Ott, W.; Dorr, B. A.; Shaw, W. M.; Sun, G. L.; Lu, T. K.; Ellis, T. Living Materials with Programmable Functionalities Grown from Engineered Microbial Co-cultures. Nat. Mater. 2021, *20*, 691-700.

31. Maharjan, S.; Alva, J.; Cámara, C.; Rubio, A. G.; Hernández, D.; Delavaux, C.; Correa, E.; Romo, M. D.; Bonilla, D.; Santiago, M. L.; Li, W.; Cheng, F.; Ying, G.; Zhang,

Y. S. Symbiotic Photosynthetic Oxygenation within 3D-Bioprinted Vascularized Tissues. Matter 2021, *4* (1), 217-240.

32. Lee, S. Y.; Kim, H. U.; Chae, T. U.; Cho, J. S.; Kim, J. W.; Shin, J. H.; Kim, D. I.; Ko, Y.-S.; Jang, W. D.; Jang, Y.-S. A Comprehensive Metabolic Map for Production of Bio-based Chemicals. Nat. Cat. 2019, *2* (1), 18-33.

33. Heveran, C. M.; Williams, S. L.; Qiu, J.; Artier, J.; Hubler, M. H.; Cook, S. M.; Cameron, J. C.; Srubar, W. V. Biomineralization and Successive Regeneration of Engineered Living Building Materials. Matter 2020, *2* (2), 481-494.

34. Qin, W.; Wang, C. Y.; Ma, Y. X.; Shen, M. J.; Li, J.; Jiao, K.; Tay, F. R.; Niu, L. N. Microbe-Mediated Extracellular and Intracellular Mineralization: Environmental, Industrial, and Biotechnological Applications. Adv. Mater. 2020, *32* (22), 1907833.

35. Xin, A.; Su, Y.; Feng, S.; Yan, M.; Yu, K.; Feng, Z.; Hoon Lee, K.; Sun, L.; Wang, Q. Growing Living Composites with Ordered Microstructures and Exceptional Mechanical Properties. Adv. Mater. 2021, 2006946.

36. Shah, N.; Ul-Islam, M.; Khattak, W. A.; Park, J. K. Overview of Bacterial Cellulose Composites: A Multipurpose Advanced Material. Carbohydr. Polym. 2013, *98* (2), 1585-1598.

37. Torres, F. G.; Arroyo, J. J.; Troncoso, O. P. Bacterial Cellulose Nanocomposites: An All-nano Type of Material. Mater. Sci. Eng. C 2019, *98*, 1277-1293.

38. Wang, J.; Tavakoli, J.; Tang, Y. Bacterial Cellulose Production, Properties and Applications with Different Culture Methods - A Review. Carbohydr. Polym. 2019, *219*, 63-76.

39. Gao, M.; Li, J.; Bao, Z.; Hu, M.; Nian, R.; Feng, D.; An, D.; Li, X.; Xian, M.; Zhang, H. A Natural In Situ Fabrication Method of Functional Bacterial Cellulose Using a Microorganism. Nat. Commun. 2019, *10* (1), 437.

40. Gromovykh, T. I.; Pigaleva, M. A.; Gallyamov, M. O.; Ivanenko, I. P.; Ozerova, K. E.; Kharitonova, E. P.; Bahman, M.; Feldman, N. B.; Lutsenko, S. V.; Kiselyova, O. I. Structural Organization of Bacterial Cellulose: The Origin of Anisotropy and Layered Structures. Carbohydr. Polym. 2020, *237*, 116140.

41. Khakalo, A.; Tanaka, A.; Korpela, A.; Orelma, H. Delignification and Ionic Liquid Treatment of Wood toward Multifunctional High-Performance Structural Materials. ACS Appl. Mater. Interfaces 2020, *12* (20), 23532-23542.

42. de Oliveira Barud, H. G.; da Silva, R. R.; da Silva Barud, H.; Tercjak, A.; Gutierrez, J.; Lustri, W. R.; de Oliveira, O. B. J.; Ribeiro, S. J. L. A Multipurpose Natural

and Renewable Polymer in Medical Applications: Bacterial Cellulose. Carbohydr. Polym. 2016, *153*, 406-420.

43. Guan, Q. F.; Yang, H. B.; Han, Z. M.; Zhou, L. C.; Zhu, Y. B.; Ling, Z. C.; Jiang, H. B.; Wang, P. F.; Ma, T.; Wu, H. A.; Yu, S. H. Lightweight, Tough, and Sustainable Cellulose Nanofiber-derived Bulk Structural Materials with Low Thermal Expansion Coefficient. Sci. Adv. 2020, *6* (18), eaaz1114.

44. Liu, X.; Souzandeh, H.; Zheng, Y.; Xie, Y.; Zhong, W.-H.; Wang, C. Soy Protein Isolate/Bacterial Cellulose Composite Membranes for High Efficiency Particulate Air Filtration. Compos. Sci. Technol. 2017, *138*, 124-133.

45. Huang, C.; Ji, H.; Guo, B.; Luo, L.; Xu, W.; Li, J.; Xu, J. Composite Nanofiber Membranes of Bacterial Cellulose/Halloysite Nanotubes as Lithium Ion Battery Separators. Cellulose 2019, *26* (11), 6669-6681.

46. Ma, L.; Bi, Z.; Xue, Y.; Zhang, W.; Huang, Q.; Zhang, L.; Huang, Y. Bacterial Cellulose: An Encouraging Eco-Friendly Nano-Candidate for Energy Storage and Energy Conversion. J. Mater. Chem. A 2020, *8* (12), 5812-5842.

47. Shao, W.; Wang, S.; Liu, H.; Wu, J.; Zhang, R.; Min, H.; Huang, M. Preparation of Bacterial Cellulose/Graphene Nanosheets Composite Films with Enhanced Mechanical Performances. Carbohydr. Polym. 2016, *138*, 166-171.

48. Zhu, Z. S.; Qu, J.; Hao, S. M.; Han, S.; Jia, K. L.; Yu, Z. Z. alpha-Fe_2O_3 Nanodisk/Bacterial Cellulose Hybrid Membranes as High-Performance Sulfate-Radical-Based Visible Light Photocatalysts under Stirring/Flowing States. ACS Appl. Mater. Interfaces 2018, *10* (36), 30670-30679.

49. Wang, F.; Kim, H.-J.; Park, S.; Kee, C.-D.; Kim, S.-J.; Oh, I.-K. Bendable and Flexible Supercapacitor Based on Polypyrrole-Coated Bacterial Cellulose Core-Shell Composite Network. Compos. Sci. Technol. 2016, *128*, 33-40.

50. Awadhiya, A.; Kumar, D.; Rathore, K.; Fatma, B.; Verma, V. Synthesis and Characterization of Agarose–Bacterial Cellulose Biodegradable Composites. Polym. Bull. 2016, *74* (7), 2887-2903.

51. Wahid, F.; Hu, X. H.; Chu, L. Q.; Jia, S. R.; Xie, Y. Y.; Zhong, C. Development of Bacterial Cellulose/Chitosan Based Semi-Interpenetrating Hydrogels with Improved Mechanical and Antibacterial Properties. Int. J. Biol. Macromol. 2019, *122*, 380-387.

52. Yang, Y.; Huang, C.; Gao, G.; Hu, C.; Luo, L.; Xu, J. Aramid Nanofiber/Bacterial Cellulose Composite Separators for Lithium-Ion Batteries. Carbohydr. Polym. 2020, *247*, 116702.

53. Jasim, A.; Ullah, M. W.; Shi, Z.; Lin, X.; Yang, G. Fabrication of Bacterial Cellulose/Polyaniline/Single-Walled Carbon Nanotubes Membrane for Potential Application as Biosensor. Carbohydr. Polym. 2017, *163*, 62-69.

54. Vu, C. M.; Nguyen, D. D.; Sinh, L. H.; Pham, T. D.; Pham, L. T.; Choi, H. J. Environmentally Benign Green Composites Based on Epoxy Resin/Bacterial Cellulose Reinforced Glass Fiber: Fabrication and Mechanical Characteristics. Polym. Test. 2017, *61*, 150-161.

55. Jiao, S.; Zhou, A.; Wu, M.; Hu, H. Kirigami Patterning of MXene/Bacterial Cellulose Composite Paper for All-Solid-State Stretchable Micro-Supercapacitor Arrays. Adv. Sci. 2019, *6* (12), 1900529.

56. Cazon, P.; Vazquez, M.; Velazquez, G. Environmentally Friendly Films Combining Bacterial Cellulose, Chitosan, and Polyvinyl Alcohol: Effect of Water Activity on Barrier, Mechanical, and Optical Properties. Biomacromolecules 2020, *21* (2), 753-760.

57. Shimizu, Y.; Sakakibara, K.; Akimoto, S.; Tsujii, Y. Effective Reinforcement of Poly(methyl methacrylate) Composites with a Well-Defined Bacterial Cellulose Nanofiber Network. ACS Sustain. Chem. Eng. 2019, *7* (15), 13351-13358.

58. Pal, S.; Nisi, R.; Stoppa, M.; Licciulli, A. Silver-Functionalized Bacterial Cellulose as Antibacterial Membrane for Wound-Healing Applications. ACS Omega 2017, *2* (7), 3632-3639.

59. Xu, Q.; Wei, C.; Fan, L.; Peng, S.; Xu, W.; Xu, J. A Bacterial Cellulose/Al_2O_3 Nanofibrous Composite Membrane for a Lithium-Ion Battery Separator. Cellulose 2017, *24* (4), 1889-1899.

60. Cazón, P.; Velazquez, G.; Vázquez, M. Characterization of Mechanical and Barrier Properties of Bacterial Cellulose, Glycerol and Polyvinyl Alcohol (PVOH) Composite Films with Eco-Friendly UV-Protective Properties. Food Hydrocoll. 2020, *99*, 105323.

61. Dai, L.; Nan, J.; Tu, X.; He, L.; Wei, B.; Xu, C.; Xu, Y.; Li, S.; Wang, H.; Zhang, J. Improved Thermostability and Cytocompatibility of Bacterial Cellulose/Collagen Composite by Collagen Fibrillogenesis. Cellulose 2019, *26* (11), 6713-6724.

62. Erbas Kiziltas, E.; Kiziltas, A.; Rhodes, K.; Emanetoglu, N. W.; Blumentritt, M.; Gardner, D. J. Electrically Conductive Nano Graphite-Filled Bacterial Cellulose Composites. Carbohydr. Polym. 2016, *136*, 1144-1151.

63. Rogalsky, S.; Bardeau, J.-F.; Makhno, S.; Babkina, N.; Tarasyuk, O.; Cherniavska, T.; Orlovska, I.; Kozyrovska, N.; Brovko, O. New Proton Conducting Membrane Based on Bacterial Cellulose/Polyaniline Nanocomposite Film Impregnated with Guanidinium-Based Ionic Liquid. Polymer 2018, *142*, 183-195.

64. Yue, L.; Liu, F.; Mekala, S.; Patel, A.; Gross, R. A.; Manas-Zloczower, I. High Performance Biobased Epoxy Nanocomposite Reinforced with a Bacterial Cellulose Nanofiber Network. ACS Sustain. Chem. Eng. 2019, *7* (6), 5986-5992.

65. Busuioc, C.; Ghitulica, C. D.; Stoica, A.; Stroescu, M.; Voicu, G.; Ionita, V.; Averous, L.; Jinga, S. I. Calcium Phosphates Grown on Bacterial Cellulose Template. Ceram. Int. 2018, *44* (8), 9433-9441.

66. Cheng, Z.; Ye, Z.; Natan, A.; Ma, Y.; Li, H.; Chen, Y.; Wan, L.; Aparicio, C.; Zhu, H. Bone-Inspired Mineralization with Highly Aligned Cellulose Nanofibers as Template. ACS Appl. Mater. Interfaces 2019, *11* (45), 42486-42495.

67. Ccorahua, R.; Troncoso, O. P.; Rodriguez, S.; Lopez, D.; Torres, F. G. Hydrazine Treatment Improves Conductivity of Bacterial Cellulose/Graphene Nanocomposites Obtained by a Novel Processing Method. Carbohydr. Polym. 2017, *171*, 68-76.

68. Chen, Y.; Zhou, X.; Lin, Q.; Jiang, D. Bacterial Cellulose/Gelatin Composites: *In Situ* Preparation and Glutaraldehyde Treatment. Cellulose 2014, *21* (4), 2679-2693.

69. Cheng, K.-C.; Catchmark, J. M.; Demirci, A. Effect of Different Additives on Bacterial Cellulose Production by Acetobacter Xylinum and Analysis of Material Property. Cellulose 2009, *16* (6), 1033-1045.

70. Keskin, Z.; Sendemir Urkmez, A.; Hames, E. E. Novel Keratin Modified Bacterial Cellulose Nanocomposite Production and Characterization for Skin Tissue Engineering. Mater. Sci. Eng. C 2017, *75*, 1144-1153.

71. Dayal, M. S.; Catchmark, J. M. Mechanical and Structural Property Analysis of Bacterial Cellulose Composites. Carbohydr. Polym. 2016, *144*, 447-453.

72. Wang, X.; Tang, J.; Huang, J.; Hui, M. Production and Characterization of Bacterial Cellulose Membranes with Hyaluronic Acid and Silk Sericin. Colloids Surf. B 2020, *195*, 111273.

73. Gea, S.; Bilotti, E.; Reynolds, C. T.; Soykeabkeaw, N.; Peijs, T. Bacterial Cellulose–Poly(vinyl alcohol) Nanocomposites Prepared by an In-Situ Process. Mater. Lett. 2010, *64* (8), 901-904.

74. Guan, Q.-F.; Han, Z.-M.; Luo, T.-T.; Yang, H.-B.; Liang, H.-W.; Chen, S.-M.; Wang, G.-S.; Yu, S.-H. A General Aerosol-Assisted Biosynthesis of Functional Bulk Nanocomposites. Natl. Sci. Rev. 2019, *6* (1), 64-73.

75. Wan, Y.; Yang, S.; Wang, J.; Gan, D.; Gama, M.; Yang, Z.; Zhu, Y.; Yao, F.; Luo, H. Scalable Synthesis of Robust and Stretchable Composite Wound Dressings by Dispersing Silver Nanowires in Continuous Bacterial Cellulose. Compos., Part B 2020, *199*, 108259.

76. Luo, H.; Dong, J.; Yao, F.; Yang, Z.; Li, W.; Wang, J.; Xu, X.; Hu, J.; Wan, Y. Layer-by-Layer Assembled Bacterial Cellulose/Graphene Oxide Hydrogels with Extremely Enhanced Mechanical Properties. Nanomicro Lett. 2018, *10* (3), 42.

77. Guan, Q.-F.; Ling, Z.-C.; Han, Z.-M.; Yang, H.-B.; Yu, S.-H. Ultra-Strong, Ultra-Tough, Transparent, and Sustainable Nanocomposite Films for Plastic Substitute. Matter 2020, *3* (4), 1308-1317.

78. Zhang, Q.; Qu, D.-H.; Tian, H.; Feringa, B. L. Bottom-Up: Can Supramolecular Tools Deliver Responsiveness from Molecular Motors to Macroscopic Materials? Matter 2020, *3* (2), 355-370.

2

Scalable Bacterial Production of Moldable and Recyclable Biomineralized Cellulose with Tunable Mechanical Properties

Abstract: While urgently needed, sustainable structural materials with excellent impact-resistance properties are challenging to produce, especially in a scalable fashion and with control over 3D shape. Here, bacterial cellulose (BC) and bacterially-precipitated calcium carbonate are self-assembled into a layered structure reminiscent of the structure of tough biomineralized material in nature (nacre, bone, and dentin). The fabrication method consists of biomineralizing BC to form an organic/inorganic mixed slurry, in which calcium carbonate crystal size is controlled with bacterial poly(γ-glutamic acid) and magnesium ions. This slurry self-assembles into a layered material due to fiber-crystal binding and entanglements. A high toughness of 22 MJ m^{-3} is achieved, five-fold higher than pure BC. The fabrication method is rapid (12 hours of biomineralization), and readily scalable, without involving toxic chemicals. The resulting material shows high impact and fire resistance. Notably, the biomineralized BC can be repeatedly recycled and molded into any desired 3D shape and size using a simple kitchen blender and sieve. This fully biodegradable composite is well-suited for use as component in daily life applications, including furniture, helmets, and protective garments.

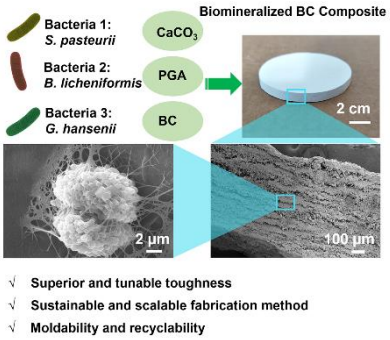

The content of this chapter is based on:
Kui Yu, Ewa M. Spiesz, Srikkanth Balasubramanian, Dominik T. Schmieden, Anne S. Meyer, and Marie-Eve Aubin-Tam. *Cell Reports Physical Science*, accepted for publication.

2.1 Introduction

Petroleum-based high-performance structural materials play a vital role in the aerospace, biomedical, construction, and automotive industries due to their low cost, excellent mechanical properties, and large production scale.[1-3] However, the manufacture and usage of such materials cause multiple irreversible damages to the environment, including accumulation of plastic waste, chemical pollution, energy-wasting, and climate change.[2] To reduce these negative effects on the planet, recyclable and sustainable structural materials fabricated in a green manner under mild conditions are highly demanded.[4] The most abundant biodegradable polymer on earth, cellulose, draws high levels of attention as a raw material for the production of sustainable structural materials.[5] Generally, plant-derived cellulose containing impurities such as lignin is used despite the fact that it requires an environmentally-unfriendly delignification process to obtain cellulose nanofibers.[6] In contrast, bacterial cellulose (BC) has gained interest in recent years due to its high purity, which is obtained with sustainable and mild processing conditions.[7] BC is an extracellular biopolymer secreted by certain microorganisms in the form of a hydrogel-like pellicle at the air-liquid interface.[8] Multiple advantages of BC, including its nanofibrous microstructure, light weight, low cost, biocompatibility, and biodegradability, make it an ideal candidate for producing the next generation of sustainable structural materials.[9] However, pure BC is brittle because of its high crystallinity. Even though BC possesses good tensile strength, its toughness is not sufficient for several applications with impact resistance requirements (*e.g.*, helmets, protective garments). Also, pure BC is an organic material, which is less fire resistant compared to inorganic materials, limiting its range of applications.

To acquire BC-based materials with a combination of high tensile strength and toughness, which are often mutually exclusive,[10] several *in situ* and *ex situ* methods including wet drawing,[11] wet spinning,[12] twisting,[13] and tape-peeling[14] have been developed. However, most of these methods focus on the production of one-dimensional (1D) fibers[15] or two-dimensional (2D) films,[16] while three-dimensional (3D) BC bulk materials are rarely reported. This difficulty in producing 3D materials based on BC at a large scale is mainly due to BC losing over 99 % of its weight upon drying, resulting in thin films with thicknesses from several centimeters to below 0.1 mm (**Figure S2.1**). More recently, a 3D BC bulk material[9] was developed by adhering multiple BC layers and polymers together using a hot-pressing technique. However, high numbers of BC layers are needed to obtain the final 3D BC

composites, and the hot-pressing process is highly energy-consuming, which would greatly increase the material and energy costs during industrial-scale production.

To lower the material costs, tune the fire retardance and mechanical properties (such as stiffness, strength, and toughness), and achieve the sustainable fabrication of 3D BC bulk composites, we combine BC with calcium carbonate ($CaCO_3$).[17] $CaCO_3$ is one of the most abundant inorganic raw materials in nature and is widely used in high-performance bioinspired structural materials.[18-22] While the preparation of $CaCO_3$-containing composites is easily realized with a mineralization method wherein $CaCO_3$ crystals are grown gradually on a supportive matrix,[18] the mineralization of BC still remains challenging. Due to the dense structure and abundance of hydrogen bonding within BC networks, inorganic $CaCO_3$ crystals cannot easily penetrate and enter into a bulk BC hydrogel matrix[20] without the assistance of external force.[18, 23] Producing a highly mineralized BC (containing over 50 *wt*% of $CaCO_3$) *via* direct mineralization of bulk BC without external force, requires weeks and months of repeated work, while the resulting material still does not possess competitive mechanical properties,[23] let alone large-scale production.[24] Organizing mineralized BC into an ordered bulk material with homogeneous inorganic crystal distribution and competitive mechanical properties remains a challenge and is of critical importance in developing BC-based 3D structural materials.

Here, we develop a hierarchical self-assembly approach to produce large-scale, shape- and size-controlled biomineralized BC composites with tunable mechanical properties, under mild conditions following a sustainable, easy, and industrially-scalable protocol (**Figure 2.1**). Three different types of bacteria are used to produce the components that make up this composite. Bulk BC hydrogels are mechanically disintegrated into a fibrous suspension, followed by bacterially-induced $CaCO_3$ biomineralization[25-27] to form an inorganic-organic mixed slurry. The crystal size and distribution can be adjusted by another bacterially-produced biopolymer: poly(γ-glutamic acid) (PGA).[28] The bacterial slurry can then self-assemble into a material with a layered microstructure, achieving a toughness of 22 MJ m^{-3}, which is over five-fold higher than that of pure BC. The resultant layered structure of $CaCO_3$ separated by organic polymers (BC and PGA) is reminiscent of the hierarchical structures of tough biomineralized materials found in nature,[4] such as nacre, bone or dentin. The homogeneous distribution of inorganic crystals together with the extensive crystal-fiber connections within the BC matrix enable the formation of stiff and tough 3D materials. This bacterially-produced composite can be molded into different geometries, is recyclable, and shows promise for use in such applications as furniture, protective garments, *etc*.

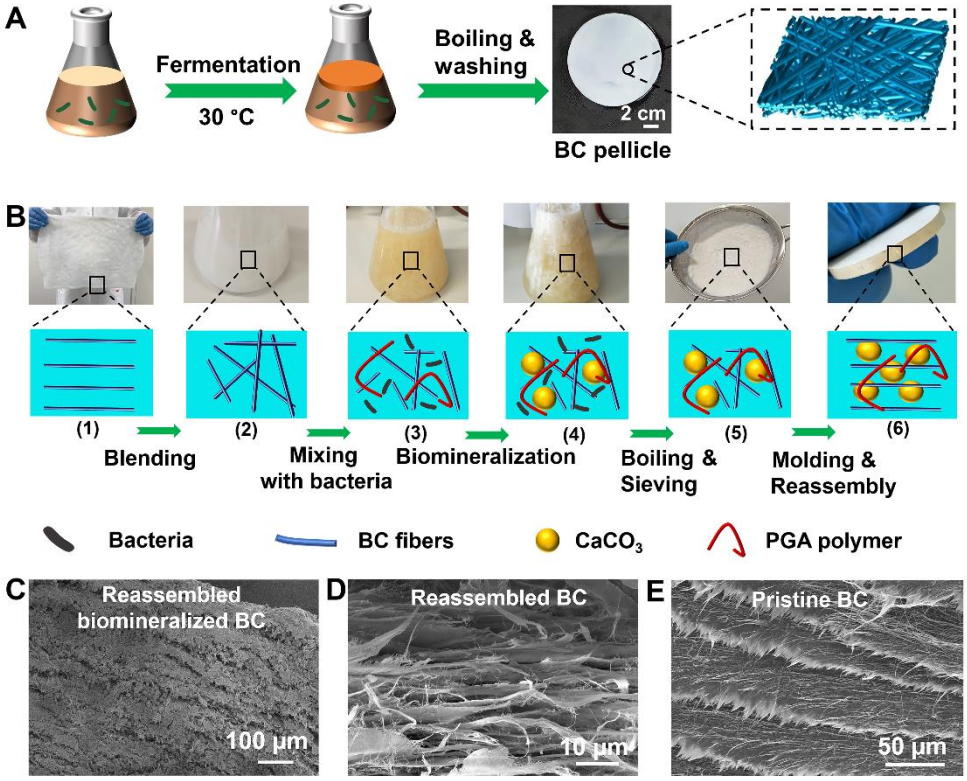

Figure 2.1 Biomineralized BC fabrication. (A) Fabrication procedure of BC, including a static *in situ* fermentation at 30 °C, boiling with sodium hydroxide, and washing with distilled water. The BC pellicle shows a hydrogel-like appearance and a nano-fibrous layered microstructure. (B) Fabrication procedure of the biomineralized BC, from step (1) to (6): (1) to (2) blending the BC hydrogel into a fibrous suspension, (2) to (3) mixing the BC fibrous suspension with the bacteria mineralization ingredients ($CaCl_2$, urea, bacteria, medium, and PGA), (3) to (4) biomineralization, (4) to (5) boiling and sieving the biomineralized slurry to remove the bacteria and medium, (5) to (6) molding the purified biomineralized BC slurry, and solvent-evaporation-induced self-assembly. The final material shown on the picture was polished with sandpaper. (C-E) Scanning electron microscope (SEM) images of the cross sections of (C) reassembled biomineralized BC composite, (D) reassembled BC, and (E) pristine BC.

2.2 Results and Discussion

Biological production and morphology of biomineralized bacterial cellulose

To achieve the sustainable and scalable fabrication of BC-biomineralized 3D structural materials with excellent mechanical properties, a bacterially-induced $CaCO_3$

biomineralization method[29, 30] was used in combination with a solvent-evaporation-induced self-assembly method (**Figure 2.1**). BC was produced by microbial fermentation with a cellulose-producing strain, *Gluconacetobacter hansenii* (*G. hansenii*).[31] After 2 weeks of growth, a wet BC pellicle was formed at the air-liquid interface (**Figure 2.1A**). This material was boiled with 1 *w/v*% sodium hydroxide solution and washed with water to remove impurities. To increase the degree of mineralization of the BC, the BC network was mechanically disintegrated (**Figure 2.1B**), so that the contact interface area between $CaCO_3$ and BC would be greatly increased during mineralization. For biomineralization, the disintegrated BC fibers were mixed in a bacterial growth medium containing *Sporosarcina pasteurii* (*S. pasteurii*), urea, and 10 mM of calcium chloride ($CaCl_2$) (**Figure S2.2**). *S. pasteurii* secrete the enzyme urease, which cleaves urea into ammonia and CO_3^{2-}, resulting in a pH increase and the formation of calcium carbonate ($CaCO_3$) crystals.[17] During this biomineralization procedure, the BC fibers were dispersed in the liquid and thus were able to become highly mineralized (**Figure 2.1B**). This biomineralized BC slurry was then purified by boiling on a heating plate for sterilization, washing with water to remove the unreacted residuals and the medium, and finally air-drying. Thermal gravimetric analysis (TGA) showed 60 *wt*% $CaCO_3$ content in these samples (**Figure S2.3**).

Due to the high aspect-ratio of BC fibrils, pure BC suspension by mechanically disintegration has been shown to be able to reassemble into a layered structure after drying, similar to that of pristine BC (**Figure 2.1C**, **D**).[32, 33] Therefore, we suspect our biomineralized BC composite might also represent a layered structure because of the self-assembly ability of the BC fibrous suspension.

After the biomineralization and the purification steps, we used SEM to assess the microstructure of the air-dried biomineralized BC/$CaCO_3$ slurry. Remarkably, we observed that BC could reassemble into a layered structure with $CaCO_3$ crystals entrapped within the layers (**Figure 2.1C**, **Figure 2.2A, B**). Due to the high aspect-ratio of BC fibrils, pure BC suspensions formed by mechanical disintegration reassembled into a layered structure after drying (**Figure 2.1D**), similar to that of pristine BC (**Figure 2.1E**). Therefore, our biomineralized BC composite likely adopted a layered structure because of this ability of the BC fibrous suspension to self-assemble.

SEM imaging of these samples revealed large $CaCO_3$ crystals (110 ± 40 μm crystal size) (**Figure 2.2A, C**) and a non-uniform cross-sectional layered morphology (**Figure 2.2B**) with a layer thickness of 130 ± 50 μm (**Figure 2.2D**). The relatively broad distribution in layer

thickness (**Figure 2.2D**) is likely attributable to the broad crystal size distribution (**Figure 2.2C**) and large crystal size (**Figure 2.2A**).

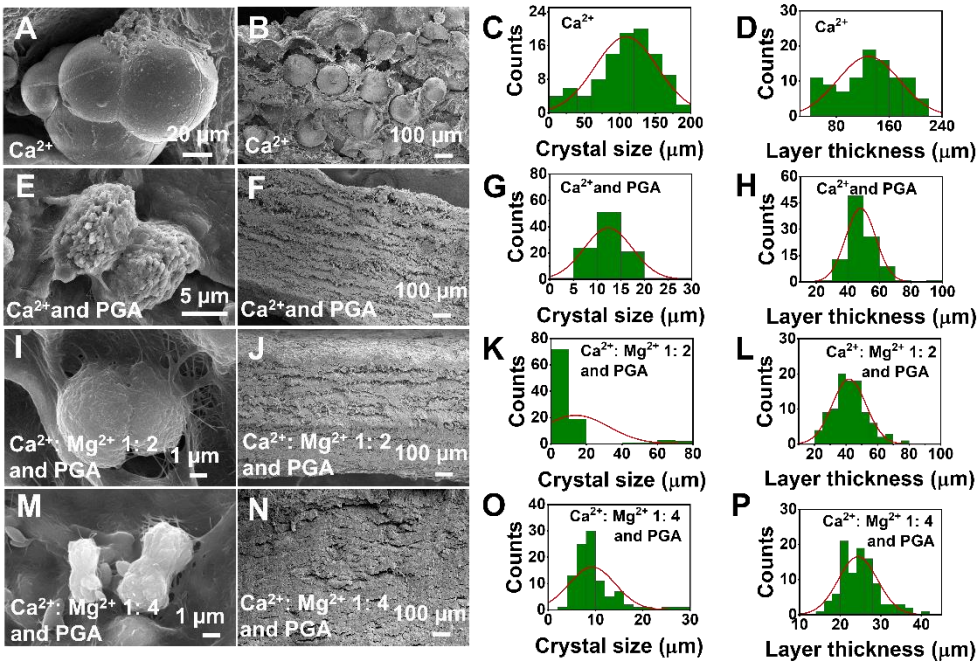

Figure 2.2 Morphology of biomineralized BC composites. (A, E, I, M) Representative SEM images of crystals within the biomineralized BC with (C, G, K, O) associated crystal size distributions. (B, F, J, N) SEM images of the material cross-sections and (D, H, L, P) layer thickness distributions of biomineralized BC composites. Biomineralized BC samples were fabricated either (A-D) without or (E-P) with PGA in the biomineralization medium; and with either (A-H) only Ca^{2+}, or with a Ca^{2+}: Mg^{2+} ratio of (I-L) 1: 2 or (M-P) 1: 4 in the biomineralization medium.

We then attempted to obtain a more homogeneous layer distribution by reducing the $CaCO_3$ crystal sizes. Also, the presence of large crystals are likely to result in stress concentration[34] in certain structural features of the material, and result in poor overall mechanical properties of the material.[35] To reduce the crystal size and in turn the layer thickness, chemically produced poly (acrylic acid) can be incorporated into the biomineralization medium, as the abundant carboxyl groups can act as binding sites for crystal growth and regulate the crystal size distribution.[36] Here, instead of poly (acrylic acid), which is produced with the use of toxic chemicals,[37] we incorporated a similar polymer that can be bacterially produced, PGA.[28] PGA is a water-soluble, renewable polyamide polymer[38]

produced by *Bacillus licheniformis*. PGA displays abundant carboxyl groups on its molecular backbone[39] that can provide binding sites for calcium ions (Ca^{2+}) during $CaCO_3$ mineralization.[40] When PGA was added to the medium for bacterial biomineralization, both the crystal size (12 ± 5 μm) (**Figure 2.2E, G**) and the layer thickness (48 ± 10 μm) (**Figure 2.2F, H**) were significantly reduced compared to samples without PGA in the biomineralization medium (**Figure 2.2A-D**) ($p < 0.01$). We therefore conclude that the addition of PGA helps to form a layered structure with thinner and more narrowly-distributed layer thicknesses, which is important for constructing layered bioinspired materials.[4] Therefore, unless indicated otherwise, the rest of the biomineralization procedures in this study were carried out in the presence of PGA.

To further reduce the crystal size, the formulation of biomineralization medium needed to be further optimized. In traditional chemical mineralization approaches, magnesium ions (Mg^{2+}) can be introduced to regulate the crystal size and morphology, as they inhibit the growth of $CaCO_3$ crystals.[41] We therefore added Mg^{2+} into the bacterial biomineralization system. Varying the Ca^{2+}/ Mg^{2+} molar ratio in the biomineralization medium, while keeping the same overall ion concentration of 10 mM, resulted in different crystal sizes and morphologies (**Figure 2.2I-P**). With a Ca^{2+}: Mg^{2+} ratio of 1: 2 in the biomineralization medium, the crystal diameter was 15 ± 19 μm (**Figure 2.2I, K**), while with a Ca^{2+}: Mg^{2+} ratio of 1: 4, the crystal diameter dropped to 9.3 ± 4.9 μm (**Figure 2.2M, O**). Notably, the samples with both Ca^{2+} and Mg^{2+} assembled into a finely-layered structure with a layer thickness of 42 ± 11 μm when the Ca^{2+}: Mg^{2+} ratio was 1: 2 (**Figure 2.2J, L**), and 24 ± 5 μm when Ca^{2+}: Mg^{2+} ratio was 1: 4 (**Figure 2.2N, P**). X-ray diffraction (XRD) indicated that the $CaCO_3$ crystals in the biomineralized BC composites (Ca: Mg 1:4 with PGA) adopted a calcite polymorph (**Figure S2.4**)

In summary, the layered structure of our material derives from the reassembly of BC fibers upon drying. After biomineralization, BC fibers are entangled with $CaCO_3$ crystals. During the drying procedure, BC fibers tend to aggregate together due to hydrogen bonding interactions, through which $CaCO_3$ crystals can be entrapped into the reassembled BC network. The addition of PGA and Mg^{2+} could regulate the biomineralization procedure *via* inhibition of the crystal growth[41, 42] and reduce the crystal diameter, which reduces the final layer thickness of our material.

The layered biomineralized BC composites (Ca^{2+}: Mg^{2+} 1: 4) could be produced in large scale (**Figure 2.3A**, material diameter of 30 cm) and repeatedly deconstructed and molded into a wide variety of desired shapes (**Figure 2.3B**). The material recycle procedure was

achieved by immersing the biomineralized BC material into water for 2 days. The softened biomineralized BC, together with water, was then re-blended with a simple kitchen blender into a slurry again. The slurry and water mixture was poured into a sieve, transferred into a mold of the desired shape, and air-dried to self-assemble into another biomineralized BC material. One single molded composite was able to be re-molded many times.

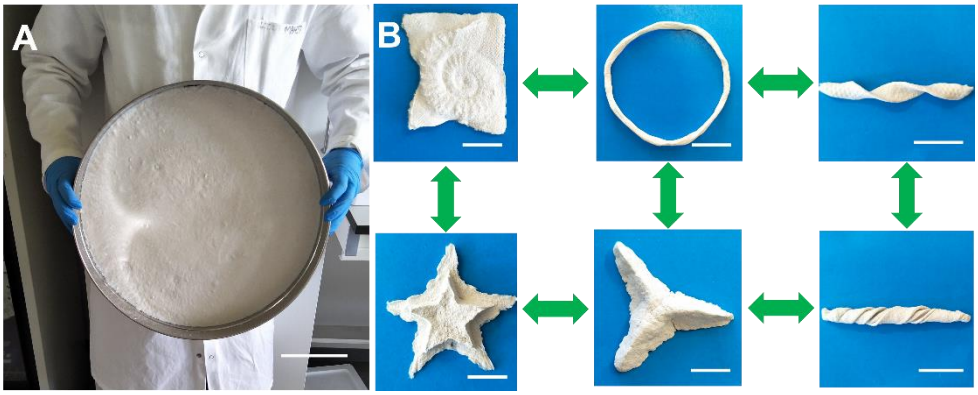

Figure 2.3 Recyclability of the biomineralized BC composites. (A) A 30-cm-diameter biomineralized BC object (Ca^{2+}: Mg^{2+} 1: 4), showing the possibility for mass production of the biomineralized BC. Scale bar = 10 cm. (B) Biomineralized BC composites (Ca^{2+}: Mg^{2+} 1: 4) produced in a variety of shapes. The shape and size of the resulting material was tunable based on the shape of the mold. All these shapes were fabricated from the same piece of material that was repeatedly remolded into different shapes. Scale bar = 2 cm.

Mechanical properties of biomineralized BC composites

Inspired by nacre, which is a natural $CaCO_3$ material possessing high toughness values due to their special layered "brick and mortar" structure,[43] we hypothesized that the layered crystal-containing structure of our biomineralized BC composites likely plays a role in their mechanical properties.[18-20] The mechanical properties were therefore assessed with tensile testing (**Figure 2.4**). Specifically, we investigated the elongation at break and tensile strength values of the biomineralized BC composites, which are the two important factors contributing to the final toughness values of a material.[43] Compared to pure BC, the elongation at break of biomineralized BC is significantly higher ($p < 0.01$) (**Figure 2.4A**). For samples produced with different Ca^{2+} content in the bacterial biomineralization medium ranging from 2.5 mM to 20 mM, the elongation at break varied from 8.0 ± 0.4 % (pure BC) to 44.4 ± 1.8 % (2.5 mM Ca^{2+}), 56.6 ± 0.4 % (5.0 mM Ca^{2+}), then reaching its highest value (73.0 ± 1.1 %) for samples with 10 mM Ca^{2+} in the bacterial biomineralization medium (**Figure 2.4A**) and finally decreasing to 17.9 ± 1.1 % (20.0 mM Ca^{2+}). Since the elongation at break is an

important factor contributing to a material's toughness, 10 mM was selected to be the optimal Ca^{2+} concentration in the bacterial biomineralization medium in order to maximize toughness. However, when Ca^{2+} content increases from 2.5 mM to 20 mM in the biomineralization medium, the ultimate tensile strength drops significantly ($p < 0.01$), from 82.4 ± 0.6 MPa (pure BC) to 49.7 ± 1.4 MPa (2.5 mM Ca^{2+}), 29.3 ± 0.9 MPa (5.0 mM Ca^{2+}), 15.5 ± 0.4 MPa (10.0 mM Ca^{2+}) and 11.4 ± 0.1 MPa (20.0 mM Ca^{2+}) (**Figure 2.4A**). This reduction in tensile strength is likely due to the higher volume fraction of $CaCO_3$ crystals, which occupy the majority of the composite's volume and increase the brittleness of the material, decreasing its strength.

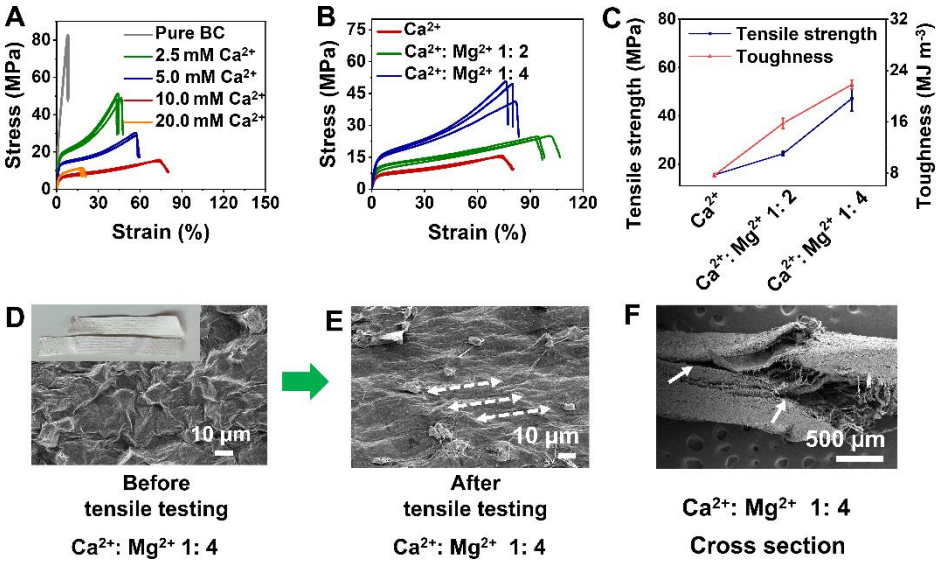

Figure 2.4 Mechanical properties of the biomineralized BC composites. (A) Tensile stress-strain curves of biomineralized BC with different Ca^{2+} content in the biomineralization medium. (B) Tensile stress-strain curves, (C) tensile strength, and toughness values of biomineralized BC with and without Mg^{2+} ions in the biomineralization medium. (D, E) Optical and SEM images of the surface morphology of the biomineralized BC composite with Ca^{2+}: Mg^{2+} ratio of 1: 4 (D) before and (E) after tensile testing. Arrows represent stretched sample wrinkles after the application of load. (F) SEM images of the cross-section of the biomineralized BC composite with Ca^{2+}: Mg^{2+} ratio of 1: 4 after tensile testing. Arrows indicate delamination in the specimen. All the samples in this figure were made with PGA.

Since the addition of PGA and Mg^{2+} into the biomineralization medium reduced the crystal size (**Figure 2.2**), we assessed any resultant effect on the mechanical properties *via*

tensile testing. With a Ca^{2+} and Mg^{2+} molar ratio of 1: 4, the material showed enhanced tensile strength (47.2 ± 5.2 MPa, **Figure 2.4B, C** and **Table S2.1**) while displaying a high elongation at break (79.1 ± 2.8 %). The biomineralized BC composites (Ca^{2+}: Mg^{2+} 1: 4) showed a sharp increase in tensile strength before breaking (**Figure 2.4B**) in the final region of the stress-strain curve (strain-hardening), as would be expected from the breakage of the numerous crystal-fiber connections (**Figure S2.5**). Because of this simultaneous increase in tensile strength and elongation at break, the toughness of the Mg^{2+}-containing biomineralized BC composite (Ca^{2+}: Mg^{2+} 1: 4) was as high as 21.8 ± 0.7 MJ m^{-3} (**Figure 2.4C**, **Table S2.1**), which was 183 % higher than that of the sample without Mg^{2+} (7.7 ± 0.3 MJ m^{-3}) and 445 % higher than that of pure BC (4.0 ± 0.2 MJ m^{-3}). This increase in tensile strength and toughness correlates with the reduced crystal size, and thus with an increased in crystal density. In these composites, more entanglements would be present between $CaCO_3$ crystals and BC fibers (**Figures 2.4D**), thus more energy would be needed to break the specimen. Besides, PGA might also help in improving toughness, since it can act as a viscoelastic glue in composite materials.[17] We therefore compared elongation at break values of biomineralized BC composites with and without PGA (produced with 10 mM Ca^{2+}), and found that indeed, the samples with PGA showed an elongation at break of 73.0 ± 1.1 % (**Figure 2.4A**), which is higher compared to samples without PGA (59.4 ± 7.2 %, **Figure S2.6**).

To further understand the mechanisms leading to such high toughness, both optical and SEM images of the biomineralized BC composites (Ca^{2+}: Mg^{2+} 1: 4) before and after tensile testing were obtained. Unlike pure BC, the biomineralized BC composites were not fully broken after tensile testing but showed a marked increase in length (**Figure 2.4D**), also reflected in the high elongation at break. SEM results (**Figure 2.4D-E**) showed that the wrinkled surfaces before testing (**Figure 2.4D**, SEM image) of the biomineralized BC composite specimens (Ca^{2+}: Mg^{2+} 1: 4) became elongated (**Figure 2.4E**), which can explain the high elongation at break values. Meanwhile, delamination where layers separate from one another (**Figure 2.4F**, white arrows) and breakage of fiber-crystal bonds (**Figure 2.4F**) occurred during failure under tension.

We also tested how well our biomineralized BC composites could resist compression. When a 100-kN force was applied to compress the biomineralized BC composites (Ca^{2+}: Mg^{2+} 1: 4), the specimen became denser, with a reduction in thickness from 10 mm to 3.7 mm after compression (**Figure S2.7A, B**). Compression tests showed that our biomineralized BC composites were extremely compressible (**Figure S2.7**), not breaking even under a compression force as high as 100 kN. To elucidate the origin of such high compressibility, the surface (**Figure S2.7C**) and cross-section morphology (**Figure S2.7D**) of the compressed

specimens (Ca^{2+}: Mg^{2+} 1: 4) were imaged. A high density of microcracks (**Figure S2.7C**) was observed on the surface of the compressed specimens, while the layered cross-section morphology (**Figure S2.7D**) remained intact. These microcracks might allow the material to absorb the energy from the applied compression force, resulting in the compressible nature of the biomineralized BC composites, which may protect against extreme compression forces.

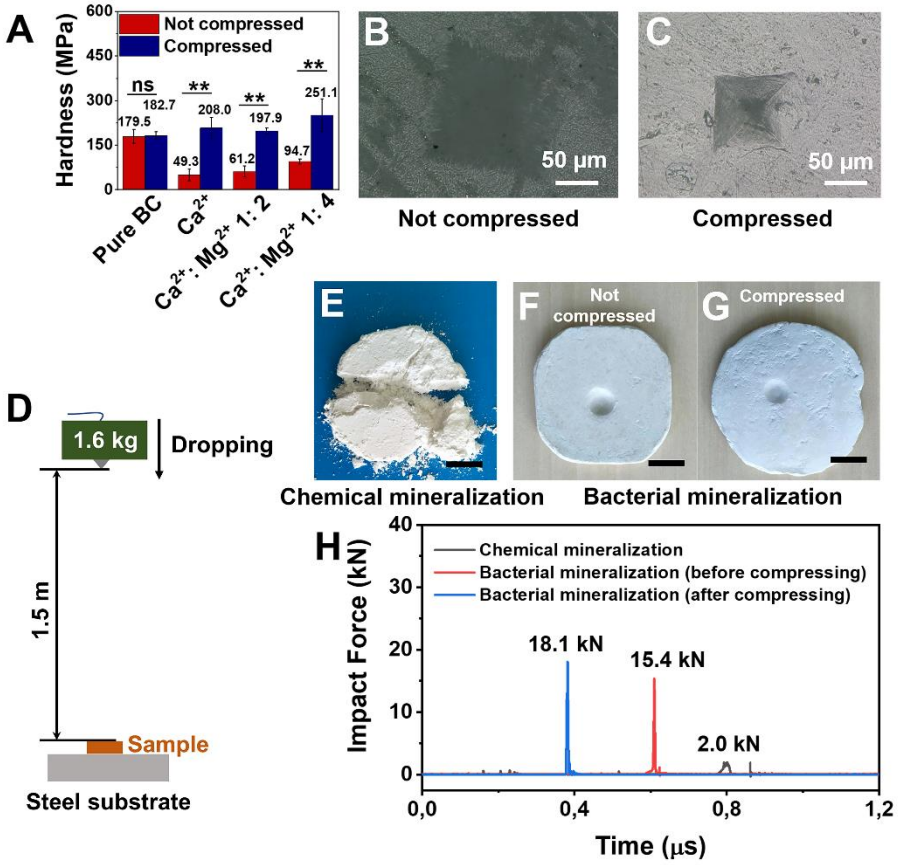

Figure 2.5 Hardness and impact resistance tests of the biomineralized BC composites. (A) Hardness values for pure BC and biomineralized BC composites before and after compression. (B, C) Optical microscope images of the biomineralized BC composite after hardness testing (Ca^{2+}: Mg^{2+} 1: 4) (B) without and (C) with compression. All the samples in this figure were made with PGA. ** $p < 0.01$, significant; ns, not significant. Error bars represent standard deviations. (D) The impact dropping tower and (E-G) the samples after impact resistance testing. The sample thickness in E-G is 8 mm. Scale bar = 2 cm. (H) The corresponding force-time curves during the impact resistance testing.

Since our material was highly compressible, we considered using compression as an additional (optional) processing step in the material fabrication. To test the influence of compression on the mechanical properties of the materials, tensile tests were carried out on the materials after being compressed with 100 kN of force (**Figure S2.8**). The compressed specimens showed an increase in ultimate tensile strength and a decrease in elongation at break compared with the non-compressed specimens (**Table S2.1**). The decrease in elongation at break could be due to the reduced surface roughness from the compression procedure (**Figure S2.7C**). However, compared to pure BC (elongation at break: 6.7 ± 1.3 %, **Table S2.1**), the compressed biomineralized BC composites still showed relatively high values for elongation at break (over 45 %), which might be attributable to the intact layered structure.

The hardness (**Figure 2.5A**) and toughness of the materials were assessed before and after compression. In nonmineralized BC samples, the hardness values of the pure air-dried BC film remained similar before (179.5 ± 23.1 MPa) and after (182.7 ± 13.0 MPa) compressing. The biomineralized composite samples had hardness values up to more than three times lower than that of pure BC, with 49.3 ± 19.7 MPa (only Ca^{2+}), 61.2 ± 18.7 MPa (Ca^{2+}: Mg^{2+} 1: 2), and 94.7 ± 9.1 MPa (Ca^{2+}: Mg^{2+} 1: 4). Nevertheless, after being pressed with a 100 kN compression force, the hardness values increased significantly ($p < 0.01$) to 208.0 ± 36.2 MPa (only Ca^{2+}), 197.9 ± 9.1 MPa (Ca^{2+}: Mg^{2+} 1: 2), and 251.1 ± 55.2 MPa (Ca^{2+}: Mg^{2+} 1: 4) and became even higher than that of pure BC (182.7 ± 13.0 MPa). Optical microscope images of the biomineralized composites (Ca^{2+}: Mg^{2+} 1: 4) after hardness testing (**Figure 2.5B**, **C**) showed that the indentation diameter for the compressed sample was smaller than the noncompressed specimen, consistent with an increase in hardness after compression.[44] This increase in hardness values indicates that we can tune the hardness of biomineralized BC by compression. Notably, the compressed samples retained almost the same toughness values (**Table S2.1**) compared with their non-compressed counterparts (**Figure S2.8**, **Table S2.1**).

To evaluate the impact resistance of the biomineralized BC composites, we used a dropping tower (**Figure 2.5D**). A mass of 1.6 kg was lifted to 1.5 m and released to hit the tested material with a speed of 5.0 m s^{-1} upon contacting the material. To test whether the specific mineralization method had an influence on the composite toughness, a control sample containing the same BC and Ca^{2+} concentration in the mineralization medium (10 mM Ca^{2+}), was prepared by traditional chemical mineralization in which $CaCl_2$ was reacted with Na_2CO_3 in a BC[23] slurry while stirring. Impact resistance testing of this sample resulted

in a sharp, brittle disintegration (**Figure 2.5E**); while the biomineralized BC composite (Ca^{2+}: Mg^{2+} 1: 4) with the same thickness (8 mm-thick) was not broken (**Figure 2.5F**), showing that the biomineralized BC composite exhibited higher impact-resistance than the chemically-mineralized sample. The biomineralized BC composite (Ca^{2+}: Mg^{2+} 1: 4) after compression was also tested by the impact resistance experiment (**Figure 2.5G**) and showed no observable breakage, also demonstrating higher impact resistance than the chemically-mineralized sample. The force-time curves (**Figure 2.5H**) from the impact resistance testing indicated that both the noncompressed and compressed biomineralized BC composites (Ca^{2+}: Mg^{2+} 1: 4) showed high peak impact resistance force values (18.1 kN, 15.4 kN), which is 7-9 times higher than the chemically-mineralized sample (2 kN). The higher impact resistance of biomineralized BC can be attributed to its higher toughness (**Table S1**).

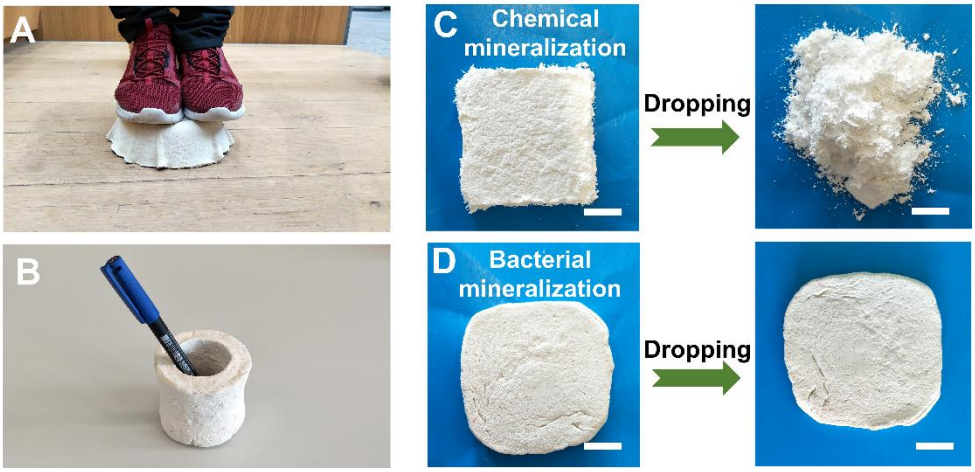

Figure 2.6 Examples for the applications of the biomineralized BC composites. Biomineralized BC composites (Ca^{2+}: Mg^{2+} = 1: 4) molded into (A) a stool shape, and (B) a cup. Composites produced with the (C) chemical method and (D) bacterial biomineralization method before (left) and after (right) dropping from a 10 m height three consecutive times. All the samples in this figure were made with PGA. Scale bars correspond to 2 cm.

Since the bacterial biomineralized BC slurry was easily molded into different complex shapes and thicknesses (**Figures 2.3B**, **2.6A**, **B**) by simply fitting the slurry into a mold shape, we fabricated a stool and a cup. Such molded composite materials could withstand, as an example, a 70 kg person standing on it (hollow stool, **Figure 2.6A**), or be dropped from over 10 m height multiple times without any visible breakage (solid shape of 8 mm thickness, **Figure 2.6D**).

However, the chemically–mineralized sample disintegrated into pieces after dropping three times from a height of 10 m (**Figure 2.6C**). The chemically-mineralized BC composites could be broken easily by hand, vulnerable to far weaker forces than the large forces during impact tests. To assess the cause of this reduced impact resistance, we compared the structure of the biologically-mineralized and the chemically-mineralized samples. Two chemical mineralization methods were used here, either based on the reaction of $CaCl_2$ with Na_2CO_3[23] (as for previous samples) or using gas diffusion.[47] Surprisingly, these two chemical approaches to form mineralized BC composites did not produce materials that demonstrate a layered structure (**Figure S2.9A, B**). The SEM images showed aggregated BC phases (**Figure S2.9A**, white arrows), separated by large clusters of $CaCO_3$, in contrast to the finely-layered structure obtained *via* bacterial biomineralization (**Figure 2.2**), confirming the importance of the layers to obtain favorable mechanical properties, as also shown for nacre[45] and nacre mimicking composites.[18] In biomineralized BC, the BC fibers were found to connect in between the layers to form fiber bridges (**Figure S2.2**) and to physically wrap around $CaCO_3$ crystals (**Figure S2.5**). These crystal-fiber entanglements might be the cause of the vastly different self-assembly behavior observed between the chemical and bacterial mineralization approaches.

To assess the fire resistance properties of the biomineralized BC composites, specimens were exposed to the outer cone of the flame of a Bunsen burner. A pure organic filtrated BC sample, fabricated following the same procedure as biomineralized BC, without the addition of *S. pasteurii* bacteria, was used as a control. This control sample caught on fire immediately upon contact with the flame (**Figure S2.10A**) while the biomineralized BC resisted fire when exposed to a flame for 1 min (**Figure S2.10B**).

Since our biomineralized BC composite could be remolded into new shapes, we also tested the mechanical properties (**Figure S2.11**, **Table S2.1**) of the remolded samples (Ca^{2+}: Mg^{2+} = 1: 4). The tensile strength and toughness values of the remolded biomineralized BC composites did not significantly differ in comparison with their original counterparts.

Table 2.1 Comparison of the mechanical properties of the biomineralized BC composites with literature.

Samples	Tensile Strength [MPa]	Elongation at Break [%]	Toughness [MJ m^{-3}]	Hardness [MPa]	References
Pure BC	148.1 ± 13.4	4.5 ± 0.1	4.9 ± 0.8	–	14
Natural nacre	60-70	< 1	0.2-2	950	45, 46
Biomineralized BC	–	–	–	370	24
Cellulose nanofiber nacre	60-133	1-6	0.5-3	200-500	47
Gelatin-$CaCO_3$ nacre	30-97	3.1-12.5	–	–	22
Matrix-directed mineralized nacre	16-20	0.09-0.12	–	1650	18
Biomineralized cross-lamella nacre	43.6 ± 4.5	< 1	0.3 ± 0.7	–	48
Acrylonitrile butadiene styrene (ABS) plastic	30-43	10-50	0.14-2.73	835	49-51
Ca^{2+}: Mg^{2+} 1: 4 and PGA	47.2 ± 5.2	79.1 ± 2.8	21.8 ± 0.7	94.7 ± 9.1	This work
Ca^{2+}: Mg^{2+} 1: 4 and PGA - compressed	50.6 ± 1.9	54.0 ± 11.1	21.3 ± 4.2	251.1 ± 55.2	This work

2.3 Conclusions

We produce impact resistant biomineralized BC composites with high and tunable toughness and stiffness via a combination of an environmentally-friendly bacterial biomineralization procedure and an evaporation-induced self-assembly process. Our layered bacterially produced composites show a toughness (21.8 ± 0.7 MJ m^{-3}) over five folds higher than that of BC (4.0 ± 0.2 MJ m^{-3}). The mechanical properties of this material are tunable by adjusting the biomineralization components and post processing method, where toughness values could be improved from 7.7 ± 0.3 MJ m^{-3} to 21.8 ± 0.7 MJ m^{-3} by adding Mg^{2+} and hardness values could be improved from 94.7 ± 9.1 MPa to 251.1 ± 55.2 MPa by compressing.

The most commonly used method to fabricate layered structures containing $CaCO_3$ is layer-by-layer mineralization.[17, 20, 21] However, such methods are time-consuming and labor-intensive, and are challenging to apply for large-scale material production. A previous approach applying direct mineralization of a bulk substrate requires multiple mineralization cycles,[24] and only a limited mineral content is achievable, with most of the crystals only attached onto the surface of the substrate. To overcome this challenge, an external force has

been previously utilized to push the mineralization solution into a pre-designed matrix,[18] to reach a mineral content similar to natural nacre. While this material possesses excellent toughness, such a fabrication approach is technically difficult and produces lower tensile strength (38 MPa) and elongation at break (0.13 %) compared to the material produced here. More recently, a $CaCO_3$-based mineralized synthetic nacre was prepared with a gas diffusion method,[48] creating in a mineral-interlocking microstructure to improve the mechanical properties. This material has a tensile strength (43.6 MPa) close to that of our material (50.6 MPa), but a significantly smaller elongation at break (0.9 % *vs* 54.0 %). Overall, our biomineralized BC composites show competitive strength and toughness values compared to most of the biomineralized synthetic nacre as well as to other natural or synthetic tough materials, including commercial ABS plastic (**Table 2.1**).

In addition to producing excellent mechanical properties, our fabrication procedure is based on easy processing under mild conditions compared to other impact-resistant materials, the fabrication of which is typically technically difficult[52] or energy-consuming,[14] with limited shape control of the resultant materials. As the biomineralization process could be completed within 12 hours and the biomineralized BC slurry could self-assemble into a multi-layered structure by simply drying in the air, the whole fabrication procedure of our biomineralized BC composites is much faster compared to the month-long continual work of a layer-by-layer mineralization method[17] and the years-long biomineralization processes of natural nacre in nature.[45] Here, the fabrication procedure is fast, ecologically-friendly and readily scalable. Notably, this material could be recycled with a simple kitchen blender and a sieve, which is promising and convenient for daily life applications. Due to these features, this fully biodegradable, highly tough material shows multiple promising applications in daily human life, including production of furniture, cellphone holders, helmets, and protective garments.

2.4 References

1. Mohanty, A. K.; Vivekanandhan, S.; Pin, J.-M.; Misra, M. Composites from Renewable and Sustainable Resources: Challenges and Innovations. Science 2018, *362*, 536–542.

2. Zhang, F.; Lan, X.; Peng, H.; Hu, X.; Zhao, Q. A “Trojan Horse” Camouflage Strategy for High‐Performance Cellulose Paper and Separators. Adv. Funct. Mater. 2020, 2002169.

3. Zhu, Y.; Romain, C.; Williams, C. K. Sustainable Polymers from Renewable Resources. Nature 2016, *540* (7633), 354-362.

4. Wegst, U. G. K.; Bai, H.; Saiz, E.; Tomsia, A. P.; Ritchie, R. O. Bioinspired Structural Materials. Nat. Mater. 2015, *14* (1), 23-36.

5. Tu, H.; Zhu, M.; Duan, B.; Zhang, L. Recent Progress in High-Strength and Robust Regenerated Cellulose Materials. Adv. Mater. 2020, 2000682.

6. Khakalo, A.; Tanaka, A.; Korpela, A.; Orelma, H. Delignification and Ionic Liquid Treatment of Wood toward Multifunctional High-Performance Structural Materials. ACS Appl. Mater. Interfaces 2020, *12* (20), 23532-23542.

7. Ma, L.; Bi, Z.; Xue, Y.; Zhang, W.; Huang, Q.; Zhang, L.; Huang, Y. Bacterial Cellulose: An Encouraging Eco-Friendly Nano-Candidate for Energy Storage and Energy Conversion. J. Mater. Chem. A 2020, *8* (12), 5812-5842.

8. Gao, M.; Li, J.; Bao, Z.; Hu, M.; Nian, R.; Feng, D.; An, D.; Li, X.; Xian, M.; Zhang, H. A Natural In Situ Fabrication Method of Functional Bacterial Cellulose Using a Microorganism. Nat. Commun. 2019, *10* (1), 437.

9. Guan, Q.-F.; Yang, H.-B.; Han, Z.-M.; Zhou, L.-C.; Zhu, Y.-B.; Ling, Z.-C.; Jiang, H.-B.; Wang, P.-F.; Ma, T.; Wu, H.-A.; Yu, S.-H. Lightweight, Tough, and Sustainable Cellulose Nanofiber-Derived Bulk Structural Materials with Low Thermal Expansion Coefficient. Sci. Adv. 2020, *6*, eaaz1114.

10. Ritchie, R. O. The Conflicts between Strength and Toughness. Nat. Mater. 2011, *10* (11), 817-822.

11. Wang, S.; Jiang, F.; Xu, X.; Kuang, Y.; Fu, K.; Hitz, E.; Hu, L. Super-Strong, Super-Stiff Macrofibers with Aligned, Long Bacterial Cellulose Nanofibers. Adv. Mater. 2017, *29* (35), 1702498.

12. Yao, J.; Chen, S.; Chen, Y.; Wang, B.; Pei, Q.; Wang, H. Macrofibers with High Mechanical Performance Based on Aligned Bacterial Cellulose Nanofibers. ACS Appl. Mater. Interfaces 2017, *9* (24), 20330-20339.

13. Gao, H.-L.; Zhao, R.; Cui, C.; Zhu, Y.-B.; Chen, S.-M.; Pan, Z.; Meng, Y.-F.; Wen, S.-M.; Liu, C.; Wu, H.-A.; Yu, S.-H. Bioinspired Hierarchical Helical Nanocomposite Macrofibers Based on Bacterial Cellulose Nanofibers. Natl. Sci. Rev. 2020, *7* (1), 73-83.

14. Wu, Z.; Chen, S.; Wu, R.; Sheng, N.; Zhang, M.; Ji, P.; Wang, H. Top-down Peeling Bacterial Cellulose to High Strength Ultrathin Films and Multifunctional Fibers. Chem. Eng. J. 2020, *391*, 123527.

15. Rahman, M. M.; Netravali, A. N. Aligned Bacterial Cellulose Arrays as “Green” Nanofibers for Composite Materials. ACS Macro Lett. 2016, *5* (9), 1070-1074.

16. Wang, S.; Li, T.; Chen, C.; Kong, W.; Zhu, S.; Dai, J.; Diaz, A. J.; Hitz, E.; Solares, S. D.; Li, T.; Hu, L. Transparent, Anisotropic Biofilm with Aligned Bacterial Cellulose Nanofibers. Adv. Funct. Mater. 2018, *28* (24), 1707491.

17. Spiesz, E. M.; Schmieden, D. T.; Grande, A. M.; Liang, K.; Schwiedrzik, J.; Natalio, F.; Michler, J.; Garcia, S. J.; Aubin-Tam, M.-E.; Meyer, A. S. Bacterially Produced, Nacre-Inspired Composite Materials. Small 2019, *15* (22), 1805312.

18. Mao, L.-B.; Gao, H.-L.; Yao, H.-B.; Liu, L.; Colfen, H.; Liu, G.; Chen, S.-M.; Li, S.-K.; Yan, Y.-X.; Liu, Y.-Y.; Yu, S.-H. Synthetic Nacre by Predesigned Matrix-Directed Mineralization. Science 2016, *354* (6308), 107-110.

19. Chen, Y.; Fu, J.; Dang, B.; Sun, Q.; Li, H.; Zhai, T. Artificial Wooden Nacre: A High Specific Strength Engineering Material. ACS Nano 2020, *14* (2), 2036-2043.

20. Farhadi-Khouzani, M.; Schütz, C.; Durak, G. M.; Fornell, J.; Sort, J.; Salazar-Alvarez, G.; Bergström, L.; Gebauer, D. A $CaCO_3$/Nanocellulose-Based Bioinspired Nacre-Like Material. J. Mater. Chem. A 2017, *5* (31), 16128-16133.

21. Finnemore, A.; Cunha, P.; Shean, T.; Vignolini, S.; Guldin, S.; Oyen, M.; Steiner, U. Biomimetic Layer-by-Layer Assembly of Artificial Nacre. Nat. Commun. 2012, *3*, 966.

22. Li, X. Q.; Zeng, H. C. Calcium Carbonate Nanotablets: Bridging Artificial to Natural Nacre. Adv. Mater. 2012, *24* (47), 6277-6282.

23. Liu, X.; Zhou, Y.; Pei, C. Mimetic Biomineralization Matrix Using Bacterial Cellulose Hydrogel and Egg White to Prepare Various Morphologies of $CaCO_3$. CrystEngComm 2018, *20* (32), 4536-4540.

24. Cheng, Z.; Ye, Z.; Natan, A.; Ma, Y.; Li, H.; Chen, Y.; Wan, L.; Aparicio, C.; Zhu, H. Bone-Inspired Mineralization with Highly Aligned Cellulose Nanofibers as Template. ACS Appl. Mater. Interfaces 2019, *11* (45), 42486-42495.

25. Phillips, A. J.; Gerlach, R.; Lauchnor, E.; Mitchell, A. C.; Cunningham, A. B.; Spangler, L. Engineered Applications of Ureolytic Biomineralization: A Review. Biofouling 2013, *29* (6), 715-733.

26. Heveran, C. M.; Williams, S. L.; Qiu, J.; Artier, J.; Hubler, M. H.; Cook, S. M.; Cameron, J. C.; Srubar, W. V. Biomineralization and Successive Regeneration of Engineered Living Building Materials. Matter 2020, *2* (2), 481-494.

27. Heveran, C. M.; Liang, L.; Nagarajan, A.; Hubler, M. H.; Gill, R.; Cameron, J. C.; Cook, S. M.; Srubar, W. V. Engineered Ureolytic Microorganisms Can Tailor the Morphology and Nanomechanical Properties of Microbial-Precipitated Calcium Carbonate. Sci. Rep. 2019, *9* (1), 14721.

28. Yu, Y.; Yan, F.; Chen, Y.; Jin, C.; Guo, J. H.; Chai, Y. Poly-gamma-Glutamic Acids Contribute to Biofilm Formation and Plant Root Colonization in Selected Environmental Isolates of Bacillus subtilis. Front. Microbiol. 2016, *7*, 1811.

29. Qin, W.; Wang, C. Y.; Ma, Y. X.; Shen, M. J.; Li, J.; Jiao, K.; Tay, F. R.; Niu, L. N. Microbe-Mediated Extracellular and Intracellular Mineralization: Environmental, Industrial, and Biotechnological Applications. Adv. Mater. 2020, *32* (22), 1907833.

30. Ghosh, T.; Bhaduri, S.; Montemagno, C.; Kumar, A. *Sporosarcina pasteurii* can Form Nanoscale Calcium Carbonate Crystals on Cell Surface. PLoS One 2019, *14* (1), 0210339.

31. Florea, M.; Reeve, B.; Abbott, J.; Freemont, P. S.; Ellis, T. Genome Sequence and Plasmid Transformation of the Model High-Yield Bacterial Cellulose Producer *Gluconacetobacter hansenii* ATCC 53582. Sci. Rep. 2016, *6*, 23635.

32. Li, Q.; Gao, R.; Wang, L.; Xu, M.; Yuan, Y.; Ma, L.; Wan, Z.; Yang, X. Nanocomposites of Bacterial Cellulose Nanofibrils and Zein Nanoparticles for Food Packaging. ACS Appl. Nano Mater. 2020, *3* (3), 2899-2910.

33. Santmarti, A.; Zhang, H.; Lappalainen, T.; Lee, K.-Y. Cellulose Nanocomposites Reinforced with Bacterial Cellulose Sheets Prepared from Pristine and Disintegrated Pellicle. Compos., Part A 2020, *130*, 105766.

34. Ghayoor, H.; Hoa, S. V.; Marsden, C. C. A Micromechanical Study of Stress Concentrations in Composites. Compos., Part B 2018, *132*, 115-124.

35. Mi, D.; Xia, C.; Jin, M.; Wang, F.; Shen, K.; Zhang, J. Quantification of the Effect of Shish-Kebab Structure on the Mechanical Properties of Polypropylene Samples by Controlling Shear Layer Thickness. Macromolecules 2016, *49* (12), 4571-4578.

36. Tom, S.; Jin, H. E.; Heo, K.; Lee, S. W. Engineered Phage Films as Scaffolds for $CaCO_3$ Biomineralization. Nanoscale 2016, *8* (34), 15696-15701.

37. Llauro, M.-F.; Loiseau, J.; Boisson, F.; Delolme, F.; Ladavière, C.; Claverie, J. Unexpected End-Groups of Poly(Acrylic Acid) Prepared by RAFT Polymerization. J. Polym. Sci. Pol. Chem. 2004, *42* (21), 5439-5462.

38. Moradali, M. F.; Rehm, B. H. A. Bacterial Biopolymers: From Pathogenesis to Advanced Materials. Nat. Rev. Microbiol. 2020, *18* (4), 195-210.

39. Ogunleye, A.; Bhat, A.; Irorere, V. U.; Hill, D.; Williams, C.; Radecka, I. Poly-Gamma-Glutamic Acid: Production, Properties and Applications. Microbiology 2015, *161*, 1-17.

40. Arias, J. L.; Ferna´ndez, M. A. S. Polysaccharides and Proteoglycans in Calcium Carbonate-based Biomineralization. Chem. Rev. 2008, *108*, 4475–4482.

41. Davis, K. J.; Dove, P. M.; Yoreo, J. J. D. The Role of Mg^{2+} as an Impurity in Calcite Growth. Science 2000, *290* (5494), 1134-1137.

42. Tsortos, A.; Nancollas, G. H. The Role of Polycarboxylic Acids in Calcium Phosphate Mineralization. J. Colloid Interface Sci. 2002, *250* (1), 159-167.

43. Wegst, U. G. K.; Bai, H.; Saiz, E.; Tomsia, A. P.; Ritchie, R. O. Bioinspired Structural Materials. Nat. Mater. 2015, *14* (1), 23-36.

44. Shahdad, S. A.; McCabe, J. F.; Bull, S.; Rusby, S.; Wassell, R. W. Hardness Measured with Traditional Vickers and Martens Hardness Methods. Dent. Mater. 2007, *23* (9), 1079-1085.

45. Barthelat, F. Nacre from Mollusk Shells: A Model for High-Performance Structural Materials. Bioinspir. Biomim. 2010, *5* (3), 035001.

46. Kakisawa, H.; Sumitomo, T. The Toughening Mechanism of Nacre and Structural Materials Inspired by Nacre. Sci. Technol. Adv. Mater. 2011, *12* (6), 064710.

47. Yan, Y.-X.; Yao, H.-B.; Yu, S.-H. Nacre-Like Ternary Hybrid Films with Enhanced Mechanical Properties by Interlocked Nanofiber Design. Adv. Mater. Interfaces 2016, *3* (17), 1600296.

48. Raut, H. K.; Schwartzman, A. F.; Das, R.; Liu, F.; Wang, L.; Ross, C. A.; Fernandez, J. G. Tough and Strong: Cross-Lamella Design Imparts Multifunctionality to Biomimetic Nacre. ACS Nano 2020, *14* (8), 9771-9779.

49. Bai, X.; Isaac, D. H.; Smith, K. Reprocessing Acrylonitrile–butadiene–styrene Pastics: Structure–property Relationships. Polym. Eng. Sci. 2007, *47* (2), 120-130.

50. Mamaghani Shishavan, S.; Azdast, T.; Rash Ahmadi, S. Investigation of the Effect of Nanoclay and Processing Parameters on the Tensile Strength and Hardness of Injection Molded Acrylonitrile Butadiene Styrene–organoclay Nanocomposites. Mater. Des. 2014, *58*, 527-534.

51. Ching, E. C. Y.; Poon, W. K. Y.; Li, R. K. Y.; Mai, Y.-W. Effect of Strain Rate on the Fracture Toughness of Some Ductile Polymers Using the Essential Work of Fracture (EWF) Approach. Polym. Eng. Sci. 2000, *40* (12), 2558-2568.

52. Yin, Z.; Hannard, F.; Barthelat, F. Impact-Resistant Nacre-Like Transparent Materials. Science 2019, *364* (6447), 1260-1263.

2.5 Supplementary Information

Materials

D(+)-glucose monohydrate and di-sodium hydrogen phosphate (≥ 99.0%) were obtained from Carl Roth GmbH. All other chemicals were purchased from Sigma-Aldrich.

Preparation of BC slurry

For cellulose production, *Gluconacetobacter hansenii* (*G. hansenii* ATCC® 53582™) were grown statically at 30 °C in HS medium (5 g L^{-1} tryptone, 5 g L^{-1} yeast extract, 2.7 g L^{-1} disodium hydrogen phosphate, 1.5 g L^{-1} citric acid, and 20 g L^{-1} glucose). The BC pellicle formed at the air-liquid interface was harvested after 15 days of incubation and boiled on a heating plate at 100 °C with a 1 *w/v*% solution of sodium hydroxide for 10 min to kill the bacteria. The pellicle was then washed and immersed in distilled water several times to remove the impurities. The washing steps were repeated until the pellicles turned pure white. For the BC slurry preparation, 120 mL of water was mixed with 30 g wet BC pellicle, and the BC pellicle/water mixture was mechanically homogenized into a fibrous suspension with a kitchen blender for 5 min. The BC slurry was then autoclaved and stored at 4 °C.

Preparation of bacterial PGA

Bacterial PGA is produced based on the previously reported procedure.[1] Briefly, overnight cultures of *Bacillius licheniformis* (*B. licheniformis* NBRC12107, NBRC, Japan) grown in BL medium (10 g L^{-1} peptone, 2 g L^{-1} yeast extract and 1 g L^{-1} $MgSO_4 \cdot H_2O$) were added at 1.5 *v/v*% to autoclaved PGA production medium (20 g L^{-1} L-glutamic acid, 13.6 g L^{-1} sodium citrate monobasic, 80 g L^{-1} glycerol, 7 g L^{-1} NH_4Cl, 0.5 g L^{-1} KH_2PO_4, 0.244 g L^{-1} $MgSO_4$, 0.04 g L^{-1} $FeCl_3 \cdot 6H_2O$, 0.15 g L^{-1} $CaCl_2 \cdot 2H_2O$, 0.1 g L^{-1} $MnSO_4 \cdot H_2O$, pH was adjusted to 7.5 with NaOH) and incubated at 30 °C for 48 h at 180 rpm. After incubation, the viscous PGA solution was centrifuged at 8200 ×g for 15 min at 4 °C to remove the bacteria. The polymer solution was diluted with twice the volume of ethanol. The precipitated PGA polymer was then dried at 50 °C for 2 days.

Bacterially-induced biomineralization

Sporosarcina pasteurii bacteria (*S. pasteurii* DSM-33, ATCC 11859, DSMZ, Germany) were inoculated into 50 mL SP2 medium (20 g L^{-1} yeast extract, 10 g L^{-1} NH_4Cl, 10 μM $NiCl_2$, pH was adjusted to 8.5 with NaOH) and incubated for 48 h at 28 °C at 180 rpm. The bacterial solution was centrifuged at 1500 ×g for 15 min. The supernatant was removed, and the bacteria pellet was re-suspended with 25 mL of fresh SP2 medium and 25 mL of sterile 40 *w/v*% glycerol. The SP2 glycerol stocks were stored at -80 °C for use.

The slurry mixture for biomineralization consisted of 400 mL L^{-1} BC slurry (120 g wet BC hydrogel), 20 g L^{-1} urea, 10 g L^{-1} tryptone, 5 g L^{-1} yeast extract, 10 g L^{-1} NH_4Cl, 1 mL L^{-1} of SP2 glycerol stock, 1 g L^{-1} PGA and $CaCl_2{\cdot}2H_2O$/$MgCl_2{\cdot}6H_2O$ solution. The overall concentrations of Ca^{2+}/Mg^{2+} in the medium are listed here for each condition tested: 2.5 mM only Ca^{2+}: 2.5 mM $CaCl_2{\cdot}2H_2O$; 5.0 mM only Ca^{2+}: 5 mM $CaCl_2{\cdot}2H_2O$; 10.0 mM only Ca^{2+}: 10 mM $CaCl_2{\cdot}2H_2O$; 20.0 mM only Ca^{2+}: 20 mM $CaCl_2{\cdot}2H_2O$; 1: 2 Ca^{2+}: Mg^{2+}: 3.33 mM $CaCl_2{\cdot}2H_2O$ and 6.67 mM $MgCl_2{\cdot}6H_2O$; 1: 4 Ca^{2+}: Mg^{2+}: 2 mM $CaCl_2{\cdot}2H_2O$ and 8 mM $MgCl_2{\cdot}6H_2O$. The slurry containing bacteria was incubated statically at 28 °C for 12 h for biomineralization. There was no difference in pH change during $CaCO_3$ precipitation with and without addition of PGA, which was utilized to adjust the crystal morphology.

Self-assembly of bacterial composites

After biomineralization, the slurry was boiled during 10 min for sterilization, and the liquid medium was removed by filtering the slurry with a kitchen sieve and rinsing with distilled water. The condensed mud-like slurry was then molded into various shapes and sizes. Finally, the material was dried for 2 days to form the resulted composites.

For the control sample of pure filtrated BC, all the formulations and post treatment methods were similar to those for the biomineralized BC composites (10 mM Ca^{2+} concentration in the biomineralization medium) except that no *S. pasteurii* bacteria were added into the biomineralization medium.

For the control samples for weight-drop testing, a chemical mineralization method was used. Briefly, 10 mM of Na_2CO_3 was added into the 400 mL L^{-1} BC slurry (120 g wet BC hydrogel) with 10 mM $CaCl_2{\cdot}2H_2O$ and 1 g L^{-1} PGA solution while stirring. The resultant BC-$CaCO_3$ mixture was vacuum filtrated and dried in the fume hood for 2 days.

For the gas diffusion method,[2] 10 g BC bulk hydrogel or 10 g blended BC suspension was placed into a Petri dish and mixed with 20 mL 5M $CaCl_2{\cdot}2H_2O$, the mixture was then put into a sealed desiccator containing a beaker filled with 100 g $(NH_4)_2CO_3$ powder. The mineralization was carried out for 7 days.

Characterization

SEM:

The sample morphology was observed with a scanning electron microscope (SEM, JEOL JSM 6010 LA). Samples were sputter-coated with gold-palladium at 20 mA for 60 s. The imaging was carried out under SEI mode at 5-15 kV in vacuum. Crystal diameters and layer thickness values were measured with the Image J software from SEM images taken over 100 different regions within the samples.

Tensile testing:

The tensile properties were measured using a Zwick LF7M10 universal testing machine with a 10 kN load cell; the grip distance was 10 mm; and the samples were tested with a loading rate of 2 mm min^{-1}. At least three specimens per group were measured for the data presented. The toughness of the biomineralized BC composites was calculated according to the equation (2.1):

$$U = \int_0^{\varepsilon_f} \sigma \, d_\varepsilon \qquad (2.1)$$

where U is the energy per volume absorbed, σ is the stress, ε is the strain, and ε_f is the elongation at break.

Compression testing:

The compression testing was carried out using a Zwick LF7M19 universal testing machine with a 250 kN load cell. The samples were compressed to 80 % of their initial height and recovered until the compression force became zero. The samples were tested with a loading rate of 5 mm min^{-1}. At least three specimens per group were measured for the data presented.

Hardness testing:

Specimens for microindentation were embedded into an epoxy resin (Epofix Cold-Setting Embedding Resin, volume ratio of epoxy and hardener was 15:2) and polished with decreasing grades of polishing papers (SiC foils #1200, #2000 and #4000, Struers) to obtain a mirror surface. Vickers hardness measurements were performed under the test force 0.2 kgf (further denoted as HV0.2) using an Automatic MicroHardness Tester (Struers Dura Scan 70). The embedded samples were indented by a standard Vickers indenter (L 5 mm, Ø 6 mm), with at least 8 indents performed for each sample. An optical microscope (OM, VH-Z250R, KEYENCE, USA) was used to image the surface morphology after hardness measurements.

Impact resistance testing:

The samples were placed onto a flat stainless-steel table, then a dropping tower (1.6 kg) with a steel tip (tip diameter = 5 mm) was lifted to the maximum height (1.5 m) and released. The maximum speed was 5.0 m s^{-1}. At least three specimens were measured for each sample type.

Dropping experiment:

The materials were brought to a height of over 10 meters inside a building and dropped to the ground floor. Each sample was dropped three times. Samples were photographed before and after dropping.

TGA:

Thermal properties were measured using a thermogravimetry analysis machine (TGA, Mettler Toledo) at 30-1000 °C, with a heating rate of 10 °C min^{-1} in an air atmosphere. At

600 °C, the mass of pure BC reached 0 %, while the mass of $CaCO_3$ remained at 100 % of its initial value. Therefore, the $CaCO_3$ content in the final composite can be represented from the mass ratio values at 600 °C.

XRD:

X-ray diffraction (XRD) was carried out with a Bruker D8 Advance diffractometer Bragg-Brentano geometry and Lynxeye position sensitive detector, Cu K_α radiation. The parameters used here consist of divergence slit V12, scatter screen height 5 mm, 45 kV 40 mA, sample spinning, and detector settings: LL 0.11, W 0.14. Measurements were carried out with a coupled θ -2θ scan of 10° - 110°, step size of 0.021°, and a counting time of 1 s per step. Data evaluation was carried out with Bruker software DiffracSuite.EVA vs 4.3.

Fire-resistant testing:

The specimens were exposed to the outer cone flame of a Bunsen burner.

Statistical Analysis:

Statistical analysis was performed on https://astatsa.com/. The groups were compared with one-way (single factor) ANOVA with post-hoc Tukey's HSD (honest significant difference) tests. $p < 0.01$, significant.

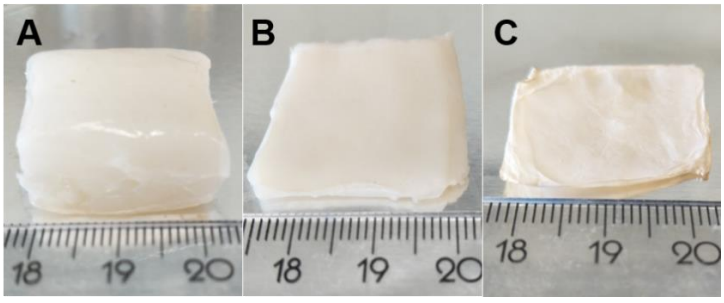

Figure S2.1 Optical images of wet BC hydrogel (A) before (thickness is 10 mm) and (B) after squeezing, and (C) after air-dried BC. BC loses over 99 % of its weight after drying in air and becomes a 2D film.

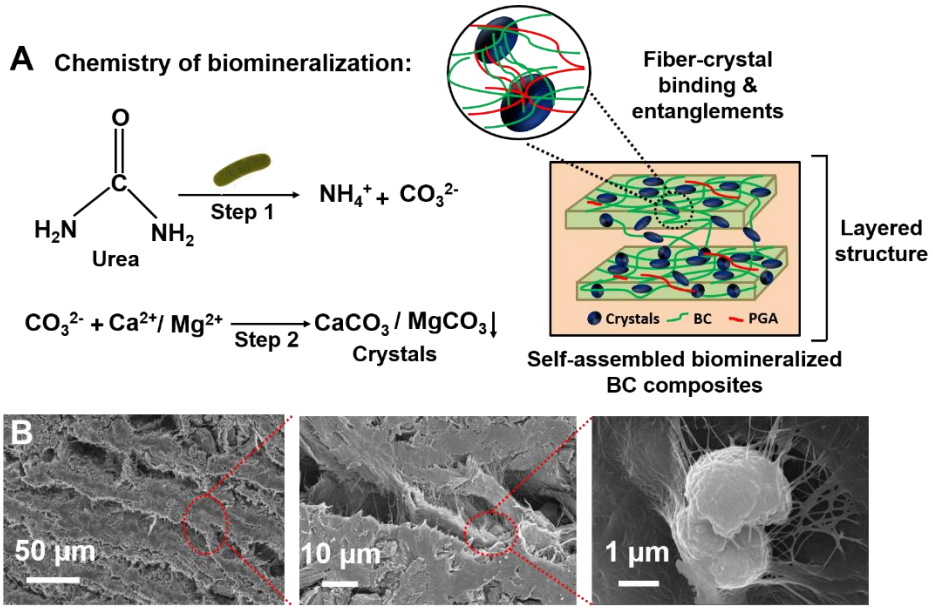

Figure S2.2 (A) Schematic of the bacterial biomineralization procedure, resulting in biomineralized cellulose composites with a layered structure. (B) SEM images of the cross-section of biomineralized BC composites (Ca^{2+}: Mg^{2+} 1: 4, with PGA) at differing magnifications, showing the layered structure (left), the cellulose interlayer connections (middle), and the entangled crystal-fiber morphology (right).

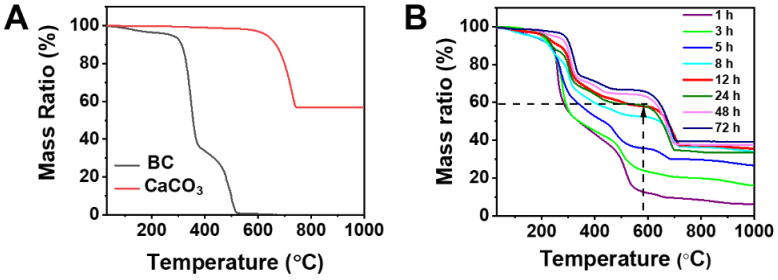

Figure S2.3 (A) TGA curves of pure BC and $CaCO_3$ crystals; (B) TGA curves of the biomineralized BC composites with 10 mM Ca^{2+} in the biomineralization medium, taken at different time points during mineralization. The dotted lines indicate the remaining mass ratio of crystals (60 % at 600 °C). An increasing $CaCO_3$ content was found for longer biomineralization durations, reaching 60 % after the first 12 hours and then increasing by less than 10 % between 12 hours and 72 hours of biomineralization. Therefore, a relatively high degree of biomineralization can be achieved within 12 hours.

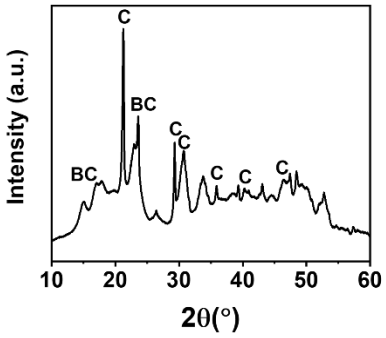

Figure S2.4 XRD spectra of the biomineralized BC composite (Ca: Mg 1:4 with PGA). The $CaCO_3$ crystals in the final composite show a calcite (C) morphology.

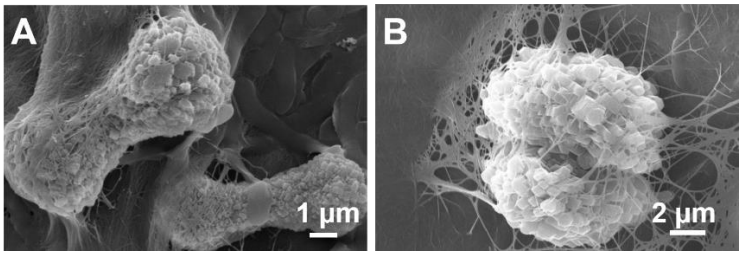

Figure S2.5 SEM images of the cross-section of the crystal-fiber binding morphology in the final materials. Both A and B are images of biomineralized BC produced with a Ca^{2+}: Mg^{2+} ratio of 1: 4 and PGA.

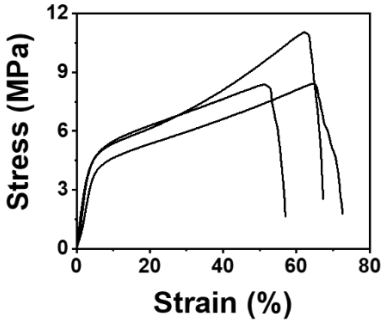

Figure S2.6 Tensile stress-strain curves of biomineralized BC composites produced with 10 mM Ca^{2+} in the biomineralization medium and without PGA.

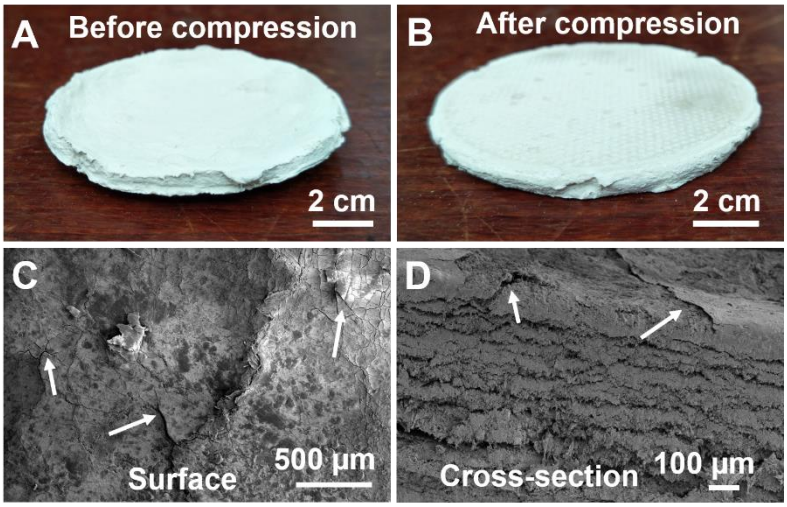

Figure S2.7 The biomineralized BC composite (Ca^{2+}: Mg^{2+} 1: 4) (A) before and (B) after compressing. The compression force applied to the sample surface was 100 kN. SEM images of the (C) surface and (D) cross-section of biomineralized BC (Ca^{2+}: Mg^{2+} 1: 4) after compression. Microcracks (white arrows) were observed on the specimens' surface (C), while the layered structure (D) was still present after compression.

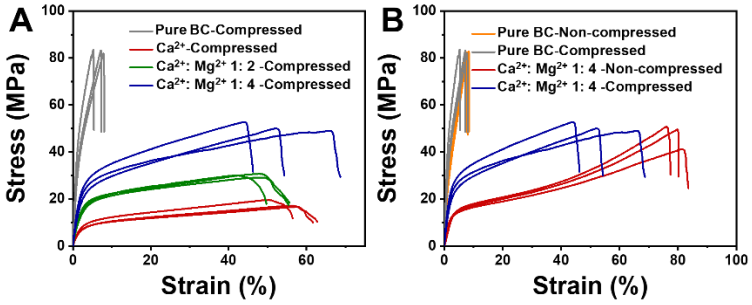

Figure S2.8 (A) Tensile stress-strain curves of the compressed pure BC and biomineralized BC composites. (B) Comparison of the tensile stress-strain curves for compressed and non-compressed pure BC and biomineralized BC composite (Ca^{2+}: Mg^{2+} 1: 4).

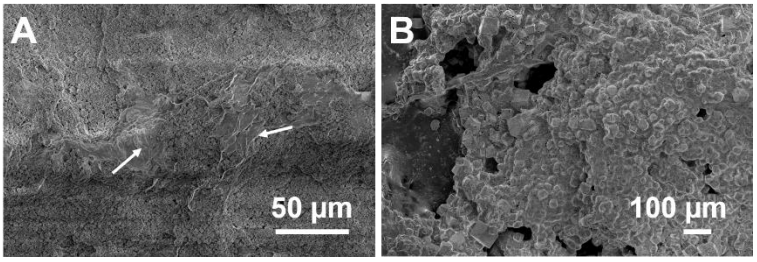

Figure S2.9 SEM images of the mineralized BC produced *via* (A) a chemical reaction by reacting $CaCl_2$ with Na_2CO_3, or *via* (B) a gas diffusion method. Both of these two methods did not produce a homogeneous interconnection between BC and the inorganic crystals. The BC fibers tended to aggregate together (Figure A, white arrows), while the inorganic crystals were not produced within the organized BC networks.

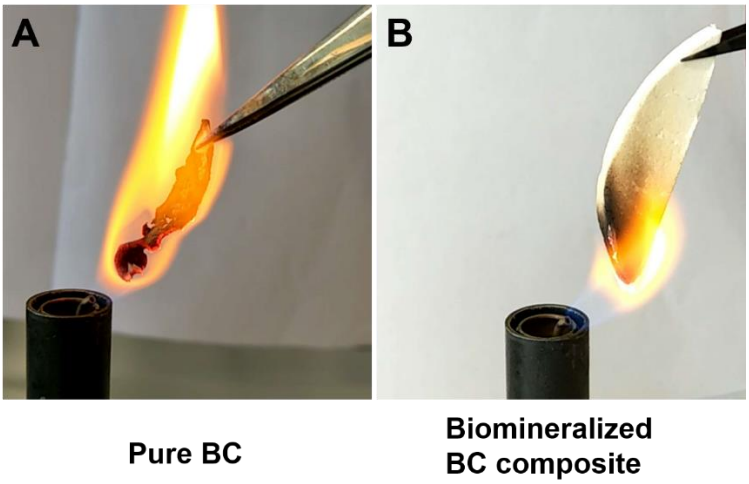

Figure S2.10 Optical images of (A) pure BC exposed to a flame for 1 second and (B) biomineralized BC composite (Ca^{2+}: Mg^{2+} 1: 4) exposed to a flame for 1 minute. Due to the high inorganic crystal content, the biomineralized BC composite showed fire retardant abilities throughout 1 minute of direct exposure to the flame (B), while pure BC ignited immediately upon contact with the flame (A).

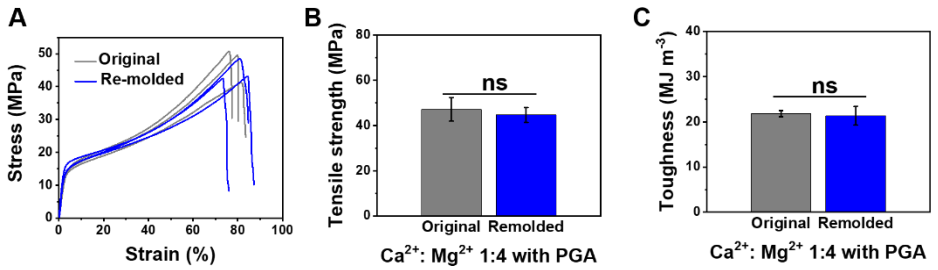

Figure S2.11 The tensile properties (A-C) of the original and the re-molded biomineralized BC composites (Ca: Mg 1:4 with PGA). The tensile strength and toughness values of the re-molded biomineralized BC composites remain unchanged compared to their original counterparts. ns, not significant.

Table S2.1 Mechanical properties of the biomineralized BC composites.

Samples	Tensile Strength [MPa]	Elongation at Break [%]	Toughness [MJ m^{-3}]	Hardness [MPa]
Pure BC and PGA	82.4 ± 0.6	8.0 ± 0.4	4.0 ± 0.2	179.5 ± 23.1
Ca^{2+} (without PGA)	9.3 ± 1.5	59.4 ± 7.2	3.9 ± 0.6	Not measured
Ca^{2+} and PGA	15.5 ± 0.4	73.0 ± 1.1	7.7 ± 0.3	49.3 ± 19.7
Ca^{2+}: Mg^{2+} 1: 2 and PGA	24.3 ± 1.0	95.7 ± 4.7	15.8 ± 0.8	61.2 ± 18.7
Ca^{2+}: Mg^{2+} 1: 4 and PGA	47.2 ± 5.2	79.1 ± 2.8	21.8 ± 0.7	94.7 ± 9.1
Pure BC and PGA -compressed	82.9 ± 0.8	6.7 ± 1.3	3.7 ± 0.6	182.7 ± 13.0
Ca^{2+} and PGA -compressed	17.8 ± 1.6	54.7 ± 3.9	7.4 ± 0.1	208.0 ± 36.2
Ca^{2+}: Mg^{2+} 1: 2 and PGA -compressed	30.0 ± 0.8	45.6 ± 3.4	11.6 ± 0.6	197.9 ± 9.1
Ca^{2+}: Mg^{2+} 1: 4 and PGA -compressed	50.6 ± 1.9	54.0 ± 11.1	21.3 ± 4.2	251.1 ± 55.2
Ca^{2+}: Mg^{2+} 1: 4 and PGA-remolded	44.7 ± 3.3	79.6 ± 5.6	21.4 ± 2.1	Not measured

References:

1. Yu, K.; Aubin-Tam, M.-E. Bacterially Grown Cellulose/Graphene Oxide Composites Infused with γ-Poly (Glutamic Acid) as Biodegradable Structural Materials with Enhanced Toughness. ACS Appl. Nano Mater. 2020, *3* (12), 12055-12063.

2. Xu, A. W.; Antonietti, M.; Cölfen, H.; Fang, Y. P. Uniform Hexagonal Plates of Vaterite $CaCO_3$ Mesocrystals Formed by Biomimetic Mineralization. Adv. Funct. Mater. 2006, *16* (7), 903-908.

3

Spiral Honeycomb Microstructured Bacterial Cellulose for Increased Strength and Toughness

Abstract: Natural materials, such as nacre and silk, exhibit both high strength and toughness due to their hierarchical structures highly organized at the nano-, micro-, and macroscales. Bacterial cellulose (BC) presents a hierarchical fibril structure at the nanoscale. At the microscale, however, BC nanofibers are distributed randomly. Here, BC self-assembles into a highly organized spiral honeycomb microstructure giving rise to high tensile strength (315 MPa) and a high toughness value (17.8 MJ m^{-3}), with pull-out and de-spiral morphologies observed during failure. Both experiments and finite element simulations indicate improved mechanical properties resulting from the honeycomb structure. The mild fabrication process consists of an *in-situ* fermentation step utilizing poly (vinyl alcohol), followed by a post-treatment including freezing-thawing and boiling. This simple self-assembly production process is scalable, does not require toxic chemicals, and enables the fabrication of light, strong, and tough hierarchical composites with tunable shape and size.

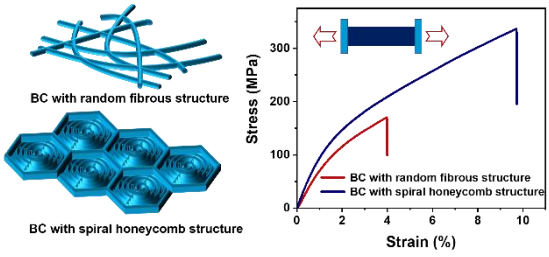

The content of this chapter is based on:
Kui Yu, Srikkanth Balasubramanian, Helda Pahlavani, Mohammad J. Mirzaali, Amir A. Zadpoor and Marie-Eve Aubin-Tam, *ACS Applied Materials& Interfaces*, 2020, 12 (45), 50748-50755.

3.1 Introduction

High-performance materials that combine lightweight, high strength, and high toughness are highly demanded in the aerospace, biomedical, and construction industries. However, strength and toughness are generally considered mutually exclusive properties in man-made materials.[1] In biological systems on the other hand, there are multiple examples of strong and tough materials (*e.g.*, spider silk,[2] nacre,[3] bone,[4] and wood[5]). This is achieved *via* their hierarchical structure, which is highly ordered from the molecular and microscale up to the macroscale.[6] The construction of highly organized hierarchical structures is key to produce high-performance structural materials.[7, 8]

To achieve such hierarchical structures, different types of materials could be used, including organic materials (*e.g.*, polymers,[9] carbon-based[10]), inorganic materials (*e.g.*, calcium carbonate[11]), or a combination of both.[12] Among those materials, natural biopolymers are drawing increasing attention due to their bioinspired nature, current environmental concerns, and the need for sustainable materials.[9] Cellulose is a particularly interesting example of such green biopolymers. As the most abundant biopolymer in nature, cellulose, in the form of nanofibers, widely exists in most plants and wood structures,[13] as well as in the biofilms surrounding some microorganisms (*e.g.* in *Gluconacetobacter hansenii*).[14] Cellulose nanofibers themselves consist of a hierarchical fibril structure originating from the strong intramolecular and intermolecular hydrogen bonding, resulting in high tensile strength and elastic modulus.[13] Therefore, cellulose nanofibers are ideal building blocks for constructing high-performance materials with organized mesoscale structures.[15] In particular, bacterial cellulose (BC) is secreted in large quantities by bacteria in the form of a hydrogel-like biofilm.[16] This biofilm consists of randomly distributed single BC nanofibers,[17] which possess the same organized fibril structure as plant cellulose,[18] exhibiting high crystallinity and good mechanical performance.[19] To obtain BC nanofibers, the most frequently used method is to mechanically disintegrate the wet BC hydrogel pellicles.[20] These BC nanofibers are then recombined together using techniques, such as wet spinning[20] or 3D printing.[21] These *ex situ* methods, however, destroy the naturally layered BC structure and weaken its mechanical performance significantly.[22] To increase the tensile strength and toughness of BC, an organized BC microstructure is desired.[23] Several methods, including wet stretching,[23] twisting and tape peeling,[24] can produce an aligned BC microstructure based on the natural BC network. These methods could demonstrate that

aligning BC at the microscale enhances the mechanical performance significantly, but they are usually highly energy-intensive and show limited scalability.

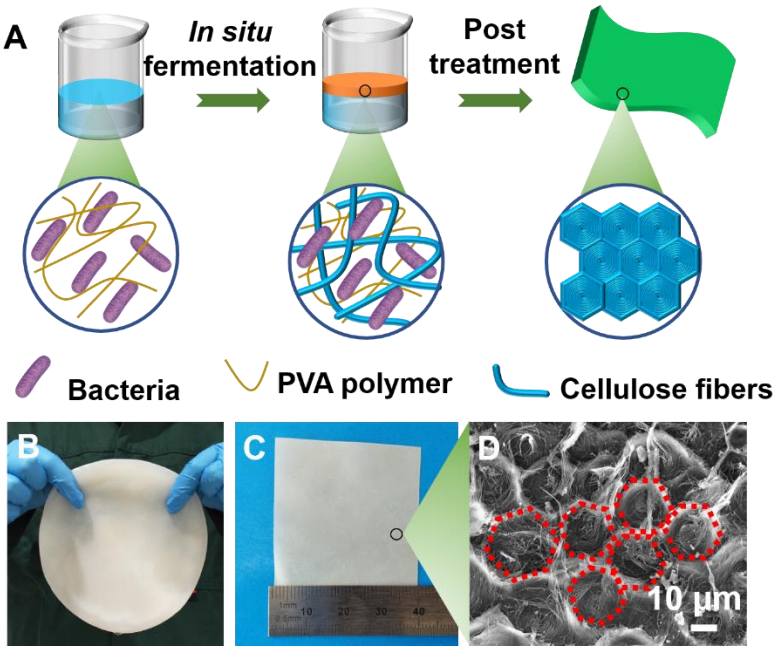

Figure 3.1 Fabrication and characterization of the self-assembled spiral honeycomb bacterial cellulose film. (A) Illustration of fabrication procedure of BC film with honeycomb structure. PVA was added to the fermentation medium. The film was formed at the air-liquid interface and was processed with a freezing-thawing, boiling, washing, and drying procedure. (B) Optical image of BC wet pellicle before air-drying. (C) Optical image of honeycomb BC film. (D) Scanning electron microscope (SEM) image of BC film, showing a spiral honeycomb microstructure.

Here, we report the formation of a highly organized spiral honeycomb microstructure in BC films *via* a self-assembly process under mild conditions that combines an *in situ* fermentation and a post-treatment procedure (**Figure 3.1**). During the BC growing procedure, poly (vinyl alcohol) (PVA), a water-soluble additive often used during BC fermentation to regulate BC's biological[25] and mechanical property,[26] was added to the fermentation medium and BC wet pellicles were harvested at the air-liquid interface. We then applied a freezing-thawing (FT) procedure, followed by boiling, washing and air-drying. These mild treatments provide a green and scalable alternative to the fabrication of nanofibrous BC with tailored shapes and sizes, and interestingly, lead to the self-assembly of the material into a spiral honeycomb microstructure. These honeycomb films exhibit higher

tensile strength and higher toughness compared to BC films of same composition but without a spiral honeycomb architecture. Hexagonal honeycomb structures are abundant in nature and are capable of adjusting the mechanical performance of various materials.[27] Furthermore, in honeycomb microstructured samples, nanofibers are densely packed in a spiral form, which is an efficient way to enhance stretchability.[28]

3.2 Results and Discussion

Biofabrication procedure and morphology of composites

In this work, cellulose nanofibers are produced by *G. hansenii*, a strain of bacteria with high cellulose production yield.[14] Cellulose from plant or wood is generally not pure, containing lignin, hemicellulose, pectin, *etc.*,[29] and an environmentally unfriendly delignification procedure is needed.[30] On the contrary, BC consists of pure cellulose without those impurities,[31] and is therefore an advantageous building block in manufacturing cellulose-based advanced materials.[8] A straightforward approach to produce BC-based composites is *in situ* fermentation,[32] which consists of simply dissolving water-soluble polymers into the fermentation medium during cellulose production by the bacteria. The produced BC nanofibers tend to aggregate at the air-liquid interface, forming a random nanofibrous network held together *via* strong hydrogen bonding. The liquid medium, including the dissolved polymers, is then entrapped into the BC, resulting in a homogeneous spread of water-soluble polymers into the BC network. For these polymers to remain in the composites, crosslinking methods are generally used.[33]

Here, the *in situ* fabrication procedure consists of adding PVA at 10 *w/v*% into the *G. hansenii* fermentation medium. After 10 days of culturing at 30 ˚C, BC/PVA pellicles were harvested at the air-liquid interface. To crosslink PVA, these pellicles were frozen at -20 ˚C for 24 hours and brought to room temperature to thaw for 6 hours. This FT procedure was repeated 5 times, and then the material was boiled in water for sterilization, immersed in water for washing, and finally dried in air (**Figure 3.1A, B, C**).

Interestingly, a highly organized layered spiral honeycomb structure is observed in these films (**Figure 3.2A-F** and **Figure S3.1**, 10 % PVA-BC-FT samples). SEM images of horizontal sections (**Figure 3.2A-C**) reveal that BC nanofibers are spirally and densely packed to form a hexagonal microunit, with borders of these microunits consisting of aligned and entangled BC nanofibers. This results in a honeycomb morphology with spiral BC nanofibers (**Figure 3.2D-F**). While the 10 % PVA-BC-FT film keeps the layered structure of natural BC (**Figure S3.2A**), the microscale arrangement in each layer is changed from the

randomly distributed nanofibers seen in natural BC (**Figure S3.2B**) to a spiral honeycomb structure.

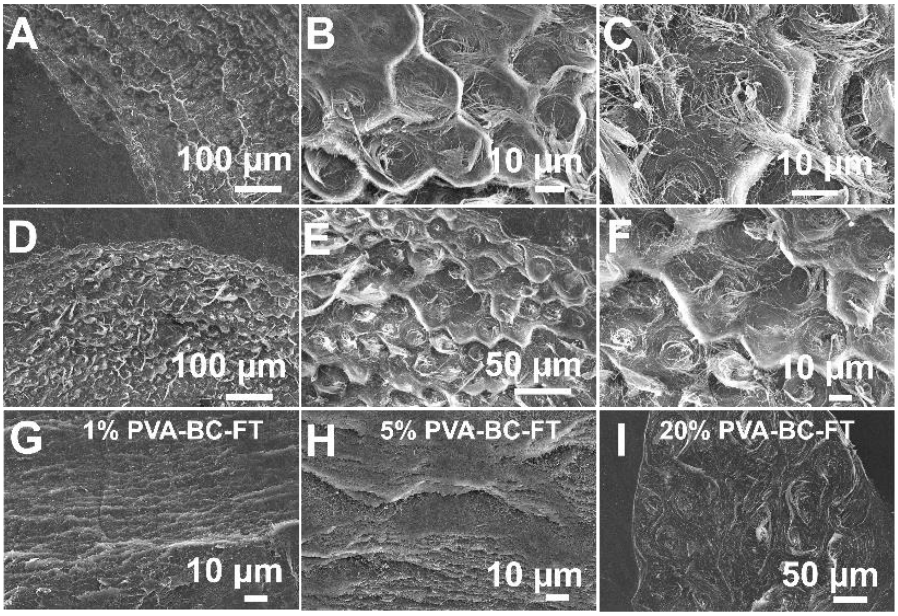

Figure 3.2 SEM images of the bacterial cellulose films. (A-C) horizontal sections and (D-F) cross-sections of 10 % PVA-BC-FT composite film. SEM images of the cross-section of (G) 1 % PVA-BC-FT, (H) 5 % PVA-BC-FT and (I) 20 % PVA-BC-FT.

To investigate the underlying mechanisms behind the formation of such a structure, we vary the PVA concentration in the fermentation medium between 1 *w/v*% and 20 *w/v*%. The sample cross-sections show a random fibrous structure for both 1 *w/v*% PVA (1 % PVA-BC-FT, **Figure 3.2G**) and 5 *w/v*% PVA (5 % PVA-BC-FT, **Figure 3.2H**), as observed in natural BC. However, the samples with 20 *w/v*% PVA (20 % PVA-BC-FT, **Figure 3.2I** and **Figure S3.3**) show a spiral fibrous structure. This structure is not identical to the hexagonal spiral honeycomb structure seen in the samples with 10 *w/v*% PVA (10 % PVA-BC-FT). Indeed, the spiral unit diameter increases to 50 µm for 20 % PVA-BC-FT as compared to 23 µm in the case of 10 % PVA-BC-FT. Therefore, the PVA concentration in the initial fermentation medium is of key importance for the formation of the spiral structure. Spirals tend to be formed when the PVA concentration exceeds 10 *w/v*% while 10 *w/v*% is the optimal concentration for the formation of ordered spiral hexagonal structures.

To assess whether PVA concentration is the only factor influencing the structure, the FT was omitted from the fabrication method. The 10 % PVA-BC-FT samples are compared to

10 % PVA-BC, produced following the same procedure except for the FT. Interestingly, there is no honeycomb or spiral structure observed in 10 % PVA-BC (**Figure S3.4**). The FT process is therefore essential to the formation of spiral honeycombs. From these results, both the PVA concentration in the fermentation medium and the post-treatment process are crucial factors contributing to the formation of this fibrous honeycomb structure.

The presence of PVA in the honeycomb composites is confirmed with Fourier Transform Infrared Spectra (FTIR) (**Figure S3.5**). Thermal Gravimetry Analysis (TGA) reveals that only a small amount of PVA is present in the final honeycomb film since the TGA of pure BC and that of honeycomb composites are similar (**Figure S3.6**). PVA in the composites is likely washed away during the post-treatment procedure. During the FT procedure, PVA polymer chains are expected to become more organized to form PVA crystals,[34] which could act as physical crosslinking points. Upon boiling, PVA polymer chains in the crystal rearrange and become less organized due to heating, causing the PVA to be water-soluble again. Before this heating procedure, PVA is spread homogeneously in the BC network and acts as a plasticizer. As the PVA polymer chain is rich in hydrogen bonds, PVA may interfere with the hydrogen bonding between the cellulose fibrils.[32] The hydrogen bonds in the original BC fibers, may, consequently, be weakened, resulting in the rearrangement of the random BC nanofibers and initiating a self-assembly process that leads to the formation of the spiral honeycomb structure in the post-treatment. Meanwhile, as no honeycomb structure were observed without FT, the PVA crystals during FT[34] might act as a template to form the highly ordered structure: the BC fibers could reorganize into the honeycomb spirals based on the PVA crystal template. During the boiling procedure, this PVA crystal template is removed while the spiral honeycomb structure remains in the composites. This could explain why a higher amount of PVA contributes to the formation of the spiral structure.

Bacterial viability and yield of materials production

We then assess whether the yield of BC/PVA composite produced depends on the bacterial viability, which can be influenced by the presence of PVA. To study this, the wet thickness of fermented BC is measured after different fermentation times (5, 10, 15 days), with and without PVA, and the corresponding amount of viable bacteria is assessed. In all sample types, the bacteria viability reaches a maximum after 5 days of fermentation (**Figure 3.3A**). After 5 and 10 days of culture, bacterial viability in pure BC and BC/PVA composites is similar. After 15 days, however, pure BC shows higher bacteria viability. Therefore, the addition of PVA in the fermentation medium lowers the number of viable bacteria only for periods longer than 10 days. The dry weight yield of all specimens remains unchanged after

10 days (**Figure 3.3B**), because bacteria entrapment into the BC pellicle and limited contact with oxygen restricts BC production after 10 days.[35] The wet thickness, wet weight and dry weight measurements (**Figure 3.3B**, **Figure S3.7A**, **B**) all show a decrease in composite production when more PVA is present. This decrease in wet thickness is probably due to the viscosity change when the polymer is added, as shown before.[33, 36] The viscosity of the fermentation medium increased significantly after adding PVA, especially for the highest concentrations, thus decreasing the oxygen transfer rate and cell migration, and slowing down BC production rate.[16, 36] As long as PVA concentration is below 10 *w/v*%, we could harvest BC/PVA composites with a wet thickness exceeding 4.0 mm after 10 days of fermentation, which is thick enough to perform mechanical testing.

The film shape and size are easily tailored by adjusting the shape and size of the fermentation vessel (**Figure S3.7C**, **D**, **E**). The entire fermentation step is carried out under mild conditions without using or generating any toxic chemicals. The fabrication process is scalable, green, and environmentally-friendly.

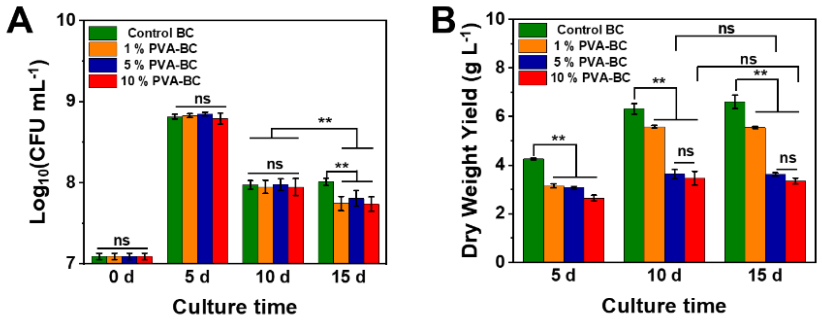

Figure 3.3 Bacterial viability during fermentation and the yield of the fermented BC/ PVA pellicle. (A) Colony forming units (CFUs) measurements, (B) dry weight yield. ** $p < 0.01$, significant; ns, insignificant.

Tensile properties of the BC/PVA composites

The microstructure of a material influences its mechanical performance. Honeycomb structures are commonly observed in nature, and are seen in many biological systems like wood,[5] turtle shells,[37] bamboo[38] and cork.[39] The honeycomb microstructure of wood, which is formed through a different mechanism,[5, 40] is demonstrated to be one of the reasons that wood possesses excellent mechanical properties,[27] hence the growing interest in mimicking this structure.[41] The random fibrous structure of natural BC, originating from the bacteria moving freely in all directions during fermentation,[42] limits its mechanical properties. Therefore, the microscale spiral honeycomb structure observed here in the 10 % PVA-BC-

FT samples are likely to affect BC's mechanical properties. Tensile tests are performed to test

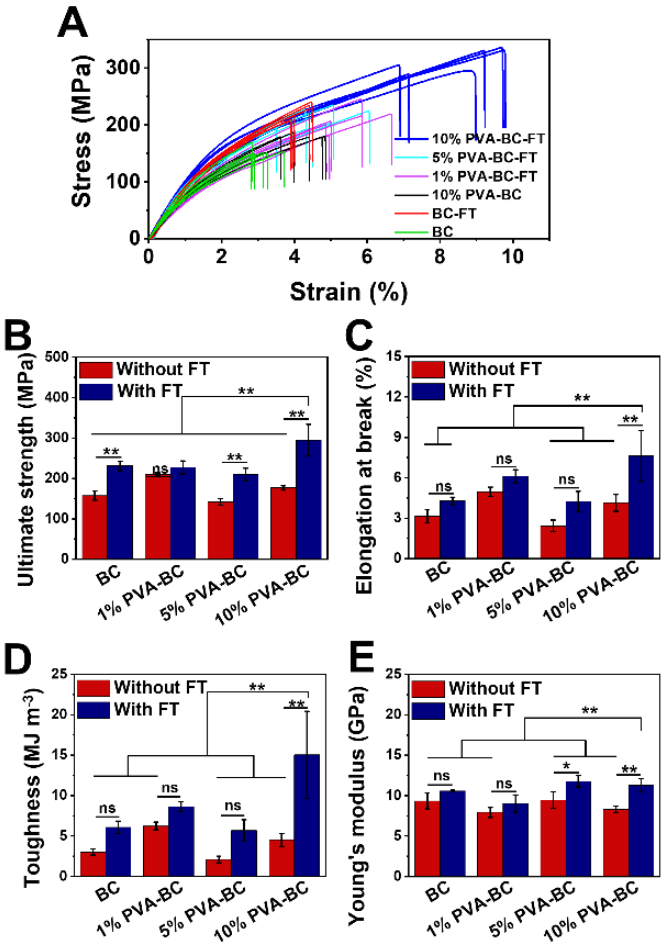

Figure 3.4 Tensile properties of the BC/PVA composite film with and without FT. (A) Stress-strain curves, (B) ultimate strength, (C) elongation at break, (D) toughness, and (E) Young's moduli. ** $p < 0.01$, significant; ns, insignificant.

this. The 10 % PVA-BC-FT samples show a significantly higher ultimate strength (314.98 ± 20.51 MPa, **Figure 3.4A-B**) and elongation at break (8.58 % ± 1.27 %, **Figure 3.4C**) when compared to the other groups. Comparing the samples that have undergone the FT procedure to the ones which have not, we find that 10 % PVA-BC-FT and BC-FT (ultimate strength: 223.07 ± 13.82 MPa; elongation at break: 4.19 % ± 0.29 %) show higher ultimate strength

and higher elongation at break than 10 % PVA-BC (ultimate strength: 176.66 ± 5.59 MPa; elongation at break: 4.14 % ± 0.63 %) and BC (ultimate strength: 153.89 ± 8.21 MPa; elongation at break: 3.10 % ± 0.35 %,), see **Figure 3.4B-C**. This indicates that the FT procedure improves the tensile properties of BC. The ultimate strength of 1 % PVA-BC-FT (211.64 ± 21.45 MPa, **Figure 3.4B**) and 5 % PVA-BC-FT (217.41 ± 13.96 MPa, **Figure 3.4B**) are close to that of BC-FT. Therefore, the main reason for this sharp increase in the ultimate strength of 10 % PVA-BC-FT is not the addition of PVA, but rather its different microstructure. Due to the contributions from a high tensile strength and a higher elongation at break, 10 % PVA-BC-FT shows a toughness (17.76 ± 3.63 MJ m^{-3}), which is significantly higher than that of BC (2.89 ± 0.33 MJ m^{-3}, **Figure 3.4D**). The Young's modulus of the 10 % PVA-BC-FT composite does not increase significantly as compared to most other specimen types, with Young's moduli of all sample types varying between 7.41 ± 0.85 GPa and 11.24 ± 0.63 GPa (**Figure 3.4E**). In conclusion, the improved mechanical properties of 10 % PVA-BC-FT are most likely linked to its nanofibrous layered structure and honeycomb microstructure. PVA was previously added to the fermentation medium to form BC/PVA composites.[33, 43] In these studies, however, the maximum tensile strength was smaller (less than 55 MPa), different post-treatment methods were used, and no honeycomb structure was observed. The BC/PVA composite film was compared with other cellulose-based composite films and showed competitive tensile strength and toughness values when compared to other BC-based composites fabricated under mild conditions (**Table S3.1**).

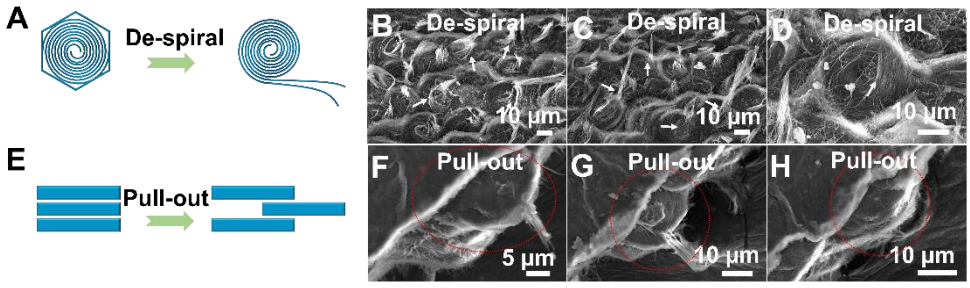

Figure 3.5 The de-spiral and pull-out breaking mechanisms of the bacterial cellulose films with honeycomb microstructure. Schematic of (A) de-spiral and (E) pull-out; SEM images of the (B-D) de-spiral morphology and (F-H) pull-out morphology of the honeycomb BC film after tensile testing.

To further understand the failure mechanism of this new material, cross-sections of the 10 % PVA-BC-FT specimens after tensile testing are imaged, showing fibrous de-spiral (**Figure 3.5A-D** and **Figure S3.8**) and pull-out morphologies (**Figure 3.5E-H**). The pull-out

morphology was previously reported in other layered materials and was suggested to be responsible for the toughness enhancement during failure.[44-46] This failure process can absorb more energy under tension, thus could contribute to the high strength and toughness measured in this honeycomb nanofibrous material.

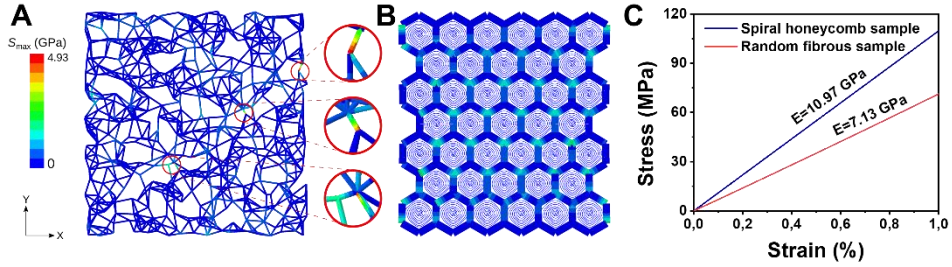

Figure 3.6 Numerical simulation results of the BC film with honeycomb and random microstructure. Stress distribution in (A) random structure and (B) spiral honeycomb structure. (C) Stress-strain curve of random and spiral honeycomb structures predicted by FE simulations.

Finite element simulations

To study the mechanistic aspects of how the spiral honeycomb structure improves BC mechanical properties, numerical simulations are carried out. In the random structure, a high level of localized stress concentrations is observed in some regions of the structure (**Figure 3.6A**). These regions are prone to failure for a higher level of applied strains. In contrast, the stress is more uniformly distributed in the spiral honeycomb structure (**Figure 3.6B**). Moreover, the maximum principal stress in the spiral honeycomb structure is lower than the maximum stress in the random structure ($(S_{max})_{Spiral\ honeycomb}$ =2.22 GPa, $(S_{max})_{Random}$=4.81 GPa) when both structures are subjected to the same level of axial strain. The computational models are limited to the elastic regime and we do not include any plasticity and post-yielding in the model. Nevertheless, the computational models confirm that the structures with random networks tend to break at a lower strain level due to the inhomogeneous stress distribution throughout the structure as compared to spiral honeycomb lattice structures. Moreover, the predicted numerical elastic moduli (slope of curves in **Figure 3.6C**) agree with the experimental observations showing higher elastic modulus for the structures with spiral honeycomb lattices given the fact that both models had similar overall densities. The small differences between the numerical and experimental results could be due to the simplifications considered for the simulation of these intricate structures.

3.3 Conclusions

The natural biopolymer bacterial cellulose possesses an organized fibril structure at the nanoscale. At the microscale however, the BC nanofibers are distributed randomly. To further increase the tensile strength and toughness of BC, it is important but still remains challenging to control the organization of BC at the microscale. Here, we demonstrate the combination of an *in situ* biofabrication of BC with 10 *w/v*% PVA with a post treatment procedure including freezing-thawing, boiling, washing and air-drying, to generate a strong and tough BC film with a highly organized spiral nanofibrous honeycomb microstructure. At high enough concentration, PVA likely affects the hydrogen-bond network of BC fibrils. The weakened BC fibers could therefore self-assemble in the observed spirals with a highly organized hexagonal microunit. As a result, this honeycomb BC film shows a 2X increase (from 154 MPa for BC to 315 MPa for honeycomb BC) in tensile strength and a 5X increase (from 2.9 MJ m^{-3} for BC to 17.8 MJ m^{-3} for honeycomb BC) in toughness compared to the BC samples with random nanofibrous structure. The sharp increase in mechanical properties is due to this special honeycomb structure, because materials of similar composition with no honeycomb structure show reduced tensile strength and toughness. In addition to experiments, finite element simulations also indicate improved mechanical properties resulting from the honeycomb structure. Furthermore, shape, size, and thickness of this material are controllable by simply adjusting the shape and size of the culture vessel and the cultivation time. This fabrication method provides a green and mild platform for incorporating beneficial polymers into BC to produce materials with superior mechanical properties and complex biomimetic structures on a large scale.

3.4 References

1. Wegst, U. G. K.; Bai, H.; Saiz, E.; Tomsia, A. P.; Ritchie, R. O. Bioinspired Structural Materials. Nat. Mater. 2015, *14* (1), 23-36.

2. Wang, Q.; Schniepp, H. C. Strength of Recluse Spider's Silk Originates from Nanofibrils. ACS Macro Lett. 2018, *7* (11), 1364-1370.

3. Barthelat, F. Nacre from Mollusk Shells: A Model for High-Performance Structural Materials. Bioinspir. Biomim. 2010, *5* (3), 035001.

4. Armiento, A. R.; Hatt, L. P.; Sanchez Rosenberg, G.; Thompson, K.; Stoddart, M. J. Functional Biomaterials for Bone Regeneration: A Lesson in Complex Biology. Adv. Funct. Mater. 2020, 1909874.

5. Gibson, L. J. The Hierarchical Structure and Mechanics of Plant Materials. J. R. Soc. Interface 2012, *9* (76), 2749-2766.

6. Huang, W.; Restrepo, D.; Jung, J. Y.; Su, F. Y.; Liu, Z.; Ritchie, R. O.; McKittrick, J.; Zavattieri, P.; Kisailus, D. Multiscale Toughening Mechanisms in Biological Materials and Bioinspired Designs. Adv. Mater. 2019, *31* (43), 1901561.

7. Spiesz, E. M.; Schmieden, D. T.; Grande, A. M.; Liang, K.; Schwiedrzik, J.; Natalio, F.; Michler, J.; Garcia, S. J.; Aubin-Tam, M. E.; Meyer, A. S. Bacterially Produced, Nacre-Inspired Composite Materials. Small 2019, *15* (22), 1805312.

8. Gao, H.-L.; Zhao, R.; Cui, C.; Zhu, Y.-B.; Chen, S.-M.; Pan, Z.; Meng, Y.-F.; Wen, S.-M.; Liu, C.; Wu, H.-A.; Yu, S.-H. Bioinspired Hierarchical Helical Nanocomposite Macrofibers Based on Bacterial Cellulose Nanofibers. Natl. Sci. Rev. 2020, *7* (1), 73-83.

9. Moradali, M. F.; Rehm, B. H. A. Bacterial Biopolymers: From Pathogenesis to Advanced Materials. Nat. Rev. Microbiol. 2020, *18* (4), 195-210.

10. Malho, J. M.; Laaksonen, P.; Walther, A.; Ikkala, O.; Linder, M. B. Facile Method for Stiff, Tough, and Strong Nanocomposites by Direct Exfoliation of Multilayered Graphene into Native Nanocellulose Matrix. Biomacromolecules 2012, *13* (4), 1093-1099.

11. Chen, Y.; Fu, J.; Dang, B.; Sun, Q.; Li, H.; Zhai, T. Artificial Wooden Nacre: A High Specific Strength Engineering Material. ACS Nano 2020, *14* (2), 2036-2043.

12. Mao, L. B.; Gao, H. L.; Yao, H. B.; Liu, L.; Colfen, H.; Liu, G.; Chen, S. M.; Li, S. K.; Yan, Y. X.; Liu, Y. Y.; Yu, S. H. Synthetic Nacre by Predesigned Matrix-directed Mineralization. Science 2016, *354* (6308), 107-110.

13. Wei, P.; Cai, J.; Zhang, L. High‐Strength and Tough Crystalline Polysaccharide‐Based Materials. Chin. J. Chem. 2020, *38* (7), 761-771.

14. Florea, M.; Reeve, B.; Abbott, J.; Freemont, P. S.; Ellis, T. Genome Sequence and Plasmid Transformation of the Model High-Yield Bacterial Cellulose Producer *Gluconacetobacter hansenii* ATCC 53582. Sci. Rep. 2016, *6*, 23635.

15. Mittal, N.; Ansari, F.; Gowda, V. K.; Brouzet, C.; Chen, P.; Larsson, P. T.; Roth, S. V.; Lundell, F.; Wagberg, L.; Kotov, N. A.; Soderberg, L. D. Multiscale Control of Nanocellulose Assembly: Transferring Remarkable Nanoscale Fibril Mechanics to Macroscale Fibers. ACS Nano 2018, *12* (7), 6378-6388.

16. Wang, J.; Tavakoli, J.; Tang, Y. Bacterial Cellulose Production, Properties and Applications with Different Culture Methods - A Review. Carbohydr. Polym. 2019, *219*, 63-76.

17. Wu, Z. Y.; Liang, H. W.; Chen, L. F.; Hu, B. C.; Yu, S. H. Bacterial Cellulose: A Robust Platform for Design of Three Dimensional Carbon-Based Functional Nanomaterials. Acc. Chem. Res. 2016, *49* (1), 96-105.

18. Wang, S.; Jiang, F.; Xu, X.; Kuang, Y.; Fu, K.; Hitz, E.; Hu, L. Super-Strong, Super-Stiff Macrofibers with Aligned, Long Bacterial Cellulose Nanofibers. Adv. Mater. 2017, *29* (35), 1702498.

19. Gao, M.; Li, J.; Bao, Z.; Hu, M.; Nian, R.; Feng, D.; An, D.; Li, X.; Xian, M.; Zhang, H. A Natural In Situ Fabrication Method of Functional Bacterial Cellulose Using a Microorganism. Nat. Commun. 2019, *10* (1), 437.

20. Yao, J.; Chen, S.; Chen, Y.; Wang, B.; Pei, Q.; Wang, H. Macrofibers with High Mechanical Performance Based on Aligned Bacterial Cellulose Nanofibers. ACS Appl. Mater. Interfaces 2017, *9* (24), 20330-20339.

21. Gutierrez, E.; Burdiles, P. A.; Quero, F.; Palma, P.; Olate-Moya, F.; Palza, H. 3D Printing of Antimicrobial Alginate/Bacterial-Cellulose Composite Hydrogels by Incorporating Copper Nanostructures. ACS Biomater. Sci. Eng. 2019, *5* (11), 6290-6299.

22. Guan, Q.-F.; Han, Z.-M.; Luo, T.-T.; Yang, H.-B.; Liang, H.-W.; Chen, S.-M.; Wang, G.-S.; Yu, S.-H. A General Aerosol-Assisted Biosynthesis of Functional Bulk Nanocomposites. Natl. Sci. Rev. 2019, *6* (1), 64-73.

23. Wang, S.; Li, T.; Chen, C.; Kong, W.; Zhu, S.; Dai, J.; Diaz, A. J.; Hitz, E.; Solares, S. D.; Li, T.; Hu, L. Transparent, Anisotropic Biofilm with Aligned Bacterial Cellulose Nanofibers. Adv. Funct. Mater. 2018, *28* (24), 1707491.

24. Wu, Z.; Chen, S.; Wu, R.; Sheng, N.; Zhang, M.; Ji, P.; Wang, H. Top-down Peeling Bacterial Cellulose to High Strength Ultrathin Films and Multifunctional Fibers. Chem. Eng. J. 2020, *391*, 123527.

25. Wahid, F.; Wang, F. P.; Xie, Y. Y.; Chu, L. Q.; Jia, S. R.; Duan, Y. X.; Zhang, L.; Zhong, C. Reusable Ternary PVA Films Containing Bacterial Cellulose Fibers and Epsilon-Polylysine with Improved Mechanical and Antibacterial Properties. Colloids Surf. B Biointerfaces 2019, *183*, 110486.

26. Osorio, M.; Velásquez-Cock, J.; Restrepo, L. M.; Zuluaga, R.; Gañán, P.; Rojas, O. J.; Ortiz-Trujillo, I.; Castro, C. Bioactive 3D-Shaped Wound Dressings Synthesized from Bacterial Cellulose: Effect on Cell Adhesion of Polyvinyl Alcohol Integrated In Situ. Int. J. Polym. Sci. 2017, *2017*, 3728485.

27. Zhang, Q.; Yang, X.; Li, P.; Huang, G.; Feng, S.; Shen, C.; Han, B.; Zhang, X.; Jin, F.; Xu, F.; Lu, T. J. Bioinspired Engineering of Honeycomb Structure – Using Nature to Inspire Human Innovation. Prog. Mater. Sci. 2015, *74*, 332-400.

28. Rehman, M. U.; Rojas, J. P. Optimization of Compound Serpentine–Spiral Structure for Ultra-Stretchable Electronics. Extreme Mech. Lett. 2017, *15*, 44-50.

29. Si, X.; Lu, F.; Chen, J.; Lu, R.; Huang, Q.; Jiang, H.; Taarning, E.; Xu, J. A Strategy for Generating High-Quality Cellulose and Lignin Simultaneously from Woody Biomass. Green Chem. 2017, *19* (20), 4849-4857.

30. Khakalo, A.; Tanaka, A.; Korpela, A.; Orelma, H. Delignification and Ionic Liquid Treatment of Wood toward Multifunctional High-Performance Structural Materials. ACS Appl. Mater. Interfaces 2020, *12* (20), 23532-23542.

31. Ma, L.; Bi, Z.; Xue, Y.; Zhang, W.; Huang, Q.; Zhang, L.; Huang, Y. Bacterial Cellulose: An Encouraging Eco-Friendly Nano-Candidate for Energy Storage and Energy Conversion. J. Mater. Chem. A 2020, *8* (12), 5812-5842.

32. Ray, D.; Sain, S. In Situ Processing of Cellulose Nanocomposites. Compos., Part A 2016, *83*, 19-37.

33. Castro, C.; Vesterinen, A.; Zuluaga, R.; Caro, G.; Filpponen, I.; Rojas, O. J.; Kortaberria, G.; Gañán, P. In Situ Production of Nanocomposites of Poly(Vinyl Alcohol) and Cellulose Nanofibrils from Gluconacetobacter Bacteria: Effect of Chemical Crosslinking. Cellulose 2014, *21* (3), 1745-1756.

34. Yokoyama E.; Masada I.; Shimamura K.; Ikawa T.; Monobe, K. Morphology and Structure of Highly Elastic Poly(Vinyl Alcohol) Hydrogel Prepared by Repeated Freezing-and-Melting. Colloid & Polym. Sci. 1986, *264*, 595-601

35. Ruka, D. R.; Simon, G. P.; Dean, K. M. Altering the Growth Conditions of *Gluconacetobacter xylinus* to Maximize the Yield of Bacterial Cellulose. Carbohydr. Polym. 2012, *89* (2), 613-622.

36. Chen, Y.; Zhou, X.; Lin, Q.; Jiang, D. Bacterial Cellulose/Gelatin Composites: *In Situ* Preparation and Glutaraldehyde Treatment. Cellulose 2014, *21* (4), 2679-2693.

37. Naleway, S. E.; Porter, M. M.; McKittrick, J.; Meyers, M. A. Structural Design Elements in Biological Materials: Application to Bioinspiration. Adv. Mater. 2015, *27* (37), 5455-5476.

38. Chen, C.; Li, Z.; Mi, R.; Dai, J.; Xie, H.; Pei, Y.; Li, J.; Qiao, H.; Tang, H.; Yang, B.; Hu, L. Rapid Processing of Whole Bamboo with Exposed, Aligned Nanofibrils toward a High-Performance Structural Material. ACS Nano 2020, *14* (5), 5194-5202.

39. Miranda, I.; Gominho, J.; Pereira, H. Cellular Structure and Chemical Composition of Cork from the Chinese Cork Oak (Quercus Variabilis). J. Wood Sci. 2013, *59* (1), 1-9.

40. Wodzicki, T. J. Natural Factors Affecting Wood Structure. Wood Sci. Tech. 2001, *35*, 5-26.

41. Yu, Z. L.; Qin, B.; Ma, Z. Y.; Gao, Y. C.; Guan, Q. F.; Yang, H. B.; Yu, S. H. Emerging Bioinspired Artificial Woods. Adv. Mater. 2020, 2001086.

42. Rahman, M. M.; Netravali, A. N. Aligned Bacterial Cellulose Arrays as "Green" Nanofibers for Composite Materials. ACS Macro Lett. 2016, *5* (9), 1070-1074.

43. Castro, C.; Zuluaga, R.; Rojas, O. J.; Filpponen, I.; Orelma, H.; Londoño, M.; Betancourt, S.; Gañán, P. Highly Percolated Poly(Vinyl Alcohol) and Bacterial Nanocellulose Synthesized In Situ by Physical-Crosslinking: Exploiting Polymer Synergies for Biomedical Nanocomposites. RSC Adv. 2015, *5* (110), 90742-90749.

44. Wang, J.; Cheng, Q.; Lin, L.; Jiang, L. Synergistic Toughening of Bioinspired Poly(vinyl alcohol)-Clay-Nanofibrillar Cellulose Artificial Nacre. ACS Nano 2014, *8* (3), 2739-2745.

45. Zhao, H.; Yue, Y.; Zhang, Y.; Li, L.; Guo, L. Ternary Artificial Nacre Reinforced by Ultrathin Amorphous Alumina with Exceptional Mechanical Properties. Adv. Mater. 2016, *28* (10), 2037-42.

46. Yan, Y.-X.; Yao, H.-B.; Yu, S.-H. Nacre-Like Ternary Hybrid Films with Enhanced Mechanical Properties by Interlocked Nanofiber Design. Adv. Mater. Interfaces 2016, *3* (17), 1600296.

3.5 Supplementary Information

Materials, strain and culture conditions

Poly (vinyl alcohol) (PVA, M_w 89000-98000, 99+% hydrolyzed), tryptone (Pancreatic digest of casein), yeast extract, agar, citric acid monohydrate (ACS reagent, ≥ 99.0%) and cellulase from *Trichoderma reesei* (aqueous solution, ≥ 700 units g^{-1}) were purchased from Sigma-Aldrich. D(+)-glucose monohydrate, sodium chloride (NaCl), and di-sodium hydrogen phosphate (≥ 99.0%) were obtained from Carl Roth GmbH.

The cellulose producing strain *Gluconacetobacter hansenii* (ATCC® 53582™) was propagated in Hestrin-Schramm (HS) medium (5.0 g L^{-1} tryptone, 5.0 g L^{-1} yeast extract, 2.7 g L^{-1} disodium hydrogen phosphate, 1.5 g L^{-1} citric acid and 20 g L^{-1} glucose) at 30 °C under static conditions for 3 days to obtain the BC pellicle. The inoculum for bacterial fermentation was prepared by treating the BC pellicle with cellulase at 180 rpm at 30 °C overnight. The solution was then centrifuged (4 °C, 3220×g centrifuge speed, 10 mins) to remove the cellulase, and the bacterial pellet was re-suspended in fresh HS medium to obtain an OD_{600} of 1. We then used 1 *v/v* % of this solution as the inoculum.

Growing composite materials by bacteria

PVA powder was dissolved into HS medium at concentrations of 1 *w/v*%, 5 *w/v*%, and 10 *w/v*%, followed by boiling in a kitchen microwave oven for 5 mins and cooling. This process was repeated three times to sterilize the solution. After that, the polymer/medium solution was inoculated with *G. hansenii* bacteria (*Gluconacetobacter hansenii* ATCC® 53582™ bacteria were obtained from the American Type Culture Collection (ATCC)). Fermentation was then carried out at 30 °C for 10 days under static conditions. The nanofibrous polymer composites were formed at the air-liquid interface such that the shape of the composite pellicle was determined by the shape of the fermentation chamber (flask or rectangular box-like) and the material thickness was established by the culture time.

Post-treatment of the nanofibrous composites

After fermentation, the freshly formed solid pellicle was transferred to a plastic petri dish and treated with a “freezing-thawing” method. Briefly, the solid pellicle was stored at -20 °C to be frozen for 24 hours and was, then, left to thaw at room temperature for 6 hours. The PVA inside the composites is known to crosslink by the crystals formed after repeating this “freezing-thawing” procedure for 5 times.[1] After crosslinking, the pellicles were boiled to kill the bacteria and washed with distilled water for 3 days to remove the unreacted

polymers and impurities, followed by drying in the air to form the final polymer/cellulose nanofibrous composite films.

Characterization of the BC/PVA nanofibrous composites

The material morphology was observed by scanning electron microscopy (SEM, JEOL JSM 6010 LA). The material was sputter-coated with gold-palladium at 20 mA for 60 s and was observed at 5-15 kV under vacuum. SEM was carried out on the specimens after the boiling and washing steps.

To check for the presence of polymers inside the composites, FTIR (Perkin Elmer, Spectrum 100) equipped with an attenuated total reflection (ATR) accessory was used. The FTIR spectra were the average of 20 scans in the 550-4000 cm^{-1} range at a resolution of 4 cm^{-1}.

TGA (Mettler Toledo) was assessed at 30-1000 °C with a heating rate of 10 °C min^{-1} in the air atmosphere. Derivative Thermogravimetry (DTG), the first derivative of the TGA curve, was also plotted (**Figure S3.6B**).

The tensile tests were performed using a Zwick/Roell Z010 universal testing machine with a 500 N load cell and 1 kN grips. The measuring distance between the clamps was 10 mm and the samples were tested with a loading rate of 2 mm/min. At least six specimens per group were measured for the data presented here.

Measuring the bacterial viability and composite yield

The effects of adding PVA on the bacterial viability was assessed with the colony-forming unit (CFU) measurements. Briefly, *G. hansenii* with/without added PVA was cultured for 0, 5, 10, and 15 days statically at 30 °C. After the respective incubation times, the cellulase treatment was carried out by adding cellulase to the above and incubating the resulting mixture at 30 °C overnight at 180 rpm. Then, the treated solutions were centrifuged to remove the cellulase, medium, and PVA. The bacterial pellet was re-suspended in the same initial volume of saline (0.9 *w/v*% NaCl). Dilutions of this in the range of 10^{0}-10^{-8} were made and 20 µL of each dilution was spotted on HS agar plates (supplemented with 2 *v/v*% acetic acid). The plates were then incubated at 30 °C for 3 days and the number of colonies was enumerated and the Log_{10} (CFU/mL) was calculated.

The yield of the composite materials was assessed by measuring the wet thicknesses of the different composite pellicle specimens (of varying culturing times) with a Vernier caliper. The wet and dried sample weights were measured using a weighing balance.

Finite element simulations

For numerical simulation, a nonlinear finite element (FE) solver (Abaqus Standard 6. 14) was used. The geometry of the random structures was created in Matlab (R2018b)

software, and was then imported as an input file into Abaqus software. We used the quadratic Timoshenko beam element (B22) since these elements allow for axial deformations, bending, and shear. Each nanofiber was simulated as a beam with a circular cross-section and a diameter of 0.059 mm. Each strut of the honeycomb unit cell was assumed to consist of 5000 parallel nanofibers and to have a rectangular cross-section with a width (W) of 0.059 mm and a length (L) of 5 mm. Therefore, the out-of-plane thickness (T) of both structures was considered 0.059 mm. The dimensions (W×H) of the random structure and spiral honeycomb were considered to be 8 × 8 mm^2 and 138 × 138 mm^2, respectively. The level of connectivity of the random structure which was defined as the average connectivity of all nodes,[2] was considered 5.5. This value was selected in a way that both random structure and honeycomb have equal densities.

An elastic material model was used for both structures (E=125 GPa and ν=0.2). The appropriate values for elastic properties were obtained via calibration and the initial range for Young's moduli was selected based on previous studies.[3, 4] In both models, a uniaxial displacement-controlled stretch test in the y direction (**Figure 3.6A, B**) was simulated. To this aim, two reference points were defined on the top and bottom of the structure, which were kinematically coupled with their corresponding nodes at the top and bottom of the structure. A displacement boundary condition corresponding to 1 % strain was applied to the top reference point while all degrees of freedom of the bottom reference point were constrained. The normal stress, σ = F/A, was defined as the ratio of the reaction force, F, to the initial cross-section area, $A = W \times T$.

Statistics

Statistical analyses were performed on https://astatsa.com/. The experimental groups were compared using one-way (single factor) ANOVA with post-hoc Tukey's HSD (honest significant difference) tests.

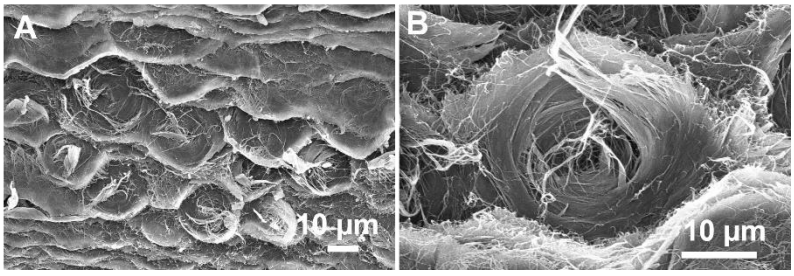

Figure S3.1 SEM images of the spiral honeycomb microstructure (sample 10 % PVA-BC-FT). (A) and (B) are the same specimen imaged at different magnifications.

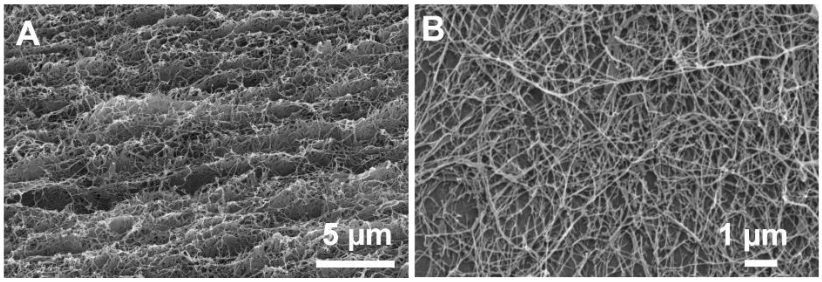

Figure S3.2 The cross section (A) and the surface morphology (B) of air-dried BC. It shows a nanofibrous layered structure.

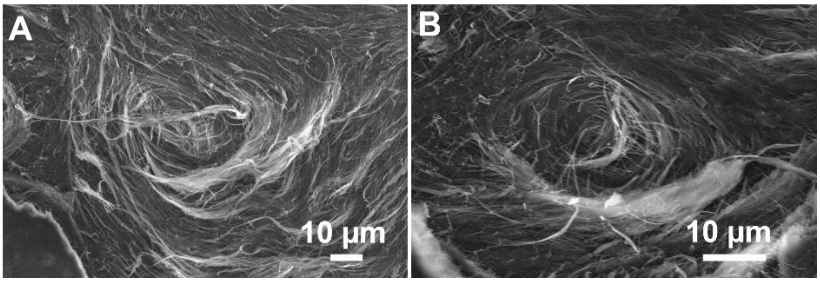

Figure S3.3 SEM images of the spiral structure (20 % PVA-BC-FT sample). (A) and (B) represent two different specimens.

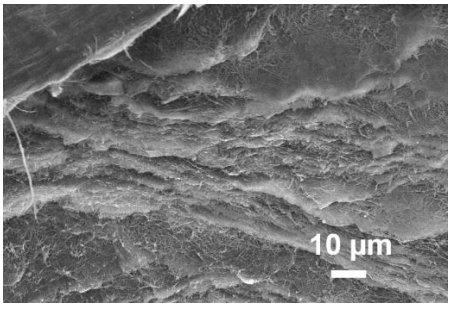

Figure S3.4 SEM image of 10 % PVA-BC sample, where no freezing-thawing procedure was carried out. It shows a similar structure to that of natural BC, with no special circular or honeycomb structure observed.

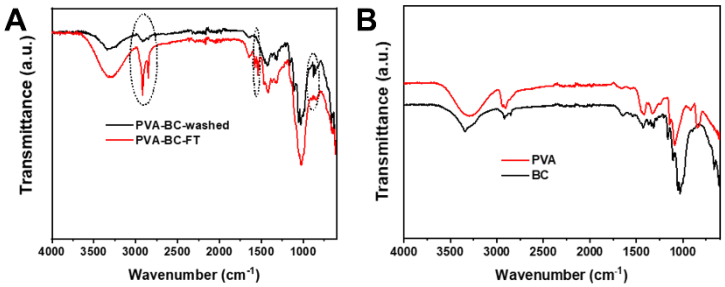

Figure S3.5 FTIR spectra of the BC/PVA composites (A) and their individual components (B).

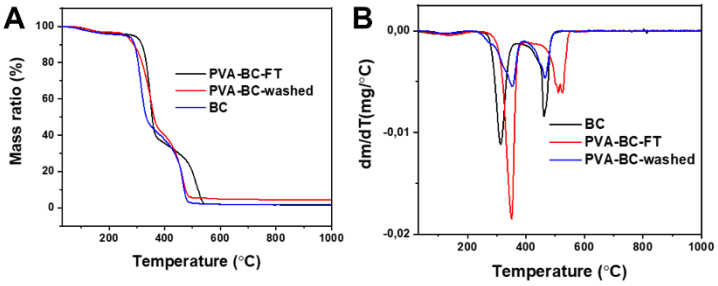

Figure S3.6 TGA (A) and DTG (B) curve of the BC based samples.

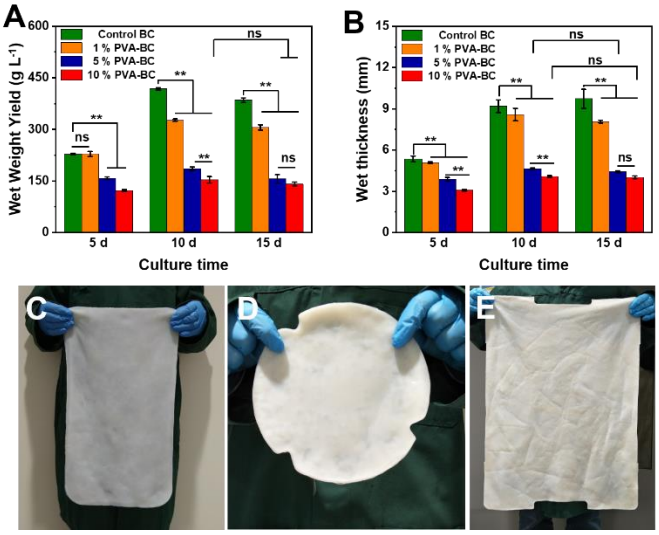

Figure S3.7 Yield and optical images of the BC/ PVA wet hydrogel after fermentation. (A) wet weight yield (B) wet thickness of pure BC and BC/PVA composites after different fermentation periods. The 1 %, 5 % and 10 %

represent the PVA concentrations in the initial fermentation medium. (C, D, E) Photos of BC/PVA composite films (before drying) after 10 days fermentation with different shapes and sizes. ** $p < 0.01$, significant; ns, insignificant.

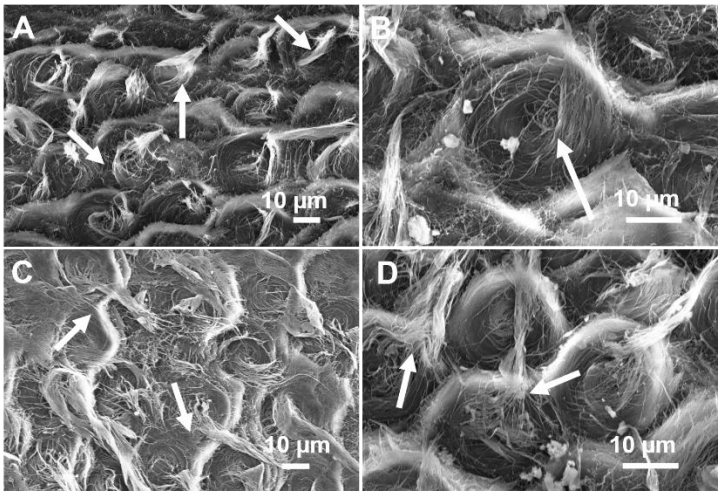

Figure S3.8 SEM images of the de-spiral morphology of the honeycomb specimen after failure (10 % PVA-BC-FT sample). The different panels (A-D) represent different magnifications. De-spiral morphologies (white arrows) are shown in all the images.

Table S3.1 Comparison of tensile strength and toughness values among the cellulose-based film materials

Type of cellulose-based film	Tensile strength [MPa]	Tensile toughness [MJ m^{-3}]	References
BC/ poly(methyl methacrylate)	69.0 - 71.0	4.7 - 7.6	5
BC/ poly(acrylated epoxidized soybean oil)	68.0 - 95.0	1.0 - 1.4	6
BC/ reduced graphene oxide	102.0	8.2	7
BC electrospun fiber	20.0	12.6	8
BC/ Alginate	1.6	2.2	9
Core-shell washed coaxial spinning cellulose fiber	172.0	11.4	10
Cellulose nanofiber	140.0	11.2	11
Tap peeling BC *	731.8	36.4	12
Wet drawn BC *	1005.3	24.7	13
BC-FT	223.1	2.9	This work
10 % PVA-BC-FT	315.0	17.8	This work

* These films were processed with a hot-pressing technique. Hot pressing is an energy consuming technique suited for small pieces of materials, to make them denser. We avoided using hot pressing in our processing to keep our production mild and scalable.

References

1. Osorio, M.; Velásquez-Cock, J.; Restrepo, L. M.; Zuluaga, R.; Gañán, P.; Rojas, O. J.; Ortiz-Trujillo, I.; Castro, C. Bioactive 3D-Shaped Wound Dressings Synthesized from Bacterial Cellulose: Effect on Cell Adhesion of Polyvinyl Alcohol Integrated In Situ. Int. J. Polym. Sci. 2017, *2017*, 3728485.

2. Mirzaali, M. J.; Pahlavani, H.; Zadpoor, A. A. Auxeticity and Stiffness of Random Networks: Lessons for the Rational Design of 3D Printed Mechanical Metamaterials. Appl. Phys. Lett. 2019, *115* (2), 021901.

3. Wang, S.; Jiang, F.; Xu, X.; Kuang, Y.; Fu, K.; Hitz, E.; Hu, L. Super-Strong, Super-Stiff Macrofibers with Aligned, Long Bacterial Cellulose Nanofibers. Adv. Mater. 2017, *29* (35), 1702498.

4. Walker, K. T.; Goosens, V. J.; Das, A.; Graham, A. E.; Ellis, T. Engineered Cell-to-Cell Signalling within Growing Bacterial Cellulose Pellicles. Microb. Biotechnol. 2019, *12* (4), 611-619.

5. Santmarti, A.; Teh, J. W.; Lee, K. Y. Transparent Poly(methyl methacrylate) Composites Based on Bacterial Cellulose Nanofiber Networks with Improved Fracture Resistance and Impact Strength. ACS Omega 2019, *4* (6), 9896-9903.

6. Santmarti, A.; Zhang, H.; Lappalainen, T.; Lee, K.-Y. Cellulose Nanocomposites Reinforced with Bacterial Cellulose Sheets Prepared from Pristine and Disintegrated Pellicle. Compos., Part A 2020, *130*, 105766.

7. Dhar, P.; Pratto, B.; Gonçalves Cruz, A. J.; Bankar, S. Valorization of Sugarcane Straw to Produce Highly Conductive Bacterial Cellulose/ Graphene Nanocomposite Films through In Situ Fermentation: Kinetic Analysis and Property Evaluation. J. Clean. Prod. 2019, *238*, 117859.

8. Zhijiang, C.; Ping, X.; Shiqi, H.; Cong, Z. Soy Protein Nanoparticles Modified Bacterial Cellulose Electrospun Nanofiber Membrane Scaffold by Ultrasound-Induced Self-Assembly Technique: Characterization and Cytocompatibility. Cellulose 2019, *26* (10), 6133-6150.

9. Sulaeva, I.; Hettegger, H.; Bergen, A.; Rohrer, C.; Kostic, M.; Konnerth, J.; Rosenau, T.; Potthast, A. Fabrication of Bacterial Cellulose-Based Wound Dressings with Improved Performance by Impregnation with Alginate. Mater. Sci. Eng. C 2020, *110*, 110619.

10. Reyes, G.; Lundahl, M. J.; Alejandro-Martin, S.; Arteaga-Perez, L. E.; Oviedo, C.; King, A. W. T.; Rojas, O. J. Coaxial Spinning of All-Cellulose Systems for Enhanced

Toughness: Filaments of Oxidized Nanofibrils Sheathed in Cellulose II Regenerated from a Protic Ionic Liquid. Biomacromolecules 2020, *21* (2), 878-891.

11. Tanpichai, S.; Biswas, S. K.; Witayakran, S.; Yano, H. Optically Transparent Tough Nanocomposites with a Hierarchical Structure of Cellulose Nanofiber Networks Prepared by the Pickering Emulsion Method. Compos., Part A 2020, *132*, 105811.

12. Wu, Z.; Chen, S.; Wu, R.; Sheng, N.; Zhang, M.; Ji, P.; Wang, H. Top-down Peeling Bacterial Cellulose to High Strength Ultrathin Films and Multifunctional Fibers. Chem. Eng. J. 2020, *391*, 123527.

13. Wang, S.; Li, T.; Chen, C.; Kong, W.; Zhu, S.; Dai, J.; Diaz, A. J.; Hitz, E.; Solares, S. D.; Li, T.; Hu, L. Transparent, Anisotropic Biofilm with Aligned Bacterial Cellulose Nanofibers. Adv. Funct. Mater. 2018, *28* (24), 1707491.

4

Bacterially grown Cellulose/ Graphene Oxide Composites Infused with γ-poly (glutamic acid) as Biodegradable Structural Materials with Enhanced Toughness

Abstract: Bioinspired bacterial cellulose (BC) composites are next generation renewable materials that exhibit promising industrial applications. However, large-scale production of inorganic/organic BC composites by *in situ* fermentation remains difficult. The methods based on BC mechanical disintegration impair the mechanical property of BC dried films, while the static *in situ* fermentation methods fail to incorporate inorganic particles within the BC network due to the limited diffusion ability. Furthermore, the addition of other components in the fermentation medium significantly interferes with the production of BC. Here, a tough BC composite with a layered structure reminiscent of the tough materials found in nature (*e.g.*, nacre, dentin, bone) is prepared using a semi-static *in situ* fermentation method. The bacterially produced biopolymer γ-poly (glutamic acid) (PGA), together with graphene oxide (GO), are introduced into the BC fermentation medium. The resulting dried BC-GO-PGA composite film shows a high toughness (36 MJ m^{-3}), which makes it one of the toughest BC composite films reported. In traditional *in situ* fermentation methods, the addition of a

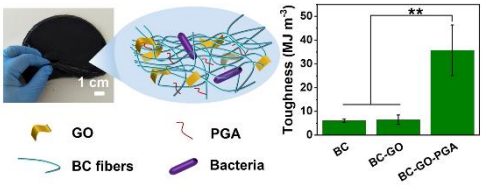

The content of this chapter is based on:
Kui Yu and Marie-Eve Aubin-Tam, *ACS Applied Nano Materials*, 2020, 3 (12), 12055-12063.

second component significantly reduces the wet thickness of the final composites. However, in this report, we show that addition of both PGA and GO to the fermentation medium show a synergistic effect in increasing the wet thickness of the final BC composites. By gently agitating the solution, GO particles get entrapped into the BC network, as the formed pellicles can move below the liquid level and the GO particles suspended in the liquid can be entrapped into the BC network. Compared to other methods, this method achieves high toughness while using a mild and easily scalable fabrication procedure. These bacterially produced composites could be employed in the next generation of biodegradable structural high-performance materials, construction materials and tissue engineering scaffolds (tendon, ligament, skin) that require high toughness.

4.1 Introduction

With the increasing concern of environmental pollution, plastic waste and energy shortage worldwide, the green fabrication of renewable bio-based materials is urgently needed.[1] Biodegradable biopolymers including polyesters (poly(hydroxyalkanoate) (PHA),[2] polylactide (PLA),[3] polyethylene furanoate (PEF)[3]), polysaccharides (cellulose,[4] chitin,[5] alginate[6]), and polyamides (γ-poly(glutamic acid) (PGA),[6] silk,[7] collagen[8]), are drawing increasing attention. Among them, cellulose is the most abundant biopolymer found in nature.[9] Due to its hierarchical fibril structure and excellent mechanical strength, cellulose has become a desirable building block for the construction of high-performance structural materials.[4, 10] However, plant-based cellulose is generally associated with hemicellulose, lignin, pectin,[11] and the extraction of pure cellulose from nature requires a chemically hazardous delignification process.[12] An environmentally friendly alternative is bacterial cellulose (BC), which is secreted by microorganisms (*e.g.*, Acetobacter[13]) in the form of a hydrogel-like pellicle.[14] In contrast to plant cellulose, BC is chemically pure (with almost 100 % cellulose content[15]) and can be produced in large scale at the air-liquid interface with a static fermentation method under mild conditions.[16] The BC pellicle consists of a layered nanofibrous microstructure,[11] a promising matrix substrate for making biomimetic materials.[17]

Although BC shows excellent mechanical performance, pure BC dried films lack certain properties such as high toughness values (over 5 MJ m^{-3})[18] and biocompatibility,[19] which limits its applications in various fields.[20] To endow BC dried film with certain functions and broaden the possible applications, functional additives, including biopolymers[21] and inorganic particles, need to be incorporated into the fibrous network of BC.[22] The preparation of BC composites can be done with an *ex situ* method that involves mechanical crushing the BC wet pellicle into a BC fiber dispersion and blending it with other components.[23-25] This method destroys the natural fibrous layered structure of BC pellicle and may impair the mechanical performance of the final BC composites. The mechanical disintegration may also reduce the tensile strength of reorganized BC dried films compared to pristine BC dried films.[26] To avoid this disadvantage, it is preferred to maintain the natural structure of BC. For incorporation of a second component into the BC structure, *in situ* impregnation[27] or vacuum filtration[28] methods are generally used. However, when it comes to viscous polymers, the vacuum filtration is time-intensive, while the natural impregnation procedure without external force may result in an inhomogeneous polymer distribution in the BC network.

Therefore, the incorporation of viscous polymers and inorganic particles without using toxic chemicals or external force into the BC fibrous network while maintaining its native structure is difficult, but attractive for the fabrication of BC-based high-performance composites.

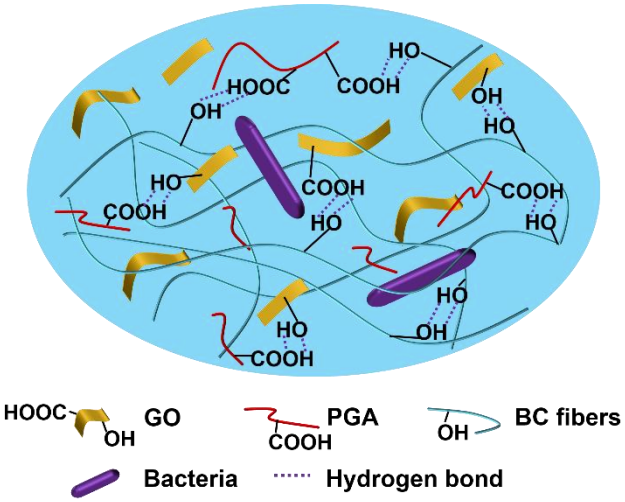

Figure 4.1 Schematic of the hydrogen bonding interactions among PGA, GO and BC fibers.

Static *in situ* fermentation provides a perfect solution to this problem. During the static fermentation process, water-soluble polymers or inorganic dispersions are added directly to the initial fermentation medium before the BC solid pellicle is formed.[20] The dissolved polymers or suspended particles are mixed together with the medium and thus become trapped into the newly formed BC fibril network, resulting in the formation of BC composites.[20] To incorporate inorganic particles into BC *via in situ* fermentation, sedimentation of inorganic particles should be avoided during the fermentation. Therefore, particles with abundant surface charges or polar groups, like graphene oxide (GO), are favorable. Also, the use of such additives may interfere with BC growth,[29, 30] resulting in low yields, hence increased production costs for industrial applications.[29] The fabrication of inorganic particle-BC composites with a static *in situ* fermentation method has thus been restricted to thin films with an overall wet thickness smaller than 2 mm,[31] because the particles can only remain suspended in the BC fermentation medium for a short time. After being precipitated, the particles cannot be entrapped in the surface BC fibers.[20] Therefore, such static *in situ* fermentation methods fail to produce BC nanocomposites due to the limited diffusion of the nanoscale units from the liquid medium to the upper surface layer of growing BC.[26]

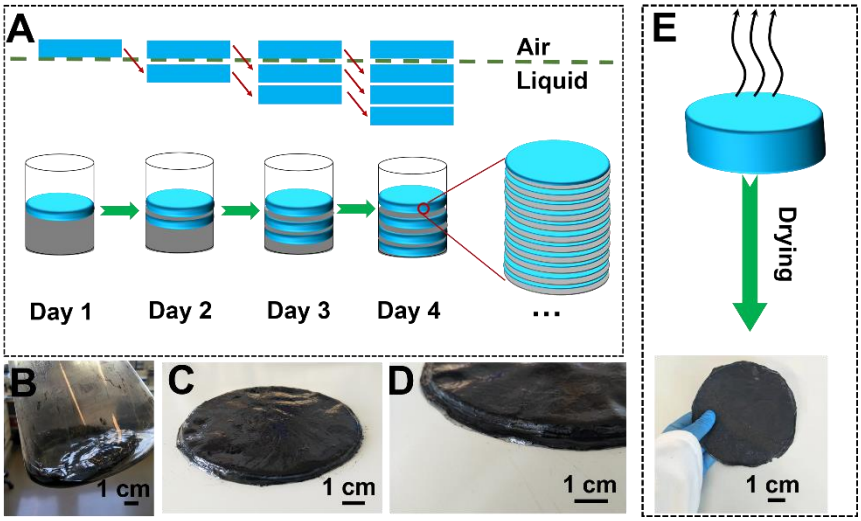

Figure 4.2 Fabrication procedure of the BC-GO-PGA composites. (A) Scheme of the fabrication method during the semi-static *in situ* fermentation, where the earlier formed layers are moved below the surface while the newly formed layers are formed at the air liquid interface; (B-D) optical images of the BC-GO-PGA composites after semi-static *in situ* fermentation; (E) the BC-GO-PGA film after drying.

Here, a BC composite material with enhanced yield is produced under mild conditions by a semi-static *in situ* fermentation method (**Figures 4.1**, **4.2**), where newly formed BC composite layers are shaken below the air-liquid interface once a day by simply moving the fermentation flask. A bacterially produced biopolymer, PGA, as well as GO are added to the initial fermentation medium. Due to the combined effect of PGA and GO, the yield (wet thickness) of the resulting material increases significantly. The yield is even slightly higher than when pure BC is produced, which is hardly achievable by other static *in situ* fermentation methods, where the wet thickness of the final composites is generally reduced after the addition of a second component in the initial fermentation medium. The resulting material shows a considerably high toughness (36 MJ m^{-3}), making it one of the toughest BC membrane reported so far. Compared to other methods, this membrane is fabricated under mild conditions and shows promising features for use as the next generation of biodegradable structural high-performance materials, construction materials, and in tissue engineering applications (tendon, ligament, skin) due to its enhanced yield and scalability.

4.2 Results and Discussion

Fabrication of BC-GO-PGA composites

Compared to *ex situ* methods,[23-25] *in situ* biofabrication methods,[20] based on the addition of components into the initial fermentation medium is a straight-forward approach to incorporate other elements into the BC network. Water soluble polymers[22, 30] are widely used in static *in situ* BC fermentation since they mix readily with the bacterial medium and become trapped in the BC network. However, it is difficult to insert inorganic particles into the BC network as these particles tend to be unstable at the ionic strength required in the bacterial fermentation medium.[20] The agitated *in situ* fermentation method[32] keeps the inorganic particles suspended in the liquid medium and inserts those particles into the BC network during fermentation. However, this method can only produce small (usually less than 1 centimeter) BC pieces[33] that are dispersed in the solution, instead of a bulk BC material.

To overcome these problems, we developed a semi-static *in situ* fermentation method (**Figure 4.2A**). In an Erlenmeyer flask, PGA and GO were mixed with Hestrin-Schramm (HS) medium. The fermentation was carried out at 30 ˚C under static conditions with the cellulose producing strain *Gluconacetobacter hansenii* (*G. hansenii*). A thin layer of BC composites was formed at the air-liquid interface after 1 day of culturing. This thin layer can be submerged below the liquid level (**Figure 4.2A**) by simply shaking the Erlenmeyer flask once. The BC pellicle composites (**Figure 4.2B-D**) were obtained by daily repeating this static incubating-shaking procedure.

Compared to pure BC, the addition of PGA reduced the wet thickness of the resulting BC-PGA composite throughout the fermentation procedure (**Figure 4.3A**) from 5.4 ± 0.2 mm (day 5), 9.2 ± 0.5 mm (day 10), and 9.8 ± 0.6 mm (day 15) for BC alone; to 1.7 ± 0.1 mm (day 5), 2.6 ± 0.1 mm (day 10) and 2.5 ± 0.2 mm (day 15) for the BC with PGA. Notably, there was no significant difference in wet thickness values between 10 days and 15 days of fermentation (**Figure 4.3A**), both with and without PGA. Therefore, a period of 10 days was selected as fermentation time for all other composites produced in this study.

To assess whether the GO content and the addition of PGA influence the yield of the composite materials produced, wet thicknesses were measured after 10 days of fermentation (**Figure 4.3B-F**). The wet thickness values dropped from 10 ± 1 mm to 5.0 ± 0.2 mm when the GO content in the fermentation medium was increased from 0.03 mg mL^{-1} to 0.67 mg mL^{-1} without any PGA in the medium (**Figure 4.3B**, **E**, **S4.1**). Although higher yield (wet thickness) could be obtained at lower GO concentration (0.03 mg mL^{-1}), sedimentation

(**Figure 4.3E**, **F**) occurred at lower GO content (0.03 mg mL^{-1}) in the fermentation medium. At 0.03 mg mL^{-1} GO content, the bottom surface of the BC composite material, which is the surface in contact with the solution, showed a yellow color (**Figure 4.3C**, similar to that of pure BC), suggesting that the GO particles cannot be incorporated into the BC network. However, at higher GO concentration (0.67 mg mL^{-1}), the BC composites showed a black color on their bottom surface (**Figure 4.3C**), which indicates that GO particles were successfully incorporated into the BC network. Therefore, the entrapment of GO into the BC network only happens at high enough GO concentration, where the yield of the final composites is significantly reduced. These conflicting properties restrain the *in situ* biofabrication of BC-GO composites.

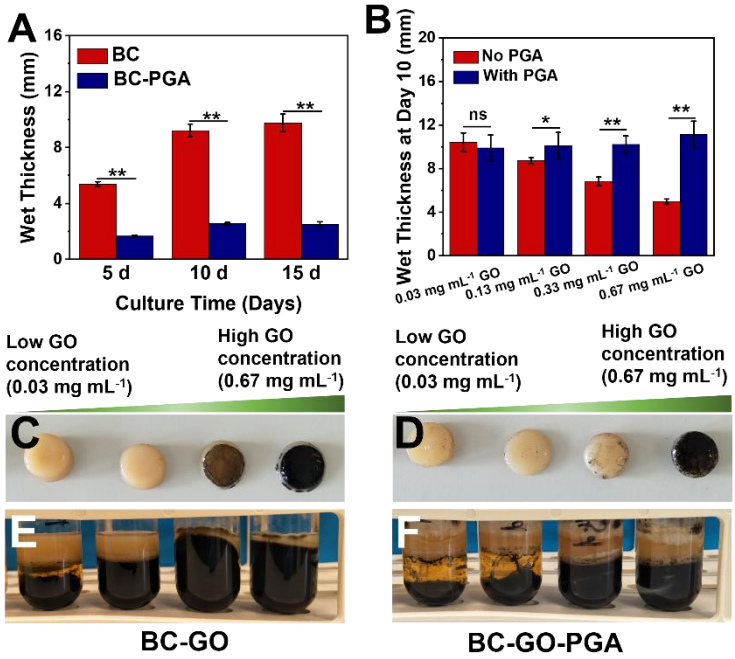

Figure 4.3 Yield of the BC-GO composites during *in situ* fermentation. (A) Wet thickness over the course of fermentation (with and without the addition of PGA) at different time points. (B) Comparison of the wet thickness with different GO concentrations in the initial fermentation medium (after 10 days of culturing). (C-D) Optical images of the BC-GO composites (bottom side, which is in contact with the liquid) without (C) and with (D) PGA at different GO concentrations (from left to right: 0.03 mg mL^{-1}, 0.13 mg mL^{-1}, 0.33 mg mL^{-1}, 0.67 mg mL^{-1}) in the initial fermentation medium after 10 days of *in situ* fermentation. (E-F) Optical images of the fermentation broth without (E) and with (F) PGA after 10 days of static culturing. * $p < 0.05$, ** $p < 0.01$, significant; *ns*: not significant.

Interestingly, the addition of PGA to the fermentation medium resulted in the formation of BC-GO-PGA composites (**Figure 4.3B**, **F**, **S4.1**). The wet thickness of BC-GO-PGA composites showed similar values at low and high GO concentrations, *i.e.*, a thickness of 10 ± 1 mm at 0.03 mg mL^{-1} GO and 11 ± 1 mm at 0.67 mg mL^{-1} GO. Both BC-PGA (2.6 ± 0.1 mm) and BC-GO similarly showed reduced wet thicknesses compared to that of pure BC (9.2 ± 0.5 mm), while the synergistic addition of PGA together with GO resulted in an increase in wet thicknesses for BC-GO-PGA, reaching values varying from 10 ± 1 mm to 11 ± 1 mm (**Figure 4.3B**).

The synergistic effect of PGA and GO on the yield of the final composite can be explained by a reduction of BC crystallinity. The crystallization process was shown to be a rate limiting step during BC production.[34] Negatively charged water-soluble polymers have been used as additives to enhance the yield by reducing BC crystallinity.[35] These polymers can absorb *via* hydrogen bonds onto BC microfibrils, and their negatively charged groups thus prevent the aggregation BC microfibrils due to electrostatic repulsion.[36] In our situation, the addition of negatively charged PGA failed to increase the yield, most likely because it increased significantly the viscosity of the fermentation medium. The polymer viscosity influences the diffusion of water-soluble polymers into the BC microfibril network. When GO was added to the fermentation medium together with PGA, the medium viscosity was reduced compared to PGA alone, thus promoting the diffusion of PGA onto the surface of each BC microfibril, resulting in the reduction of crystallinity and the enhanced yield of the final composites.

At high GO concentration (0.67 mg mL^{-1}), BC-GO-PGA showed enhanced yield (**Figure 4.3B**) and GO particles could be entrapped into the BC network (**Figure 4.3D**), however only a small fraction of the full thickness of BC-GO-PGA composites presented a mixed structure, manifested by a black color (**Figure 4.3C**, **E**, **D**, **F**). This is because the top layer of the composite (**Figure 4.3E**, **F**) was not in contact with GO in the fermentation medium.

To solve this problem, we used a semi-static fermentation method (**Figure 4.2**). After one day of static culturing, a thin layer of BC-GO-PGA composite was formed. We then gently shook the flask containing this thin layer of BC-GO-PGA film at the air-liquid interface to position the film below the liquid level and left the fermentation flask static for another day. This allowed the grown BC to contact the GO containing fermentation medium and form new BC-GO-PGA layers. After 10 days of daily treatment (once a day), BC-GO-PGA composites could be formed, with a completely colored hydrogel-like morphology (**Figures 4.2B-D**, **4.4E**).

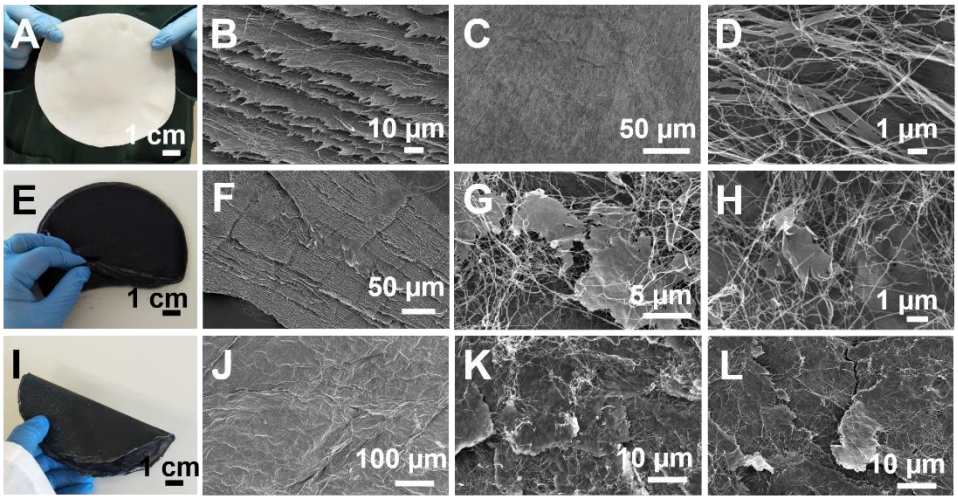

Figure 4.4 Characterization of layered composites. (A) Optical image of BC-PGA wet hydrogel by *in situ* fermentation before drying. SEM images of (B) the cross-section, (C) surface morphology and (D) fiber morphology of the BC-PGA composite material after drying. Optical images of the *in situ* fermented BC-PGA-GO composite material (E) before and (I) after drying. SEM images of (F-H) the cross-section morphology and (J-L) the surface morphology of the *in situ* fermented BC-GO-PGA composites after drying in air.

Morphology of the BC-GO-PGA composites

After an *in situ* fermentation procedure, the fermented BC composites would normally be purified following the traditional BC purification method, where BC pellicles are boiled with 1 *w/v*% of sodium hydroxide (NaOH) solution and washed with distilled water.[37] This method, however, might result in the loss of PGA during the washing step due to its water-soluble nature.[38] To keep PGA within the fermented BC network, we used a calcium chloride ($CaCl_2 \cdot 2H_2O$) solution, instead of NaOH, when boiling the fermented composites. During this process, calcium ions (Ca^{2+}) can bind with the carboxyl groups (-COOH) in the PGA backbone to form a complex that resists solubilization in water. Fourier-transform infrared spectroscopy (FTIR) results (**Figure S4.2**) confirm the presence of PGA in the final composites. Furthermore, "freezing-thawing" (FT) procedures have been proven to be an effective way of improving the crystallinity and tensile properties of BC composites.[39] Therefore, after the boiling procedure with Ca^{2+},[40] we treated our specimens with a FT process, where the BC composites were placed inside a -20˚C freezer during 24 hours and then thawed at room temperature for 6 hours. After repeating this FT process 5 times, the BC composites were washed with water until the pH of the water reaches 7. Hereafter, we refer

to this whole post-treatment procedure as "CaFT". After this CaFT procedure, the BC wet pellicles were air-dried in the fume hood to form the final composite material (**Figure 4.4I**). The addition of PGA did not influence the optical appearance of BC, with both BC-PGA-CaFT (**Figure 4.4A**) and pure BC (**Figure S4.3**) showing a white hydrogel-like appearance. Scanning electron microscope (SEM) images of BC-PGA-CaFT (**Figure 4.4B**, **C**, **D**) showed layered nanofibrous structures comparable to that of pure BC (**Figure S4.4**). However, after the addition of GO in the fermentation medium, the BC-GO-PGA-CaFT samples obtained *via* the semi-static method showed a black color due to the insertion of GO in the BC matrix (**Figure 4.4E**, **I**). SEM images of BC-GO-PGA-CaFT (**Figure 4F-H**, **J-L**) showed that GO particles are inserted into the layered nanofibrous network of BC, with GO being entangled and associated with BC nanofibers (**Figure 4.4G**, **H**, **K**, **L**). It should be noted that BC-GO-PGA-CaFT dried films showed a wrinkled surface morphology (**Figure 4.4J**) while the surface morphology of BC-PGA-CaFT dried films was rather smooth (**Figure 4.4C**). The formation of this wrinkled structure in the GO containing sample is likely due to the large surface area of GO flakes, which tend to become curly, aggregate and absorb on the surface of BC fibers.[41, 42]

Thermogravimetric analysis (TGA) curves (**Figure S4.5**) showed that the residual mass values of BC-GO-CaFT and BC-GO-PGA-CaFT lie between the ones of pure GO and BC-PGA-CaFT, confirming the presence of GO in the final composites. The GO content in the final composites can be calculated based on the residual mass ratio of TGA curves,[26] and the BC-GO-PGA dried films showed a ~50 *wt*% GO content. X-ray diffraction (XRD) analysis (**Figure S4.6**) revealed that the peaks present in the BC-GO-PGA-CaFT sample become less sharp compared to those of BC-PGA-CaFT, thus further confirming the presence of GO in the final composites.

Tensile properties of the BC-GO-PGA composites

To assess whether the post treatment methods have any influence on the mechanical properties of BC-PGA composites, tensile tests were carried out. After 10 days of static fermentation in presence of PGA, the BC wet pellicles were treated using 4 different methods: (1) by simply boiling in water (BC-PGA-water), (2) by boiling in a $CaCl_2 \cdot 2H_2O$ solution (BC-PGA-Ca), (3) by boiling in water followed by the FT procedure (BC-PGA-FT), or (4) by a combination of boiling in a $CaCl_2 \cdot 2H_2O$ solution followed by the FT procedure (BC-PGA-CaFT). The tensile tests (**Figure 4.5A**) show that the CaFT post-treatment procedure increased both the ultimate tensile strength and the elongation at break of the BC-PGA composites significantly. Compared to BC-PGA boiled in water (BC-PGA-water), BC-PGA-

CaFT showed a 36 % increase in ultimate tensile strength (from 180 ± 20 MPa to 250 ± 20 MPa) and a 72 % increase in elongation at break (from 5.1 ± 0.8 % to 8.7 ± 0.5 %) (**Table S4.1**). Due to the beneficial effect of CaFT on tensile properties of BC-PGA composites, all the GO-containing specimens were post-treated with the CaFT method.

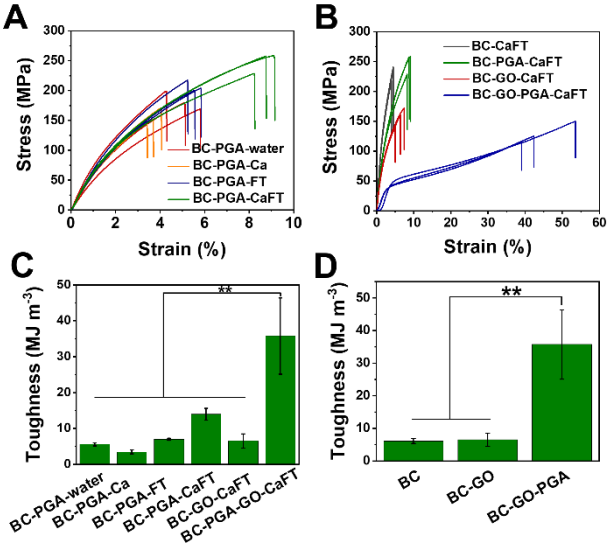

Figure 4.5 Tensile properties of the composite materials. (A) Stress-strain curves of BC-PGA composites with different post treatment methods after *in situ* fermentation. (B) Stress-strains curves of the fermented composites after CaFT treatment. (C) Comparison of toughness values of the BC-GO-PGA composite with other specimens. (D) Comparison of toughness values of BC, BC-GO and BC-GO-PGA. These three specimen types are treated with CaFT. ** $p < 0.01$, significant.

From the previous analysis, we could demonstrate that GO inserts into the BC network when the GO content in the initial fermentation broth was 0.67 mg mL^{-1}, therefore we used 0.67 mg mL^{-1} of GO here. After 10 days of semi-static *in situ* fermentation, BC-GO composites with and without PGA were post-treated with the CaFT procedure. Tensile tests (**Figure 4.5B**) revealed that BC-GO-PGA-CaFT showed a significant increase in elongation at break value (45 ± 8 %) compared to BC-CaFT (4.3 ± 0.3 %), BC-PGA-CaFT (8.7 ± 0.5 %) and BC-GO-CaFT (8.7 ± 0.5 %). A lower elastic modulus value was obtained for BC-GO-PGA-CaFT dried films (1.8 ± 0.4 GPa, **Table S4.1**) compared to BC-PGA-CaFT (7.2 ± 2.2 GPa) and BC-CaFT (10 ± 2 GPa). Furthermore, the overall toughness value of BC-GO-PGA-CaFT reached up to 36 ± 11 MJ m^{-3}, which is significantly higher than all other specimens (**Figure 4.5C-D**, **Table S4.1**).

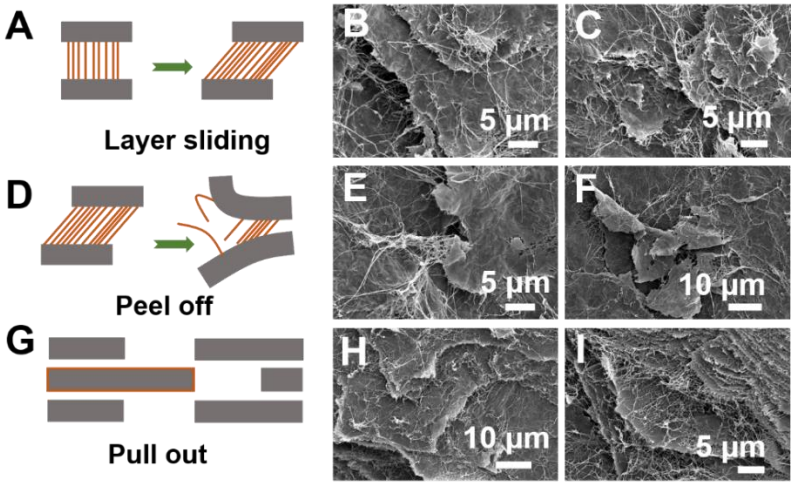

Figure 4.6 Proposed breaking mechanism of the BC-GO-PGA composites. (A-C) Layer sliding, (D-F) peel off and (G-I) pull out morphologies are observed from SEM of the failure cross-section.

The considerably higher toughness for BC-GO-PGA-CaFT dried film samples is explained by the higher elongation at break. To understand the underlying mechanism behind this increase in elongation at break, the cross-section morphology of BC-GO-PGA-CaFT dried films after tensile testing were examined (**Figure 4.6**). Instead of a catastrophic failure, BC-GO-PGA-CaFT dried films showed a progressive failure morphology, with layer sliding[43] (**Figure 4.6A-C**), peel off[44] (**Figure 4.6D-F**) and pull out[43] (**Figure 4.6G-I**) morphologies observed. Additionally, BC-GO-PGA-CaFT dried films showed a wrinkled surface morphology (**Figure 4.4J**), and during the tensile testing, the wrinkles might extend and absorb energy, thus increasing the elongation at break. Therefore, the wrinkled structure might also be one of the reasons for the high toughness values. Moreover, the addition of PGA itself can also contribute to the increase in toughness, as shown previously for other types of composites,[45, 46] since BC-PGA-CaFT showed higher toughness (**Table S4.1**, 14 ± 2 MJ m^{-3}) than BC-CaFT (6.1 ± 0.8 MJ m^{-3}). In summary, the combined effects of several mechanisms including a progressive failure accompanied by layer sliding, peel off and pull out, a wrinkled morphology, as well as the addition of PGA, could all contribute to the fact that the BC-GO-PGA-CaFT dried film were significantly tougher compared to the other specimens.

Comparison with other BC based materials

Because of its layered nanofibrous structure, and its mild and scalable production capability, BC draws increasing attention for the fabrication of bioinspired high-performance structural materials.[17, 47, 48] To insert other components into the BC fibrous network, multiple methods, including mechanical disintegration,[23-25] *in situ* post impregnation,[37] *in situ* vacuum filtration[28] and *in situ* fermentation,[48] are being developed. Among these methods, *in situ* fermentation is the most promising method,[20] as it is less energy consuming, carried out in mild conditions and can easily achieve a homogeneous distribution of other components into the BC network. However, it is problematic to insert inorganic particles into the BC network with a static *in situ* fermentation method, due to the limited diffusion of these particles to the air-liquid interface.[26] Compared to all these BC composites fabrication methods, the semi-static *in situ* fermentation method in this study provides an easily implemented approach to incorporate inorganic particles into a BC nanofibrous network. Due to the addition of PGA, the yield of final composite material increases significantly and the BC-GO-PGA shows a relatively high yield compared to other BC based composites produced *via in situ* fermentation (**Table S4.2**). The BC-GO-PGA-CaFT specimens show an excellent toughness value (36 MJ m^{-3}), which is among the highest reported for BC composites and BC based high performance materials so far (**Table 4.1**).

Table 4.1 Comparison of toughness values among the cellulose-based film materials.

type of cellulose-based film	tensile toughness [MJ m^{-3}]	references
Alkali treated cellulose	6.3	49
BC-GO	8.2	47
CNF (cellulose nanofiber)-GO	14	50
Wet stretched and hot-pressed BC	25	51
Double-cross-linked cellulose	28	52
Hot pressed and tap-peeled BC	36	53
Anisotropic plant cellulose	41	54
BC-PGA-CaFT	14	This work
BC-GO-PGA-CaFT	36	This work

4.3 Conclusions

A BC-GO-PGA composite material with a bioinspired layered morphology was prepared following a semi-static *in situ* fermentation method. This BC-GO-PGA composite material is one of the toughest BC composite membranes reported. GO particles were inserted successfully into the BC nanofibrous structure by a daily shaking procedure. Notably, after the addition of the bacterial polymer PGA, the yield (wet thickness) of the final BC composites increased significantly, which is hardly achievable by other static *in situ* fermentation methods, where the wet thickness of the final composites is generally reduced after the addition of components in the initial fermentation medium. Compared to other methods, this approach is mild and easily scalable. BC and PGA are both bacterially produced, making this an environmentally friendly biofabrication method for bioinspired high-performance structural materials. Due to these advantages, this material shows promising applications as protective garments, or as biodegradable structural high-performance materials, construction materials and tissue engineering scaffolds (tendon, ligament, skin) that require high toughness.

4.4 References

1. Mohanty, A. K.; Vivekanandhan, S.; Pin, J.-M.; Misra, M. Composites from Renewable and Sustainable Resources: Challenges and Innovations. Science 2018, *362*, 536.

2. Meereboer, K. W.; Misra, M.; Mohanty, A. K. Review of Recent Advances in the Biodegradability of Polyhydroxyalkanoate (PHA) Bioplastics and Their Composites. Green Chem. 2020, *22*, 5519-5558.

3. Zhu, Y.; Romain, C.; Williams, C. K. Sustainable Polymers from Renewable Resources. Nature 2016, *540* (7633), 354-362.

4. Ray, U.; Zhu, S.; Pang, Z.; Li, T. Mechanics Design in Cellulose-Enabled High-Performance Functional Materials. Adv. Mater. 2020, 2002504.

5. Bai, L.; Kamarainen, T.; Xiang, W.; Majoinen, J.; Seitsonen, J.; Grande, R.; Huan, S.; Liu, L.; Fan, Y.; Rojas, O. J. Chirality from Cryo-Electron Tomograms of Nanocrystals Obtained by Lateral Disassembly and Surface Etching of Never-Dried Chitin. ACS nano 2020, *14* (6), 6921-6930.

6. Moradali, M. F.; Rehm, B. H. A. Bacterial Biopolymers: From Pathogenesis to Advanced Materials. Nat. Rev. Microbiol. 2020, *18* (4), 195-210.

7. Yoshioka, T.; Tsubota, T.; Tashiro, K.; Jouraku, A.; Kameda, T. A Study of the Extraordinarily Strong and Tough Silk Produced by Bagworms. Nat. Commun. 2019, *10* (1), 1469.

8. Ling, S.; Chen, W.; Fan, Y.; Zheng, K.; Jin, K.; Yu, H.; Buehler, M. J.; Kaplan, D. L. Biopolymer Nanofibrils: Structure, Modeling, Preparation, and Applications. Prog. Polym. Sci. 2018, *85*, 1-56.

9. Tu, H.; Zhu, M.; Duan, B.; Zhang, L. Recent Progress in High-Strength and Robust Regenerated Cellulose Materials. Adv. Mater. 2020, 2000682.

10. Kontturi, E.; Laaksonen, P.; Linder, M. B.; Nonappa; Groschel, A. H.; Rojas, O. J.; Ikkala, O. Advanced Materials through Assembly of Nanocelluloses. Adv. Mater. 2018, *30* (24), 1703779.

11. Gromovykh, T. I.; Pigaleva, M. A.; Gallyamov, M. O.; Ivanenko, I. P.; Ozerova, K. E.; Kharitonova, E. P.; Bahman, M.; Feldman, N. B.; Lutsenko, S. V.; Kiselyova, O. I. Structural Organization of Bacterial Cellulose: The Origin of Anisotropy and Layered Structures. Carbohydr. Polym. 2020, *237*, 116140.

12. Khakalo, A.; Tanaka, A.; Korpela, A.; Orelma, H. Delignification and Ionic Liquid Treatment of Wood toward Multifunctional High-Performance Structural Materials. ACS Appl. Mater. Interfaces 2020, *12* (20), 23532-23542.

13. Florea, M.; Reeve, B.; Abbott, J.; Freemont, P. S.; Ellis, T. Genome Sequence and Plasmid Transformation of the Model High-Yield Bacterial Cellulose Producer *Gluconacetobacter hansenii* ATCC 53582. Sci. Rep. 2016, *6*, 23635.

14. Gao, M.; Li, J.; Bao, Z.; Hu, M.; Nian, R.; Feng, D.; An, D.; Li, X.; Xian, M.; Zhang, H. A Natural In Situ Fabrication Method of Functional Bacterial Cellulose Using a Microorganism. Nat. Commun. 2019, *10* (1), 437.

15. Ma, L.; Bi, Z.; Xue, Y.; Zhang, W.; Huang, Q.; Zhang, L.; Huang, Y. Bacterial Cellulose: An Encouraging Eco-Friendly Nano-Candidate for Energy Storage and Energy Conversion. J. Mater. Chem. A 2020, *8* (12), 5812-5842.

16. Wang, J.; Tavakoli, J.; Tang, Y. Bacterial Cellulose Production, Properties and Applications with Different Culture Methods - A Review. Carbohydr. Polym. 2019, *219*, 63-76.

17. Guan, Q.-F.; Ling, Z.-C.; Han, Z.-M.; Yang, H.-B.; Yu, S.-H. Ultra-Strong, Ultra-Tough, Transparent, and Sustainable Nanocomposite Films for Plastic Substitute. Matter 2020, *3*, 1-10.

18. Yu, K.; Balasubramanian, S.; Pahlavani, H.; Mirzaali, M. J.; Zadpoor, A. A.; Aubin-Tam, M. E. Spiral Honeycomb Microstructured Bacterial Cellulose for Increased Strength and Toughness. ACS Appl. Mater. Interfaces 2020, *12* (45), 50748-50755.

19. de Oliveira Barud, H. G.; da Silva, R. R.; da Silva Barud, H.; Tercjak, A.; Gutierrez, J.; Lustri, W. R.; de Oliveira, O. B. J.; Ribeiro, S. J. L. A Multipurpose Natural and Renewable Polymer in Medical Applications: Bacterial Cellulose. Carbohydr. Polym. 2016, *153*, 406-420.

20. Shah, N.; Ul-Islam, M.; Khattak, W. A.; Park, J. K. Overview of Bacterial Cellulose Composites: A Multipurpose Advanced Material. Carbohydr. Polym. 2013, *98* (2), 1585-1598.

21. Eichhorn, S. J.; Dufresne, A.; Aranguren, M.; Marcovich, N. E.; Capadona, J. R.; Rowan, S. J.; Weder, C.; Thielemans, W.; Roman, M.; Renneckar, S.; Gindl, W.; Veigel, S.; Keckes, J.; Yano, H.; Abe, K.; Nogi, M.; Nakagaito, A. N.; Mangalam, A.; Simonsen, J.; Benight, A. S.; Bismarck, A.; Berglund, L. A.; Peijs, T. Review: Current International Research into Cellulose Nanofibres and Nanocomposites. J. Mater. Sci. 2010, *45* (1), 1-33.

22. Torres, F. G.; Arroyo, J. J.; Troncoso, O. P. Bacterial Cellulose Nanocomposites: An All-nano Type of Material. Mater. Sci. Eng. C 2019, *98*, 1277-1293.

23. Fang, Q.; Zhou, X.; Deng, W.; Zheng, Z.; Liu, Z. Freestanding Bacterial Cellulose-Graphene Oxide Composite Membranes with High Mechanical Strength for Selective Ion Permeation. Sci. Rep. 2016, *6*, 33185.

24. Zhu, Z. S.; Qu, J.; Hao, S. M.; Han, S.; Jia, K. L.; Yu, Z. Z. Alpha- Fe_2O_3 Nanodisk/Bacterial Cellulose Hybrid Membranes as High-Performance Sulfate-Radical-Based Visible Light Photocatalysts under Stirring/Flowing States. ACS Appl. Mater. Interfaces 2018, *10* (36), 30670-30679.

25. Cabañas-Romero, L. V.; Valls, C.; Valenzuela, S. V.; Roncero, M. B.; Pastor, F. I. J.; Diaz, P.; Martínez, J. Bacterial Cellulose–Chitosan Paper with Antimicrobial and Antioxidant Activities. Biomacromolecules 2020, *21* (4), 1568-1577.

26. Guan, Q.-F.; Han, Z.-M.; Luo, T.-T.; Yang, H.-B.; Liang, H.-W.; Chen, S.-M.; Wang, G.-S.; Yu, S.-H. A General Aerosol-Assisted Biosynthesis of Functional Bulk Nanocomposites. Natl. Sci. Rev. 2019, *6* (1), 64-73.

27. Yano, H.; Sugiyama, J.; Nakagaito, A. N.; Nogi, M.; Matsuura, T.; Hikita, M.; Handa, K. Optically Transparent Composites Reinforced with Networks of Bacterial Nanofibers. Adv. Mater. 2005, *17* (2), 153-155.

28. Ccorahua, R.; Troncoso, O. P.; Rodriguez, S.; Lopez, D.; Torres, F. G. Hydrazine Treatment Improves Conductivity of Bacterial Cellulose/Graphene Nanocomposites Obtained by a Novel Processing Method. Carbohydr. Polym. 2017, *171*, 68-76.

29. Ruka, D. R.; Simon, G. P.; Dean, K. M. In Situ Modifications to Bacterial Cellulose with the Water Insoluble Polymer Poly-3-Hydroxybutyrate. Carbohydr. Polym. 2013, *92* (2), 1717-1723.

30. Chen, Y.; Zhou, X.; Lin, Q.; Jiang, D. Bacterial Cellulose/Gelatin Composites: *In Situ* Preparation and Glutaraldehyde Treatment. Cellulose 2014, *21* (4), 2679-2693.

31. Luo, H.; Dong, J.; Yao, F.; Yang, Z.; Li, W.; Wang, J.; Xu, X.; Hu, J.; Wan, Y. Layer-by-Layer Assembled Bacterial Cellulose/Graphene Oxide Hydrogels with Extremely Enhanced Mechanical Properties. Nanomicro Lett. 2018, *10* (42), 1-10.

32. Nandgaonkar, A. G.; Wang, Q.; Fu, K.; Krause, W. E.; Wei, Q.; Gorga, R.; A. Lucia, L. A One-Pot Biosynthesis of Reduced Graphene Oxide (RGO)/ Bacterial Cellulose (BC) Nanocomposites. Green Chem. 2014, *16* (6), 3195-3201.

33. Campano, C.; Balea, A.; Blanco, A.; Negro, C. Enhancement of the Fermentation Process and Properties of Bacterial Cellulose: A Review. Cellulose 2015, *23* (1), 57-91.

34. Haigler, C. H.; White, A. R.; Brown, R. M. J.; Cooper, K. M. Alteration of In Vivo Cellulose Ribbon Assembly by Carboxymethylcellulose and Other Cellulose Derivatives. J. Cell Biol. 1982, *94*, 64-69.

35. Cheng, K.-C.; Catchmark, J. M.; Demirci, A. Effect of Different Additives on Bacterial Cellulose Production by Acetobacter Xylinum and Analysis of Material Property. Cellulose 2009, *16* (6), 1033-1045.

36. Hirai, A.; Tsuji, M.; Yamamoto, H.; Horii, F. *In Situ* Crystallization of Bacterial Cellulose III. Infuences of Different Polymeric Additives on the Formation of Microfibrils as Revealed by Transmission Electron Microscopy. Cellulose 1998, *5*, 201-213.

37. Cazon, P.; Vazquez, M.; Velazquez, G. Environmentally Friendly Films Combining Bacterial Cellulose, Chitosan, and Polyvinyl Alcohol: Effect of Water Activity on Barrier, Mechanical, and Optical Properties. Biomacromolecules 2020, *21* (2), 753-760.

38. Cao, M.; Feng, J.; Sirisansaneeyakul, S.; Song, C.; Chisti, Y. Genetic and Metabolic Engineering for Microbial Production of Poly-Gamma-Glutamic Acid. Biotechnol. Adv. 2018, *36* (5), 1424-1433.

39. Millon, L. E.; Wan, W. K. The Poly Vinyl Alcohol-Bacterial Cellulose System as a New Nanocomposite for Biomedical Applications. J. Biomed. Mater. Res. B Appl. Biomater. 2006, *79* (2), 245-253.

40. Butylina, S.; Geng, S.; Oksman, K. Properties of As-Prepared and Freeze-Dried Hydrogels Made from Poly(Vinyl Alcohol) and Cellulose Nanocrystals Using Freeze-Thaw Technique. Eur. Polym. J. 2016, *81*, 386-396.

41. Hu, K. M.; Liu, Y. Q.; Zhou, L. W.; Xue, Z. Y.; Peng, B.; Yan, H.; Di, Z. F.; Jiang, X. S.; Meng, G.; Zhang, W. M. Delamination‐Free Functional Graphene Surface by Multiscale, Conformal Wrinkling. Adv. Funct. Mater. 2020, *30* (34), 2003273.

42. Liu, W.; Liu, N.; Yue, Y.; Rao, J.; Cheng, F.; Su, J.; Liu, Z.; Gao, Y. Piezoresistive Pressure Sensor Based on Synergistical Innerconnect Polyvinyl Alcohol Nanowires/Wrinkled Graphene Film. Small 2018, *14* (15), 1704149.

43. Wegst, U. G. K.; Bai, H.; Saiz, E.; Tomsia, A. P.; Ritchie, R. O. Bioinspired Structural Materials. Nat. Mater. 2015, *14* (1), 23-36.

44. Alsaadi, M.; Erkliğ, A. Effect of Perlite Particle Contents on Delamination Toughness of S-Glass Fiber Reinforced Epoxy Matrix Composites. Compos. Part B: Eng. 2018, *141*, 182-190.

45. Spiesz, E. M.; Schmieden, D. T.; Grande, A. M.; Liang, K.; Schwiedrzik, J.; Natalio, F.; Michler, J.; Garcia, S. J.; Aubin-Tam, M. E.; Meyer, A. S. Bacterially Produced, Nacre-Inspired Composite Materials. Small 2019, *15* (22), 1805312.

46. Liang, K.; Spiesz, E. M.; Schmieden, D. T.; Xu, A. W.; Meyer, A. S.; Aubin-Tam, M. E. Bioproduced Polymers Self-Assemble with Graphene Oxide into Nanocomposite Films with Enhanced Mechanical Performance. ACS Nano 2020, *14* (11), 14731–14739.

47. Dhar, P.; Pratto, B.; Gonçalves Cruz, A. J.; Bankar, S. Valorization of Sugarcane Straw to Produce Highly Conductive Bacterial Cellulose / Graphene Nanocomposite Films through In Situ Fermentation: Kinetic Analysis and Property Evaluation. J. Clean. Prod. 2019, *238*, 117859.

48. Dhar, P.; Etula, J.; Bankar, S. B. In Situ Bioprocessing of Bacterial Cellulose with Graphene: Percolation Network Formation, Kinetic Analysis with Physicochemical and Structural Properties Assessment. ACS Appl. Bio Mater. 2019, *2* (9), 4052-4066.

49. Nan, F.; Nagarajan, S.; Chen, Y.; Liu, P.; Duan, Y.; Men, Y.; Zhang, J. Enhanced Toughness and Thermal Stability of Cellulose Nanocrystal Iridescent Films by Alkali Treatment. ACS Sustain. Chem. Eng. 2017, *5* (10), 8951-8958.

50. Zhang, T.; Zhang, X.; Chen, Y.; Duan, Y.; Zhang, J. Green Fabrication of Regenerated Cellulose/Graphene Films with Simultaneous Improvement of Strength and Toughness by Tailoring the Nanofiber Diameter. ACS Sustain. Chem. Eng. 2017, *6* (1), 1271-1278.

51. Wang, S.; Li, T.; Chen, C.; Kong, W.; Zhu, S.; Dai, J.; Diaz, A. J.; Hitz, E.; Solares, S. D.; Li, T.; Hu, L. Transparent, Anisotropic Biofilm with Aligned Bacterial Cellulose Nanofibers. Adv. Funct. Mater. 2018, *28* (24), 1707491.

52. Wei, P.; Huang, J.; Lu, Y.; Zhong, Y.; Men, Y.; Zhang, L.; Cai, J. Unique Stress Whitening and High-Toughness Double-Cross-Linked Cellulose Films. ACS Sustain. Chem. Eng. 2018, *7* (1), 1707-1717.

53. Wu, Z.; Chen, S.; Wu, R.; Sheng, N.; Zhang, M.; Ji, P.; Wang, H. Top-down Peeling Bacterial Cellulose to High Strength Ultrathin Films and Multifunctional Fibers. Chem. Eng. J. 2020, *391*, 123527.

54. Ye, D.; Lei, X.; Li, T.; Cheng, Q.; Chang, C.; Hu, L.; Zhang, L. Ultrahigh Tough, Super Clear, and Highly Anisotropic Nanofiber-Structured Regenerated Cellulose Films. ACS Nano 2019, *13* (4), 4843-4853.

4.5 Supplementary Information

Experimental Section

Materials, Strain and Medium:

D(+)-glucose monohydrate, and di-sodium hydrogen phosphate (≥ 99.0%) were obtained from Carl Roth GmbH. Other chemicals were purchased from Sigma-Aldrich.

The cellulose producing strain *Gluconacetobacter hansenii* (ATCC® 53582™) was inoculated in Hestrin-Schramm (HS) medium (5.0 g L^{-1} tryptone, 5.0 g L^{-1} yeast extract, 2.7 g L^{-1} disodium hydrogen phosphate, 1.5 g L^{-1} citric acid and 20 g L^{-1} glucose) at 30 ˚C under static conditions for 3 days to obtain the BC pellicle at the air-liquid interface. The inoculum for bacterial fermentation was prepared by treating the BC pellicle with cellulase from *Trichoderma reesei* (aqueous solution, ≥ 700 units g^{-1}) on a shaking platform at 180 rpm at 30 ˚C overnight. The solution was then centrifuged (4 ˚C, 3220 ×g centrifuge speed, 5 mins) to remove the cellulase and supernatant, and the bacterial pellet was re-suspended in fresh HS medium to obtain an OD_{600} of 1. A 1 *v/v* % of this solution was then used as the inoculum.

Preparation of bacterial PGA:

Overnight cultures of *Bacillus licheniformis* (*B. licheniformis* NBRC12107, NBRC, Japan) grown in BL medium (10 g L^{-1} peptone, 2 g L^{-1} yeast extract and 1 g L^{-1} $MgSO_4 \cdot H_2O$) (1.5 *v/v*%) were added to autoclaved PGA production medium (20 g L^{-1} L-glutamic acid, 13.6 g L^{-1} sodium citrate monobasic, 80 g L^{-1} glycerol, 7 g L^{-1} NH_4Cl, 0.5 g L^{-1} KH_2PO_4, 0.24 g L^{-1} $MgSO_4$, 0.04 g L^{-1} $FeCl_3 \cdot 6H_2O$, 0.15 g L^{-1} $CaCl_2 \cdot 2H_2O$, 0.1 g L^{-1} $MnSO_4 \cdot H_2O$, pH was adjusted to 7.5) and incubated at 30 ˚C for 48 hours on a platform shaking at 180 rpm. After incubation, the formed viscous PGA solution was centrifuged at × 8200 g for 15 min at 4 ˚C to remove the bacteria. The polymer solution was mixed with over twice the volume of ethanol. The precipitated PGA polymer was then dried in the oven at 50 ˚C for 2 days. The dried PGA solid polymer was UV treated overnight and dissolved into sterilized distilled water at 1 *w/v*% concentration for use.

Preparation of the fermentation medium:

The total volume of the fermentation medium was fixed at 12 mL. 8 mL of HS medium and 120 μL of bacteria were added to each glass tube. For the samples with PGA, 2 mL of 1 *w/v*% PGA solution was added. 0.05 mL, 0.1 mL, 0.5 mL or 1 mL of 8 mg mL^{-1} GO solutions were added to different tubes. Finally, sterilized distilled water was added to make sure that the total volume in each tube was exactly 12 mL. These fermentation broths with different

GO concentrations (0.03 mg mL^{-1}, 0.13 mg mL^{-1}, 0.33 mg mL^{-1}, and 0.67 mg mL^{-1}) were then incubated at 30 ˚C for 24 hours.

Semi-static in situ fermentation:

The above GO containing fermentation broths were incubated at 30 ˚C in static conditions. After a period of 24 hours, a thin film formed at the air-liquid interface. The incubation flask was gently shaken so that the solid BC pellicle was submerged below the liquid level, and the flask was left in a static position for another 24 hours of fermentation. This procedure was repeated daily until the end of the fermentation. The BC pellicle remained close to the air-liquid interface after being shaken gently, likely due to the presence of BC nanofibers in the liquid (**Figure S4.7**), which increased the density of the liquid. Unless specified, all BC pellicles in this study were prepared following this semi-static *in situ* fermentation method.

Post-treatment of the composites:

After fermentation, the solid pellet was transferred into a beaker, filled with 200 mL of 1M $CaCl_2 \cdot 2H_2O$ solution. The pellet was boiled on a heating plate for 10 mins to kill the bacteria. After cooling down, the pellet was transferred into a -20 ˚C freezer for 24 hours and then thawed at room temperature for 6 hours. After repeating this FT process 5 times, the BC composites were washed with water until the pH of the water reached 7. After this "CaFT" procedure, the BC wet pellicles were dried in the fume hood for 7 days to form the resulting composites and stored in a glass desiccator with reduced pressure for further testing. To check the moisture content, the air-dried films were further oven-dried at 50 ˚C for 48 hours. The air-dried films showed similar morphology and moisture content compared to the air-and-oven-dried films (**Figure S4.8**).

Characterization of the BC composites:

The wet thicknesses of the different composite pellicles of varying culturing times were measured with a Vernier caliper.

The materials' morphology was observed by SEM (JEOL JSM 6010 LA). The material was sputter-coated with gold-palladium at 20 mA for 60 s and was observed at 5-15 kV with SEI mode under vacuum.

FTIR (Perkin Elmer, Spectrum 100) equipped with an attenuated total reflection (ATR) accessory was carried out with the average of 20 scans in the 550-4000 cm^{-1} range at a resolution of 4 cm^{-1}.

TGA (Mettler Toledo) was performed at 30-1000 ˚C with a heating rate of 10 ˚C min^{-1} in nitrogen atmosphere. The GO content in the final BC-GO-PGA dried film was calculated by TGA[1] according to equation (4.1):

$$wt\%_{(GO)} = \frac{\varphi_0 - \varphi_{polymer}}{\varphi_{GO} - \varphi_{polymer}} \times 100\% \quad (4.1)$$

Where φ_0 is the total residual ratio of TGA for BC-GO-PGA dried film under nitrogen atmosphere, $\varphi_{polymer}$ is the residual ratio of BC-PGA dried film under the same measurement conditions, and φ_{GO} is the residual ratio of pure GO under the same testing conditions.

XRD (Bruker D8 Advance, Bruker AXS) was carried out by an Ultima III X-Ray diffractometer (Rigaku Co. Ltd., Japan). Ni-filtered Cu K_α radiation (λ = 0.1542 nm) was generated from 40 kV voltage and 40 mA current, with a LynyEye detector, Cobalt (with Iron filter) source, Bragg Brentano (reflection mode) geometry, a step size of 0.02˚ and scan speed of 2˚/min between 2θ = 5˚- 60˚.

Tensile testing:

For tensile strength testing, the samples were prepared by drying the wet pellicle in a fume hood during 7 days. These dried films were cut into rectangular shapes with dimensions of 50 × 7 mm^2 and stored into a glass desiccator with reduced pressure before tensile testing. The tensile testing was performed using a Zwick/Roell Z010 universal testing machine with a 500 N load cell and 1 kN grips. The grip distance was 10 mm and the tests were carried out with a loading rate of 2 mm min^{-1} under ambient lab conditions, with a temperature of 23 °C and 45 % humidity.

Statistics:

Statistical analyses were performed on https://astatsa.com/. The experimental groups were compared using one-way (single factor) ANOVA with post-hoc Tukey's HSD (honest significant difference) tests.

Figure S4.1 Side view of BC-GO composites obtained by *in situ* fermentation. Without PGA, the sample thickness decreases at higher GO concentration in fermentation medium. After the addition of PGA, the sample thickness remains similar at various GO concentrations. GO could penetrate into the BC network (black area) only at higher GO concentrations.

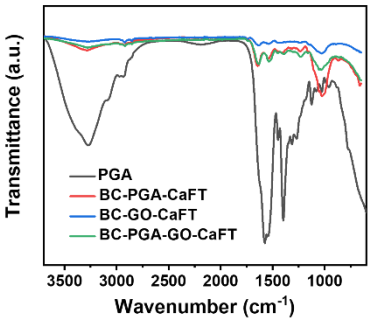

Figure S4.2 FTIR spectra of the *in situ* fermented BC composites.

Figure S4.3 Optical images of pure BC wet pellicle after treatment with CaFT.

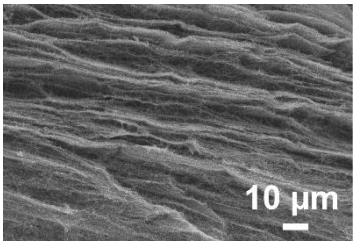

Figure S4.4 SEM image of the cross-section of a freeze-dried pure BC film.

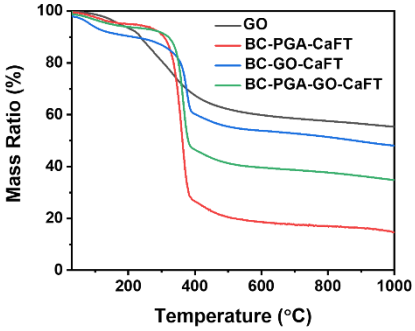

Figure S4.5 TGA curves of the *in situ* fermented BC composites.

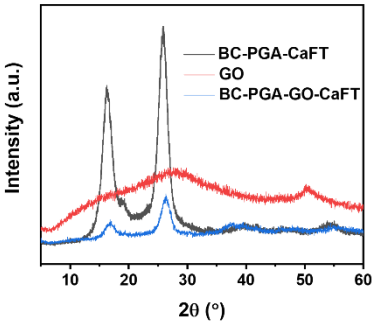

Figure S4.6 XRD spectra of the *in situ* fermented BC composites.

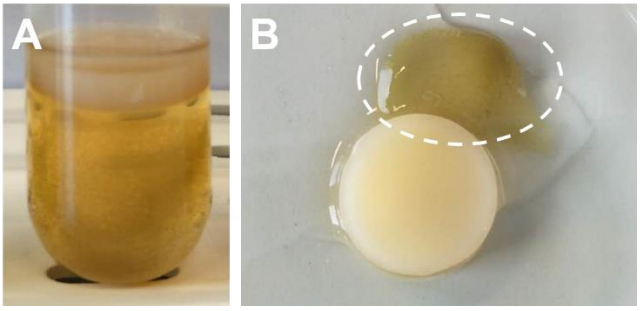

Figure S4.7 Optical images of fermented BC pellicles. (A) Tube with a solid BC pellicle floating in the liquid medium. (B) Optical image of a solid BC pellicle connected to a gel-like suspension (white dashed circle). This gel-like suspension comes from the liquid medium during fermentation.

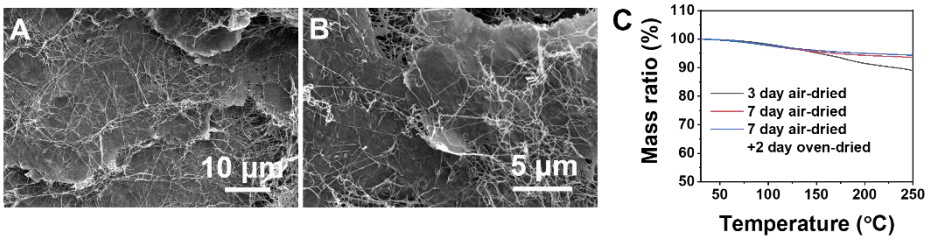

Figure S4.8 SEM images and TGA curves of air-dried (7 days) BC-GO-PGA film and air-dried and further oven dried BC-GO-PGA film. The air-dried BC-GO-PGA film (A) shows similar morphology to the air-dried and oven dried BC-GO-PGA film (B). The TGA curves (C) show that there is minimal difference from water loss.

Table S4.1 Tensile properties of *in situ* fermented BC composites (mean ± standard deviation).

Sample ID	Tensile Strength [MPa]	Elongation at Break [%]	Young's Modulus [GPa]	Toughness [MJ m^{-3}]
BC-CaFT	230.9 ± 11.9	4.3 ± 0.3	10.0 ± 2.3	6.1 ± 0.8
BC-PGA-water	182.8 ± 15.1	5.1 ± 0.8	7.1 ± 1.7	5.6 ± 0.4
BC-PGA-Ca	158.2 ± 11.1	3.7 ± 0.3	7.1 ± 2.3	3.5 ± 0.6
BC-PGA-FT	207.2 ± 9.1	5.5 ± 0.3	7.5 ± 6.4	7.0 ± 0.3
BC-PGA-CaFT	248.3 ± 17.0	8.7 ± 0.5	7.2 ± 2.2	14.0 ± 1.6
BC-GO-CaFT	157.8 ± 16.4	6.3 ± 1.2	6.1 ± 0.7	6.5 ± 2.0
BC-GO-PGA-CaFT	130.5 ± 17.4	44.9 ± 7.6	1.8 ± 0.4	35.7 ± 10.6

Table S4.2 Dry weight yield of BC based composites formed *via in situ* fermentation.

Sample ID	Dry weight yield (g L^{-1})	References
BC-Polyethylene glycol 400	2.2-5.4	2
BC-cyclodextrin	5.8-6.6	2
BC-carboxyl methyl cellulose	7.2	3
BC-Poly vinyl alcohol	3.8	4
BC-gelatin	0.5	5
BC-alginate	0.8-1.0	3
BC-PGA-CaFT	2.9	This work
BC-GO-CaFT	4.8	This work
BC-GO-PGA-CaFT	6.3	This work

References:

1. Guan, Q.-F.; Han, Z.-M.; Luo, T.-T.; Yang, H.-B.; Liang, H.-W.; Chen, S.-M.; Wang, G.-S.; Yu, S.-H. A General Aerosol-Assisted Biosynthesis of Functional Bulk Nanocomposites. Natl. Sci. Rev. 2019, *6* (1), 64-73.

2. Heßler, N.; Klemm, D. Alteration of Bacterial Nanocellulose Structure by In Situ Modification Using Polyethylene Glycol and Carbohydrate Additives. Cellulose 2009, *16* (5), 899-910.

3. Cheng, K.-C.; Catchmark, J. M.; Demirci, A. Effect of Different Additives on Bacterial Cellulose Production by *Acetobacter Xylinum* and Analysis of Material Property. Cellulose 2009, *16* (6), 1033-1045.

4. Yu, K.; Balasubramanian, S.; Pahlavani, H.; Mirzaali, M. J.; Zadpoor, A. A.; Aubin-Tam, M. E. Spiral Honeycomb Microstructured Bacterial Cellulose for Increased Strength and Toughness. ACS Appl. Mater. Interfaces 2020, *12* (45), 50748-50755.

5. Chen, Y.; Zhou, X.; Lin, Q.; Jiang, D. Bacterial Cellulose/Gelatin Composites: *In Situ* Preparation and Glutaraldehyde Treatment. Cellulose 2014, *21* (4), 2679-2693.

5

Three-dimensional Patterning of Engineered Biofilms with a Do-it-yourself Bioprinter

Abstract: Biofilms are aggregates of bacteria embedded in a self-produced spatially-patterned extracellular matrix. Bacteria within a biofilm develop enhanced antibiotic resistance, which poses potential health dangers, but can also be beneficial for environmental applications such as purification of drinking water. The further development of anti-bacterial therapeutics and biofilm-inspired applications will require the development of reproducible, engineerable methods for biofilm creation. Recently, a novel method of biofilm preparation using a modified three-dimensional (3D) printer with a bacterial ink has been developed. This article describes the steps necessary to build this efficient, low-cost 3D bioprinter that offers multiple applications in bacterially-induced materials processing. The protocol begins with an adapted commercial 3D printer in which the extruder has been replaced with a bio-ink dispenser connected to a syringe pump system enabling a controllable, continuous flow of bio-ink. To develop a bio-ink suitable for biofilm printing, engineered *Escherichia coli* bacteria were suspended in a solution of alginate, so that they solidify in contact with a surface containing calcium. The inclusion of an inducer chemical within the printing substrate drives expression of biofilm proteins within the printed bio-ink. This method enables 3D printing of various spatial patterns composed of discrete layers of printed biofilms. Such spatially-controlled biofilms can serve as model systems and can find applications in multiple fields that have a wide-ranging impact on society, including antibiotic resistance prevention or drinking water purification, among others.

The content of this chapter is based on:
Ewa M Spiesz,* **Kui Yu,*** Benjamin A. E. Lehner, Dominik T. Schmieden, Marie-Eve Aubin-Tam, Anne S. Meyer. *Journal of Visualized Experiments*, 2019, 147, e59477.
* equal contributions.

5.1 Introduction

There is currently an increasing need to develop environmentally-friendly, sustainable solutions for the production of spatially-patterned materials, due to the expanding number of markets for such materials.[1] This article presents a simple, economical method for the production of such materials and therefore offers a large spectrum of future applications. The method presented here allows three-dimensional (3D) printing of spatially-patterned structures using a bio-ink containing living bacteria. Bacteria remain viable within the printed structures for over one week, enabling the bacteria to perform natural or engineered metabolic activities. Printed bacteria can thereby produce and deposit desired components within the printed structure, for example creating a functional cross-linked biofilm.[2]

Traditional methods for the production of advanced materials involve high energy expenditures (*e.g.*, high temperatures and/or pressures) and can produce large quantities of chemical waste, often toxic substances that require cost-extensive utilization.[3, 4] In contrast, multiple bacterial species are able to produce materials that can be readily applicable in various industries. These materials include polymers such as polyhydroxyalkanoates (PHA)[5] or poly(glycolide-co-lactide) (PGLA),[6] bacterial cellulose,[7] bacterial concrete materials,[8] biomimetic composites,[9] amyloid-based adhesives,[10] or bio-based electrical switches,[11] among others. Moreover, bacterial production of valuable materials typically takes place at near-ambient temperatures and pressures and in aqueous environments, without requiring or producing toxic compounds. While producing materials with bacteria has been demonstrated in the literature and some industrial applications have already emerged,[12, 13] a reliable method for spatial patterning of such materials remains a challenge.

This article demonstrates a straight-forward method of converting a low-cost commercial 3D printer into a 3D bacterial printer. The protocol shows how to prepare a bio-ink containing and sustaining the living bacteria, as well as how to prepare substrates onto which the 3D printing can be performed. This method is appropriate to use with a variety of natural and engineered bacterial strains able to produce materials. These bacteria can be spatially distributed within a 3D printed structure and still continue their metabolic activity, which will result in a spatial distribution of the desired materials produced by the bacteria.

This printing method enables additive manufacturing of biofilms, aggregates of bacteria surrounded by a self-produced extracellular matrix. Biofilms are heterogeneous 3D networks in which proteins, polymers, bacterial cells, oxygen, and nutrients are all spatially structured.[14] While in the form of a biofilm, bacteria exhibit an increased antibiotic resistance

and structural robustness, making them difficult to eradicate from surfaces including medical catheters and implants. The key to biofilm properties, and also the largest challenge to biofilm research, seems to be the heterogeneity of biofilms.[15-17] Production of spatially-controlled model biofilms is of special interest as it would allow for either reproducing or tuning the spatial patterns of biofilm components, aiding the understanding of the stable deposition of biofilms on virtually any surface in nature.

This article presents a method for the production of biofilms using 3D-printed hydrogels containing engineered *E. coli* bacteria that produce biofilm proteins in the presence of an inducer, as well as methods of verification of biofilm formation.[2] The major extracellular matrix components of these biofilms are curli amyloid fibers[18] that contain self-assembled *CsgA* proteins. When engineered *E. coli* bacteria are induced to express *CsgA* proteins, they form a stable model biofilm that protects the cells against being washed off of the printing surface. Such a 3D printed biofilm can be spatially controlled and can serve as a useful research tool for the investigation of multiscale biofilm structure-function mechanics or materiomics.[19] These bespoke biofilms will aid the understanding of the principles of biofilm formation and their mechanical properties, enabling further research into the mechanisms of antibiotic resistance among other applications.

5.2 Protocol

Conversion of a commercial 3D printer into a 3D bioprinter

a. Remove the extruder and the heater of a commercial 3D printer (Table of Materials) from the printer frame, and unplug the wiring controlling these elements from the main circuit board (**Figure 5.1A**). Since the sensor that controls the operational temperature of the printer needs to be functional to communicate with the printer software, remove from the printing software the algorithm that delays printing until operational temperature is reached.

b. Connect a pipette tip (200 µL tip) *via* silicon tubing (inner diameter of 1 mm) to a 5 mL syringe loaded into a syringe pump. Mount the pipette tip onto the 3D printer extruder head as a replacement for the original extruder (**Figure 5.1B**).

c. If more than one type of bio-ink will be used, mount additional tubing system(s) and pipette tip(s) to the printer.

Substrate preparation for 3D printing

a. Add 4 mL of 5 M $CaCl_2$ solution to 400 mL of 1 *w/v*% agar dissolved in Luria-Bertani broth (LB) medium, supplemented with appropriate antibiotics and inducers (here 34 µg/mL chloramphenicol and 0.5 % rhamnose).

b. Dispense 20 mL of the LB-agar solution into each 150 mm × 15 mm Petri dish. Dry 30 min at room temperature with the lid half-open.

NOTE: The protocol can be paused here by storing these printing substrates at 4 °C for up to several days.

Bio-ink preparation

a. Prepare a sodium alginate solution (3 *w/v*%), and heat to the boiling point three times to sterilize the solution. Store at 4 °C until used.

b. Grow *E. coli* MG1655 PRO Δ*csgA* ompR234 (*E. coli* Δ*csgA*) bacteria carrying plasmids pSB1C3-green fluorescent protein (GFP) (constitutive GFP expression)[2] or pSB1C3-GFP-*CsgA* (constitutive GFP expression, rhamnose-inducible *CsgA* expression) overnight at 37 °C with shaking at 250 rpm in 50 mL of LB medium containing 34 μg mL^{-1} chloramphenicol and 0.5 % rhamnose.

c. Centrifuge the cell culture for 5 min at 3220 ×g to pellet the bacteria. Remove the supernatant.

d. Re-suspend the bacteria pellet in 10 mL of LB medium and add 10 mL of sodium alginate (3 *w/v*%).

3D printing process

a. Install and open the 3D printing software (Table of Materials) on a computer. Connect the 3D printer to the computer. Move the printhead to its home position by clicking the home button for the X, Y, and Z axes.

b. For each print, place a prepared printing substrate onto a particular location on the printing bed.

c. Calibrate the height of the printhead in the Z axis.

Raise the printhead to a height of 22 mm under manual control, so that it will not collide with the edge of the petri dish when moving to the desired position. Position the printhead overtop of the plate, and move it down until the pipette tip contacts the printing surface. Assign this Z-axis position as Z_1 (the height of the printing surface).

Raise the printhead, and move it outside of the plate area by manual control in the X, Y, and Z axes. If the working distance between the printhead and the plate surface is defined as Z_2, enter $Z_1 + Z_2$ into the printing program as the Z-value during printing.

d. Program the printing shape by a self-developed point-by-point coordinate-determined method according to the desired trajectory.

If the desired trajectory is a straight line, define only the start and end points. Including additional points on curved lines will result in smoother curves. Move the printhead manually to every point sequentially, and record the coordinates of these points in order. Enter all of

these coordinates as well as the printhead moving speed for each printed segment into the G-code editor.

e. Both before and after printing, lift the printhead to a distance higher than the plate edge (20 mm), and move directly out of the plate region. Save this program as a G-code file and load directly for use in subsequent prints, while re-measuring the Z axis height for each new printing substrate.

NOTE: See **Table 5.1** for an example G-code for printing a square.

Table 5.1 Programming process and explanations of G-code for printing a square.

G-code commands	Tasks
G1 Z20 F9000	Lift the z-axis to 20 mm height with 9000 mm/min moving speed.
G1 X95 Y65 F9000	Move to the starting point of the first line with 9000 mm/min moving speed.
G1 Z6 F9000	Move downwards in the z-direction to a proper (here z=6mm) printing distance.
G1 X95 Y105 F300	End point of the first line and starting point of the second line.
G1 X135 Y105	End point of the second line and starting point of the third line.
G1 X135 Y65	End point of the third line and starting point of the fourth line.
G1 X95 Y65	End point of the fourth line and the starting point of the first line; a square is formed.
G1 Z20 F9000	Lift the z-axis to 20 mm height with 9000 mm/min.
G1 X55 Y40 F9000	Move to a coordinate (55, 40) outside of the petri dish range.

f. Load the pre-programmed G-code file. Open the G-code editor in the software, and program in the commands for printing the desired shape. At each command line, the position of the printhead may be changed in the X, Y, and/or Z axis. Input the Z value during all printing steps as $Z_1 + Z_2$ (height of printing surface + working distance).

NOTE: The moving speed is also adjustable; 9000 mm min^{-1} is a suitable value for typical printing rates.

g. Load the liquid bio-ink into syringe(s), and mount them in the syringe pump(s) of the 3D bioprinter.

h. Print the bio-ink onto the printing substrate by clicking the Print button.

i. During printing, control the printhead movement entirely by the software. Manually start the syringe pump before the printhead comes into contact with the printing surface.

NOTE: The coordination of the syringe pump and the printer is empirically determined depending on the extrusion speed, the speed at which the printhead moves to the first print point, and the initial position of the printhead. If the initial printhead position is 20 mm, with a printhead speed of 9000 mm min^{-1} and an extrusion speed of 0.1 mL h^{-1}, start the syringe pump immediately after the printing is started. If the extrusion speed is changed from

0.1 mL h^{-1} to 0.3 mL h^{-1}, then wait 2−3 s to start the syringe pump after the printing is started.

j. Stop the syringe pump as soon as the printhead arrives at the last point of printing. Halt the syringe pump before the printhead lifts up at the end of the printing process, otherwise excess bio-ink will drop onto the printing substrate and reduce the printing resolution.

k. For the construction of 3D structures, control all movements of the printhead in the G-code editor. Type in the printing height of the first layer. Increase the Z-value in the G-code by 0.2 millimeters for the second layer to increase the printing height. Thereafter, increase the Z-value by 0.1 millimeters when moving to a higher layer. Do not move the plate during the printing process.

l. To measure the width and height of the printed hydrogel, use a steel ruler placed underneath or alongside the sample.

Growing and testing the effectiveness of biofilm production by E. coli

a. Incubate the printed samples at room temperature for 3−6 days to allow the production of biofilm components (curli fibers). Image the plates using a camera or fluorescent scanner.

b. To dissolve the alginate matrix, add 20 mL of 0.5 M sodium citrate solution (pH = 7 adjusted with NaOH) to the printing substrates, and incubate for 2 h with 30 rpm shaking at room temperature. Discard the liquid and image the plates again to compare with the images of the plates before citrate treatment.

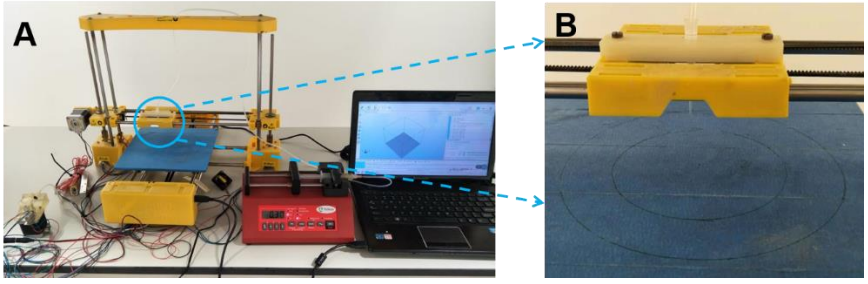

Figure 5.1 Photos showing the conversion of a commercial 3D printer into a 3D bioprinter. (A) The components of the 3D bioprinter after conversion from a commercial 3D printer. (B) The bio-ink extruder formed by a tubing system attached to a pipette tip. Additional printing tips can be added in the second printhead hole or by adding additional holes to the printhead, for use in printing multiple types of bio-ink.

5.3 Results

The first step for successful 3D printing of biofilms is converting a commercial 3D printer into a bioprinter. This conversion is achieved by removing the extruder and heater of the printer, designed for printing with a polymeric ink, and replacing these with components appropriate for printing bio-ink containing living bacteria (**Figure 5.1A**). The extruder is replaced by a pipette tip (or tips, if multiple bio-inks will be used in the printing process) attached to a tubing system connected to a syringe pump (**Figure 5.1B**). The successful conversion of the commercial printer into a bioprinter can be assessed based on the ability to transfer desired bio-ink(s) from the syringe pump through the tubing system and pipette tip(s) onto a printing surface without leaking or heating the bio-ink. If the tubing bulges due to the flow of bio-ink during printing, it may be replaced by tubing with thicker walls. It should be noted that this printing technique should be able to work with any type of commercial 3D printer for which tubing can be attached to the printhead.

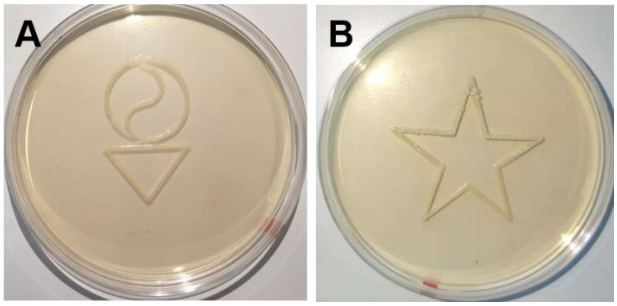

Figure 5.2 Examples of 3D bioprinted patterns containing *E. coli* pSB1C3-GFP-CsgA. These images were taken two days after printing. This printing resolution was obtained with pumping speed 0.3 mL h^{-1}, printhead movement speed 300 mm min^{-1}, and working distance 0.2 mm. The G-codes for printing these shapes may be found in the Supplemental Files.

The 3D bioprinter can create bacteria-encapsulating hydrogels in a variety of two-dimensional (2D) and 3D shapes (**Figure 5.2**). Calcium ions in the printing substrate induce solidification (chelation of calcium ions with alginate carboxyl groups) of the bio-ink upon printing, converting the liquid bio-ink into a solid hydrogel. The resolution of bioprinting will depend on the extrusion speed, the size of the pipette tip, the speed of the printhead, the volume and concentration of $CaCl_2$ solution added to the agar solution, the flatness of the printing surface, and the viscosity of the bio-ink used. The concentration of $CaCl_2$ solution

has a great influence on hydrogel sharpness. Four different concentrations of $CaCl_2$ (0.1 M, 0.2 M, 1 M, and 5 M) were sampled, and only 5 M $CaCl_2$ solution resulted in hydrogel that did not become blurred after printing. Therefore, 5 M was chosen as the optimal concentration of $CaCl_2$ solution.

In an earlier version of this protocol, the $CaCl_2$ solution was applied onto the surface of the agar plate rather than mixed into the agar solution before pouring the agar plate. When using this version, the volume of the $CaCl_2$ solution has a critical influence over printing quality and resolution. When using a 150 × 15 mm Petri dish, applying a volume of calcium chloride solution of more than 100 μL (or 30 μL for a 90-mm Petri dish) results in too much liquid remaining on the printing surface. This liquid may spread unevenly when the plate is moved, which can change the working distance and cause blockage of the pipette tip. Too much volume of $CaCl_2$ can also cause printed hydrogels to float and slide across the solution, changing the shape and position of the printed hydrogel. If the volume of calcium chloride solution is too small, some regions of the plate may not receive $CaCl_2$ solution and will have poor hydrogel solidification. In this improved protocol, adding the $CaCl_2$ solution directly into the agar solution prior to pouring the agar plate resulted in substantially less moisture on the surface of the printing substrate compared to the surface-applied method, resulting in dramatically improved printing resolution.

Table 5.2 The optimal printing parameters for hydrogels with high resolution. Five points were measured for each condition. The average value and standard deviation are shown in the table.

Extrusion speed (mL/h)	Printhead moving speed (mm/min)	Gel width (mm)
0.1	100	1.6 ± 0.1
0.1	200	1.1 ± 0.1
0.1	300	1.0 ± 0.1
0.3	300	1.8 ± 0.1
0.3	400	1.2 ± 0.1
0.3	500	0.9 ± 0.1
0.5	200	2.2 ± 0.2
0.5	1200	1.2 ± 0.2
0.7	200	2.8 ± 0.1
0.7	1200	1.3 ± 0.1

The extrusion speed and printhead movement are interdependent and can be tuned in a coordinated manner to alter the printing resolution. For example, if the printer is operated with extrusion speed between 0.1 mL h^{-1} and 0.5 mL h^{-1} with a constant printhead movement speed of 300 mm min^{-1}, the diameter of the printed hydrogel increases with the increase of extrusion speed.[2, 20] At extrusion speeds over 0.5 mL h^{-1}, the outer edges of the printed lines of hydrogel change from straight, parallel lines to wavy lines, and the line width also increases. The velocity of the printhead also has an influence on the printing resolution. With a constant extrusion speed of 0.3 mL h^{-1}, increasing the speed of the printhead from 300 mm min^{-1} to 500 mm min^{-1} results in the width of the printed hydrogel becoming narrower, decreasing from 1.8 mm to 0.9 mm. If the printhead moving speed is over 500 mm min^{-1}, the gel line will easily become discontinuous. For a 200 µL pipette tip and the bio-ink used in the current study, several combinations of the printing resolution are considered optimal (**Table 5.2**). At pumping speed 0.3 mL h^{-1}, printhead movement speed 500 mm min^{-1}, and working distance 0.2 mm, printed hydrogel is produced with a width of approximately 0.9 mm.

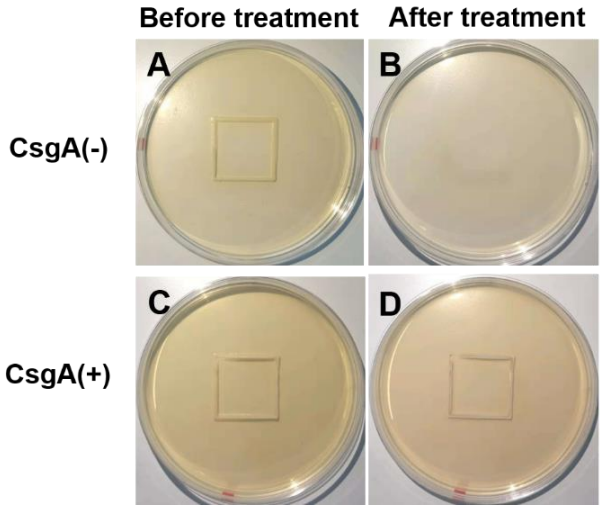

Figure 5.3 A method of verifying whether biofilm components have been produced by *E. coli* bacteria within a printed pattern. When printed *E. coli* contained a plasmid that did not encode for curli induction, the printed pattern was completely dissolved by sodium citrate treatment (A and B). When *E. coli* containing a plasmid encoding inducible curli proteins was used, the printed biofilm was resistant to sodium citrate treatment (C and D). The programming process and explanations of the G-code for printing this square pattern are provided in **Table 5.1**.

One crucial achievement of the bacterial 3D printing method is its ability to create engineered biofilms. To create an engineered and spatially-controlled biofilm, the bacteria should not only survive the 3D printing process but should also produce biofilm components while remaining within the printed pattern. The engineered *E. coli* bacteria used in this protocol, *E. coli ΔcsgA* bacteria carrying the plasmid pSB1C3-GFP-CsgA, enable controllable expression of curli proteins. The use of a csgA-knockout strain ensures that *CsgA* protein is only expressed when it is induced from a plasmid with rhamnose. The bacteria export the induced *CsgA* protein subunits, which then self-assemble[21] onto *CsgB* proteins on the bacterial outer membrane[22] to form curli fibers. These amyloid-like fibers are the major proteinaceous components of biofilm extracellular matrix: a connected network of proteins and polymers in which the bacteria are embedded. The printed alginate matrix of the 3D-printing bio-ink lends physical support and structure to the bacteria during the curli production process. The use of constitutive GFP expression allows for visualization and quantification of printed cells *via* fluorescence imaging.

In order to assess whether the formation of biofilm was successful, the alginate matrix was dissolved using a sodium citrate solution, and the shape of the printed bio-ink was assessed after the citrate treatment (**Figure 5.3**). In the case of bio-ink without the inducible curli production plasmid, the printed pattern was completely dissolved after the sodium citrate treatment, signifying that no biofilm curli network had formed (**Figure 5.3A, B**). In the case of bacteria containing the inducible curli production plasmid, the gel was not dissolved after sodium citrate treatment (**Figure 5.3C, D**). This result indicates that the printed bacteria were able to form a curli network extensive enough to stabilize the printed pattern of bacteria.[2]

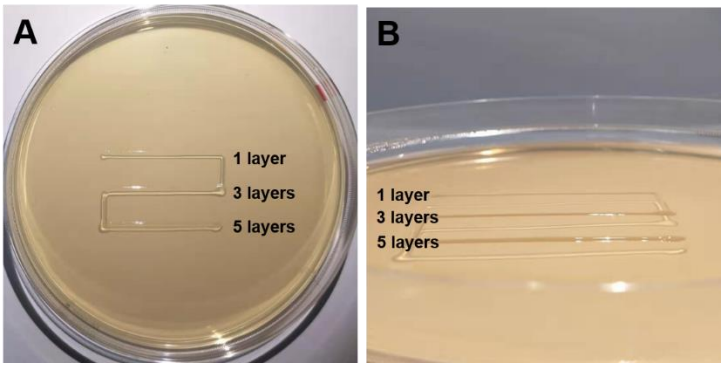

Figure 5.4 Top view (A) and side view (B) of multi-layered printed structures containing E. coli pSB1C3-GFP-CsgA. This sample was printed with pumping speed 0.3 mL h^{-1}, printhead movement speed 200 mm min^{-1}, and working distance 0.2 mm.

To construct multi-layered structures, additional layers were printed (**Figure 5.4**) by adjusting the print height and print trajectory in the G-code editor. Increasing the number of printed layers in a sample caused the width and the height of the printed structures to increase incrementally (**Figure 5.5**),[2, 20] but even 5-layer printed structures could be created with a resolution of millimeters to sub-millimeters. When *E. coli* engineered to inducibly produce curli proteins were printed into multi-layered structures, sodium citrate treatment did not dissolve the samples, whereas multi-layer structures containing non-curli-producing *E. coli* were dissolved in sodium citrate solution (**Figure 5.6**). This experiment demonstrates that engineered biofilms can be created in multi-layered, three-dimensional printed structures, as well as in single-layer printed structures.

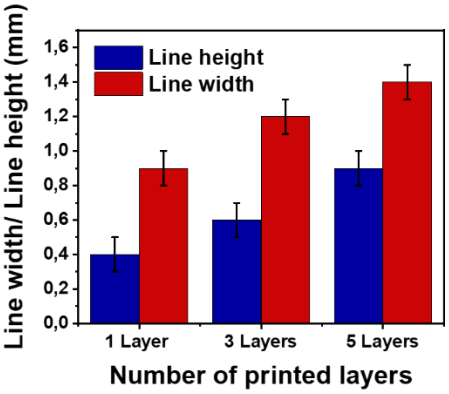

Figure 5.5 The line width and height of printed hydrogels containing different numbers of printed layers. The measurements were performed on samples printed with pumping speed 0.3 mL h^{-1}, printhead movement speed 500 mm min^{-1}, and working distance 0.2 mm.

5.4 Discussion

The protocol presented here for 3D printing of engineered biofilms has two critical steps. First is the preparation of the agar printing surface, which is the most critical factor to producing a specific printing resolution. It is important to ensure that the printing surface is flat and that the pipette tip on the printhead is positioned at the correct height from the surface. If the surface is not flat, the working distance will change during the printing process. If the working distance is less than 0.1 mm, the $CaCl_2$ solution could enter inside the pipette tip and cause hydrogel formation, causing the pipette tip to become clogged. If the working distance is more than 0.3 mm, the gel cannot be printed continuously. The optimal working distance in this study is 0.2 mm. Good approaches for preparing flat agar printing surfaces are to use

larger-diameter Petri dishes (150-mm-diameter Petri dish rather than a 90-mm-diameter plate), place the plates on a flat table, pour the agar solution with fast and even speed, and avoid moving the agar plate during its solidification.

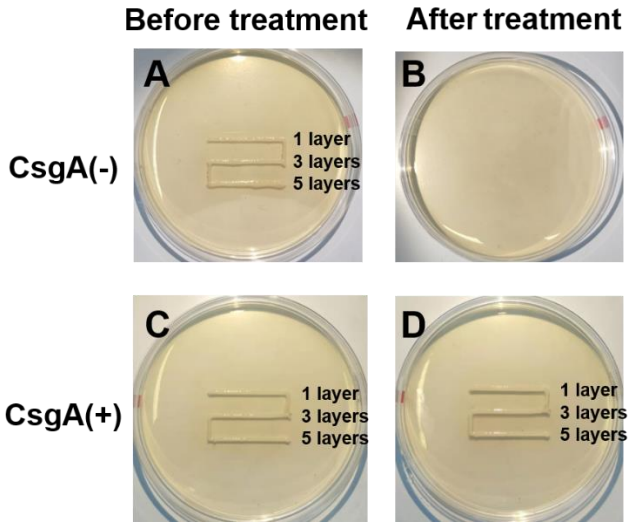

Figure 5.6 A method of verifying whether biofilm components have been produced by *E. coli* bacteria within multi-layer printed structures. Engineered *E. coli* was printed into 1-, 3-, or 5-layer hydrogels and incubated for 6 days. When the printed *E. coli* contained a plasmid that did not encode for curli induction, the printed pattern was completely dissolved by sodium citrate treatment (A and B). When the printed *E. coli* contained a plasmid encoding inducible curli proteins, the printed biofilm was resistant to sodium citrate treatment (C and D).

The second critical step is the selection of desired printing parameters including pumping speed, viscosity of the bio-ink used, and printhead speed, which determine the resulting printing resolution. To select these parameters in an efficient manner, the user can sample several extreme values for printhead speed with a constant extrusion rate, noting the width of the printed hydrogel for each set of conditions. Then, repeat this experiment with 4 other extrusion rates. Next, take the five combinations that produced the best printing resolution for the application, and vary both printing parameters (pumping and printhead speeds) in smaller and smaller steps until the desired resolution is obtained.

The thickness of the printed lines has an impact on the ability of the printed engineered bacteria to form stable biofilms. Under optimal printing conditions (pumping speed 0.3 mL h^{-1}, printhead speed 300 mm min^{-1}, and working distance 0.2 mm), printed lines of bio-ink will produce stable biofilms after 3-6 days of incubation at room temperature. If the lines

become thicker, such as by increasing the pumping speed, the middle regions of each line may not be induced sufficiently to produce citrate-stable biofilms.

When printing a multi-layer bio-ink hydrogel, each printed layer is solidified upon contacting the calcium ions that have diffused into the previous printed layer. Since the Ca^{2+} concentration in the printing substrate is high, Ca^{2+} ions can rapidly diffuse up through the lower layers. Therefore, the upper layers can be printed immediately after the previous layers have been printed, simply by adjusting the print height in the G-code editor. Additionally, the printing distance of the upper layer should be restricted to only 0.1−0.2 mm higher than the printing distance of the previous layer. If the added printing distance is less than 0.1 mm, the tip will drag across the first layer and reduce the resolution of the printed hydrogel. If the added printing distance is larger than 0.2 mm, the bio-ink will form drops of liquid during extrusion, causing the printed hydrogel to become discontinuous.

The current bioprinting approach enables the production of reproducible, spatially-controlled engineered biofilms, suitable for use in the study of biofilm mechanical properties or biological resistance of biofilm bacteria to various factors including antibiotics, surfactants, *etc*. This capability ensures a direct usability of the proposed method. The development of higher-precision do-it-yourself (DIY) bioprinters will likely be possible by maintaining the printing working distance but lowering the pumping speed and the moving speed of the printhead, or by sampling different extruder geometries and bio-ink chemistries. With future improvements to the printing resolution, additional applications can be enabled such as tissue engineering or drug delivery. The 3D bioprinting approach described here should also be able to be expanded to printing additional types of bacteria species that are biocompatible with our alginate-based bio-ink. The current protocol provides sufficient sterility by repeatedly boiling the bio-ink during preparation, using sterile syringes and printing tips, and utilizing antibiotics in both the bio-ink and printing plate. Future experiments using wild-type bacteria may require additional sterilization measures such as replacing or disinfecting the tubing system between prints.

To the authors' best knowledge, the presented method (originally developed in Lehner et al.[20]) is the first published example of an additive manufacturing style for 3D printing of bacteria. In the first part of this protocol, this general method is described in detail for the 3D printing of bacteria, which is applied to the production of engineered biofilms.[2] Multiple future applications of 3D-printed biofilms are possible using this method. In nature, multiple bacterial systems have evolved that create various types of biofilms, of which in this article a single system was explored. Multiple other systems can be easily examined by creating 3D-printed biofilms with other bacterial systems, such as *Bacillus subtilis* or *Acetobacter xylinum*.

Alternative methods[23, 24] have also been developed for spatial patterning of bacteria at high resolution using optical signals. These approaches require more expensive, complicated equipment to achieve them in comparison to this printer, and are only suitable for patterning of genetically engineered bacteria.

The ability to spatially pattern 3D-printed biofilms with this method can allow for the creation of engineered biofilms that reproduce the spatial heterogeneity of natural biofilms.[17] Because of the highly detailed arrangement of protein and polymeric fibers within a biofilm, bacteria in a biofilm state achieve a much higher resistance to chemical and physical stimuli, such as an increased resistance to antibiotics as compared to the same bacteria in a planktonic state. Moreover, bacteria within a biofilm show an increased resistance to fluid flow, making the maintenance and sterility of implantable medical devices much more difficult.[25] Printed engineered biofilms that attempt to reproduce the specific spatial distributions of biofilm components are powerful tools for studying the mechanisms by which bacteria within a biofilm achieve resistance phenotypes.

5.5 References

1. Tibbitt, M. W.; Rodell, C. B.; Burdick, J. A.; Anseth, K. S. Progress in Material Design for Biomedical Applications. Proc. Natl. Acad. Sci. USA 2015, *112* (47), 14444-14451.

2. Schmieden, D. T.; Basalo Vazquez, S. J.; Sanguesa, H.; van der Does, M.; Idema, T.; Meyer, A. S. Printing of Patterned, Engineered *E. coli* Biofilms with a Low-Cost 3D Printer. ACS Synth. Biol. 2018, *7* (5), 1328-1337.

3. Mao, L.-B. M.; Gao, H.-L.; Yao, H.-B.; Liu, L.; Cölfen, H.; Liu, G. L.; Chen, S.-M.; Li, S.-K.; Yan, Y.-X.; Liu, Y.-Y.; Yu, S.-H. Synthetic Nacre by Predesigned Matrix-Directed Mineralization. Science *354* (6308), 107-110.

4. Gao, H. L.; Chen, S. M.; Mao, L. B.; Song, Z. Q.; Yao, H. B.; Colfen, H.; Luo, X. S.; Zhang, F.; Pan, Z.; Meng, Y. F.; Ni, Y.; Yu, S. H. Mass Production of Bulk Artificial Nacre with Excellent Mechanical Properties. Nat. Commun. 2017, *8* (1), 287.

5. Poirier, Y.; Nawrath, C.; Somerville, C. Production of Polyhydroxyalkanoates, a Family of Biodegradable Plastics and Elastomers, in Bacteria and Plants. Bio Technol. 1995, *13*, 142-150.

6. Choi, S. Y.; Park, S. J.; Kim, W. J.; Yang, J. E.; Lee, H.; Shin, J.; Lee, S. Y. One-Step Fermentative Production of Poly(Lactate-co-Glycolate) from Carbohydrates in *Escherichia coli*. Nat. Biotechnol. 2016, *34* (4), 435-440.

7. Mohammadi, P.; Toivonen, M. S.; Ikkala, O.; Wagermaier, W.; Linder, M. B. Aligning Cellulose Nanofibril Dispersions for Tougher Fibers. Sci. Rep. 2017, *7* (1), 11860.

8. Jonkers, H. M. Bacteria-Based Self-Healing Concrete. Heron 2011, *56*, 1-2.

9. Schmieden, D. T.; Meyer, A. S.; Aubin-Tam, M.-E. Using Bacteria to Make Improved, Nacre-Inspired Materials. MRS Adv. 2016, *1* (8), 559-564.

10. Zhong, C.; Gurry, T.; Cheng, A. A.; Downey, J.; Deng, Z.; Stultz, C. M.; Lu, T. K. Strong Underwater Adhesives Made by Self-Assembling Multi-Protein Nanofibres. Nat. Nanotechnol. 2014, *9* (10), 858-866.

11. Chen, A. Y.; Deng, Z.; Billings, A. N.; Seker, U. O.; Lu, M. Y.; Citorik, R. J.; Zakeri, B.; Lu, T. K. Synthesis and Patterning of Tunable Multiscale Materials with Engineered Cells. Nat. Mater. 2014, *13* (5), 515-523.

12. Gatenholm, P.; Klemm, D. Bacterial Nanocellulose as a Renewable Material for Biomedical Applications. MRS Bull. 2011, *35* (3), 208-213.

13. Rodriguez-Carmona, E.; Villaverde, A. Nanostructured Bacterial Materials for Innovative Medicines. Trends Microbiol. 2010, *18* (9), 423-430.

14. Hung, C.; Zhou, Y.; Pinkner, J. S.; Dodson, K. W.; Crowley, J. R.; Heuser, J.; Chapman, M. R.; Hadjifrangiskou, M.; Henderson, J. P.; Hultgren, S. J. *Escherichia coli* Biofilms Have an Organized and Complex Extracellular Matrix Structure. mBio 2013, *4* (5), e00645-13.

15. Donlan, R. M.; Costerton, J. W. Biofilms: Survival Mechanisms of Clinically Relevant Microorganisms. Clin. Microbiol. Rev. 2002, *15* (2), 167-193.

16. Wu, H.; Moser, C.; Wang, H. Z.; Hoiby, N.; Song, Z. J. Strategies for Combating Bacterial Biofilm Infections. Int. J. Oral Sci. 2015, *7* (1), 1-7.

17. Stewart, P. S.; Franklin, M. J. Physiological Heterogeneity in Biofilms. Nat. Rev. Microbiol. 2008, *6* (3), 199-210.

18. Kikuchi, T.; Mizunoe, Y.; Takade, A.; Naito, S.; Yoshida, S.-i. Curli Fibers Are Required for Development of Biofilm Architecture in *Escherichia coli* K-12 and Enhance Bacterial Adherence to Human Uroepithelial Cells. Microbiol. Immunol. 2005, *49* (9), 875-884.

19. Cranford, S.; Buehler, M. J. Materiomics: Biological Protein Materials, From Nano to Macro. Nanotechnol. Sci. Appl. 2010, *3*, 127-148.

20. Lehner, B. A. E.; Schmieden, D. T.; Meyer, A. S. A Straightforward Approach for 3D Bacterial Printing. ACS Synth. Biol. 2017, *6* (7), 1124-1130.

21. Wang, X.; Smith, D. R.; Jones, J. W.; Chapman, M. R. In Vitro Polymerization of a Functional *Escherichia coli* Amyloid Protein. J. Biol. Chem. 2007, *282* (6), 3713-3719.

22. Hammar, M.; Bian, Z.; Normark, S. Nucleator-Dependent Intercellular Assembly of Adhesive Curli Organelles in *Escherichia coli*. Proc. Natl. Acad. Sci. USA 1996, *93*, 6562-6566.

23. Huang, Y.; Xia, A.; Yang, G.; Jin, F. Bioprinting Living Biofilms through Optogenetic Manipulation. ACS Synth. Biol. 2018, *7* (5), 1195-1200.

24. Jin, X.; Riedel-Kruse, I. H. Biofilm Lithography Enables High-Resolution Cell Patterning *via* Optogenetic Adhesin Expression. Proc. Natl. Acad. Sci. USA 2018, *115* (14), 3698-3703.

25. Percival, S. L.; Suleman, L.; Vuotto, C.; Donelli, G. Healthcare-Associated Infections, Medical Devices and Biofilms: Risk, Tolerance and Control. J. Med. Microbiol. 2015, *64* (Pt 4), 323-334.

6

Bioprinting of Regenerative Photosynthetic Living Materials

Abstract: Living materials, which are fabricated by encapsulating living biological cells within a non-living matrix, have gained increasing attention in recent years. Their fabrication in spatially-defined patterns that are mechanically robust is essential for their optimal functional performance but is difficult to achieve. Here a bioprinting technique employing environmentally-friendly chemistry to encapsulate microalgae within an alginate hydrogel matrix is reported. The bioprinted photosynthetic structures adopt pre-designed geometries at sub-millimeter-scale resolution. A bacterial cellulose substrate confers exceptional advantages to this living material, including strength, toughness, flexibility, robustness, and retention of physical integrity against extreme physical distortions. The bioprinted materials possess sufficient mechanical strength to be self-standing, and can be detached and reattached onto different surfaces. Bioprinted materials can survive stably for a period of at least 3 days without nutrients, and their life can be further extended by transferring them to a fresh source of nutrients within this timeframe. These bioprints are regenerative, *i.e.*, they can be reused and expanded to print additional living materials. The fabrication of the bioprinted living materials can be readily up-scaled (up to ≥ 70 x 20 cm), highlighting their potential product applications including artificial leaves, photosynthetic bio-garments, and adhesive labels.

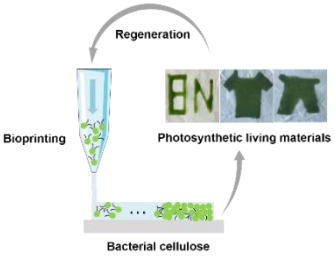

The content of this chapter is based on:
Srikkanth Balasubramanian,* **Kui Yu,*** Anne S. Meyer, Elvin Karana and Marie-Eve Aubin-Tam. *Advanced Functional Materials*, 2021, 2011162.
* equal contributions.

6.1 Introduction

Living materials are bio-hybrid structures that are composed of biological living cells (either non-engineered or genetically engineered) housed within a non-living synthetic matrix (*e.g.* organic or inorganic polymers, metals, ceramics, *etc.*).[1-3] The living cells in these materials endow them with novel functionalities such as sense-and-respond, energy production, production of high-value compounds, detoxification of harmful compounds, or self-healing capacities, among others.[1, 4, 5] Such functional living materials have been increasingly proposed for usage in potential applications including smart textiles, wearable devices, biosensors, or fermentation bioreactors.[2, 5, 6] However, controlling the spatiotemporal form of a living material, while endowing it with sufficient mechanical strength for the material to be self-standing, is hardly achievable.

3D printing has been shown to be an effective technology for the fabrication of living materials with controlled shapes and sizes. Customized living materials from nano- to macroscales can be 3D printed with high resolution into spatially defined patterns.[7-9] Materials and patterns can be designed with the aid of bioprinting such that they mimic the complex architecture, spatial organization, and time-evolving nature of living cells.[10] Living cells from different taxonomic kingdoms (including algae, bacteria, fungi, yeast, plant, and animal cells) have been effectively bioprinted for fabrication of living functional materials.[2, 11-19] Particularly, bioprinting of microalgae has gained considerable attention in the recent years.[2, 20-22] Microalgae are biotechnologically profitable unicellular microorganisms that are capable of photosynthesis.[22-25] Due to their adaptability to harsh conditions, robustness, and sustainability, microalgae have been widely used in applications such as biofuel production, bioremediation, production of high-value metabolites (food and pharmaceutical grade), and wastewater treatment,[20, 25-27] and they have been printed into silk scaffolds capable of improving air quality.[22] Bioprinting of microalgae has been predominantly performed so far using scaffolds composed of natural, cell-friendly biopolymers such as alginate,[21] carrageenan,[20] silk,[22] and starch.[28] However, these bioprinted living materials remain fragile and lack mechanical strength, for example, the tensile strength of calcium alginate film ranges between ~ 10-750 kPa,[29, 30] with toughness values ranging between ~ 2-80 J m^{-3}.[31] The fabrication of living materials that are self-standing and mechanically robust, while preserving the viability of encapsulated cells, remains a challenge.

Nature provides an inspiration for fabrication of such mechanically robust living materials.[32] Materials present in nature possess better mechanical properties than the reported

bioprinted living materials because of their hierarchical structure.[33, 34] In particular, cellulose produced by bacteria is a versatile, cell-friendly, and robust biopolymer[35-37] with excellent tensile strength (73-194 MPa)[35, 38] and toughness (2-25 MJ m^{-3}).[36, 38, 39] Bacterial cellulose is produced by the fermentation of bacteria such as *Gluconacetobacter hansenii* and *Komagataeibacter rhaeticus*.[40-42] Bacterial cellulose has a nano-fibrous architecture and absorptive capabilities,[42] which when used as a support for microalgal bioprints might allow nutrients to diffuse and reach the microalgal cells, thereby supporting their growth. Thus, we aimed to bioprint microalgae onto bacterial cellulose in order to combine the photosynthetic functionality of microalgae and the physico-mechanical properties of bacterial cellulose in the resultant living materials. Such photosynthetic self-standing living materials could be used in environmental applications such as air purification by fixing carbon dioxide and releasing oxygen and waste water treatment by trapping heavy metals and pollutants.

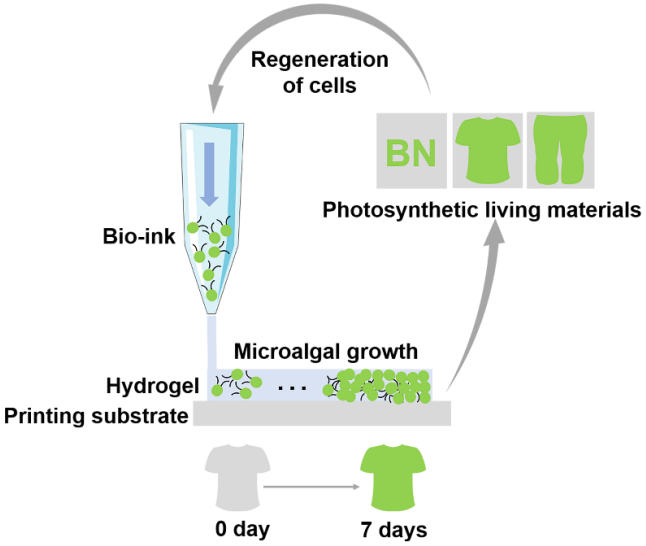

Figure 6.1 Bioprinting of photosynthetic living materials in a regenerative approach. Printing of a bio-ink (composed of sodium alginate and microalgae) onto a substrate (composed of bacterial cellulose and calcium chloride) results in the formation of an alginate hydrogel in which microalgal cells are immobilized. Placement of the bacterial cellulose overtop of a microalgal nutrient medium (minimal medium or carbon-supplemented medium) ensures microalgal growth within the bioprints on the bacterial cellulose over time. The bacterial cellulose supporting the living bioprinted microalgae can then be peeled off from the culture medium and used for various applications. Microalgal cells in the bioprints can also be regenerated and used as fresh bio-inks for further bioprinting processes.

In this study, we report a simple approach for the fabrication of living microalgal materials along with the development of cost-effective microalgal bioprinters. We employed a house-built bioprinter (**Figure S6.1**) for patterning of microalgae onto agar and bacterial cellulose substrates (**Figure 6.1**). Here we show that microalgae are capable of being bioprinted as mono- or multi-layered constructs into various pre-defined geometries and sizes. Interestingly, the bioprints can be detached from the bacterial cellulose and re-attached to a fresh bacterial cellulose surface and retain adhesion to the new surface. These bioprinted microalgal structures are resilient to physical distortions and to immersion in water, indicating their physically stable nature. The bioprinted microalgal cells exhibit high viability over a period of at least 1 month. Furthermore, the patterned microalgae in the bioprints can be regenerated for preparation of fresh bio-inks. The microalgal cells bioprinted onto bacterial cellulose could survive stably at least 3 days following removal from nutrients, with their longevity being further extended when transferred onto fresh agar. Overall, these regenerative photosynthetic living materials of microalgae bioprinted overtop of bacterial cellulose offer diverse possibilities for novel product applications including artificial leaves, photosynthetic bio-garments, and adhesive labels.

6.2 Results

Living materials can be 3D printed by depositing living cells (bio-ink) onto a non-living matrix (substrate) in a layer-by-layer fashion. Both the bio-ink composition and the nature of the printing substrate play an important role in maintaining the viability and functionality of cells in the resultant bioprinted materials as well as maintaining the overall 3D structure.

Optimal growth conditions for C. reinhardtii and their temporality in bioprinted materials over time

We investigated the growth of the microalgae *Chlamydomonas reinhardtii* (*C. reinhardtii*) on bacterial cellulose. *C. reinhardtii* can grow photoautotrophically (on CO_2 as a carbon source in the presence of light), chemotrophically/heterotrophically in the absence of light (on alternate carbon sources like acetate), or photomixotrophically (a combination of these two growth modes).[43, 44] In addition, cellulose has been demonstrated to be an alternative carbon source for the growth of *C. reinhardtii* under photomixotrophic conditions.[45] However, the growth of microalgae on bacterial cellulose has not been evaluated so far. Thus, we evaluated the growth of microalgae on bacterial cellulose when placed overtop of carbon-supplemented agar and found that microalgae can grow on bacterial cellulose in photomixotrophic condition (**Figure S6.2**). Bacterial cellulose has a nano-fibrous

architecture and absorptive capabilities,[42] which might allow the nutrients to diffuse and reach the microalgal cells, thereby supporting the microalgal growth.

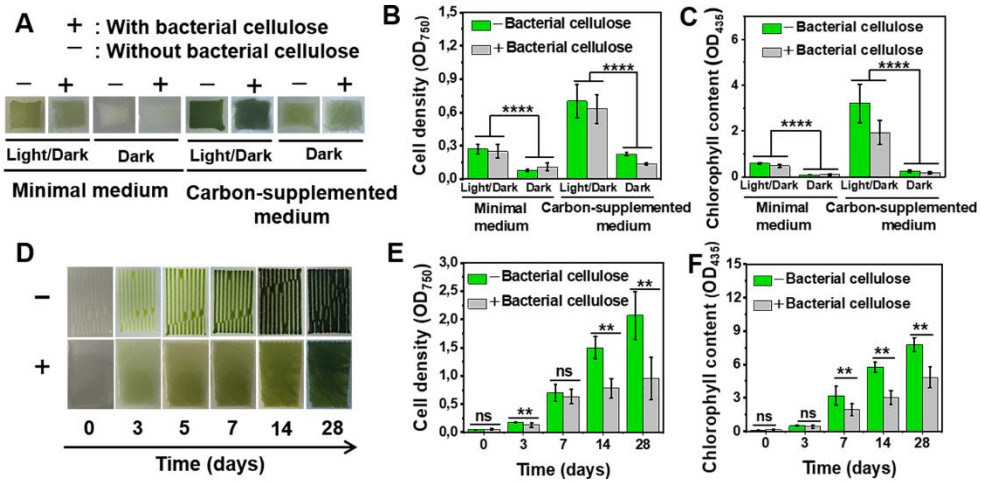

Figure 6.2 Optimal growth conditions and temporality of bioprinted microalgal materials. Bioprinted microalgae on agar (minimal medium and carbon-supplemented, indicated as "– bacterial cellulose") and on bacterial cellulose overtop of agar (minimal medium and carbon-supplemented, indicated as "+ bacterial cellulose") under light/dark and dark conditions (7 days of cultivation) were analyzed by **(A)** photographs (- : printed directly on agar without bacterial cellulose; + : printed on bacterial cellulose overtop of agar), **(B)** cell density measurement ($O.D._{750}$), and **(C)** chlorophyll content measurement ($O.D._{435}$). Growth of bioprinted microalgae over time was measured by **(D)** photographs (- : printed directly onto agar without bacterial cellulose; + : printed onto bacterial cellulose overtop of agar), **(E)** cell density measurements ($O.D._{750}$), and **(F)** chlorophyll measurements ($O.D._{435}$) during cultivation under photomixotrophic conditions. Sterile sodium chloride (0.9 *w/v*%) and DMSO served as the controls in the (**B** and **E**) cell density and (**C** and **F**) chlorophyll measurements, respectively. ns, not significant, ** $p < 0.01$ as determined by one-way (single factor) ANOVA with post-hoc Tukey's HSD, **** $p < 0.0001$ as determined by two-way ANOVA.

We then determined the optimal conditions that yield the maximum microalgal cell growth and chlorophyll content within bioprinted structures on agar (minimal or carbon-supplemented) or bacterial cellulose placed overtop of minimal or carbon-supplemented agar. Bioprints grown photomixotrophically (**Figure 6.2**) either on agar (carbon-supplemented, light/dark condition) or on bacterial cellulose (overtop of carbon-supplemented agar, light/dark condition) had the most intense green coloration (**Figure 6.2A**) and yielded the maximum cell density (**Figure 6.2B**) and chlorophyll content in comparison with the

photoautotrophic and chemotrophic conditions (**Figure 6.2C**). Incubation under dark condition (minimal medium agar) yielded no visible growth in the samples, due to the absence of carbon source and light. Thus, the photomixotrophic growth condition was seen to be optimal for growth of microalgae in the bioprints and was used in all further experiments.

The viability of bioprinted microalgal materials was investigated over time visually as well as by cell density ($O.D._{750}$) and chlorophyll ($O.D._{435}$) measurements at regular intervals of time for a total period of 4 weeks (**Figure 6.2D-F**). Immediately after printing (day 0), the calcium-alginate hydrogel matrix is transparent for samples both on carbon-supplemented agar or on bacterial cellulose overtop of carbon-supplemented agar. After 3 days of culturing, the green color of the microalgae was visible within the hydrogel matrix. Visual inspections indicated that the intensity of the green color within the bioprints increased over time (**Figure 6.2D**), consistent with results from microalgal cell density measurements, indicating a steady increase in cell density (**Figure 6.2E**). For samples bioprinted onto agar, cell density within the bioprints increased steadily throughout the 28-day incubation period, whereas samples printed onto bacterial cellulose grew more slowly and reached maximum cell density after 14 days of incubation.

Chlorophyll content of the microalgal cells within the bioprints was observed by imaging the red fluorescence of chlorophyll induced upon UV excitation[46] (**Figure S6.3**) and by chlorophyll content measurement (**Figure 6.2F**). Chlorophyll content in the bioprinted microalgae increased by ~101 fold and ~33 fold (with respect to day 0) when grown upon carbon-supplemented agar and bacterial cellulose overtop of agar during 28 days of cultivation. The higher cell density and chlorophyll content of bioprinted microalgae on agar compared to bacterial cellulose overtop of agar is likely due to lesser availability of nutrients on bacterial cellulose. In total, our data show that microalgal cells survive the bioprinting process and are able to grow consistently within the bioprinted hydrogel matrices for at least a period of 4 weeks.

We additionally measured the viability of bioprinted microalgae after extended growth on either carbon-supplemented agar or on bacterial cellulose overtop of carbon-supplemented agar, by recovering and re-growing the microalgae from the bioprints. The microalgae were able to regrow in fresh carbon-supplemented medium even after 28 days of growth, indicating their long-term viability (**Figure S6.4**).

We then assessed whether the bioprinted microalgae on bacterial cellulose would survive after removal from the nutrient source (carbon-supplemented agar). For this purpose,

we first grew the bioprints on bacterial cellulose (overtop of carbon-supplemented agar) for 7 days under photomixotrophic condition. We then removed the bacterial cellulose containing

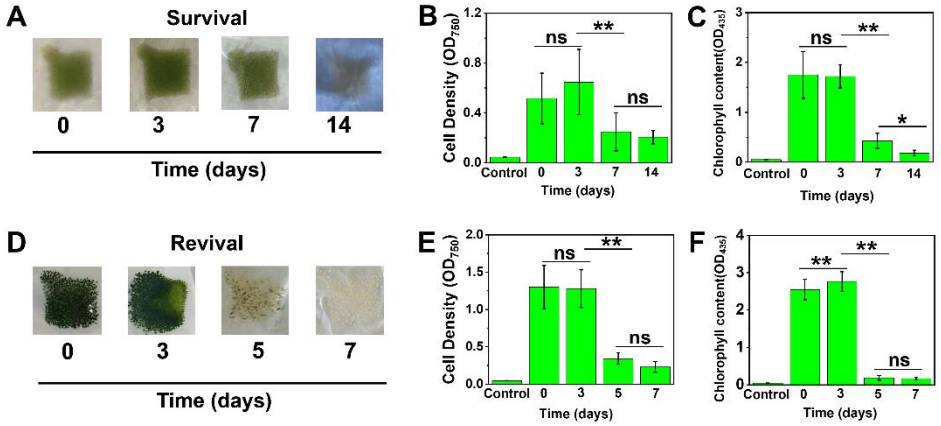

Figure 6.3 Survival (A-C) and revival (D-F) abilities of bioprinted microalgae material over time. Microalgal bioprints on bacterial cellulose were grown for 7 days under photomixotrophic conditions. The bioprints were assessed for survival after removal from carbon-supplemented agar for a total of 0, 3, 7, or 14 days. Their revival abilities were assessed by placing the microalgal bioprints back onto fresh carbon-supplemented agar for 7 days under photomixotrophic conditions. Bioprints were assessed *via* photographs **(A, D)**, cell density ($O.D._{750}$) **(B, E)** and chlorophyll ($O.D._{435}$) **(C, F)** measurements. Sterile sodium chloride (0.9 *w/v*%) and DMSO served as the controls in the (**B** and **E**) cell density and (**C** and **F**) chlorophyll measurements, respectively. ns, not significant, $*p < 0.05$, $**p < 0.01$ as determined by one-way (single factor) ANOVA with post-hoc Tukey's HSD.

the bioprinted microalgae from the carbon-supplemented agar and further incubated them under light/dark conditions. Cell density and chlorophyll measurements indicated that microalgae in the bioprints on bacterial cellulose could stably survive up to at least 3 days without contact with carbon-supplemented agar, and their growth could be revived by placing them back onto fresh carbon-supplemented agar within 3 days of survival (**Figure 6.3**). To control for whether the process of removing the bacterial cellulose from carbon-supplemented agar affected the bioprinted microalgae, we measured the cell density of microalgae bioprints on bacterial cellulose that were lifted from the carbon-supplemented agar after 7 days, transferred to a fresh carbon-supplemented agar, and incubated for another 7 days. When compared to the cell density of a bioprint grown 14 days on the same carbon-supplemented agar, this transfer process was seen not to impede, but rather to increase the cell density of the bioprinted microalgae (**Figure S6.5**). However, extended periods of incubation (≥ 5 days) without contact with carbon-supplemented agar led to an irreversible

decrease in the microalgal cell density and chlorophyll content. Thus, the bioprinted living materials can survive for a period of at least 3 days after removal from nutrient source, and their longevity can be extended by placing them back onto a fresh nutrient source within this timeframe.

To assess whether there were morphological differences between the bioprinted and the planktonic microalgal cells, we performed scanning electron microscopy (SEM). The results (**Figure S6.6**) revealed a uniform distribution of microalgal cells (with a mean cell diameter of 4-5 μm) with no morphological differences on both carbon-supplemented agar and bacterial cellulose overtop of carbon-supplemented agar. The observed cell sizes are consistent with previously reported cell sizes of *C. reinhardtii*.[25, 47]

C. reinhardtii has been shown to utilize cellulose, which is composed of D-glucose units,[48] as a carbon substrate *via* expression of endo β-1,4-glucanases. If the microalgae in the bioprints were to digest and degrade the bacterial cellulose substrate, the mechanical properties of the resulting material would be compromised and the material would be eventually degraded by the microalgae itself, which is undesirable. Hence, we assessed the cellulolytic activities of microalgae grown either planktonically in wells (8 mm in diameter) on carbon-supplemented agar containing carboxymethyl cellulose, or as bioprints on carbon-supplemented agar containing carboxymethyl cellulose, or as bioprints on bacterial cellulose overtop of carbon-supplemented agar (**Figure S6.7**). In these assays, active digestion of carboxymethyl cellulose in the agar plates is indicated by a halo formation (cellulolytic zone) around the wells due to the enzymatic secretion into the solid medium. Microalgae grown as planktonic cultures expressed cellulolytic activities on carboxymethyl cellulose (18.36 ± 0.27 mm), whereas no cellulolytic zones were observed for bioprinted microalgae on either carboxymethyl cellulose or bacterial cellulose. The lack of cellulolytic zones seen for bioprinted microalgae could be due to the alginate matrix immobilizing secreted enzymes within the bioprinted structures, which would be beneficial from a material perspective since the bacterial cellulose printing substrate would not be digested over time by the microalgae within the bioprints.

Printability of C. reinhardtii with defined patterns and printing resolution

To characterize the printability of our photosynthetic living material, *C. reinhardtii* were bioprinted in varying pre-defined basic geometrical patterns (simple, hollow, filled) as single-layered constructs or as multi-layered complex geometrical patterns (2-4 layered) in a range of sizes on carbon-supplemented agar or bacterial cellulose overtop of carbon-supplemented

agar. Samples were visually inspected after 7 days of photomixotrophic growth (**Figure 6.4A, B**). Microalgae could be bioprinted in all the pre-defined patterns and sizes (5 × 8 mm; 22 × 32 mm; 31 × 42 mm; 37 × 52 mm) both onto carbon-supplemented agar or bacterial cellulose overtop of carbon-supplemented agar. Thus, with our approach we can make at-scale bioprints by merely changing the bioprinting design parameters. Microalgae bioprinted onto bacterial cellulose could be readily peeled off from the agar support layer (**Figure S6.8**), allowing the material to be self-standing, thus considerably increasing its range of possible applications.

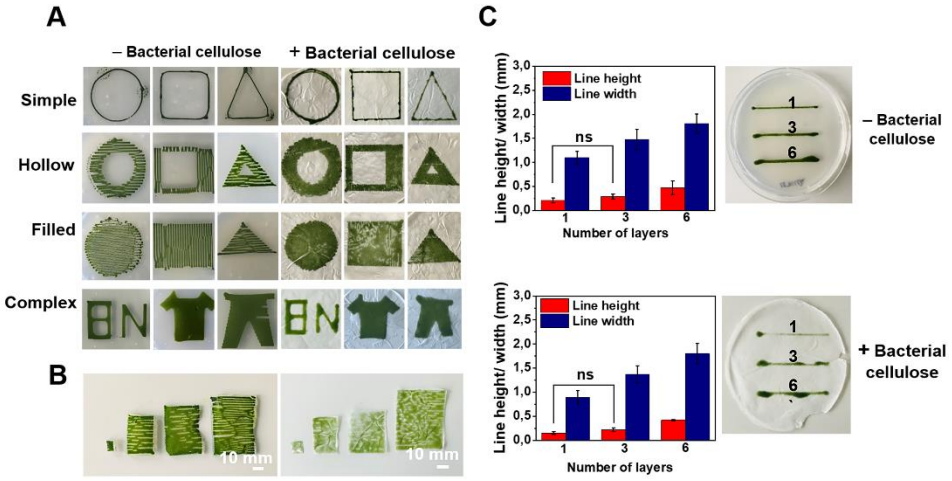

Figure 6.4 Different geometries and printing resolution of bioprinted microalgal materials. (A) Varying geometries (basic: mono-layered structure; complex: multi-layered (2-4 layer) structures) and **(B)** sizes of bioprinted microalgae on carbon-supplemented agar (left) or bacterial cellulose (right). Images were taken after 7 days of photomixotrophic growth. **(C)** Line height and width of bioprinted structures (mono-, tri-, and hexa-layered) on carbon-supplemented agar or bacterial cellulose overtop of carbon-supplemented agar. Measurements were performed after 7 days of photomixotrophic growth (n=9). ns, not significant; all the other comparisons were statistically significant (**$p < 0.01$ as determined by one-way (single factor) ANOVA with post-hoc Tukey's HSD).

The printing resolution for microalgal materials bioprinted with our house-built bioprinter was assessed by characterizing the minimum printed line height and width. We created multi-layered structures (up to 6 layers) by depositing bio-ink on top of previously printed layers in a layer-by-layer fashion. Line heights were measured to be 0.21 ± 0.05 mm (1 layer), 0.29 ± 0.05mm (3 layers), and 0.47 ± 0.14 mm (6 layers) for bioprinted microalgae on carbon-supplemented agar, whereas line heights were 0.15 ± 0.03 mm (1-layer), 0.22 ± 0.04 mm (3-layers), and 0.42 ± 0.01 mm (6-layers) on bacterial cellulose overtop of carbon-

supplemented agar (**Figure 6.4C**). Thus, the line height increased steadily as the number of bioprinted layers increased. Line widths were 1.10 ± 0.13 mm (1 layer), 1.48 ± 0.21 mm (3 layers), and 1.81 ± 0.20 mm (6 layers) for bioprinted microalgae on carbon-supplemented agar, while line widths were 0.89 ± 0.14 mm (1 layer), 1.37 ± 0.18 mm (3 layers), and 1.80 ± 0.21 mm (6 layers) on bacterial cellulose overtop of carbon-supplemented agar (**Figure 6.4C**). Thus, line width also increased as the number of bioprinted layers increased, likely due to slight spreading of the hydrogel prior to full gelation during the layer-by-layer addition. We confirmed this hypothesis by printing 10- and 20-layer structures onto both carbon-supplemented agar and bacterial cellulose overtop of carbon supplemented agar, which displayed increased line widths (**Figure S6.9**). In summary, our bioprinting strategy can produce bioprints as lines or curves with sharp millimeter-scale resolution for prints up to 6 layers tall, with a decrease in resolution for additional layers. The resolution obtained with this strategy is similar to that obtained with the bioprinting of bacteria previously reported by our groups.[11, 14, 49] The resolution is sufficiently high for applications such as biogarments, where patterning of microalgae on bacterial cellulose is desirable. Applications such as structural materials that would require an increased number of layers at higher resolution, would benefit from further improvements in 3D printing capability.

Physical stability and regenerative aspects of bioprinted living materials

In addition to removing the bioprinted microalgae living materials from agar, we were also interested in detaching it from the cellulose substrate, as this would potentially enable other types of product applications, *e.g.*, as living photosynthetic patterns and brand labels. Upon testing, we found that the microalgal bioprints could successfully be detached from bacterial cellulose and re-attached onto a fresh bacterial cellulose surface. The re-attached bioprints remained attached even after inverting them (**Figure 6.5A**).

The stability of microalgal bioprints to physical distortions is also of crucial importance to allow potential user interaction scenarios. We subjected microalgal bioprints on bacterial cellulose to physical distortions manually by folding, twisting, and crushing them at least 6 times each (**Figure 6.5B**). The microalgal bioprints on bacterial cellulose all resumed their original shapes upon unfolding, untwisting, and uncrushing, whereas pure alginate prints or microalgae bioprints not supported by bacterial cellulose were fragile and broke within one round of the folding/twisting/crushing assessments due to their poor mechanical properties (**Figure S6.10**). Thus, the bacterial cellulose support confers excellent mechanical properties to the microalgae bioprints.

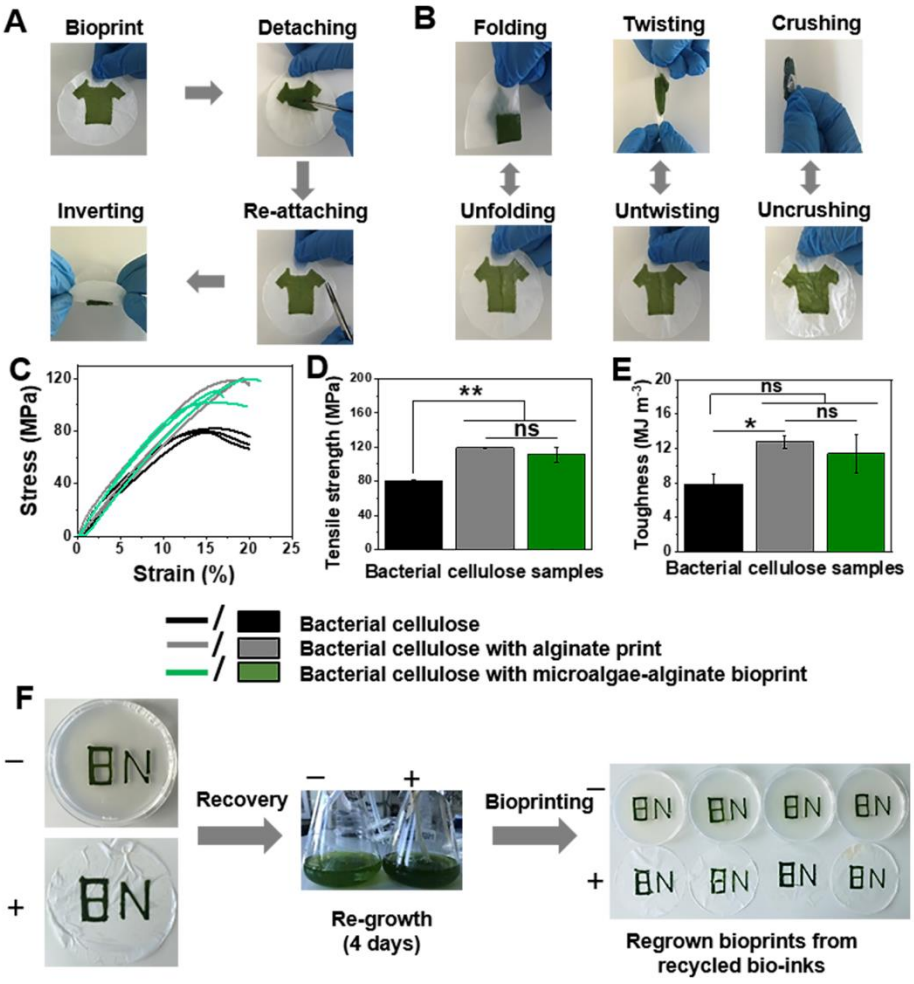

Figure 6.5 Physical stability and regenerative abilities of the bioprinted living materials. Bioprinted microalgae materials after **(A)** detachment and re-attachment onto bacterial cellulose, and **(B)** physical distortion assessments. Mechanical testing of bioprinted materials including **(C)** tensile stress-strain curves, **(D)** tensile strength, and **(E)** toughness. **(F)** Regeneration from recycled bio-inks. For regeneration, microalgae from week-old photomixotrophically grown bioprints on carbon-supplemented agar (-) or bacterial cellulose overtop of carbon-supplemented agar (+) were recovered by citrate treatment. The recovered cells were regrown in carbon-supplemented medium for 4 days, harvested for fresh bio-ink preparation, and bioprinted again. Bioprints were grown for 1 week under photomixotrophic condition and were imaged. ns, not significant; *$p < 0.05$, **$p < 0.01$ as determined by one-way (single factor) ANOVA with post-hoc Tukey's HSD.

To quantify the mechanical properties conferred by bacterial cellulose, we measured the tensile strength and toughness of (1) bacterial cellulose alone, (2) alginate printed onto bacterial cellulose (without microalgae), and (3) microalgae/alginate printed onto bacterial cellulose. The tensile strength of pure bacterial cellulose was 80.3 ±1.6 MPa, whereas the tensile strength of alginate prints on bacterial cellulose was 119.2 ± 0.9 MPa, and the tensile strength of microalgae bioprints on bacterial cellulose was 110.8 ± 8.9 MPa (**Figure 6.5C-D**). The toughness of pure bacterial cellulose was 7.9 ± 1.1 MJ m^{-3}, whereas the toughness of alginate prints on bacterial cellulose was 12.8 ± 0.8 MJ m^{-3}, and the toughness of microalgae bioprints on bacterial cellulose was 11.4 ± 2.2 MJ m^{-3} (**Figure 6.5E**). Thus, the prints on bacterial cellulose (either alginate or alginate-microalgae bioprints on bacterial cellulose) possessed higher tensile strength and higher toughness than pure bacterial cellulose samples. No significant difference was observed between the tensile strength and toughness of bacterial cellulose supporting prints made of alginate alone *versus* alginate with microalgae. Therefore, microalgae present in the bioprints did not contribute to the mechanical properties of the living material.

We evaluated the effects on the mechanical properties of the bioprinted living materials of fabrication parameters including elapsed time after printing and number of printed layers (**Figure S6.11**). The tensile strength (**Figure S6.11 A-B**) of microalgae printed onto bacterial cellulose increased significantly ($p < 0.05$) from 85.4 ± 8.9 MPa at 0 days after printing to 110.8 ± 8.9 MPa at 7 days after printing, whereas the toughness values remained unchanged over time (**Figure S6.11 C**). This increase in tensile strength could be due to increased attachment of the bioprint to the bacterial cellulose over time during the incubation period or to decrease in water content of the bioprint. Increasing the number of printed layers had no significant effect on the mechanical properties of the bioprinted living materials (**Figure S6.11 D-F**). Moreover, bioprints on bacterial cellulose were observed to retain a stable three-dimensional shape and intense green color even after 1 month of storage under ambient conditions (**Figure S6.12**).

The stability of the bioprints in water was assessed by immersing the microalgal bioprints multiple times into water and retrieving them. The bioprints remained stably attached on the bacterial cellulose and did not display observable dissolution even after 6 rounds of immersion in water (**Figure S6.13**). Bioprints on bacterial cellulose were also immersed in water for a period of one week under ambient conditions. Upon retrieval of the immersed samples, no visible distortion of the bioprinted structures was observed. We also tested the mechanical properties of the bioprinted living materials before and after immersion, and after drying the immersed materials (**Figure S6.14**). After immersion in

water for one week, the tensile strength of the bioprinted living materials dropped from 110.8 ± 8.9 MPa to 58.2 ± 1.3 MPa. However, when these wet materials were placed out of water for 7 days, the tensile strength increased to 145 ± 12.2 MPa. The values for toughness ranged between 11-16 MJ m^{-3} for all the samples without statistically significant differences. Therefore, immersion in water reduces the tensile strength of the bioprinted materials without affecting the toughness. Additionally, no visible presence or growth of microalgae in the water phase was observed during incubation, which was confirmed by measuring the $O.D._{750}$ of the water samples before immersion and after retrieval of the bioprints (**Figure S6.15**). Thus, no or minimal liberation of microalgae from the bioprints into the water occurred, which is advantageous in applications wherein the bioprints contact water without raising potential environmental concerns.[50]

The reversible polymerization chemistry of our alginate bio-ink gives rise to the possibility that the bioprinted living materials may be able to be dissolved and re-used. To test this hypothesis, we attempted to dissolve the alginate hydrogel and recover the bioprinted microalgal cells on carbon-supplemented agar or bacterial cellulose overtop of carbon-supplemented agar by treatment with sodium citrate (**Figure S6.16**). The recovered microalgal cells were regenerated in fresh carbon-supplemented medium by growth under photomixotrophic condition for 4 days. The regenerated microalgal cultures were then used to prepare fresh bio-inks with which several bioprints were made, such that one single print gave rise to multiple prints of the same dimensions, and further grown for 7 days. The fully re-grown bioprinted materials highlight the reusability and regenerative abilities of microalgae in these living materials (**Figure 6.5F**). Thus, the fabricated bioprinted living materials can be readily deconstructed following citrate treatment and used as a recycled source for the generation of more of such living materials, indicating their circular nature.[51]

Up-scaled production of bioprinted living materials

To demonstrate the applicability of this bioprinting approach, we custom-built a second, similar cost-effective bioprinter (**Figure S6.17**) suitable for bioprinting at larger scales (up to 70 x 20 cm). We could show that our bioprinted living material (of 22 x 12 cm dimension) remained flexible (**Figure 6.6**). The flexible nature of bacterial cellulose and the freedom of design achievable with bioprinting technology enables our bioprinted living materials to be used in applications like photosynthetic bio-garments, adhesive labels, blinds or curtains for windows, *etc*.

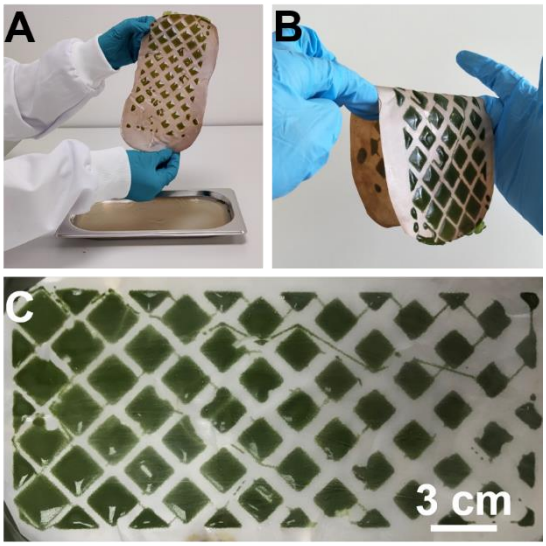

Figure 6.6 Photographs of up-scaled bioprinted living materials (22 x 12 cm) (A) Peeled-off from carbon-supplemented agar, **(B)** flexibility of the material, **(C)** overall view of the living material.

6.3 Conclusion

The printing of living cells typically involves immobilization or encapsulation of the living cells within a hydrogel matrix. Different hydrogel systems have been shown to be suitable to support cell growth while maintaining the 3D structure,[2, 9, 19, 20] however, it remains challenging to endow mechanical robustness to bioprinted structures. In this study, we report a calcium-alginate-based hydrogel system for bioprinting of *C. reinhardtii* microalgae cells overtop a cellulose substrate. Calcium-alginate-based hydrogels are easy to pattern and cell-friendly, such that the microalgal cells remain alive both during and after the bioprinting process for relatively long periods of time. Their optical transparency and selective permeability ensure efficient light transmission, mass transfer of nutrients, and diffusion of environmental CO_2 to the bioprinted microalgal cells allowing for vigorous growth. The cross-linked "egg-box" structure of the alginate hydrogel matrix exhibits pore dimensions that enable the retention of microalgal cells, while supporting the release of O_2 produced during the photosynthetic process.[21]

The immobilized or encapsulated microalgal cells in the hydrogel matrix of the bioprinted structures retain viability and exhibit increased growth and chlorophyll content

over a 4-week period of cultivation. Further, the microalgae in these living materials remain stable in terms of cell density and chlorophyll content for at least a 3-day period after removal from nutrients, and their longevity can be extended by placing them back into contact with nutrients. The fabricated living materials show resilience to physical distortions and to immersion in water. No visible release of the microalgal cells from the bioprinted living materials to surrounding water can be observed, highlighting the biosecurity features of the fabricated living materials that prevent environmental contamination. However, the potential environmental implications of these materials will still need to be closely investigated for individual applications prior to full deployment.

With our approach, we show bioprinted microalgal structures with millimeter-scale precision that support the spatio-temporal characteristics of natural microalgae. Further, this bioprinting approach is simple, scalable, and eco-friendly, involving usage of completely biodegradable components. Moreover, the costs of the bioprinters are ~250 US dollars, which is vastly cheaper than the previously reported bioprinters described for microalgal-bioprinting, which have costs ranging from 5000 to 250000 US dollars.[52, 53] Thus, the work shown here highlights the development of a cost-effective, efficient, and straight-forward bioprinting approach employing alginate-based chemistry for fabrication of resilient photosynthetic living materials.

There is a growing interest in the development of living materials that are regenerative and reusable in nature [51]. The regenerative nature of our bioprinted materials can inspire diverse future living products which require curation to extend their life or repair them, with innovative "end-of-life" scenarios. For example, if the living materials were physically damaged, the end users could extract the microalgal cells and regrow them into fresh and undamaged bioprinted structures without wasting the original cells in the material. As the bioprinted microalgae are stored within our living materials, they could be directly used as raw materials by the users for their own production of new living materials at locations unsuitable for new shipments of microalgal cultures, such as for space applications. Such novel user scenarios with living materials should be further explored via user studies in real-life settings.

Due to the sustainable nature of our approach, which employs naturally-occurring materials based on living microalgal cells and environmental-friendly biopolymers such as alginate and bacterial cellulose, as well as the physical robustness, resilience and regenerative nature of the approach, the developed bioprinted living materials could be employed in diverse applications including artificial leaves, photosynthetic bio-garments, and adhesive labels.

6.4 References

1. Nguyen, P. Q.; Courchesne, N. D.; Duraj-Thatte, A.; Praveschotinunt, P.; Joshi, N. S. Engineered Living Materials: Prospects and Challenges for Using Biological Systems to Direct the Assembly of Smart Materials. Adv. Mater. 2018, *30* (19), 1704847.

2. Johnston, T. G.; Fillman, J. P.; Priks, H.; Butelmann, T.; Tamm, T.; Kumar, R.; Lahtvee, P. J.; Nelson, A. Cell-Laden Hydrogels for Multikingdom 3D Printing. Macromol. Biosci. 2020, *20* (8), 2000121.

3. Smith, R. S. H.; Bader, C.; Sharma, S.; Kolb, D.; Tang, T. C.; Hosny, A.; Moser, F.; Weaver, J. C.; Voigt, C. A.; Oxman, N. Hybrid Living Materials: Digital Design and Fabrication of 3D Multimaterial Structures with Programmable Biohybrid Surfaces. Adv. Funct. Mater. 2019, *30* (7), 1907401.

4. Chen, A. Y.; Zhong, C.; Lu, T. K. Engineering Living Functional Materials. ACS Synth. Biol. 2015, *4* (1), 8-11.

5. Moser, F.; Tham, E.; González, L. M.; Lu, T. K.; Voigt, C. A. Light‐Controlled, High‐Resolution Patterning of Living Engineered Bacteria Onto Textiles, Ceramics, and Plastic. Adv. Funct. Mater. 2019, *29* (30), 1901788.

6. Guo, S.; Dubuc, E.; Rave, Y.; Verhagen, M.; Twisk, S. A. E.; van der Hek, T.; Oerlemans, G. J. M.; van den Oetelaar, M. C. M.; van Hazendonk, L. S.; Bruls, M.; Eijkens, B. V.; Joostens, P. L.; Keij, S. R.; Xing, W.; Nijs, M.; Stalpers, J.; Sharma, M.; Gerth, M.; Boonen, R.; Verduin, K.; Merkx, M.; Voets, I. K.; de Greef, T. F. A. Engineered Living Materials Based on Adhesin-Mediated Trapping of Programmable Cells. ACS Synth. Biol. 2020, *9* (3), 475-485.

7. Arrabito, G.; Ferrara, V.; Bonasera, A.; Pignataro, B. Artificial Biosystems by Printing Biology. Small 2020, *16* (27), 1907691.

8. Gantenbein, S.; Masania, K.; Woigk, W.; Sesseg, J. P. W.; Tervoort, T. A.; Studart, A. R. Three-Dimensional Printing of Hierarchical Liquid-Crystal-Polymer Structures. Nature 2018, *561* (7722), 226-230.

9. Balasubramanian, S.; Aubin-Tam, M. E.; Meyer, A. S. 3D Printing for the Fabrication of Biofilm-Based Functional Living Materials. ACS Synth. Biol. 2019, *8* (7), 1564-1567.

10. Liu, X.; Yuk, H.; Lin, S.; Parada, G. A.; Tang, T. C.; Tham, E.; de la Fuente-Nunez, C.; Lu, T. K.; Zhao, X. 3D Printing of Living Responsive Materials and Devices. Adv. Mater. 2018, *30* (4), 1704821.

11. Lehner, B. A. E.; Schmieden, D. T.; Meyer, A. S. A Straightforward Approach for 3D Bacterial Printing. ACS Synth. Biol. 2017, *6* (7), 1124-1130.

12. Schaffner, M.; Rühs, P. A.; Coulter, F.; Kilcher, S.; Studart, A. R. 3D Printing of Bacteria into Functional Complex Materials. Sci. Adv. 2017, *3*, eaao6804.

13. Seidel, J.; Ahlfeld, T.; Adolph, M.; Kummritz, S.; Steingroewer, J.; Krujatz, F.; Bley, T.; Gelinsky, M.; Lode, A. Green Bioprinting: Extrusion-Based Fabrication of Plant Cell-Laden Biopolymer Hydrogel Scaffolds. Biofabrication 2017, *9* (4), 045011.

14. Spiesz, E. M.; Yu, K.; Lehner, B. A. E.; Schmieden, D. T.; Aubin-Tam, M. E.; Meyer, A. S. Three-Dimensional Patterning of Engineered Biofilms with a Do-it-yourself Bioprinter. J. Vis. Exp. 2019, *147*, e59477.

15. Ning, E.; Turnbull, G.; Clarke, J.; Picard, F.; Riches, P.; Vendrell, M.; Graham, D.; Wark, A. W.; Faulds, K.; Shu, W. 3D Bioprinting of Mature Bacterial Biofilms for Antimicrobial Resistance Drug Testing. Biofabrication 2019, *11* (4), 045018.

16. Shavandi, A.; Jalalvandi, E. Biofabrication of Bacterial Constructs: New Three-Dimensional Biomaterials. Bioeng. 2019, *6* (44), 1-6.

17. Saygili, E.; Dogan-Gurbuz, A. A.; Yesil-Celiktas, O.; Draz, M. S. 3D Bioprinting: A Powerful Tool to Leverage Tissue Engineering and Microbial Systems. Bioprinting 2020, *18*, 00071.

18. Bhardwaj, A.; Vasselli, J.; Lucht, M.; Pei, Z.; Shaw, B.; Grasley, Z.; Wei, X.; Zou, N. 3D Printing of Biomass-Fungi Composite Material: A Preliminary Study. Manuf. Lett. 2020, *24*, 96-99.

19. Huang, J.; Liu, S.; Zhang, C.; Wang, X.; Pu, J.; Ba, F.; Xue, S.; Ye, H.; Zhao, T.; Li, K.; Wang, Y.; Zhang, J.; Wang, L.; Fan, C.; Lu, T. K.; Zhong, C. Programmable and Printable *Bacillus subtilis* Biofilms as Engineered Living Materials. Nat. Chem. Biol. 2019, *15* (1), 34-41.

20. Malik, S.; Hagopian, J.; Mohite, S.; Lintong, C.; Stoffels, L.; Giannakopoulos, S.; Beckett, R.; Leung, C.; Ruiz, J.; Cruz, M.; Parker, B. Robotic Extrusion of Algae-Laden Hydrogels for Large-Scale Applications. Glob. Chall. 2020, *4* (1), 1900064.

21. Lode, A.; Krujatz, F.; Brüggemeier, S.; Quade, M.; Schütz, K.; Knaack, S.; Weber, J.; Bley, T.; Gelinsky, M. Green Bioprinting: Fabrication of Photosynthetic Algae-Laden Hydrogel Scaffolds for Biotechnological and Medical Applications. Eng. Life Sci. 2015, *15* (2), 177-183.

22. Zhao, S.; Guo, C.; Kumarasena, A.; Omenetto, F. G.; Kaplan, D. L. 3D Printing of Functional Microalgal Silk Structures for Environmental Applications. ACS Biomater. Sci. Eng. 2019, *5* (9), 4808-4816.

23. Hopfner, U.; Schenck, T. L.; Chavez, M. N.; Machens, H. G.; Bohne, A. V.; Nickelsen, J.; Giunta, R. E.; Egana, J. T. Development of Photosynthetic Biomaterials for In Vitro Tissue Engineering. Acta Biomater. 2014, *10* (6), 2712-2717.

24. Homburg, S. V.; Kruse, O.; Patel, A. V. Growth and Photosynthetic Activity of *Chlamydomonas reinhardtii* Entrapped in Lens-Shaped Silica Hydrogels. J. Biotechnol. 2019, *302*, 58-66.

25. Das, A. A. K.; Bovill, J.; Ayesh, M.; Stoyanov, S. D.; Paunov, V. N. Fabrication of Living Soft Matter by Symbiotic Growth of Unicellular Microorganisms. J. Mater. Chem. B 2016, *4* (21), 3685-3694.

26. Pierobon, S. C.; Riordon, J.; Nguyen, B.; Ooms, M. D.; Sinton, D. Periodic Harvesting of Microalgae from Calcium Alginate Hydrogels for Sustained High-Density Production. Biotechnol. Bioeng. 2017, *114* (9), 2023-2031.

27. Chisti, Y. Biodiesel from Microalgae. Biotechnol. Adv. 2007, *25* (3), 294-306.

28. An, Y. J.; Guo, C. F.; Zhang, M.; Zhong, Z. P. Investigation on Characteristics of 3D Printing Using Nostoc Sphaeroides Biomass. J. Sci. Food Agric. 2019, *99* (2), 639-646.

29. Jie, G.; Kongyin, Z.; Xinxin, Z.; Zhijiang, C.; Min, C.; Tian, C.; Junfu, W. Preparation and Characterization of Carboxyl Multi-walled Carbon Nanotubes/Calcium Alginate Composite Hydrogel Nano-filtration Membrane. Mater. Lett. 2015, *157*, 112-115.

30. Drury, J. L.; Dennis, R. G.; Mooney, D. J. The Tensile Properties of Alginate Hydrogels. Biomaterials 2004, *25* (16), 3187-3199.

31. Kong, H. J.; Wong, E.; Mooney, D. J. Independent Control of Rigidity and Toughness of Polymeric Hydrogels. Macromolecules 2003, *36*, 4582-4588.

32. Gibson, L. J. The Hierarchical Structure and Mechanics of Plant Materials. J. R. Soc. Interface 2012, *9* (76), 2749-2766.

33. Wang, Q.; Schniepp, H. C. Strength of Recluse Spider's Silk Originates from Nanofibrils. ACS Macro Lett. 2018, *7* (11), 1364-1370.

34. Barthelat, F. Nacre from Mollusk Shells: A Model for High-Performance Structural Materials. Bioinspir. Biomim. 2010, *5* (3), 035001.

35. Rahman, M. M.; Netravali, A. N. Aligned Bacterial Cellulose Arrays as "Green" Nanofibers for Composite Materials. ACS Macro Lett. 2016, *5* (9), 1070-1074.

36. Wang, S.; Li, T.; Chen, C.; Kong, W.; Zhu, S.; Dai, J.; Diaz, A. J.; Hitz, E.; Solares, S. D.; Li, T.; Hu, L. Transparent, Anisotropic Biofilm with Aligned Bacterial Cellulose Nanofibers. Adv. Funct. Mater. 2018, *28* (24), 1707491.

37. Wu, Z.; Chen, S.; Wu, R.; Sheng, N.; Zhang, M.; Ji, P.; Wang, H. Top-down Peeling Bacterial Cellulose to High Strength Ultrathin Films and Multifunctional Fibers. Chem. Eng. J. 2020, *391*, 123527.

38. Santmarti, A.; Zhang, H.; Lappalainen, T.; Lee, K.-Y. Cellulose Nanocomposites Reinforced with Bacterial Cellulose Sheets Prepared from Pristine and Disintegrated Pellicle. Compos, Part A 2020, *130*, 105766.

39. Yu, K.; Balasubramanian, S.; Pahlavani, H.; Mirzaali, M. J.; Zadpoor, A. A.; Aubin-Tam, M. E. Spiral Honeycomb Microstructured Bacterial Cellulose for Increased Strength and Toughness. ACS Appl. Mater. Interfaces 2020, *12* (45), 50748-50755.

40. Florea, M.; Reeve, B.; Abbott, J.; Freemont, P. S.; Ellis, T. Genome Sequence and Plasmid Transformation of the Model High-Yield Bacterial Cellulose Producer *Gluconacetobacter hansenii* ATCC 53582. Sci. Rep. 2016, *6*, 23635.

41. Wang, J.; Tavakoli, J.; Tang, Y. Bacterial Cellulose Production, Properties and Applications with Different Culture Methods - A Review. Carbohydr. Polym. 2019, *219*, 63-76.

42. Florea, M.; Hagemann, H.; Santosa, G.; Abbott, J.; Micklem, C. N.; Spencer-Milnes, X.; de Arroyo Garcia, L.; Paschou, D.; Lazenbatt, C.; Kong, D.; Chughtai, H.; Jensen, K.; Freemont, P. S.; Kitney, R.; Reeve, B.; Ellis, T. Engineering Control of Bacterial Cellulose Production Using a Genetic Toolkit and a New Cellulose-Producing Strain. Proc. Natl. Acad. Sci. USA 2016, *113* (24), 3431-3440.

43. Therien, J. B.; Zadvornyy, O. A.; Posewitz, M. C.; Bryant, D. A.; Peters, J. W. Growth of *Chlamydomonas reinhardtii* in Acetate-Free Medium When Co-Cultured with Alginate-Encapsulated, Acetate-Producing Strains of *Synechococcus sp.* PCC 7002. Biotechnol. Biofuels 2014, *7*, 154.

44. Fischer, B. B.; Wiesendanger, M.; Eggen, R. I. Growth Condition-Dependent Sensitivity, Photodamage and Stress Response of *Chlamydomonas reinhardtii* Exposed to High Light Conditions. Plant Cell Physiol. 2006, *47* (8), 1135-1145.

45. Blifernez-Klassen, O.; Klassen, V.; Doebbe, A.; Kersting, K.; Grimm, P.; Wobbe, L.; Kruse, O. Cellulose Degradation and Assimilation by the Unicellular Phototrophic eukaryote *Chlamydomonas reinhardtii*. Nat. Commun. 2012, *3*, 1214.

46. Lagorio, M. G.; Cordon, G. B.; Iriel, A. Reviewing the Relevance of Fluorescence in Biological Systems. Photochem. Photobiol. Sci. 2015, *14* (9), 1538-1559.

47. Sathe, S.; Durand, P. M. Cellular Aggregation in *Chlamydomonas* (*Chlorophyceae*) is Chimaeric and Depends on Traits Like Cell Size and Motility. Eur. J. Phycol. 2015, *51* (2), 129-138.

48. Liu, K.; Catchmark, J. M. Enhanced Mechanical Properties of Bacterial Cellulose Nanocomposites Produced by Co-Culturing *Gluconacetobacter hansenii* and *Escherichia coli* Under Static Conditions. Carbohydr. Polym. 2019, *219*, 12-20.

49. Schmieden, D. T.; Basalo Vazquez, S. J.; Sanguesa, H.; van der Does, M.; Idema, T.; Meyer, A. S. Printing of Patterned, Engineered E. coli Biofilms with a Low-Cost 3D Printer. ACS Synth. Biol. 2018, *7* (5), 1328-1337.

50. Usher, P. K.; Ross, A. B.; Camargo-Valero, M. A.; Tomlin, A. S.; Gale, W. F. An Overview of the Potential Environmental Impacts of Large-Scale Microalgae Cultivation. Biofuels 2014, *5* (3), 331-349.

51. Heveran, C. M.; Williams, S. L.; Qiu, J.; Artier, J.; Hubler, M. H.; Cook, S. M.; Cameron, J. C.; Srubar, W. V. Biomineralization and Successive Regeneration of Engineered Living Building Materials. Matter 2020, *2* (2), 481-494.

52. Zhao, S.; Guo, C.; Kumarasena, A.; Omenetto, F. G.; Kaplan, D. L. 3D Printing of Functional Microalgal Silk Structures for Environmental Applications. ACS Biomaterials Science & Engineering 2019, *5* (9), 4808-4816.

53. Anja Lode, F. K.; Brüggemeier, S.; Quade, M.; Schütz, K.; Knaack, S.; Weber, J.; Bley, T.; and Gelinsky, M. Green Bioprinting: Fabrication of Photosynthetic Algae‐Laden Hydrogel Scaffolds for Biotechnological and Medical Applications. Engineering in Life Sciences 2015, *15*, 177-183.

6.5 Supplementary Information

Experimental section

Reagents

All chemical reagents and solvents used in this study (acetic acid, agar, ammonium chloride, calcium chloride, calcium chloride dihydrate, carboxymethyl cellulose, cellulase from *Trichoderma reesei* (aqueous solution, ⩾700 units g^{-1}), citric acid, Congo red, dimethyl sulfoxide (DMSO), disodium hydrogen phosphate, glucose, glutaraldehyde, hydrochloric acid, magnesium sulfate heptahydrate, potassium dihydrogen phosphate, sodium alginate, sodium chloride, sodium hydroxide, tris base, tryptone, and yeast extract) were purchased from Sigma-Aldrich. Phosphate solution and Hutner's trace elements were obtained from Chlamydomonas Resource Center, USA. Silicone tubing (1 × 1 mm) for bioprinting was purchased from VWR international BV.

Strains and culturing conditions

C. reinhdardtii CC-124 wild type mt(-) used in this study was purchased from Chlamydomonas Resource Center, USA. The strain was propagated under laboratory conditions for several weeks to allow for acclimation to humidity and temperature. Cultures were grown in minimal medium (Tris: 2.42 g L^{-1}, TAP salts (NH_4Cl: 5 g L^{-1}, $MgSO_4.7H_2O$: 4 g L^{-1} and $CaCl_2.2H_2O$: 2 g L^{-1}), phosphate solution: 0.03 *v/v*%, Hutner's trace elements; 0.1 *v/v*%; pH adjusted to 7.0 with hydrochloric acid) or carbon-supplemented medium (Tris: 2.42 g L^{-1}, TAP salts (NH_4Cl: 5 g L^{-1}, $MgSO_4.7H_2O$: 4 g L^{-1} and $CaCl_2.2H_2O$: 2 g L^{-1}), phosphate solution: 0.03 *v/v*%, Hutner's trace elements; 0.1 *v/v*%; pH adjusted to 7.0 with acetic acid) with sterile air bubbling at room temperature. Microalgal bioprints were subjected to light/dark (12:12 hours) cycles with a light intensity of 23 μmol m^{-2} s^{-1} using Grow light LEDs strip - Red / Blue - 4: 1 (ABC-LED, Netherlands) for a period of 7 days. Spectral data of LEDs **(Figure S6.18)** were obtained with an AQ6374 (350-1750 nm) optical spectrum analyzer.

G. hansenii (ATCC® 53582™) used for bacterial cellulose production was cultured in Hestrin-Schramm (HS) medium (tryptone: 5.0 g L^{-1}, yeast extract: 5.0 g L^{-1}, disodium hydrogen phosphate: 2.7 g L^{-1}, citric acid: 1.5 g L^{-1}, and glucose: 20 g L^{-1}) statically at 30 ºC for 3 to 4 days to obtain a bacterial cellulose pellicle. The inoculum for bacterial fermentation was prepared by treating this bacterial cellulose pellicle with cellulase (0.1 *v/v*%) with shaking at 180 rpm at 30 ºC overnight. This solution was then centrifuged at 4000 rpm for 5

min at 4 ºC, and the obtained bacterial pellet was re-suspended in fresh HS medium. A 1 *v/v*% of this solution was used as the inoculum for bacterial fermentation.

Bacterial cellulose production and purification

Bacterial cellulose was produced *in vitro* as a pellicle at the air-liquid interface by the static fermentation of *G. hansenii* in HS medium in a Petri dish (94 × 16 mm) for 7 days at 30 ºC. The produced bacterial cellulose pellicle was submerged in NaOH (1 *w/v*%) solution and boiled for 10 min to heat-kill the producing *G. hansenii*. The bacterial cellulose pellicle was then washed several times in hot water to remove the impurities and residual HS media components. Finally, the purified bacterial cellulose pellicles were air-dried and autoclaved before their use in experiments with microalgae and bioprinting.

C. reinhardtii growth on bacterial cellulose

To assess microalgal growth on bacterial cellulose, sterile bacterial cellulose samples (1 cm × 1 cm) were submerged aseptically in freshly prepared *C. reinhardtii* (10^4 cells mL^{-1}) solution and placed onto carbon-supplemented agar medium. Samples were incubated at room temperature and subjected to light/dark (12:12 hours) cycles. After 3 and 7 days of incubation, samples were visually inspected and photographed.

Bioprinting substrate preparation

To print onto agar surfaces, a Petri dish (94 × 16 mm) filled with 25 mL of minimal agar or carbon-supplemented agar with calcium chloride (0.05 M) was used as the printing substrate.

To print onto bacterial cellulose, sterile bacterial cellulose was placed overtop of freshly prepared minimal medium or carbon-supplemented agar medium supplemented with calcium chloride (0.05 M) and attached to this agar surface by addition of 500 µL calcium chloride (5 M). The surface of the bacterial cellulose was flattened with an L-shaped spreader. Plates with bacterial cellulose were sterilized by UV-treatment for 1 hour in a laminar flow chamber and then used as the printing substrate.

Bio-ink preparation

For the preparation of the bio-ink for bioprinting, 10 mL of a 7-day microalgae liquid culture (grown in carbon-supplemented medium under light/dark condition with sterile air bubbling) was spun down at 4000 rpm for 5 min, and the supernatant was discarded. Cells were re-suspended in 10 mL of minimal medium or carbon-supplemented medium. An equal volume of sodium alginate (5 *w/v*%) was added to the microalgal cell suspension and vortexed to obtain the bio-ink for the printing process. The final microalgal cell concentration was 1×10^6 cells mL^{-1}, and the sodium alginate concentration in the bio-ink was 2.5 *w/v*%.

Bioprinting

Bioprinting was performed using a modified do-it-yourself bioprinter (CoLiDo DIY) as previously described.[1, 2] Briefly, the extruder and heater of the standard bioprinter were removed and replaced with a 0.2 mL pipette tip, a silicone tubing system, and a syringe pump (**Figure S6.1**). Desired 3D structures with different shapes and sizes were designed in CoLiDo software by manually programming the G-codes. During the bioprinting, a sterile syringe was loaded with 10 mL of printer bio-ink and mounted in a syringe pump. The syringe was connected to a 0.2 mL pipette tip *via* silicone tubing (1 × 1 mm). Printing substrates were placed onto the stage, and printing was then carried out using the CoLiDo software interface. An extrusion rate of 0.5 mL h^{-1} was maintained throughout the process of bioprinting.

Cell density and chlorophyll content characterization of microalgae in the bioprints

At different time points and incubation conditions, bioprinted microalgae were incubated in a NaCl solution (0.9 *w/v*%) containing sodium citrate (55 mM) for 30 min to dissolve the alginate matrix and recover the microalgal cells.[3] Cells were centrifuged at 10000 rpm for 5 min at 4 ºC, and the cell pellet was recovered. For cell density measurements, the obtained cell pellet was dissolved in the same volume of sterile NaCl (0.9 *w/v*%), and the optical density was spectrophotometrically read at 750 nm ($O.D._{750}$) using a BioTek Epoch2 microplate reader (BioTek, USA).[4] Control wells contained sterile NaCl (0.9 *w/v*%) without microalgae.

Chlorophyll measurements were performed as described previously, with slight modifications.[3, 5] Briefly, DMSO (250 µL) was added to each cell pellet, and samples were subjected to six freeze-thaw cycles in liquid nitrogen. Then, three glass beads (5 mm in diameter) were added to each sample, and solutions were supplemented to 1 mL with DMSO. Samples were subjected to vigorous vortexing for 3 hours to ensure complete lysis of the microalgal cells. The optical absorbance of the lysate was then measured at 435 nm ($O.D._{435}$) with a BioTek Epoch2 microplate reader. Control wells contained pure DMSO. Red fluorescence of chlorophyll upon UV excitation in the bioprinted microalgae was checked by illuminating the bioprints on a UV trans-illuminator (Syngene™) using 312 nm wavelength.

Assessing optimal growth conditions of bioprinted microalgae

Microalgae were bioprinted as squares (10 × 10 mm) onto minimal medium or carbon-supplemented medium agar (- bacterial cellulose condition) or bacterial cellulose placed overtop of minimal medium or carbon-supplemented medium agar (+ bacterial cellulose condition) and incubated at room temperature under light/dark (12:12 hours) or dark conditions for 7 days. Cell density and chlorophyll measurements of these different set-ups

were carried out (as described above) for assessing the optimal growth conditions for the microalgae within the bioprints.

Evaluating the re-growth of microalgae from bioprints

Microalgae from 28 days old bioprints on carbon-supplemented agar or on bacterial cellulose overtop of carbon-supplemented agar were recovered as described above. The recovered cells were re-suspended and used as inoculum (0.1 % (*v/v*)) for re-growth in fresh carbon-supplemented medium. Re-growth was monitored in this set-up by measurement of cell density ($O.D._{750}$) following 4, 7, and 10 days of incubation under light/dark (12:12 h) conditions.

Congo red staining

The cellulolytic activity of *C. reinhardtii* was evaluated in two different ways. In the first, 1×10^6 algal cells mL^{-1} were added into an 8-mm diameter well on a carbon-supplemented agar plate additionally supplemented with 0.1 *w/v*% carboxymethylcellulose (CMC), then incubated for 7 days under light/dark (12:12 hours) conditions. In the second, algal cells were bioprinted onto a carbon-supplemented agar plate with 0.1 *w/v*% carboxymethylcellulose (CMC) or onto bacterial cellulose substrate (overtop of carbon-supplemented agar plate), then incubated for 7 days under light/dark (12:12 hours) conditions. CMC agar plates or bacterial cellulose with the bioprinted algae were stained with 20 mL Congo red (0.1 *w/v*%) for 15 min, then treated with NaCl (1 M) for 5 min as described previously.[6] The visualized zones of cellulolysis were measured, and the cellulolytic zones around the wells or bioprints were photographed.

Survival and revival abilities of microalgae in bioprinted living materials

A 1-week-old bioprinted microalgae on bacterial cellulose overtop of carbon-supplemented agar grown under light/dark (12:12 hours) conditions was used. Briefly, bacterial cellulose supporting the bioprinted microalgae was removed from the carbon-supplemented agar medium, placed aseptically into an empty Petri dish, and incubated under light/dark (12:12 hours) conditions. Survival of the microalgae on these bacterial cellulose samples was estimated by quantifying the cell density ($O.D._{750}$) and chlorophyll content ($O.D._{435}$) at defined time intervals (0, 3, 7, or 14 days post-removal from carbon-supplemented agar medium). Revival of the microalgae printed material on these bacterial cellulose samples was characterized by placing the above samples back onto carbon-supplemented agar at the indicated time points (0, 3, 5, and 7 days post-removal from carbon-supplemented agar). Samples were further incubated for 7 days, after which the cell density ($O.D._{750}$) and chlorophyll content ($O.D._{435}$) were measured.

Scanning electron microscopy

Morphology of the bioprinted microalgae was examined with a scanning electron microscope (SEM, JEOL JSM 6010 LA). Briefly, samples were fixed with glutaraldehyde (6.25 *w/v*%) in Sorenson's phosphate buffer overnight at 4 ºC, dehydrated with increasing gradients of EtOH (30, 50, 70, and 100 *v/v*%), and air-dried. Samples were then sputter-coated with gold-palladium at 20 mA for 60 s and observed at 5-15 kV under vacuum in SEI mode.

Height and thickness measurements

The height and the thickness of bioprinted microalgae (1-, 3-, 6-, 10- and 20-layered constructs) grown on carbon-supplemented agar or on bacterial cellulose overtop of carbon-supplemented agar for 7 days under light/dark (12:12 hours) conditions were measured with an optical microscope (DNT®, DigiMicro Lab 5.0). Measurements were performed on three biological replicates at different locations on each sample (n = 18). ImageJ software (National Institutes of Health, USA) was used to quantify the height and thickness values from the images obtained from optical microscopy.

Stability assessments

The bioprints were detached from the bacterial cellulose surface, re-attached onto a fresh bacterial cellulose surface, and inverted to assess the adhesion of the bioprints onto bacterial cellulose surfaces. Additionally, the stability of bioprinted microalgae on bacterial cellulose or alginate prints to physical distortion was investigated by manually folding, twisting, or crushing the samples. Samples were subsequently unfolded, untwisted, or uncrushed and imaged.

Bioprinted microalgae on bacterial cellulose were also tested for stability against water. Bioprinted samples were repeatedly immersed into a beaker filled with sterile distilled water (~450 mL) and kept immersed for 7 days at room temperature under water. Samples were then retrieved and photographed to visualize any distortion in the bioprint due to water treatment.

All the assessed samples were then stored at room temperature under ambient conditions for a 1-month period to assay for any visual changes in the bioprints.

Tensile testing of bioprinted living materials

7-day-old bioprinted microalgae on bacterial cellulose was subjected to tensile testing assessment using a Zwick LF7M10 testing machine with a 10 kN load cell. The grip distance was set as 10 mm, and the materials were tested with a loading rate of 2 mm min^{-1}. Three samples per group were measured for the data presented.

Recovery of bioprinted microalgae from agar plates with citrate treatment

The recovery of microalgae from bioprints from (carbon-supplemented agar or bacterial cellulose overtop of carbon-supplemented agar) was studied by treatment of the bioprinted agar plates or bacterial cellulose samples with 20 mL sodium citrate (0.5 M, pH 7.0) with shaking at 40 rpm for 120 min. Plates and bacterial cellulose samples were photographed before and after citrate treatment.

Re-usability and viability of microalgae in the bioprints

A 1-week-old bioprinted microalgae sample (grown under light/dark (12:12 hours) conditions) was removed from carbon-supplemented agar or bacterial cellulose overtop of carbon-supplemented agar. The bioprints were incubated in 10 mL of sterile sodium citrate (18 mM in 0.9 *w/v*% NaCl) for 30 min at room temperature to dissolve the alginate matrix. Solutions were centrifuged at 10000 rpm for 5 min at 4 ºC, and the cell pellets were re-dissolved in 10 mL of fresh carbon-supplemented medium. 1 *v/v*% of these solutions was used as an inoculum for re-growing the microalgae in carbon-supplemented medium. Cultures were incubated under light/dark (12:12 hours) conditions for 4 days at room temperature, made into fresh bio-inks (with equal volume of sodium alginate (5 *w/v*%), and bioprinted on carbon-supplemented agar or bacterial cellulose overtop of carbon-supplemented agar. Samples were then incubated under light/dark (12:12 hours) conditions for 7 days at room temperature and imaged.

Up-scaling of the living materials production

Up-scaled fabrication of bioprinted living materials was performed with a customized Creality Ender-3 Pro bioprinter within a sterile chamber (UV-C treatment) to avoid contamination (**Figure S6.17**). Square-shaped patterns were repeatedly bioprinted over the entire surface of a bacterial cellulose printing substrate sized 22 x 12 cm, overtop of carbon-supplemented agar. Bioprinted living materials were incubated under conditions of photomixotrophic growth for a period of 14 days and photographed.

Statistical analysis

All experiments were performed at least two independent times with at least 6 technical replicates. Data are expressed as mean ± SD. Statistical analyses were performed on https://astatsa.com/. The experimental groups were compared using one-way (single factor) ANOVA with post-hoc Tukey's HSD (honest significant difference) tests or two-way ANOVA. $p < 0.01$, significant.

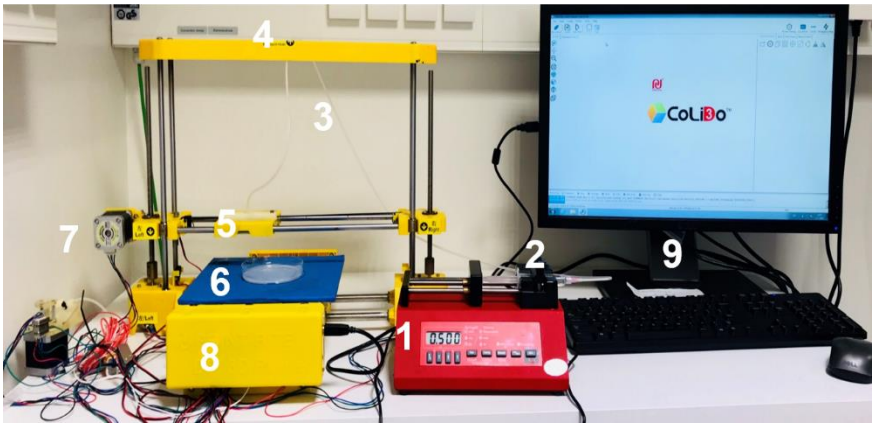

Figure S6.1 The microalgal bioprinting set-up. (1) syringe pump, (2) syringe filled with bio-ink, (3) silicone tubing, (4) printer frame, (5) extruder holder with a pipette-tip nozzle, (6) printing stage with printing substrate, (7) one of the three step-motors for positioning, (8) breadboard and hardware of the bioprinter, (9) CoLiDo bioprinting software.

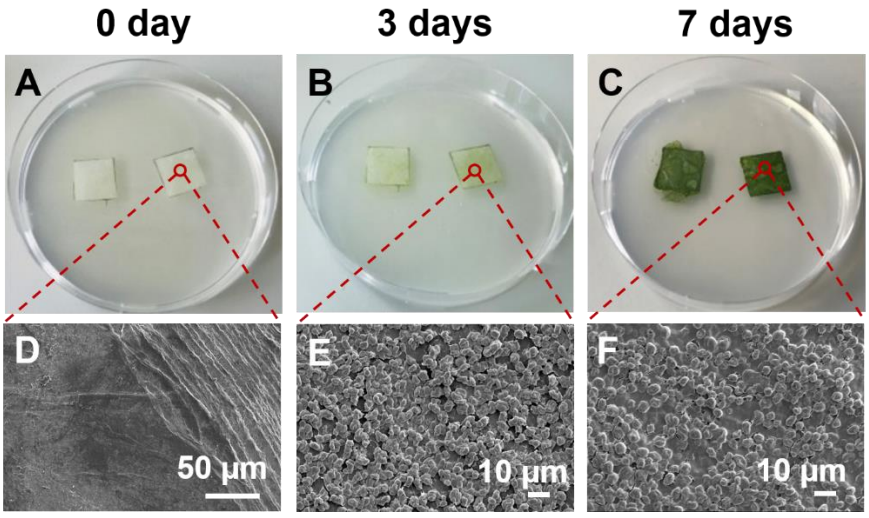

Figure S6.2 (A-C) Optical and (D-F) SEM images of *C. reinhardtii* grown on bacterial cellulose overtop of carbon-supplemented agar. Bacterial cellulose pieces were dipped in freshly prepared microalgal solution (104 cells mL^{-1}) and placed on carbon-supplemented agar and incubated for 0 day (A, D), 3 days (B, E) and 7 days (C, F).

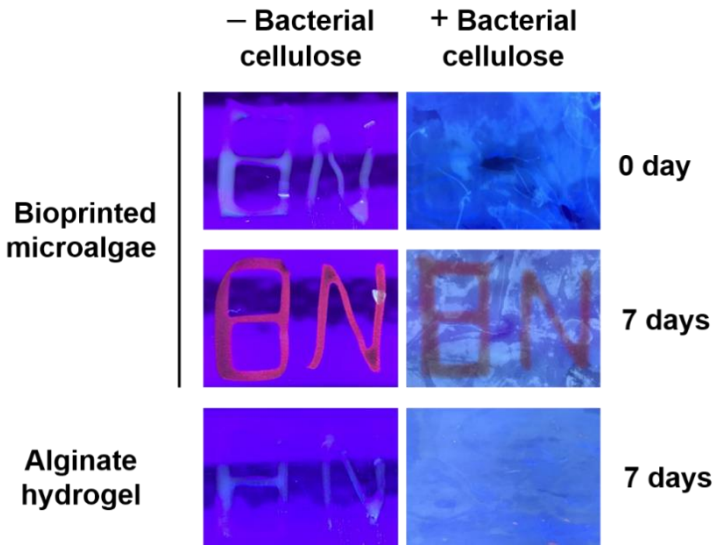

Figure S6.3 Red fluorescence of chlorophyll in bioprinted microalgae upon UV excitation. Bioprinted samples (incubated under photomixotrophic conditions for 0 or 7 days) were imaged on a UV-transilluminator.

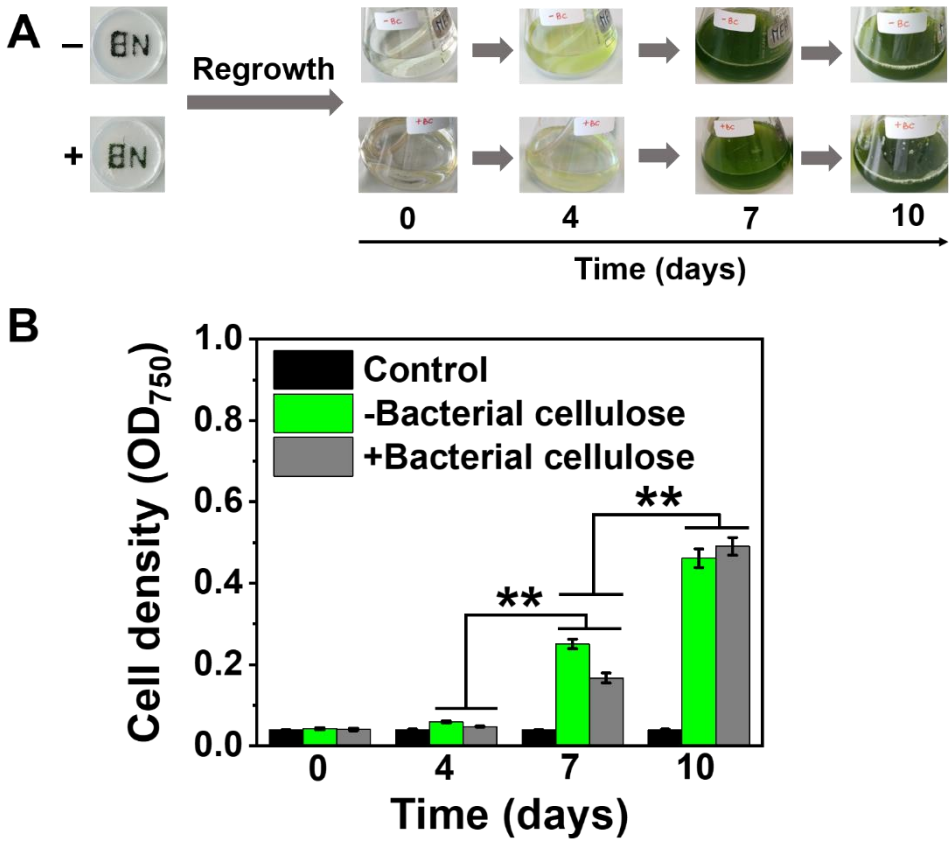

Figure S6.4 Regrowth of microalgae (A, B) in fresh carbon-supplemented medium after 28 days of growth in bioprints. Microalgae from bioprints (28-days old) on both carbon-supplemented agar and bacterial cellulose overtop of carbon-supplemented agar was recovered and used as the inoculum (0.1% (*v/v*)) for regrowth in fresh carbon-supplemented medium. Samples were incubated under light:dark conditions (12:12 h), and cell density measurements ($O.D._{750}$) were carried out at 0, 4, 7, and 10 days. ns, not significant; $^{**}p < 0.01$ as determined by one-way (single-factor) ANOVA with post-hoc Tukey's HSD.

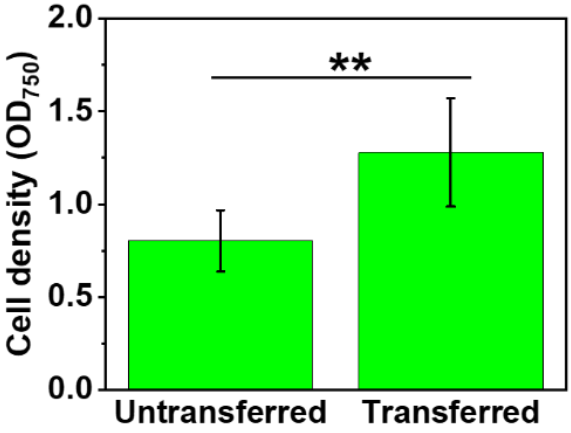

Figure S6.5 Effect on cell density of transferring microalgae bioprints to fresh carbon-supplemented agar. Cell density measurements ($O.D._{750}$) were performed on microalgae bioprinted onto bacterial cellulose overtop of carbon-supplemented agar that was grown for 14 days ("untransferred" samples), as well as on microalgae bioprinted onto bacterial cellulose that was removed from carbon-supplemented agar after 7 days of growth, then transferred to a fresh carbon-supplemented agar and grown for another 7 days ("transferred" samples). $^{**}p < 0.01$, statistically significant as determined by one-way (single factor) ANOVA with post-hoc Tukey's HSD.

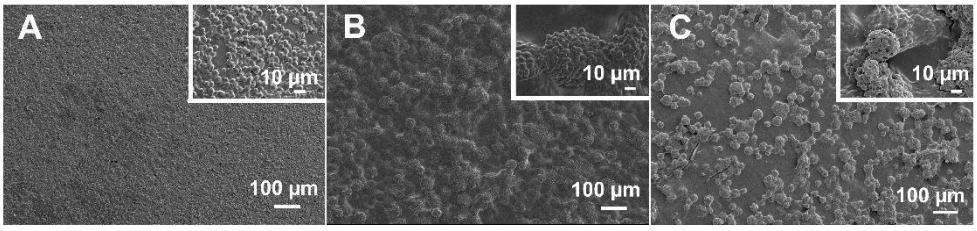

Figure S6.6 Scanning electron microscopy images of (A) *C. reinhardtii* grown as a liquid culture (devoid of alginate), (B) bioprinted *C. reinhardtii* on carbon-supplemented agar, and (C) bioprinted *C. reinhardtii* on bacterial cellulose overtop of carbon-supplemented agar. SEM images were taken following 7 days of growth under photomixotrophic condition.

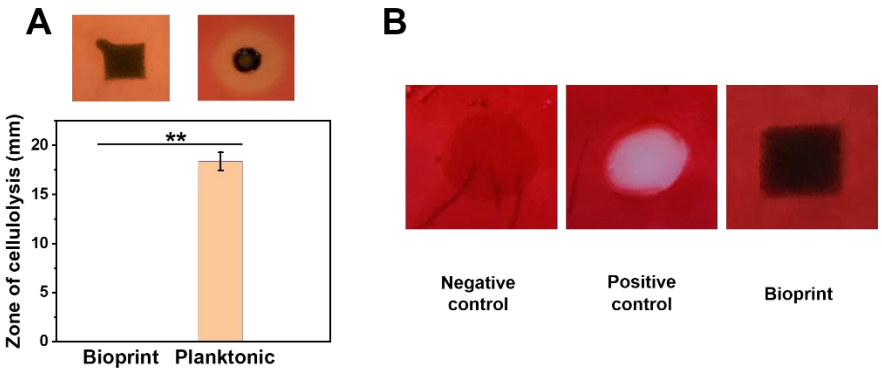

Figure S6.7 Determination of cellulolytic activities of *C. reinhardtii* using Congo red staining. (A) On carboxymethyl cellulose (0.1 *w/v*%) as the substrate. Microalgae were bioprinted or grown as planktonic culture in a well within carbon-supplemented agar (+ carboxymethyl cellulose) under photomixotrophic condition for 7 days. Congo red staining was carried out, and the zone of cellullolysis was determined. (B) On bacterial cellulose as the substrate. Microalgae were bioprinted onto bacterial cellulose overtop of carbon-supplemented agar and grown under the same conditions for 7 days and Congo red staining was performed. The negative control is bacterial cellulose incubated with 50 µL sodium chloride (0.9 *w/v* %), and the positive control is bacterial cellulose incubated with 50 µL of cellulase overnight at 30 °C. $^{**}p < 0.01$, statistically significant (determined by one-way (single factor) ANOVA with post-hoc Tukey's HSD).

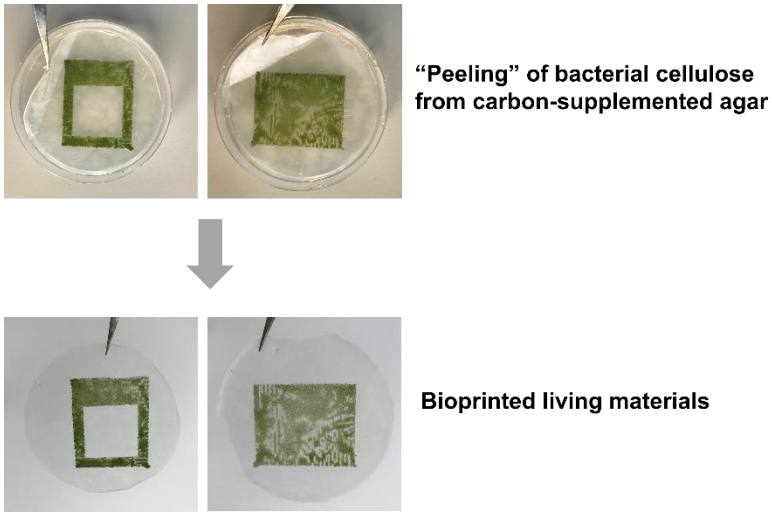

Figure S6.8 Peeling of microalgae bioprints off of agar substrates. Bacterial cellulose supporting 7-day-old bioprinted microalgae was peeled off from carbon-supplemented agar. The detached bacterial cellulose supporting the bioprinted microalgae can be directly used as a living material.

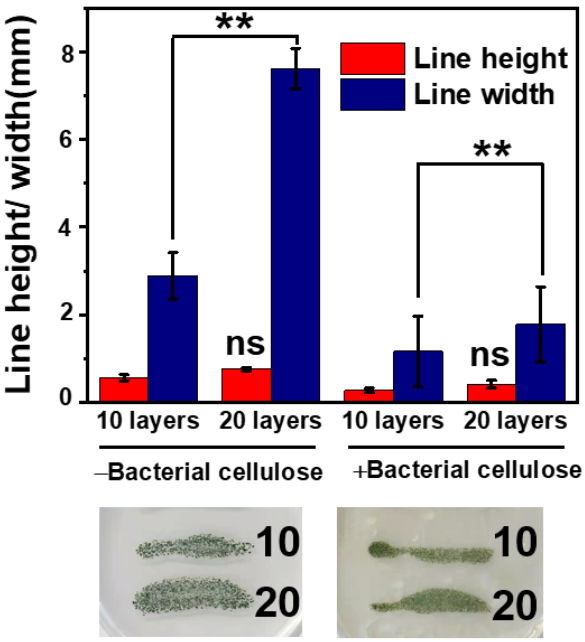

Figure S6.9 Line height and width of bioprinted 10- and 20-layer microalgal structures. Bottom images represent the bioprinted microalgal structures (10- and 20-layers) on carbon-supplemented agar (left) and on bacterial cellulose overtop of carbon-supplemented agar (right). ns, not significant (a comparison between 10 and 20 layers) ; $^{**}p < 0.01$, as determined by one-way (single factor) ANOVA with post-hoc Tukey's HSD.

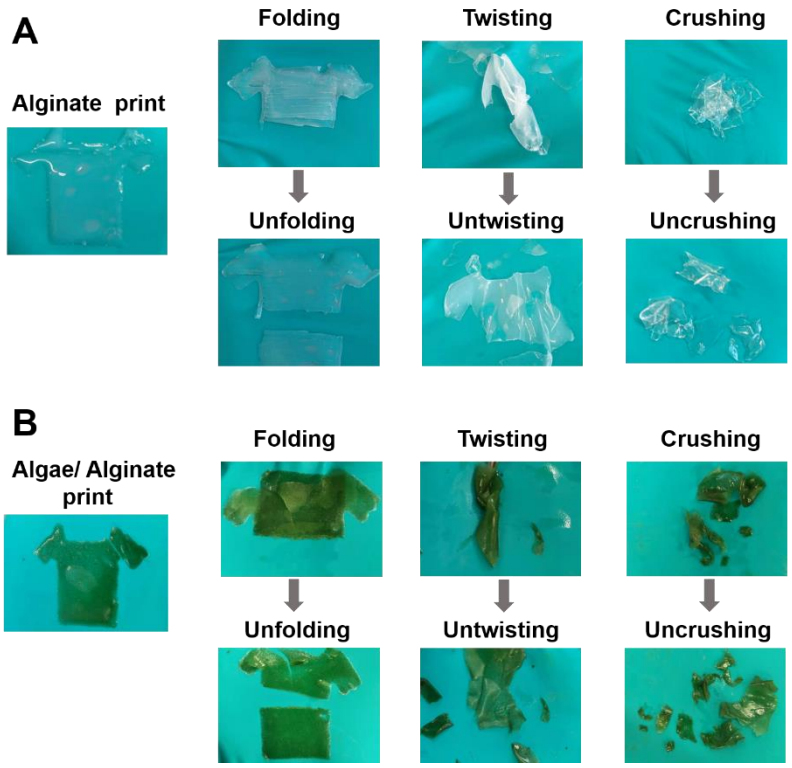

Figure S6.10 Physical stability of (A) prints of alginate (without microalgae) and (B) bioprints of alginate containing microalgae. Each print was made by printing onto bacterial cellulose (placed overtop of carbon-supplemented agar) and incubated for 7 days under photomixotrophic condition. Prints were then subjected to physical distortions and imaged.

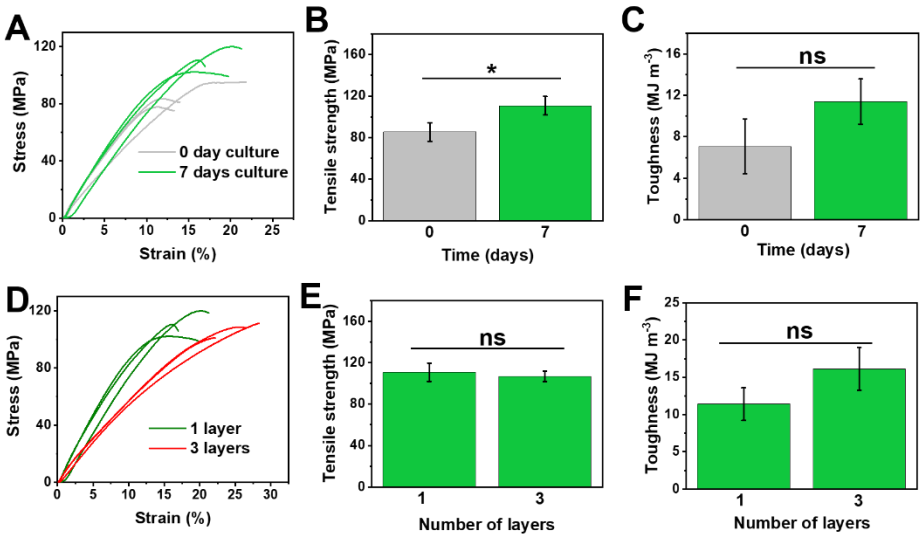

Figure S6.11 Effect of fabrication parameters (time elapsed after printing (A-C) and number of printed layers (D-F)) on the mechanical properties of bioprinted living materials. ns, not significant; *$p < 0.05$ as determined by one-way (single factor) ANOVA with post-hoc Tukey's HSD.

Figure S6.12 Stability of bioprints. Photographs of bioprinted microalgae on bacterial cellulose following 1 month of incubation under ambient conditions.

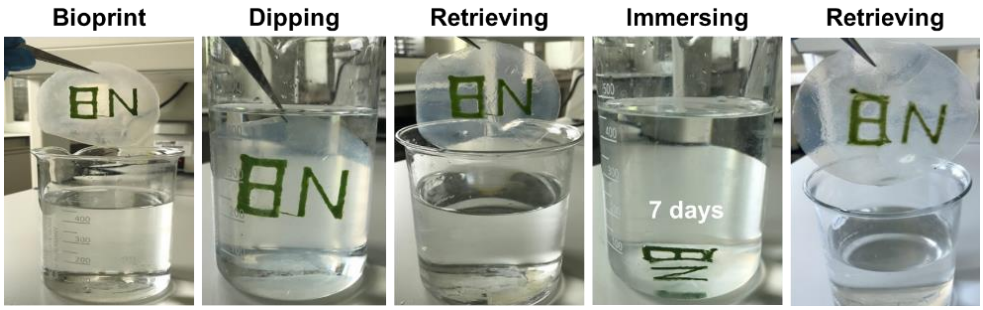

Figure S6.13 Stability of bioprints to dipping and immersion in water. Bioprinted microalgae materials were retrieved from water after dipping and immersion.

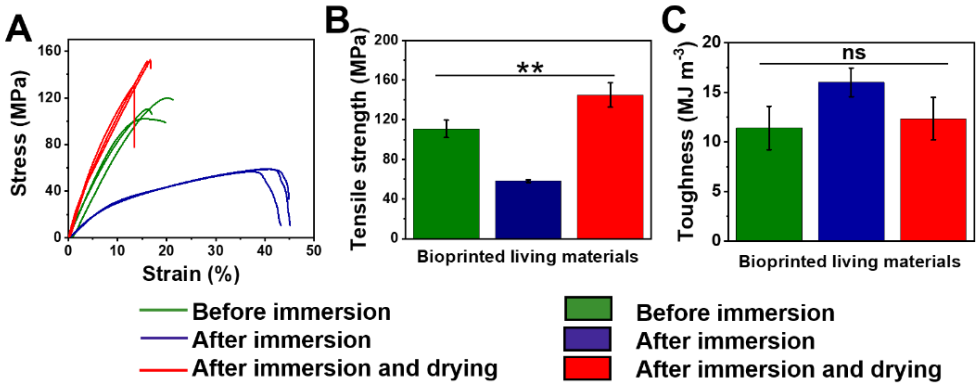

Figure S6.14 Tensile testing of bioprinted materials before and after immersion into water (A) stress-strain curves, **(B)** tensile strength, **(C)** toughness. ns, not significant; $^{**}p < 0.01$ as determined by one-way (single factor) ANOVA with post-hoc Tukey's HSD.

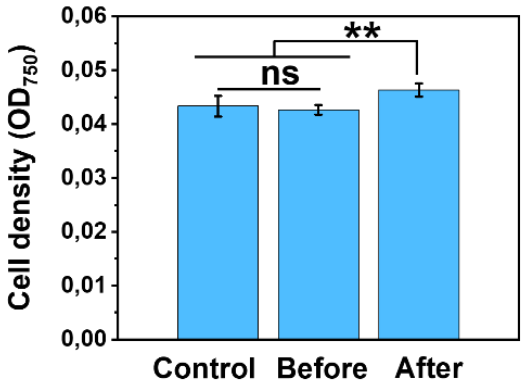

Figure S6.15 Measurements of microalgae release from bioprints on bacterial cellulose into water. Bacterial cellulose with the microalgal bioprints were immersed in water for 7 days under ambient conditions. Microalgae release from the bioprints were determined by measuring the $O.D._{750}$ of water before immersion and after retrieval of bioprints. Control consisted of water without the microalgal bioprints. ns, not significant; $^{**}p < 0.01$, statistically significant (determined by one-way (single factor) ANOVA with post-hoc Tukey's HSD).

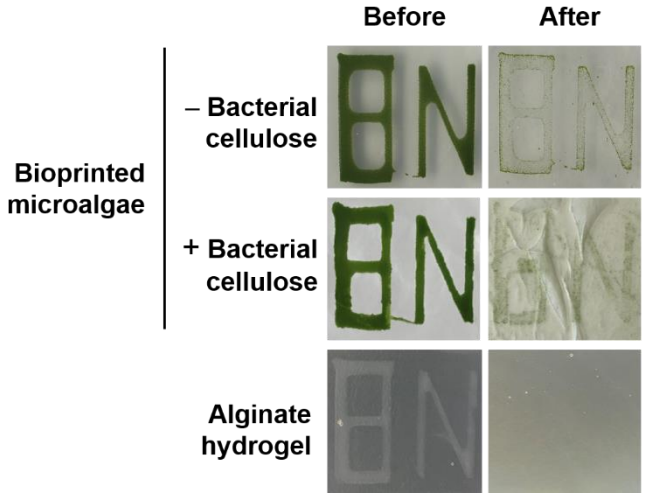

Figure S6.16 Citrate treatment of the bioprinted structures for the removal of alginate hydrogel and recovery of microalgal cells. Bioprinted structures (7 days of photomixotrophic growth) were treated with sodium citrate (0.5 M) for 2 hours with shaking at 40 rpm under ambient conditions. Bioprints were imaged before and after the citrate treatment.

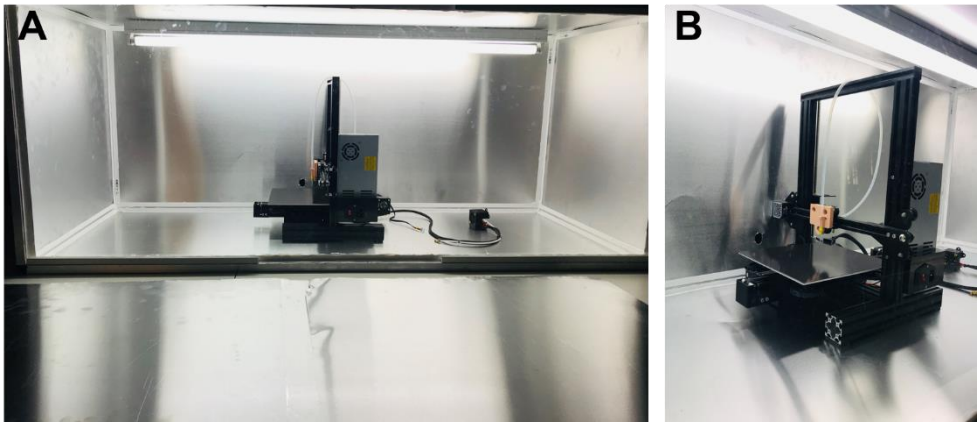

Figure S6.17 Bioprinter for scaled-up fabrication of photosynthetic living materials. (A) Overall view and (B) closer view of the bioprinting set-up.

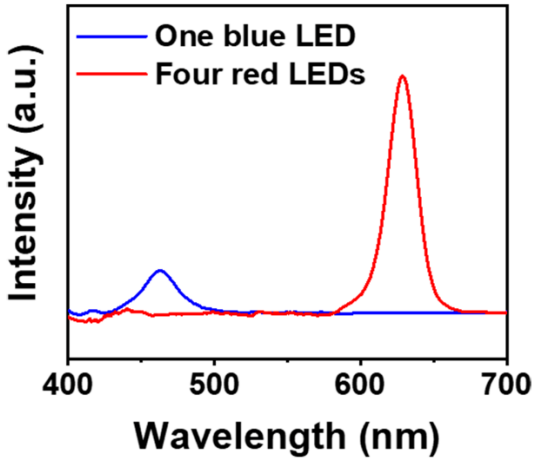

Figure S6.18 Spectra of LEDs employed for microalgae growth in the bioprints. One blue LED and four red LEDs were used for the microalgal cultivation. The red line in the spectra corresponds to the intensity measured from four red LEDs, whereas the blue line corresponds to the intensity measured from one blue LED.

References

1. Spiesz, E. M.; Yu, K.; Lehner, B. A. E.; Schmieden, D. T.; Aubin-Tam, M. E.; Meyer, A. S. Three-Dimensional Patterning of Engineered Biofilms with a Do-it-yourself Bioprinter. J. Vis. Exp. 2019, *147*, e59477.

2. Lehner, B. A. E.; Schmieden, D. T.; Meyer, A. S. A Straightforward Approach for 3D Bacterial Printing. ACS Synth. Biol. 2017, *6* (7), 1124-1130.

3. Lode, A.; Krujatz, F.; Brüggemeier, S.; Quade, M.; Schütz, K.; Knaack, S.; Weber, J.; Bley, T.; Gelinsky, M. Green Bioprinting: Fabrication of Photosynthetic Algae-Laden Hydrogel Scaffolds for Biotechnological and Medical Applications. Eng. Life Sci. 2015, *15* (2), 177-183.

4. Chioccioli, M.; Hankamer, B.; Ross, I. L. Flow Cytometry Pulse Width Data Enables Rapid and Sensitive Estimation of Biomass Dry Weight in the Microalgae *Chlamydomonas reinhardtii* and *Chlorella vulgaris*. PLoS One 2014, *9* (5), e97269.

5. Hopfner, U.; Schenck, T. L.; Chavez, M. N.; Machens, H. G.; Bohne, A. V.; Nickelsen, J.; Giunta, R. E.; Egana, J. T. Development of Photosynthetic Biomaterials for In Vitro Tissue Engineering. Acta Biomater. 2014, *10* (6), 2712-2717.

6. Blifernez-Klassen, O.; Klassen, V.; Doebbe, A.; Kersting, K.; Grimm, P.; Wobbe, L.; Kruse, O. Cellulose Degradation and Assimilation by the Unicellular Phototrophic eukaryote *Chlamydomonas reinhardtii*. Nat. Commun. 2012, *3*, 1214.

7

Conclusions and Outlook

Many biological materials (*e.g.*, spider silk,[1] wood,[2] nacre[3]) possess excellent mechanical performance due to their highly organized structure from nano-, micro- to macroscopic scales.[4] To mimic this multiscale structure, several fabrication techniques, including layer-by-layer, vacuum filtration, freeze casting, hot-pressing, *etc.*, are developed.[5] However, most of the current fabrication methods are either energy-intensive, labor-intensive, environmental-unfriendly, or with limited scalable abilities.[6] The development of green and mild fabrication methods with scalable productibility becomes increasingly important. Microbial fabrication is an emerging technique in the construction of advanced materials from microbiology perspective.[7] The mild incubation temperature, fast replicability and gene-engineered possibility of microorganisms make this technique promising in material science, especially in the mild and scalable construction of bioinspired functional materials.[8]

The three most important questions studied in this thesis are summarized here:

1. "How to produce a composite material biologically?"

Microorganisms,[8, 9] including bacteria, fungi and algae, can replicate fast, grow under mild conditions and secrete many biological enzymes, which could be used as bio-catalysts in chemical reactions[10] and in material science applications.[11] Moreover, as microorganisms require very little space to be stored and can usually stay alive upon freezing, they draw increasingly attention in the fabrication of bioinspired materials and living materials.[7, 11-13]

As one of the most important starting materials produced from microorganisms, bacterial cellulose (BC) is drawing increasing attention in the fabrication of next-generation sustainable structural materials.[14] However, pure BC lacks biocompatibility, conductivity and photosensitivity. To make full use of this new material, it is of critical importance to introduce functional components into natural BC structure.[15]

Due to the densely packed structure, it remains difficult to insert a second component within the natural BC network, especially viscous polymers, inorganic particles and living

cells.[15] Two basic methods (*ex situ* and *in situ*) were used in this thesis to solve this problem. In Chapter 2 (*ex situ*), the BC wet pellicle was mechanically disintegrated into a fibrous suspension, inorganic particles could be bacterially grown in the suspension to form a BC-based slurry, which could further self-assemble into a newly layered material. In Chapters 3 and 4 (*in situ*), viscous polymers and water-soluble inorganic particles were added into the liquid fermentation medium before BC is formed. During the BC biological fermentation procedure, these polymers and inorganic particles were entrapped into the BC network.

2. "**How to improve their mechanical properties?**"

Tensile toughness, one of the most important mechanical properties in many applications, is the amount of energy that a material can absorb before rupturing under tension. It is related to the tensile strength and elongation at break. Pure BC dried film possesses excellent tensile strength (over 100 MPa), but less elongation at break values (less than 5 %), which results in pure BC having relatively low toughness values (< 3 MJ m^{-3}). In Chapter 2, $CaCO_3$ inorganic particles were inserted into BC by disintegration, biomineralization and reassembly. The new composites showed a reduced tensile strength (51 MPa) but improved elongation at break (54 %), resulting in an overall toughness increase of the final composite (21 MJ m^{-3}). The reduction in tensile strength is because of the presence of $CaCO_3$, which brings stress concentration in the cross section; while the enhancement of the elongation at break is attributed to the BC-$CaCO_3$ crystal fiber interaction, the addition of γ-poly (glutamic acid) (PGA), and the wrinkled structure. In Chapter 3, BC-PVA composites with a spiral honeycomb structure showed both improved tensile strength (315 MPa) and elongation at break (9 %) values, with an overall toughness of 18 MJ m^{-3}. The highly organized honeycomb microstructure is the major reason for this toughness increase. In Chapter 4, the graphene oxide (GO) and BC films showed a similar tensile strength (130 MPa) and improved elongation at break value (45 %), with an enhanced toughness value (36 MJ m^{-3}), which makes it one of the toughest BC composite film. The improvement in toughness is attributed to the addition of PGA, the wrinkled structure and the GO-fiber interaction. The overall mechanical properties of the composites reported in this thesis (Chapter 2-4) and some everyday materials (natural nacre, pure BC, ABS plastics) are summarized in **Table 7.1**.

Overall, the raw components, the interface interactions and the structure organization are three major factors that influence the tensile strength, elongation at break and toughness values of a material.

Table 7.1 Comparison of the mechanical properties of the biologically produced composites with everyday materials.

Samples	Tensile Strength [MPa]	Elongation at Break [%]	Toughness [MJ m^{-3}]	References
Pure BC	148.1 ± 13.4	4.5 ± 0.1	4.9 ± 0.8	16
Natural nacre	60-70	< 1	0.2-2	3, 17
Natural wood	40-60	< 3	0.36	18
Polypropylene (PP) plastic	25.2 ± 0.2	7.2 ± 0.5	1.3 ± 0.2	19
Acrylonitrile butadiene styrene (ABS) plastic	30-43	10-50	0.14-2.73	20, 21, 22
Biomineralized BC composite	50.6 ± 1.9	54.0 ± 11.1	21.3 ± 4.2	Chapter 2
Honeycomb BC-PVA	315 ±21	8.6 ± 1.3	17.8 ± 3.6	Chapter 3
BC-GO-PGA	130.5 ± 17.4	44.9 ± 7.6	35.7 ± 10.6	Chapter 4

3. "How to spatially organize the material?"

During the biological production stage, living cells are randomly distributed into the fermentation medium, which might result in the inhomogeneous distribution of the produced components. The emerging of 3D printing technique solves this problem. 3D bioprinting is an emerging technique and remains a very useful tool in the spatial patterning of living materials. In Chapter 5 and 6, we used this technique to construct functional living materials with shapes that can be controlled spatially at the millimeter scale. In Chapter 5, we printed a calcium-alginate hydrogel containing bacteria and optimized the printing resolution. In Chapter 6, based on the same calcium-alginate hydrogel, we printed microalgae. The bioprinting was done on the top of a dried BC film, in order to improve the mechanical properties of the fragile calcium-alginate hydrogel. Notably, the presence of microalgae endows the material with photosynthetic properties, which makes it promising in diverse applications including photosynthetic skin, artificial leaves, bio-garments, photosynthetic adhesive labels, *etc*.

Although 3D printing could realize the spatial organization at submillimeter scale and macroscale, it remains difficult to design the nano- and microscale structure. To achieve the spatial organization at smaller scales (nano- and micro-), *ex situ* (Chapter 2), *in situ* (Chapter 3 and 4) and self-assembly (Chapter 2-4) techniques were utilized. In Chapter 2, the

disintegrated and biomineralized BC could self-assemble into a layered structure, with $CaCO_3$ crystals entrapped in-between the microscaled layers. In Chapter 3, PVA polymers were entrapped into the BC layers by the combination of *in situ* fermentation and self-assembly. In Chapter 4, inorganic GO particles were spatially organized into the BC layered structure with a semi *in situ* fermentation technique.

4. Limitations and future challenges

There are also several limitations that need to be noticed:

1. In the *ex situ* method, we disintegrate the natural structure of BC, which brings the reassembled material with reduced tensile strength. Due to this disadvantage, *in situ* fermentation method is better in the fabrication of BC-based composites, as BC natural structure does not have to be destroyed during the fabrication procedure.

2. The biomineralized BC composite is self-assembled by water evaporation, therefore, the material is not water resistant. To overcome this problem, coatings need to be applied on the material surface in the real application.

3. For the spiral honeycomb BC composite, due to the addition of PVA, the yield of the final composite is reduced during *in situ* fermentation, which might increase the potential cost for this material.

4. To get a whole piece of BC bulk material, the *in situ* fermentation need to be carried out under static conditions. In the static *in situ* fermentation procedure, only BC pellicles can be formed. BC with tubular or complex geometries are hardly achievable.

5. The Ca^{2+}-alginate based 3D printing technique makes it difficult to print scaffolds with more than 5 layers, as the Ca^{2+} ions need time to diffuse from bottom agar to the upper layer of sodium alginate, which makes the upper layer ink difficult to be solidified.

6. Although we printed microalgae on a BC surface, we still did not manage to insert living algal cells into BC network with *in situ* fermentation method.

In summary, microorganisms are very promising in the fabrication of advanced materials. The overall principle is to keep living microorganisms alive during the material fabrication procedure. More works need to be explored by selecting proper raw materials, living cells and processing methods. With the development of genetic engineering and synthetic biology, living microorganisms will play an increasingly important role in the fabrication of next generation sustainable bioinspired materials and functional living materials.

References:

1. Wang, Q.; Schniepp, H. C. Strength of Recluse Spider's Silk Originates from Nanofibrils. ACS Macro Lett. 2018, *7* (11), 1364-1370.

2. Chen, C.; Hu, L. Nanocellulose toward Advanced Energy Storage Devices: Structure and Electrochemistry. Acc Chem. Res. 2018, *51* (12), 3154-3165.

3. Barthelat, F. Nacre from Mollusk Shells: A Model for High-Performance Structural Materials. Bioinspir. Biomim. 2010, *5* (3), 035001.

4. Huang, W.; Restrepo, D.; Jung, J. Y.; Su, F. Y.; Liu, Z.; Ritchie, R. O.; McKittrick, J.; Zavattieri, P.; Kisailus, D. Multiscale Toughening Mechanisms in Biological Materials and Bioinspired Designs. Adv. Mater. 2019, *31* (43), 1901561.

5. Zhao, H.; Yang, Z.; Guo, L. Nacre-inspired Composites with Different Macroscopic Dimensions: Strategies for Improved Mechanical Performance and Applications. NPG Asia Mater. 2018, *10* (4), 1-22.

6. Zhao, C.; Zhang, P.; Zhou, J.; Qi, S.; Yamauchi, Y.; Shi, R.; Fang, R.; Ishida, Y.; Wang, S.; Tomsia, A. P.; Liu, M.; Jiang, L. Layered Nanocomposites by Shear-flow-induced Alignment of Nanosheets. Nature 2020, *580* (7802), 210-215.

7. Moradali, M. F.; Rehm, B. H. A. Bacterial Biopolymers: From Pathogenesis to Advanced Materials. Nat. Rev. Microbiol. 2020, *18* (4), 195-210.

8. Schaffner, M.; Ruhs, P. A.; Coulter, F.; Kilcher, S.; Studart, A. R. 3D Printing of Bacteria into Functional Complex Materials. Sci. Adv. 2017, *3* (12), eaao6804.

9. Maharjan, S.; Alva, J.; Cámara, C.; Rubio, A. G.; Hernández, D.; Delavaux, C.; Correa, E.; Romo, M. D.; Bonilla, D.; Santiago, M. L.; Li, W.; Cheng, F.; Ying, G.; Zhang, Y. S. Symbiotic Photosynthetic Oxygenation within 3D-Bioprinted Vascularized Tissues. Matter 2021, *4* (1), 217-240.

10. Lee, S. Y.; Kim, H. U.; Chae, T. U.; Cho, J. S.; Kim, J. W.; Shin, J. H.; Kim, D. I.; Ko, Y.-S.; Jang, W. D.; Jang, Y.-S. A Comprehensive Metabolic Map for Production of Bio-based Chemicals. Nat. Cat. 2019, *2* (1), 18-33.

11. Heveran, C. M.; Williams, S. L.; Qiu, J.; Artier, J.; Hubler, M. H.; Cook, S. M.; Cameron, J. C.; Srubar, W. V. Biomineralization and Successive Regeneration of Engineered Living Building Materials. Matter 2020, *2* (2), 481-494.

12. Qin, W.; Wang, C. Y.; Ma, Y. X.; Shen, M. J.; Li, J.; Jiao, K.; Tay, F. R.; Niu, L. N. Microbe-Mediated Extracellular and Intracellular Mineralization: Environmental, Industrial, and Biotechnological Applications. Adv. Mater. 2020, *32* (22), 1907833.

13. Xin, A.; Su, Y.; Feng, S.; Yan, M.; Yu, K.; Feng, Z.; Hoon Lee, K.; Sun, L.; Wang, Q. Growing Living Composites with Ordered Microstructures and Exceptional Mechanical Properties. Adv. Mater. 2021, 2006946.

14. Torres, F. G.; Arroyo, J. J.; Troncoso, O. P. Bacterial Cellulose Nanocomposites: An All-nano Type of Material. Mater. Sci. Eng. C 2019, *98*, 1277-1293.

15. Shah, N.; Ul-Islam, M.; Khattak, W. A.; Park, J. K. Overview of Bacterial Cellulose Composites: A Multipurpose Advanced Material. Carbohydr. Polym. 2013, *98* (2), 1585-1598.

16. Wu, Z.; Chen, S.; Wu, R.; Sheng, N.; Zhang, M.; Ji, P.; Wang, H. Top-down Peeling Bacterial Cellulose to High Strength Ultrathin Films and Multifunctional Fibers. Chem. Eng. J. 2020, *391*, 123527.

17. Kakisawa, H.; Sumitomo, T. The Toughening Mechanism of Nacre and Structural Materials Inspired by Nacre. Sci. Technol. Adv. Mater. 2011, *12* (6), 064710.

18. Jia, C.; Chen, C.; Kuang, Y.; Fu, K.; Wang, Y.; Yao, Y.; Kronthal, S.; Hitz, E.; Song, J.; Xu, F.; Liu, B.; Hu, L. From Wood to Textiles: Top-Down Assembly of Aligned Cellulose Nanofibers. Adv. Mater. 2018, *30* (30), 1801347.

19. Yang, B.-X.; Shi, J.-H.; Pramoda, K. P.; Goh, S. H. Enhancement of the Mechanical Properties of Polypropylene Using Polypropylene-grafted Multiwalled Carbon Nanotubes. Compos. Sci. Technol. 2008, *68* (12), 2490-2497.

20. Bai, X.; Isaac, D. H.; Smith, K. Reprocessing Acrylonitrile–butadiene–styrene Pastics: Structure–property Relationships. Polym. Eng. Sci. 2007, *47* (2), 120-130.

21. Mamaghani Shishavan, S.; Azdast, T.; Rash Ahmadi, S. Investigation of the Effect of Nanoclay and Processing Parameters on the Tensile Strength and Hardness of Injection Molded Acrylonitrile Butadiene Styrene–organoclay Nanocomposites. Mater. Des. 2014, *58*, 527-534.

22. Ching, E. C. Y.; Poon, W. K. Y.; Li, R. K. Y.; Mai, Y.-W. Effect of Strain Rate on the Fracture Toughness of Some Ductile Polymers Using the Essential Work of Fracture (EWF) Approach. Polym. Eng. Sci. 2000, *40* (12), 2558-2568.

Acknowledgements

PhD is a memorable but challenging journey that cannot be accomplished by an individual effort. I feel I am very lucky to arrive the end point of this journey. It is not my own achievement, but the result of the collaboration of many wonderful people that I would like to thank here.

First of all, I would like to thank my promotor and daily supervisor, Marie-Eve Aubin-Tam, who had the biggest influence on me during my time in Delft. Thank you very much for giving me the precious opportunity for pursuing my PhD at TU Delft. During the past three years, you gave so many suggestions on my research works, encouraged me to solve problems and think in a scientific way; you tolerated my mistakes and let me know what I should do correctly in academic publication and collaboration; you talked with me many times and helped me get rid of the financial problems and release my pressure of career development. I really appreciate that you spent so much time from your tight agenda, even during your holiday time, to give feedbacks and improve the quality of my manuscripts. Because of your contributions, I was able to complete my PhD work within three years. I really enjoy the time in MEA lab. Thanks Marie!

Yuemei, thank you for being my promotor. Thank you very much for giving me so many useful suggestions concerning presentation, thesis structure, interview, career plan, *etc.* These suggestions are very important for my personal development. Whenever I contact you, you responded my email immediately and behaved very warmly to help me. Due to your technical suggestions, we could improve the quality of the honeycomb paper quite a lot within a very short time. Without your contributions, my PhD cannot go that fast. Thank you!

I would like to thank the committee members (Prof. dr. A. A. Zadpoor, Prof. dr. G. H. Koenderink, Prof. dr. M. M. G. Kamperman, Dr. K. Masania and Prof. dr. M. Linder). Thank you for reviewing my PhD thesis and accepting to present my PhD defence ceremony.

Srikkanth, I spent most of my working time with you during my PhD, we have fruitful results and I really enjoy our wonderful collaboration. Thank you very much for sharing your previous experiences with me and encouraging me when I was in low mood. I feel very happy to work with you these years. I will remember our teamwork and brainstorming. I wish you a wonderful career in the future.

Ewa, you brought me to our nacre project and showed me all the basic experimental details, which are very important for my PhD work; you helped me with many technical problems

and gave me a lot of useful suggestions. I feel very lucky that I can learn so many things from you, thanks Ewa!

Roland, I am really happy to be your officemate. You helped me a lot with my experiments and gave me so many useful suggestions on my projects. You are a super technician with positive attitude; you always have creative ideas. I really enjoy our everyday talking in the office and I will remember you.

Ramon, I still remember that at the beginning of my PhD, we two moved all the lab stuffs from AM lab to MEA lab, it is a very tough but memorable work. I also remember that I brought many troubles to you during my PhD. Due to your tolerance to my mistakes, I was able to learn many lab regulations. You taught me the biological experiments, helped me order chemicals, reviewed most of my manuscripts. Without your help, I cannot manage my PhD projects. Thanks Ramon!

Specifically, I would like to thank many technicians from chemical engineering department, aerospace engineering faculty and industrial design faculty. Ben Norder, thank you very much for helping me with the XRD testing. You helped me test so many samples for free. Without your help, I cannot start my PhD project. Besides, thank you very much for introducing Berthil to me, who helped me a lot during my PhD. Berthil Grashof, thank you so much for your kind help with the mechanical testing. You have a huge help for my PhD work. I broke your machine many times, but you still agree me to do experiments in your lab. You introduced so many technicians (Dave, Misja, Gertjan, Durga) to me, and they helped me with different characterizations. That is how the Chapter 2 of my PhD thesis could be entirely completed. Thanks Berthil, you are definitely one of the most important person during my PhD. Dave, thank you very much for your kind help with the compression testing. I still remember that you and Berthil helped me with the compression testing during the Christmas holiday in 2019. Thanks Dave! Misja, you helped me with the impact testing, those are very important results in my PhD thesis, thanks very much! Gertjan and Durga, I would also thank you both for giving me helps with the machine training. Marlies, you helped me many times with the indentation, FTIR and 3-point bending test, thank you very much for your kind help! Bart van der Linden, you are also one of the most important person in my PhD. TGA is one of the most important characterization in my PhD projects, and I destroyed your TGA machine many times, but you still allow me to use it for free. Without your kind help, I could not imagine how could I continue my PhD projects. Thank you very much, Bart! I would also thank Mascha and Tessa from industrial design for their help with the tensile testing.

Helda, Mohammad and Amir, we had a very nice collaboration about the honeycomb paper. Thanks very much for your nice suggestions to our paper. Anne, thank you very much for

your very useful comments on my manuscripts. I really like our collaboration. Elvin, thank you for reviewing our bioprinting manuscripts and bringing new students to our lab.

I would like to thank many nice people in BN. Anke and Jan, you helped me autoclave so much medium during the past three years, and I also brought you many troubles. Sorry for the troubles and thank you very much for your kind help, I will remember you! Dominik, you helped me with many technical problems, I wish you a wonderful career development. Benjamin, you showed me how to use the 3D printer. I still remember that we took videos together with Ewa for our *JoVE* paper, thanks for your help! Wayne, you showed me the SEM in the clean room, thanks very much for your precious time, very nice to know you. Irfan, we did experiments together and you helped me a lot, I will remember our happy lab time. Chaline, you gave me many suggestions about the DE programme, thanks very much, I wish you a successful PhD. Da, thank you for answering me so many questions, your suggestions are very useful. Kuang, I am very happy about our project discussion. Tanja, I remember that I burned your hand when I moved to the MEA lab for the first time. I feel very sorry for that. You are such a nice girl and I wish you a nice PhD time. Arjen, thank you very much for joining my GO/No GO meeting and giving your feedbacks. Aurora, you are a very nice girl, thank you for giving me many useful suggestions. Jeremie, thank you very much for your suggestions about the microscope. Cecilia, thank you for helping me solve many lab problems and order petri dishes. Ward, you are my first student, and you work very hard, I wish you a nice future. Joris, you are a very smart guy, I am very happy to work with you. Arash, I really enjoy our talking and I wish you a successful PhD. Besides, I am also very happy to meet the following people: Guillermo, Martin, Diederik, Wiel, Stefan, Natasha, Lisa, Vivian, Joran, Josine, Anouk, Hein, Jeroen, Celina, Floor, Amaria, Donna, and many people in the corner with familiar faces but I do not know the name.

Meanwhile, I would like to thank my Chinese friends who make me have a wonderful time in Delft. Guotai, you are one of my best friend in Netherlands and I hope you can soon complete your PhD successfully. Jiahui, thank you for helping me and introducing Helda and Amir to me. You are very smart and hard-working. I wish you a successful PhD. Jianing, thank you very much for your help with the hardness testing. Peng Lin, thank you very much for your help with the viscosity measurement. Besides, I would like to thank Chang Liu, Xiaohui Liu, Wenjun Yang, Bowen Fan, Kailun Yang, Yongjun Men, Kai Liu, Xuerui Wang, Zilong Liu, Yu Wang, *etc*. You make my life in Netherlands enjoyable. I wish all of you a bright future.

Finally, thanks my wife Xiangxiang Zhou for 10 years' accompany and my friends' and families' support.

Curriculum Vitae

Kui Yu

24-10-1991	Born in Henan province, China
2010-2014	Bachelor in Macromolecular Materials and Engineering Jiaxing University, Zhejiang, China
2014-2017	Master of Engineering in Material Science and Engineering Donghua University, Shanghai, China
2017-2018	Researcher in Aachen-Maastricht Institute for Biobased Materials Maastricht University, Geleen, the Netherlands
2018-2021	PhD in Bioinspired Materials and Living Materials Delft University of Technology, Delft, the Netherlands

List of Publications

(13). **K. Yu**, E. M. Spiesz, S. Balasubramanian, D. T. Schmieden, A. S. Meyer, M.-E. Aubin-Tam. Scalable Bacterial Production of Moldable and Recyclable Biomineralized Cellulose with Tunable Mechanical Properties. ***Cell Reports Physical Science***, accepted for publication.

(12). **K. Yu**, S. Balasubramanian, H. Pahlavani, M. J. Mirzaali, A. A. Zadpoor, M.-E. Aubin-Tam. Spiral Honeycomb Microstructured Bacterial Cellulose for Increased Strength and Toughness. ***ACS Applied Materials & Interfaces***, 2020, 12, 45, 50748–50755.

(11). **K. Yu**, M.-E. Aubin-Tam. Bacterially Grown Cellulose/Graphene Oxide Composites Infused with γ-Poly (Glutamic Acid) as Biodegradable Structural Materials with Enhanced Toughness. ***ACS Applied Nano Materials***, 2020, 3, 12, 12055–12063.

(10). S. Balasubramanian #, **K. Yu #**, A. S. Meyer, E. Karana, M.-E. Aubin-Tam. Bioprinting of Regenerative Photosynthetic Living Materials, ***Advanced Functional Materials***, 2021, 2011162. # equal contributions.

(9). E. M. Spiesz #, **K. Yu #**, B. A. E. Lehner, D. T. Schmieden, M.-E. Aubin-Tam, A. S. Meyer. Three-dimensional Patterning of Engineered Biofilms with a Do-it-yourself Bioprinter. ***Journal of Visualized Experiments***, 2019, 147, 59477. # equal contributions.

(8). **K. Yu**, T. Zhu, Y. Wu, X. Zhou, X. Yang, J. Wang, J. Fang, H. El-Hamshary, S. S. Al-Deyab, X. Mo. Incorporation of Amoxicillin-loaded Organic Montmorillonite into Poly(ester-urethane) urea Nanofibers as a Functional Tissue Engineering Scaffold. ***Colloids and Surfaces B: Biointerfaces***, 2017, 151, 314-323.

(7). **K. Yu**, X. Zhou, M. R. El-Aassar, T. Zhu, Y. Wu, J. Wang, W. Feng, Y. Morsi, X. Mo. Preparation and Characterization of Chitosan Nanofibers Containing Silver Nanoparticles. ***Journal of Donghua University***, 2017, 34 (1), 105-110.

(6). **K. Yu**, X. Zhou, T. Zhu, T. Wu, J. Wang, J. Fang, M. R. El-Aassar, H. El-Hamshary, M. El-Newehy, X. Mo. Fabrication of Poly(ester-urethane) urea Elastomer/Gelatin Electrospun Nanofibrous Membranes for the Potential Application in Skin Tissue Engineering. ***RSC Advances***, 2016, 6 (77), 73636-73644.

(5). J. Dong, Y. Li, P. Lin, S. Leeflang, S. V. Asperen, **K. Yu**, N. Tumer, B. Norder, A. A. Zadpoor, J. Zhou. Solvent-cast 3D Printing of Magnesium Scaffolds. ***Acta Biomaterialia***, 2020, 114, 497-514.

(4). G. Li, **K. Yu**, J. Noordijk, M. H. M. Meeusen-Wierts, B. Gebben, P. A. M. oude Lohuis, A. H. M. Schotman, K. V. Bernaerts. Hydrothermal Polymerization towards Fully Biobased Polyazomethines. ***Chemical Communications***, 2020, 56, 9194-9197.

(3). T. Zhu, **K. Yu**, M. A. Bhutto, X. Guo, W. Shen, J. Wang, W. Chen, H. El-Hamshary, S. S. Al-Deyab, X. Mo. Synthesis of RGD-peptide Modified Poly(ester-urethane) urea Electrospun Nanofibers as a Potential Application for Vascular Tissue Engineering. ***Chemical Engineering Journal***, 2017, 315, 177-190.

(2). J. Wang, B. Sun, M. A. Bhutto, T. Zhu, **K. Yu**, J. Bao, Y. Morsi, H. El-Hamshary, M. El-Newehy, X. Mo. Fabrication and Characterization of Antheraea Pernyi Silk Fibroin-blended P(LLA-CL) Nanofibrous Scaffolds for Peripheral Nerve Tissue Engineering. ***Frontiers of Material Science***, 2017, 11 (1), 22-32.

(1). T. Zhu, **K. Yu**, M. A. Bhutto, J. Wang, W. Shen, W. Song, X. Zhou, H. El-Hamshary, S. S. Al-Deyab, X. Mo. A Facile Approach for the Fabrication of Nanoattapulgite/Poly(vinyl pyrrolidone)/Biopolymers Core-sheath Ultrafine Fibrous Mats for Drug Controlled Release. ***RSC Advances***, 2016, 6 (55), 49817-49823.